



Durham E-Theses

Seismic investigation of the crust and upper mantle of east Africa

Sundaraling am, K.

How to cite:

Sundaraling am, K. (1971) *Seismic investigation of the crust and upper mantle of east Africa*, Durham theses, Durham University. Available at Durham E-Theses Online: <http://etheses.dur.ac.uk/8585/>

Use policy

The full-text may be used and/or reproduced, and given to third parties in any format or medium, without prior permission or charge, for personal research or study, educational, or not-for-profit purposes provided that:

- a full bibliographic reference is made to the original source
- a [link](#) is made to the metadata record in Durham E-Theses
- the full-text is not changed in any way

The full-text must not be sold in any format or medium without the formal permission of the copyright holders.

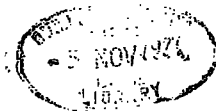
Please consult the [full Durham E-Theses policy](#) for further details.

The copyright of this thesis rests with the author.
No quotation from it should be published without
his prior written consent and information derived
from it should be acknowledged.

SEISMIC INVESTIGATION OF THE
CRUST AND UPPER MANTLE OF
EAST AFRICA.

K. Sundaralingam.

A thesis submitted for the degree of Doctor of
Philosophy in the University of Durham.



Durham, October, 1971.

C O N T E N T S

| | Page |
|---|--------|
| Acknowledgements | (i) |
| Abstract | (ii) |
| Figures | (iv) |
| Tables | (viii) |
| | |
| Chapter 1 : INTRODUCTION | |
| (1.1) General Geology | 1 |
| (1.2) Previous Geophysical work | 4 |
| (1.2.1) Surface Wave Dispersion | 4 |
| (1.2.2) Body Wave Refraction | 6 |
| (1.2.3) Spectral Response Ratio - Phinney's method | 8 |
| (1.2.4) Sn - Wave | 8 |
| (1.2.5) Seismicity | 9 |
| (1.2.6) Gravity | 9 |
| (1.2.7) Magnetic Studies | 12 |
| (1.2.8) Heat Flow | 12 |
| (1.2.9) Pole of Rotation | 13 |
| (1.2.10) The State of Stress in the Upper part of the Earth's crust | 13 |
| (1.3) Theories of Rift Formation | 14 |
| (1.4) The Present Study | 17 |
| | |
| Chapter 2 : SURFACE WAVE | |
| (2.1) Review | 19 |
| (2.2) Station Location | 25 |
| (2.3) Instrumentation | 25 |
| (2.4) Data Selection | 26 |
| | |
| Chapter 3 : ANALYSIS OF SEISMOGRAMS | |
| (3.1) Techniques for the determination of Group Velocities | 28 |
| (3.1.1) Peak and Trough Method | 28 |
| (3.1.2) Fourier Method | 28 |
| (3.1.3) Moving Window Analysis | 29 |
| (3.1.4) Multiple Filter Techniques | 30 |
| (3.2) Techniques for the determination of Phase Velocities | 33 |
| (3.2.1) Peak and Trough Correlation Method | 33 |
| (3.2.2) Fourier Analysis Method | 34 |
| (3.2.3) Correlation Techniques | 38 |
| (3.3) Data Reduction | 39 |
| (3.4) Errors | 43 |

| | Page |
|---|------|
| Chapter 4 : INVERSION OF SURFACE WAVE DISPERSION CURVES | |
| (4.1) Theoretical Study on Inversion problems | 47 |
| (4.2) Methods of Inversion | 49 |
| (4.2.1) Trial and Error Method | 49 |
| (4.2.2) Monte Carlo Inversion | 50 |
| (4.2.3) Least Square Inversion Techniques | 50 |
| (4.3) New Techniques | 54 |
| (4.3.1) The Alternating Variable Search Method | 58 |
| (4.3.2) Steepest Descent Method | 59 |
| (4.3.3) Powell - Conjugate direction Method | 60 |
| Chapter 5 : RESULTS AND INTERPRETATION | |
| (5.1) Results and Regional Comparisons | 69 |
| (5.2) Interpretation | 76 |
| (5.2.1) The Application of Steepest Descent Method | 77 |
| (5.2.2) The Application of Powell - Conjugate direction Method | 80 |
| (5.2.3) The Models | 82 |
| (5.2.4) Non-Uniqueness | 88 |
| Chapter 6 : ADDITIONAL GEOPHYSICAL STUDIES | |
| (6.1) Delay time | 93 |
| (6.1.1) The Present Study | 95 |
| (6.2) Q - measurement | 100 |
| Chapter 7 : DISCUSSION AND CONCLUSION | |
| (7.1) Discussion | 104 |
| (7.2) Conclusion | 110 |
| Computer Program : | |
| (1) Steepest Descent Method | 117 |
| (2) Powell - Conjugate direction Method | 123 |
| (3) Mapping in Hyperspace | 138 |
| References : | 146 |

(i).

ACKNOWLEDGEMENTS

I wish to thank Professor M.H.P. Bott for the privilege of working in the department. I am indebted to Dr. R.E. Long for valuable help, guidance and encouragement throughout the progress of this study.

I should like to thank Mr. Peter Marshall and his colleagues at Blacknest for their assistance and advice and for permitting me to use their SWAP computer program. I am grateful to Dr.M. Alchalabi for his assistance with computer programming.

I should like to thank Professor P.L. Willmore at the I.S.C. Edinburgh for supplying seismic records from various stations. Further, I should like to thank Professor L.R. Sykes of Lamont-Doherty Geological observatory for supplying Lwiro station records and to Dr. Paul Pomeroy of Department of Geology and Mineralogy, University of Michigan for supplying the characteristics of the instrument in operation at Lwiro. I should also like to thank Mr. K. Bram, Head, Seismological department, Lwiro for providing us with the clock error at the Lwiro station.

I would like to thank all my colleagues, in particular Mr. Alan Gooda^{cre} and Mr. Richard Backhouse for their help.

Finally, I should like to thank the University of Ceylon, Peradeniya for financial support for three years.

ABSTRACT

Interstation Rayleigh - and Love wave phase and group velocities have been determined for seismic recording stations in East Africa. Single station group velocities have also been determined for events in ^{the} African continent. The phase velocities cover the period range of 15 - 60 sec and the group velocities extend from 12 - 50 sec. The most characteristic feature of this set of Rayleigh wave phase velocity curves is that there is a definite merging of phase velocities from longer to shorter periods. The spread at 60 sec period is 0.33 km/sec whereas at 20 sec period this is reduced to 0.1 km/sec.

A Fourier analysis method is used to determine the phase velocities and Multiple filter techniques to determine the group velocities.

A number of non-linear optimization techniques have been developed to derive the shear velocity - depth structure of the crust and upper mantle from surface wave dispersion data. These techniques have a number of advantages over Least Square Inversion techniques. The Non-uniqueness problem is investigated in detail; and a method is proposed to determine the order of magnitude of the thickness of the layers to overcome such a problem.

The structural models derived show that the total thickness of the crustal layers is roughly the same throughout East Africa, and is between 34 to 42 km, except along the centre of the eastern rift valley where crustal thinning is indicated by refraction and gravity studies (Griffiths et al, 1971). There is some indication of modification of the lower crustal layer ^{towards} higher shear velocity along the flanks of the eastern rift valley system.

The upper mantle structure beneath the eastern rift valley system is similar to that beneath Iceland; further, this structure extends to

(iii)

a greater distance south of Nairobi. It seems the eastern and the western rift valley systems are separated by a shield type structure at Lake Victoria. P - delay at Addis Ababa and Nairobi is found to be nearly the same as that for stations in ^{the} western United States and Iceland. P - delay at Lwiro is about half as that at Nairobi.

The rift valley system in East Africa has not yet developed to a stage comparable to Mid-ocean ridges.

FIGURES

1. Tectonic map of East Africa.
2. The crustal structure at Addis Ababa, Nairobi and Lwiro from the spectral response ratio.
3. The crust and upper mantle structure across the eastern and western rift valley systems from gravity studies (Searle et al).
4. The crust and upper mantle structure across the Gregory rift, near ^{the} equator, from gravity studies (Khan and Mansfield).
5. Map of Bouguer - isanomalies of East Africa (in Graben Problem - Wohlenberg, 1970).
6. The crust and upper mantle structure beneath the western rift valley system from gravity studies.
7. The vertical and the N - S component ^{of} seismograms from recording stations at BUL, NAI and AAE for the event of 19 March 1966 (Rayleigh wave).
8. The location of the seismic recording stations in East Africa and the epicentre of the events used in interstation surface wave studies.
9. The epicentres of the events used for single station group velocity measurements.
10. Rayleigh wave group velocity dispersion curve for the event of 26 Feb 1964 recorded at NAI; using Multiple filter techniques.
11. A comparison of amplitude spectra for two portions of the same record, to determine the frequency content of the wave train.
12. (a) The phase velocity partial derivative with respect to shear wave velocity for Rayleigh waves
 - (b) The group velocity partial derivative with respect to shear wave velocity for Rayleigh waves.
 - (c) The phase velocity partial derivative with respect to shear wave velocity for Love waves.
 - (d) The group velocity partial derivative with respect to shear wave velocity for Love waves.
 - (e) The phase velocity partial derivative with respect to thickness

for both Love and Rayleigh waves.

- (f) The group velocity partial derivative with respect to thickness for both Love and Rayleigh waves.
13. Shear velocity - depth structure of the initial model used to calculate the partial derivatives; and phase - and group velocity for the Love and Rayleigh waves for this model.
 14. The plot of $RMSD/H$ as a function of the depth to the mid-point of the layers for the initial model.
 15. Two-dimensional section in a hyperspace formed by thickness and shear velocity (Problem of uniqueness).
 16. Rayleigh wave phase velocities for a number of interstation paths in East Africa, together with that for AFRIC model and that along the path PRE - BUL.
 17. Rayleigh wave group velocities for two interstation paths in East Africa, together with that for AFRIC model, central U.S.A. and M. Atlantic ridge type structures (Table 9).
 18. Love and Rayleigh wave phase velocities for the interstation AAE - NAI together with that for E. Pacific rise type model, M. Atlantic ridge type model and Germany model (Table 9).
 19. Rayleigh wave phase velocities for the interstation path AAE - LWI and NAI - BUL together with that for the central U.S.A. and E. Australia.
 20. Single station Rayleigh wave group velocity dispersion curve for events in African continent.
 21. Shear velocity - depth structure obtained for the interstation paths AAE - NAI, NAI - BUL and AAE - LWI using steepest descent method.
 22. The observed Rayleigh wave phase - and group velocity data points for the interstation paths AAE - NAI, NAI - BUL and AAE - LWI; together with the corresponding dispersion curve for the optimized models using Steepest descent method.
 23. The contour of the RMSD value for Rayleigh wave phase and group; and phase by varying the shear velocity of third and fourth layers of the model used to derive partial derivative (Table 7).

24. The contour of the RMSD value for Rayleigh wave phase and group; and phase by varying the shear velocity of fifth and sixth layers of the model used to derive partial derivatives (Table 7).
25. A Number of, the crust and upper mantle structures obtained for the path AAE - NAI, by inverting Rayleigh wave phase and group velocity dispersion curves of the event 20 April 1966.
26. The observed velocity data points for the path AAE - NAI and the corresponding dispersion curve for the optimized model (Powell Conjugate direction method).
27. The observed Love wave data points (Event : 26 July 67) for the path AAE - NAI and the corresponding dispersion curve for an optimized model.
28. The observed velocity data points for the path NAI - BUL, and the corresponding dispersion curve for the optimized model.
29. The observed velocity data points for the path AAE - LWI, and the corresponding dispersion curve for the optimized model.
30. The observed velocity data points for the path NAI - LWI, and the corresponding dispersion curve for the optimized model.
31. The observed velocity data points for the path BUL - LWI, and the corresponding dispersion curve for the optimized model.
32. The shear velocity - depth structure obtained by using Powell Conjugate direction method, for all the interstation paths in East Africa.
33. The contour of the RMSD value for the phase and group velocity of Rayleigh waves and phase velocity of Love waves for the path AAE - NAI, using the optimized model and varying the shear velocity of fourth and fifth layers (that is, two uppermost upper mantle layers).
34. The shear velocity - depth structure obtained from single station Rayleigh wave group velocity measurements.
35. Q against period plot for the interstation paths AAE - NAI and NAI - BUL; for Love and Rayleigh waves.
36. Tectonic map of East Africa; the red-dashed portion of the interstation paths are the regions where the anomalous upper mantle extends to a greater depth is observed. The red-hatched paths

the region where anomalous uppermost upper mantle velocity is observed.

TABLES

1. (a) The crust and upper mantle structure of Africa by Press, Ewing and Oliver (1956).
(b) The crust and upper mantle structure of southern part of East Africa by Oliver, Dorman and Sutton (1959).
2. (a) The crust and upper mantle structure of South Africa by Bloch, Hales and Landisman (1969).
(b) The crust and upper mantle structure of Africa by Gumper and Pomeroy (1970).
3. (a) The crust and upper mantle structure of western Transvaal.
(b) The crust and upper mantle structure of eastern Transvaal.
4. Interstation great circle path:- distance and azimuth.
5. Location, date, origin time and co-ordinates of earthquakes used in interstation study.
6. Location, date, origin time and co-ordinates of earthquakes used in single station group velocity study.
7. The structural detail of initial model used to derive partial derivatives.
8. Root mean square deviation corresponding to a unit change in the compressional velocity, shear velocity, density and thickness for the model in Table 7.
9. The structural detail of the Germany model, central United States model, East-Pacific rise model and Mid-Atlantic ridge model.
10. The interstation crust and upper mantle structure from Powell - conjugate direction method; together with confidence limits on the active parameters.
11. P- and S- delay times in seconds, at AAE, NAI and LMI with respect to BUL.
12. Date, origin time and epicentre of the events in African continent used to determine the Pn and Sg velocity between the station pair BUL and BHA.

13. The comparison of East African structure with that for Rhine graben and Baikal rift.
14. The comparison of East African structure with that for western United States and Iceland.

CHAPTER 1

I N T R O D U C T I O N

(1.1) General Geology

The rift system in East Africa extends some 2,300 miles, from the neighbourhood of the Limpopo river in the South to the Red Sea in the North. (Fig.1.)

The most obvious expression of the rift system is in the topography. An extensive swell occupies eastern Africa, forming a plateau some 1,000 km wide and reaching heights of 1 to 2 km above sea level. This swell, is dissected by the rift zones which comprise narrow depressions, forming the rift valleys, with neighbouring regions of even greater uplift. Here the rift shoulders reach heights of 2 to 3 km above sea level. The rift valleys are typically 25 to 60 km wide and the floor may have been displaced as much as 6 km relative to the shoulders, although infilling with sediments and volcanics has reduced the depth to about 1 km in most places (Dixey, 1956; Freud, 1965). The rift valleys show greater variations in altitude, but the fact that elevations and depressions of the floor are matched by corresponding elevations and depressions of the shoulders shows that the overall displacements are everywhere of the same general order.

The rift zone is not continuous, nor is it everywhere equally developed. They are trains of long narrow tectonic troughs, bordered by faults. Almost all the faults which border the rift and occur within them are narrow faults (Freud, 1965). Their dips range from 45° to almost vertical, but most commonly $55-70^{\circ}$. Reverse and Transverse faults are very rare. Rifts are not bordered by large single faults, but rather they are outlined by sets of steep blocks, and the faults that diverge ^{and substitute for} one another in an en echelon manner, so that they make a zig-zag pattern. It is common for one side of a rift to be much more elevated than the other,

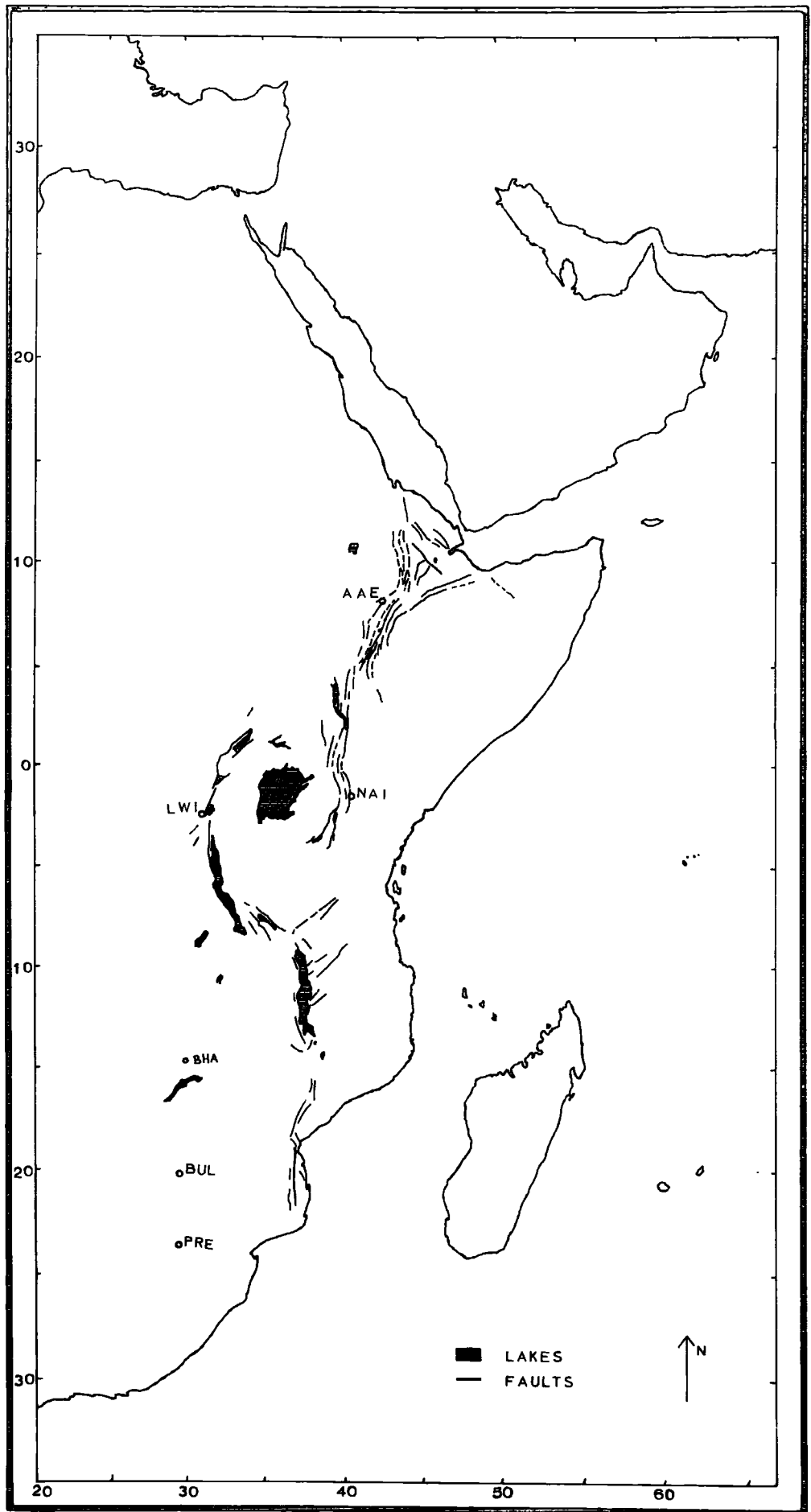


FIG. I

and the main fault may be missing on one side. The most remarkable feature of the rift is the down faulted block within the rift, shattered by numerous faults into small horsts and grabens and the almost complete absence of faults outside. The subsiding grabens, ascending shoulders, seismic activity, recent volcanism and many hot springs demonstrate that the taphrogenic activity is still in progress.

Both the general trend and the details of rift faulting are closely determined by older, mostly Pre-cambrian structures. These structures are, however, widely diverse in age and kind.

It seems clear that the bifurcation of the system into an Eastern and a Western rift is the result of deflection of the fracture systems around the Tanganika "Shield" or Craton; this consists of a gneissic complex and meta-sedimentary or meta-volcanic systems with prevalently east-west trends.

Although the most characteristic rifting is of Tertiary and later age, a similar pattern of faulting is recognisable in several sectors dating back to late Karroo or early Jurassic times. The fact that there are no older crustal structures or lineaments in this great belt of such magnitude and persistence suggests that the system has been determined by a major deep-seated crustal or sub-crustal mechanism. The occurrence of distinctive volcanic associations along many parts of the rift system is also in accord with this conclusion.

(a) The Eastern Rift:-

The Eastern or Gregory rift valley in Kenya approximates in many places, to a classic graben; its N-S trends and general regularity are evidently related to the equally regular structures of the Mozambique belt. Northwards towards the Ethiopian border, however, it splays out, again apparently largely controlled by older structures, to form a broad

zone up to about 200 miles in width, within which only a narrow and relatively insignificant trough passes from the southern end of Lake Rudolf and by way of Lake Stephanie to link with the great rift valley of Ethiopia. Southwards in Tanzania the eastern rift rapidly "degenerates" into a broad zone of faults of varying persistence and trends which define a series of tilted blocks (James, 1956; Dundas, 1965; Pallister, 1965). Control by older structures is, however, still evident.

The extensive Tertiary to recent lava fields in Ethiopia are generally recorded as being predominantly basaltic but this may well be a convenient generalization because to the south, in Kenya, although basalts (often basarites according to Kent, 1944) are widespread, phonolite is very common and is perhaps the predominant lava throughout the eastern rift and in adjacent areas such as the Uasin Gishu plateau, the Aberdare mountains and Mount Kenya. Trachytes, nephelinites, and alkali rhyolites are also well represented in these fields. Further south, in Tanzania, the lava fields give way to central volcanoes built largely by fragmental materials, mainly nephelinites and phonolites along the eastern rift and trachytes and phonolites to the east in the Kilimanyaro range. In eastern Uganda a chain of Tertiary volcanoes, largely composed of fragmental nephelinites, stretches northward from Mount Elgon (Davies, 1952), one of these, Napale (King, 1949), having an exposed ijolite carbonatite core. Further to the south and west lie the pre-Tertiary carbonatite centres of Torora, Sekulu and Bukusu (Bailey, 1964).

(b) The Western Rift:-

In Lake Albert drilling and Geophysical work have established a maximum thickness of some 8,000 ft of sediments. The faults are mostly N-E to S-W, but have an en echelon pattern which relays the movements northwards. Pleistocene faulting is evident where sediments are thrown against basement.

Further south is the off-set Lake Edward trough, which is shallow at its N-E end but deepens towards the Rwanda border; from Lake George it is defined by a series of Faults which form an en echelon pattern.

The culmination of the floor of the western rift is Lake Kivu which, as a result of a volcanic accident, drains into Lake Tanganyika and thence to the Congo. South of Lake Kivu there are lava fields largely composed of alkali (Olivine) basalts and basanites, but trachytes and trachyandesites are also represented.

Southwards from Lake Kivu the western rift swings into the 400 mile north-north-west to south-south-east belt occupied by Lake Tanganyika. The structures here have not as yet been closely studied, but appear to be relatively simple. The lake is not comparable to Lake Albert for it has a negligible sedimentary in-fill and its floor is well below sea level. The lake itself occupies sub-parallel graben defined by various pairs of faults and, towards its southern end, the rift structures extend over a width of about 100 miles, involving parallel graben and horsts, into the rejuvenated post Karroo Rukwa trough.

In the north, the western rift terminates abruptly against the strongly marked N-W to S-E trends of the Madi series of the Sudan border and parallel structures of the Aswa shear belt of Northern Uganda.

(1.2) Previous Geophysical Work

(1.2.1.) Surface Wave Dispersion:

Press, Ewing and Oliver (1956) using Rayleigh wave group velocities in the period range 10 to 70 sec, for the event in northern Algeria (36° 17' N 1° 28' E) recorded at Pietermaritzburg (South Africa) deduced the average thickness of the crust along this path to be 35 km. Further,

Press, Ewing and Oliver (1956)

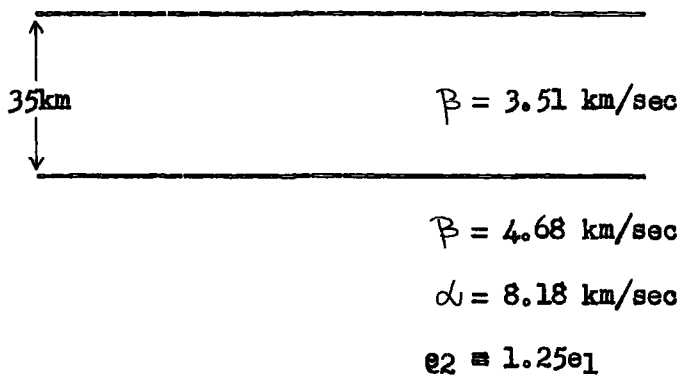


Table 1a

Oliver, Dorman and Sutton (1959)

| H km | α km/sec | β km/sec | ρ gm/cc |
|----------|-----------------|----------------|--------------|
| 2.222 | 5.2 | 3.00 | 2.55 |
| 17.778 | 6.32 | 3.65 | 2.817 |
| 20.000 | 6.58 | 3.80 | 2.922 |
| ∞ | 8.14 | 4.70 | 3.300 |

Table 1b

it is concluded that Africa and North America are identical in crustal structure (Table 1a).

Oliver, Dorman and Sutton (1959) using the second shear mode of continental Rayleigh wave for the event in Belgian Congo (9.5° S 27.5° E) recorded at Pietermaritzburg; deduced ^{the} thickness of the crust to be about 40 km. Shear velocity depth structure is same as for typical shield area. (Table 1b).

Ocal (1965) from the Love - and Rayleigh - wave group velocities in the period range 28 to 76 sec for the event Agadir earthquake (30.5° N 9.6° W) recorded at Lwiro and Skopje earthquake (42.1° N 21.5° E) recorded at Pretoria and Windhoek, ^{has} shown that the average thickness of the crust in Africa is thinner than in Europe and the thickness in ^{the} direction of Skopje to Pretoria is more than that from Agadir to Lwiro.

Bloch, Hales and Landisman (1969) have ~~been~~ determined Rayleigh wave phase velocities from an array of stations located near Johannesburg, South Africa, and from the World Wide Standard Seismic Network stations at Pretoria, Bulawayo and Windhoek. Multi-mode Rayleigh - and Love - wave group velocities have also been found from the records of a number of earthquakes originating near the Kariba Dam, and in southern Malawi. The phase velocities cover the period range 20 - 100 sec and the group velocities extend from 2 - 40 sec for the fundamental mode and 2 - 12 sec for the higher modes. The multi-mode dispersion obtained indicates that the crustal and Upper mantle velocities to the east of a line through Pretoria and Bulawayo are higher than those to the west. The phase velocities for the array area confirm the high sub-crustal shear velocities previously determined from refraction studies (Gane, Atkins, Sellschop and Seligman, 1956; Hales and Sacks, 1959). The phase - and group - velocity curves obtained for the Kariba - Pretoria path are similar to those for other shield areas. The central United States, eastern Australia and the western part of southern Africa have very similar

SASD 2
Bloch, Hales and Landisman, (1969)

| H km | α km/sec | β km/sec | ρ gm/cc |
|----------|-----------------|----------------|--------------|
| 8.0 | 5.7 | 3.50 | 2.70 |
| 12.0 | 6.2 | 3.64 | 2.90 |
| 8.0 | 6.7 | 3.84 | 2.95 |
| 8.0 | 6.9 | 3.97 | 3.00 |
| 9.0 | 7.3 | 4.24 | 3.20 |
| 25.0 | 8.1 | 4.67 | 3.30 |
| 50.0 | 8.3 | 4.80 | 3.37 |
| 150.0 | 7.8 | 4.50 | 3.37 |
| ∞ | 8.3 | 4.80 | 3.40 |

Table 2a

AFRIC MODEL
Gumper and Pomeroy, (1970)

| H km | α km/sec | β km/sec | ρ gm/cc |
|-------|-----------------|----------------|--------------|
| 7.0 | 5.90 | 3.35 | 2.70 |
| 10.5 | 6.15 | 3.55 | 2.80 |
| 18.7 | 6.60 | 3.72 | 2.85 |
| 80.0 | 8.05 | 4.63 | 3.30 |
| 100.0 | 8.20 | 4.78 | 3.44 |
| 100.0 | 8.30 | 4.65 | 3.53 |
| 80.0 | 8.70 | 4.85 | 3.70 |
| | 9.20 | 5.25 | 3.76 |

Table 2b

Rayleigh-wave phase velocities, which are lower than those for the shield areas (Table 2a).

Gumper and Pomeroy (1970) determined phase - and group - velocities of fundamental mode Rayleigh waves; Group velocities of fundamental mode Love waves and higher mode Rayleigh waves; and group velocities for sedimentary layer Rayleigh waves, for the African continent. Rayleigh wave phase velocities range from approximately 3.90 to 4.20 km/sec in the period range of 30.0 to 63.0 sec. Group velocities of fundamental mode Love and Rayleigh waves in the period range of 10.0 to 60.0 sec range from 3.35 to 4.15 km/sec and 3.00 to 3.95 km/sec respectively. As expected, for the shorter periods the velocities depend strongly upon regional structure. Group velocities of sedimentary Rayleigh waves and of higher mode Rayleigh waves have also been determined. Short period body-wave velocities were determined for this region as follows: $P_n = 8.06$ km/sec, $S_n = 4.55 - 4.72$ km/sec, and $L_g = 3.48 - 3.60$ km/sec. The observed surface wave velocities are similar to those reported for the Baltic shield and differ somewhat from those velocities found for the Canadian shield. A theoretical model that accounts for the observed velocities is derived for the African continent (Table 2b).

(1.2.2) Body Wave Refraction:

Willmore, Hales and Gane (1952); and Gane, Atkins, Sellschop and Seligman (1956) have used local earth tremors within 500 km of the seismic stations and studied the crustal structure of western Transvaal (Table 3a). The velocity values found :

$$\begin{array}{ll} P_1 = 6.18 \text{ km/sec} & P_n = 8.27 \text{ km/sec} \\ S_1 = 3.66 \text{ km/sec} & S_n = 4.73 \text{ km/sec} \end{array}$$

Crustal thickness from P and S data, 35.1 and 33.3 km respectively. These depths include about 1.3 km of superficial material of lower

Willmore, Hales and Gane (1952)
 Gane, Atkins, Scallschop, Selligman (1956)

Single Layer Crust

| | β km/sec | α km/sec |
|-------|----------------|-----------------|
| West | 3.69 | 6.23 |
| | 4.83 | 8.24 |
| | H 38.3km | H 35.5km |
| South | 3.68 | 6.09 |
| | 4.78 | 8.42 |
| | H 34.0km | H 34.7km |
| East | 3.63 | 6.20 |
| | 4.66 | 8.01 |
| | H 31.6km | H 34.1km |
| North | 3.64 | 6.20 |
| | 4.60 | 8.21 |
| | H 30.0km | H 36.6km |
| A ll | 3.66 | 6.10 |
| | 4.73 | 8.27 |
| | H 33.6km | H 35.4km |

Table 3a

Hales, Sacks (1958)

Two Layer Crust

| East | β km/sec | α km/sec |
|----------------------|-----------------------|-----------------------|
| Layer 1 | 3.62 | 6.03 |
| | H ₁ 24.8km | H ₁ 28.2km |
| Layer 2 | 4.04 | 7.19 |
| Layer 2 ¹ | | H ₂ 8.4km |
| | | H ₂ 14.7km |
| Layer 3 | 7.96 | |
| | Depth to Moho 36.6km | |

Table 3b

velocity.

There is evidence of a phase corresponding to an intermediate layer of P - velocity 6.83 km/sec; the inclusion of which brings the total depth to 39 km.

Hales and Sacks (1959) using the same procedure as Willmore et al (1952); studied crustal structure in the eastern Transvaal.

It is considered that the most satisfactory interpretation is that the crust is two-layered. The velocities in the granitic layer are 6.0 and 3.6 km/sec for P and S waves respectively. In the intermediate layer the P velocity lies between 6.7 and 7.2 km/sec, and the S velocity between 3.95 and 4.15 km/sec. The Pn velocity was found to be 7.9 km/sec and the crustal thickness 36.6 km (Table 3b).

Dopp (1964) has used small earthquakes within 100 km of the seismic stations Uvira, Lwiro, and Rumangabo, in the Western rift, to form seismic refraction profiles along the rift. He found a Pg-velocity of 5.57 km/sec in the upper part of the crust. Below this was a layer with P- wave velocity 6.76 ± 0.06 km/sec, which was separated from the upper (5.57 km/sec) layer by an interface striking N-S and dipping 15° to the west. The depths of the interface were 17, 33 and 27 km at Rumangabo, Lwiro and Uvira respectively.

The refraction work (Artificial explosion) between Lake Rudolf and Lake Hannington, along the axis of the Gregory rift by Griffiths, King, Khan and Blundall (1971) show a layer of about 20 km thickness with P- velocity of 6.4 km/sec and S- velocity of 3.5 km/sec underlying a surface layer of about 3 km thick and P- velocity of 3.0 km/sec ($S = 1.8$ km/sec). The velocity and thickness of this surface layer is assumed in the interpretation. The layer beneath the 6.4 km/sec

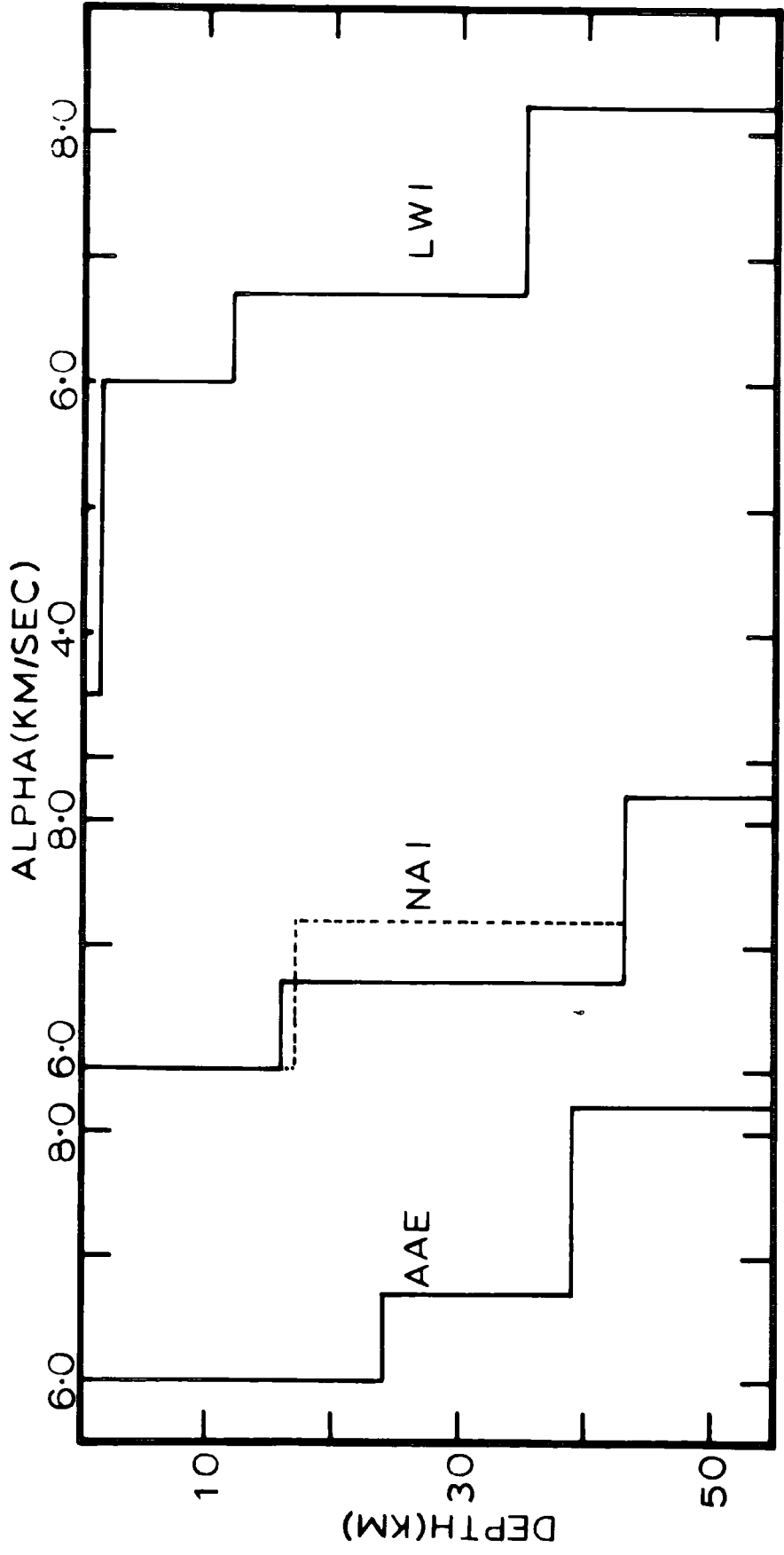


FIG. 2

layer is found to have a P- velocity of 7.5 km/sec and S- velocity of 4.53 km/sec.

(1.2.3) Spectral Response Ratio - Phinney's Method:

Crustal response ratios within the East African rift system are determined by spectral analysis of long period P wave, dominant period of 10 sec, from two Hindu Kush earthquakes observed at stations in Addis Ababa, Nairobi and Lwiro (Bonjer, Fuchs and Wohlenberg, 1969). The spectral response shows P- velocity^{ies} of 6.0 km/sec for the upper crustal layer and 6.7 km/sec for the lower crustal layer. The thickness of the crust is found to be 39 km at Addis Ababa, 43 km at Nairobi and 35 km at Lwiro (Fig. 2).

(1.2.4) Sn- Wave :

The following observations have been made from the study of the propagation of Sn phase, Sn- is a short period seismic shear wave travelling in the uppermost part of the mantle, by Molnar and Oliver (1969); and Gumper and Pomeroy (1970).

(a) Sn is observed over all paths less than 3,000 km in length that do not cross either the African rift zone or the Red sea rift.

(b) Sn does propagate across the southern part of the rift zone below approximately 10° S, but ^{not across the northern part above the equator,} however, between these two regions the data are mixed, with Sn propagating along some paths and not along other nearby paths.

It has been concluded that the above observations indicate that under the northern part of the rift zone there exists a gap in the mantle portion of the lithosphere which closes toward the southern part of the zone.

(1.2.5) Seismicity :

Fairhead (1968) has made a study of the seismicity of East Africa using the Joint Epicentral determination technique (Douglas, 1967). He relocated earthquake epicentres for the period 1955 through 1968, showing that the epicentres do tend to fall on known faults. Two focal mechanisms were also obtained, one of which indicated normal faulting and the other strike-slip faulting.

Sykes (1967); and Banghar and Sykes (1969) have shown normal and strike-slip faulting in four other East African earthquakes (in the western rift).

Tobin and others (1969) have made a detailed study of the micro seismicity of the Gregory rift. They showed that the greatest activity occurs not along the marginal faults, which are relatively quiet, but at the centre of the rift in the zone of recent, intense faulting.

Wohlenberg (1970); and Molnar and Aggarwal (1971) studying micro earthquakes over Gregory rift, ^{have} shown that there is a region in this part of the rift, from 1° S, 36° E up to Lake Rudolf where no epicentres of earthquakes with magnitude $M \geq 4$ could be localized. Further the number of observed micro earthquakes in a time - unit decreases from south to north beginning at the frontier of Tanzania and Kenya in the south to nearly 200 km in the north of Nairobi.

For all earthquakes in East Africa, the depths of focus were shallow - less than 15 km in Kenya (Molnar and Aggarwa, 1971) and less than 75 km in the western rift (Wohlenberg, 1970).

(1.2.6) Gravity :(a) Eastern Rift :-

Gravity anomaly studies over the region of rift valley system by

Kohlschütter (1899 - 1900) and Bullard (1936) shows that ; except the centre of the rift valleys, African plateau, in general, in isostatic equilibrium and floor of the rift valley is associated with high negative Bouguer anomaly.

The most important findings of the Gravity traverses in Ethiopia by Mohr and Gouin (1968, 1967) can be enumerated as follows: (1) There is a definite gravity low over the main Ethiopian rift compared with the adjacent plateau. The cause of the rift "low" is tentatively identified with underlying silicic magma chambers and their extensive volcanic effluvia (welded-tuffs, Lavas, pumite), and with thick lacustrine sediments, all deposited in the subsiding proto-rift, pre-middle Pleistocene trough.

(2) Free-air anomaly values of between 0 and -50 mgal are determined for the rift floor.

(3) The gravity 'high' over the Wonji fault belt is confirmed. The 'high' is attributed to basaltic injection into a thin crust affected by tension.

Similar gravity studies in Kenya across main rift valley system from east to west, by Sowerbutts (1969); Girdler, Fairhead, Searle and Sowerbutts (1969); Searle (1970 a,b); Baker and Wohlenberg (1971) suggest the possibility of thinning of crustal material beneath the rift valley system (Gregory rift) with overall reduction in thickness of the lithosphere in the upper mantle over a broader area. This reduction is due to upwelling of the low velocity channel near Moho. Further it is found that the volcanoes on the rift floor are associated with a positive Bouguer anomaly; this anomaly can be interpreted as being due to a basic intrusion, in the sialic crust, of about 20 km

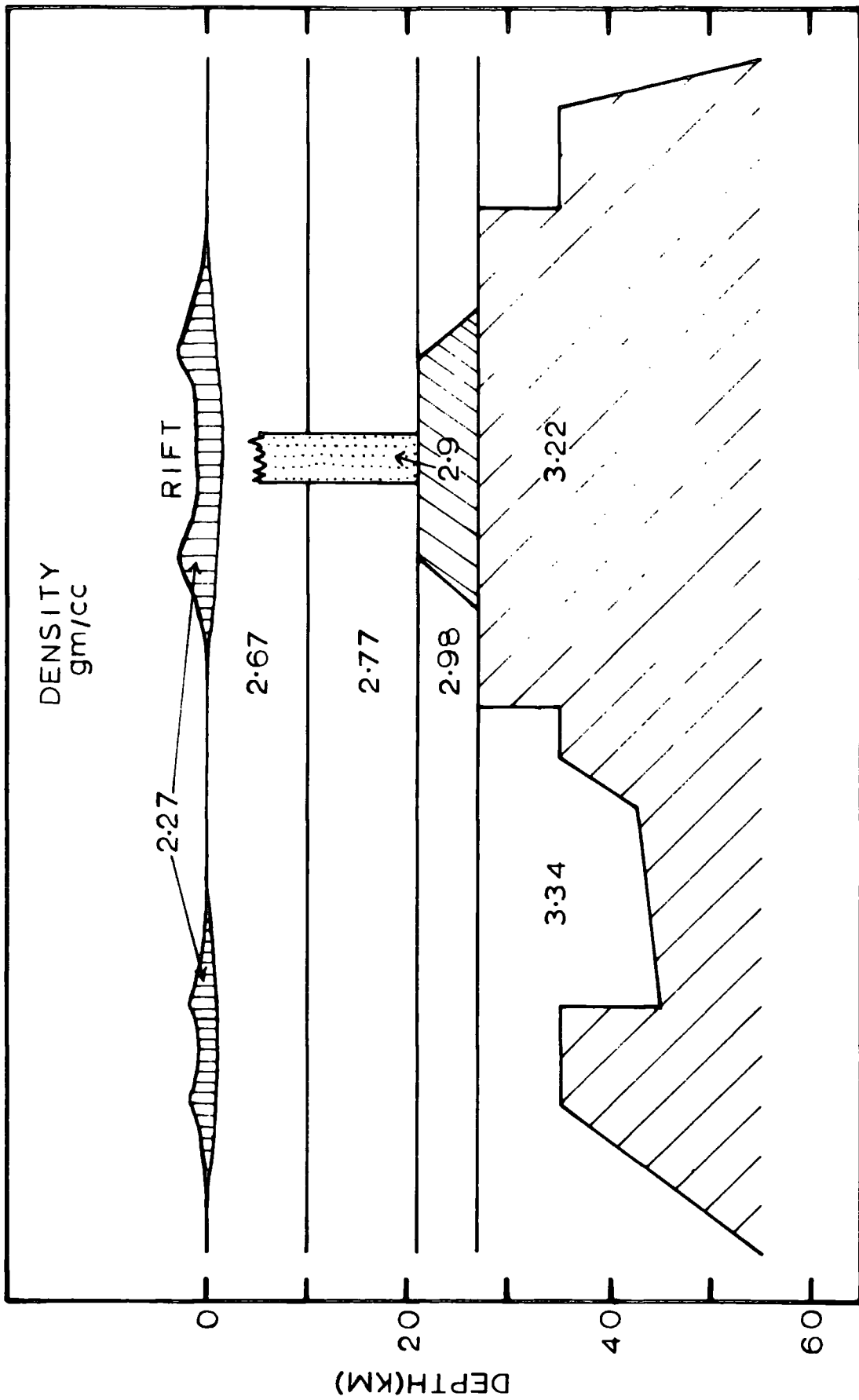


FIG. 3

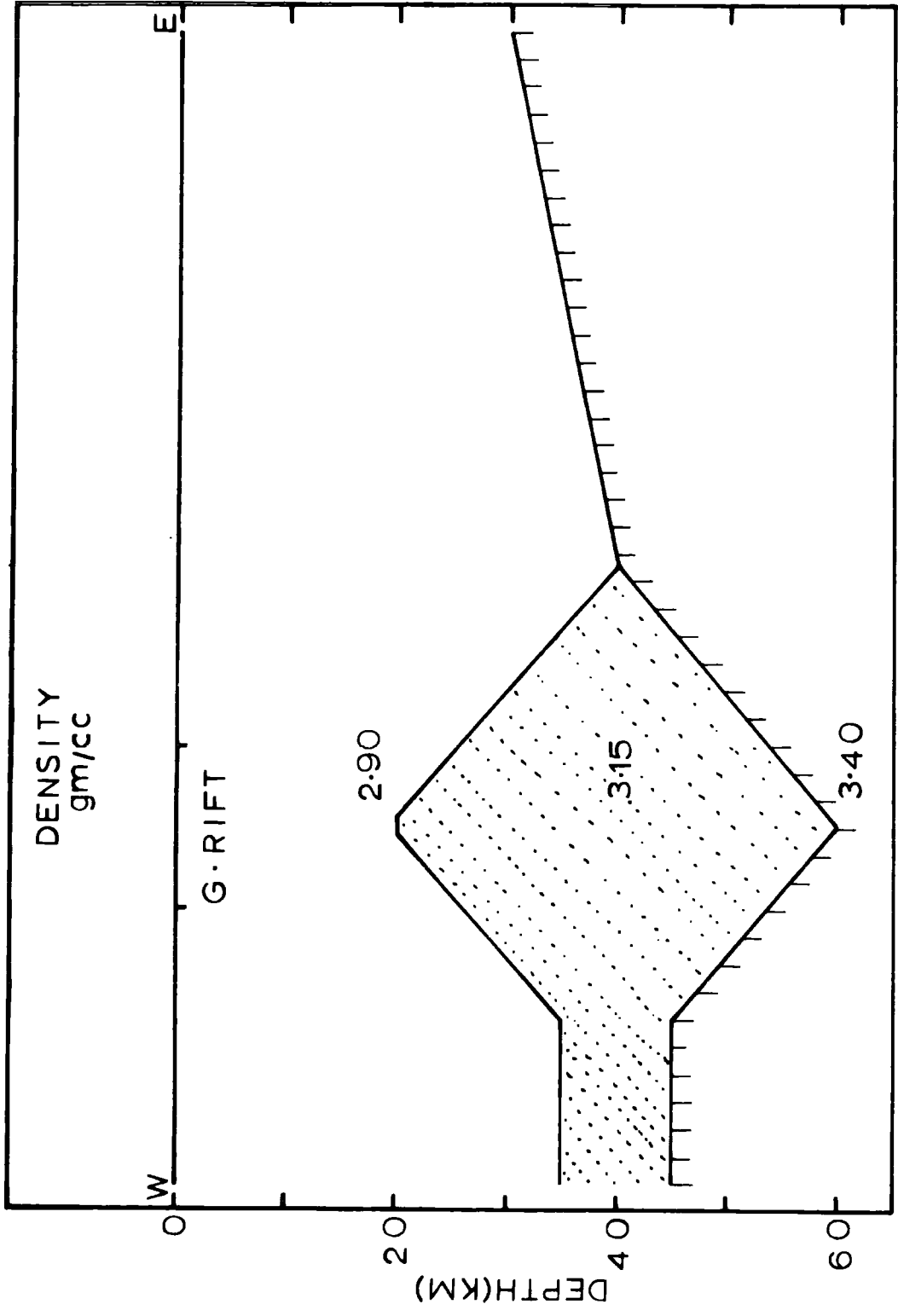
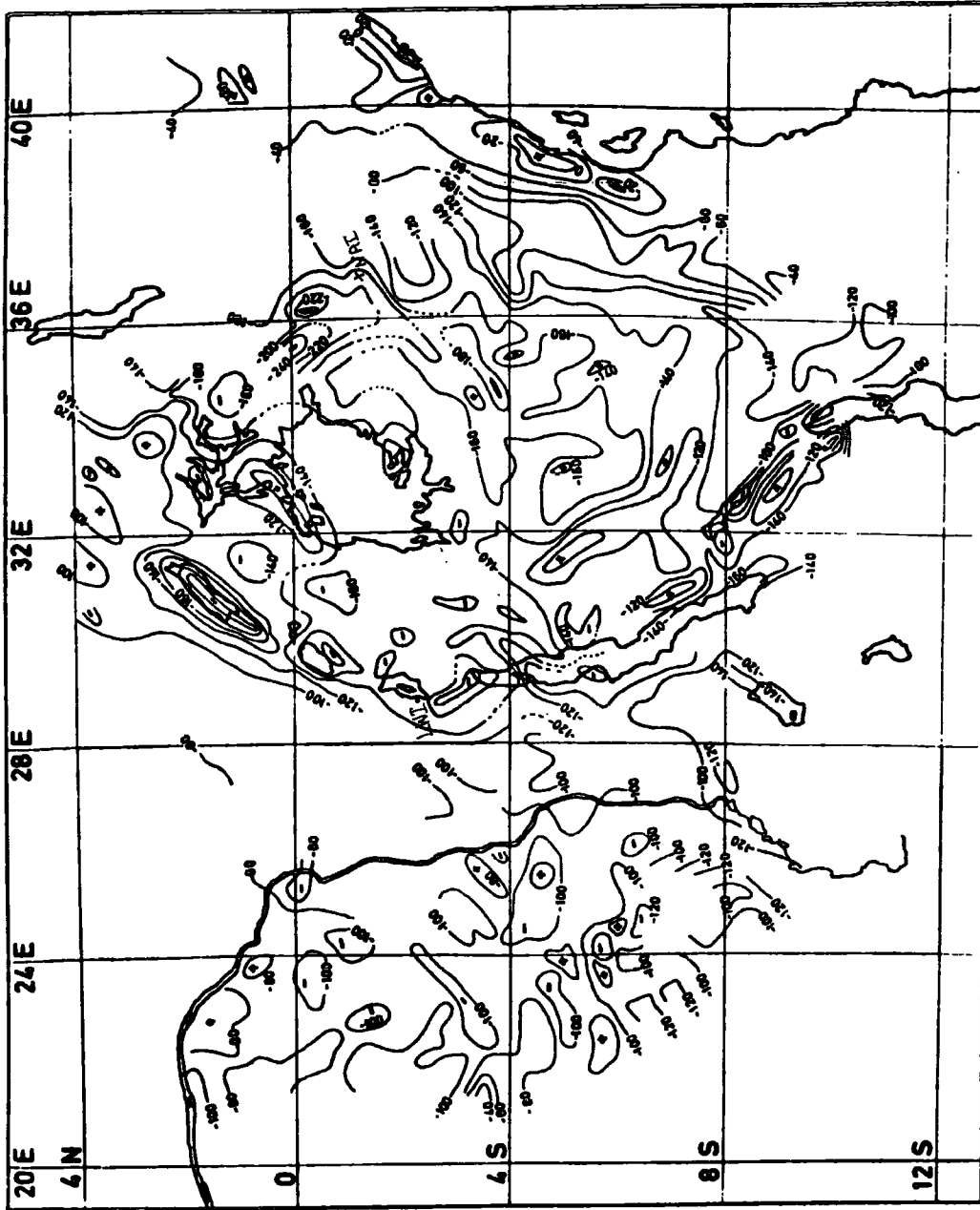


FIG. 4



Map of Bouguer-is anomalies of East Africa. The map is based on detailed investigations of: BROWN (1961, Uganda), BULLARD (1936, East Africa), JONES (1962, Rep. Dem. du Congo), KRENKEL (1925, Tanzania), and the Overseas Geology Surveys (1965, Kenya).

wide and reaching to within 1 km of the surface (Fig.3).

Khan and Mansfield (1971) suggested slightly different type of crust and Upper mantle structure for the E-W profile across the Gregory rift, near equator (Fig. 4). From the regional map of Bouguer anomaly we can see clearly the presence of lateral variation in gravity anomaly, even along the axis of the rift, with locally very low values at few places (Fig.5).

(b) Western Rift :-

Measurements by J.M. Brown in Uganda; and by Smith and Andrew (1960) in Tanzania have shown negative Bouguer anomalies associated with much of the western rift and with the Eyasi and Rukwa troughs in Tanzania. The gradient and magnitude of the Bouguer anomaly in the Albert rift show that the top of the mass-deficiency causing it must be within 1 km of the surface. Girdler (1963) found that 2 to 3 km of sediment would account for this anomaly, and such a thickness has been found in a borehole in Uganda section of the western rift (Davies, 1951).

Sutton and Grow (1969) found that the regional Bouguer gravity anomalies over the rift valleys surrounding Lakes Albert, Edward, Kivu and Tanganyika range between -100 and -140 mgal. The residual Bouguer gravity anomalies over the rift valleys are sharply defined, ranging between -70 and -80 mgal. They interpreted these anomalies in terms of a sediment or breccia - filled graben about 30 km wide bounded by high-angle normal faults 60° or steeper in dip penetrating to the mantle. The sharpness of the negative anomaly over the rift valleys suggests that the source of the anomaly is within the upper 5 km of the graben floor and is due to deficiency created by the density contrast between the sediments (2.17 gm/cc) and the basement rock (2.67 gm/cc). The Moho discontinuity beneath the entire region is probably at relatively

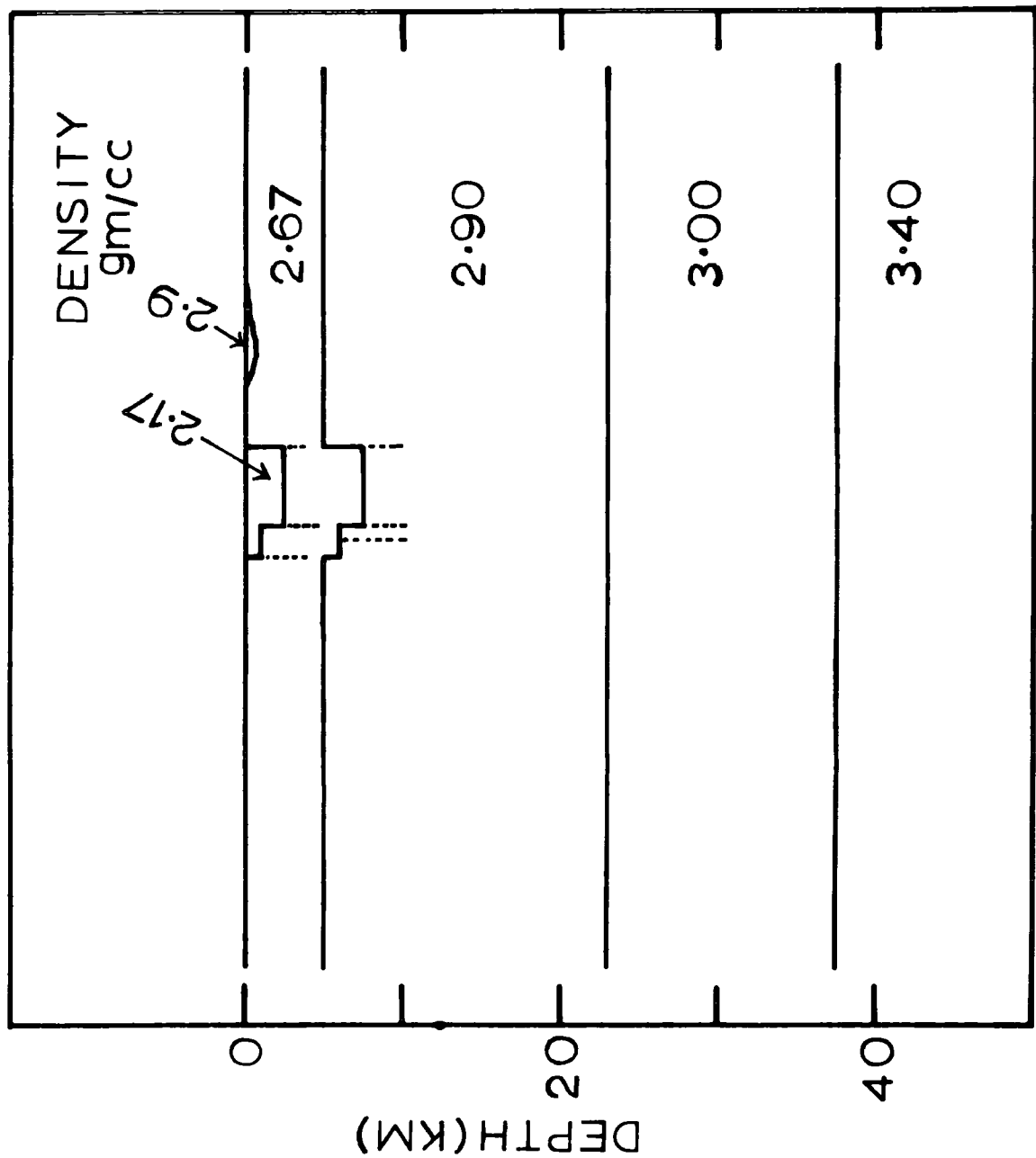


FIG. 6

uniform depths (36 - 39 km) and that the underlying mantle has normal density of 3.4 gm/cc (Fig.6).

(1.2.7) Magnetic Studies :

Hunter (1965) has reviewed previous Geomagnetic work in East Africa. The only work significant to rift valley studies has been two surveys carried out by Witham and Hoge (1961). One of these was a traverse from Toroto to Mombassa which crossed the Gregory rift valley between Eldoret and Nairobi (Hoge and Witham, 1962). Vertical and horizontal field components were measured at intervals of 3 and 6 km respectively. It was impossible to deduce anything concerning the structure of the rift, indeed the rift margins apparently caused no anomaly. The only major feature to appear on the profile was the contact between the crystalline basement and the Tertiary volcanic rocks of the rift zone, the magnetic field undergoing much more rapid variation over the volcanic than over the basement. The second survey, a traverse between Voi and Ngorongora, also failed to find any major anomaly associated with the rift valley.

A recent magnetic survey along the E-W profile, across Lake Magadi, by Wohlenberg (1971) indicate the possibility of presence of normal and reverse magnetization. Preliminary interpretation shows no lineation in magnetization which could be due to opening of the rift system.

(1.2.8) Heat Flow :

Twenty measurements of heat flow through the floor of deep Lake Malawi (central Africa) gave values ranging from 0.15 to 2.88 mcal/cm² sec. A systematic areal distribution of the values indicated regions of low heat flow at the northern and southern ends of the lake (average = 0.54 and 0.70 ucal/cm² sec respectively), separated by a central region of high heat flow (average = 2.3 ucal/cm² sec). The variability implies local heat sources within a few tens of km of the earth's surface and/or

disturbance from the local environment.

(1.2.9) Pole of Rotation :

Robert (1969) and McKenzie (1970) determine the relative motion between the plates on each side of the East African rift valley system by fitting the coast lines of the Red sea and the Gulf of Aden and determining the respective pole of rotation.

From Robert's work, pole of rotation of East African rift valley system is at 30° N 47° E and E-W extension across the Ethiopian rift is at a rate of 0.7 cm/year per limb. This rate would produce 140 km of widening of the Ethiopian rift during the last 10 myr, an amount approximately twice the width of this rift.

The pole of rotation suggested for East African rift valley system by McKenzie is at 8.5° S 31.0° E, with a rotation angle of 1.9° . The opening on the rift that has taken place varies from 65 km in northern Ethiopia to 30 km in Kenya.

There are number of geological evidence against the pole position and the amount of opening suggested in the above two works (Mohr, 1970; Baker, 1969). From geology the crustal separation in Kenya rift valley could be only about 10 km.

(.1.2.10) The State of Stress in the Upper part of the Earth's Crust:

These measurements are being performed in conjunction with the excavation of tunnels in the area of the underground power station at Kafue Gorge, 40 km from the confluence of the Kafue and Zambesi rivers (Hast, 1969).

The results of the measurement show not a tensile but a horizontal compressive stress field of large magnitude. It is interesting to note

that the direction of the fault lines of the depression areas of Lake Nyasa (or Malawi) and Lake Tanganyika is about the same as the direction of T.max in area around Kafue Gorge.

(1.3) Theories of Rift Formation

Bullard (1936) interpreted gravity anomaly over East African rift and Plateau in terms of compression. Wright (1970) suggested that the doming movements and related vulcanism could be originated because of lateral compression, induced by sea-floor spreading movements in the Atlantic and Indian ocean.

The Compression theory for the development of East African rift valley system is not accepted for several reasons: First, the results of earthquake focal mechanism studied have failed to show reverse fault movements in the rift zones (Fairhead, 1968; Sykes and Landisman, 1964; Wohlenberg, 1968). Second, detailed interpretation of Bouguer anomaly across the rift valley system (Heiskanen and Vening Meinesz, 1958) need normal fault type structure. Third, the lack of evidence of compressional force on a large scale led many geologists to doubt the theory there are local areas showing compressional features, but these can be accounted for as results of small strike-slip movements. Furthermore, there was the difficulty of explaining the great differences between the rift system and the mountain chains of the world if both were supposed to result from compressive forces. Finally, when the continuity of the East African rift system and the World rift system has been recognised (Rothe, 1954; Girdler, 1958; Ewing and Heezen, 1956) and the phenomenon of sea floor spreading had been accepted (Vine, 1966), it seemed certain that both the oceanic and the continental rifts should be the result of tensional forces.

It is generally thought that the process taking place under East African rift valley system must be very similar to that under Mid-ocean ridges (Illies, 1970; Wright, 1970; Oliver, Sykes and Iscks, 1969). That is, there is an upward convection current beneath the centre of the rift and the rift as a whole ^{is} one continuous system. The only difference is that the East African rift valley system is in an embryonic stage (Girdler et al, 1969; Harris, 1970; Wilson, 1969). One evidence based on pole of rotation of Ethiopian rift (McKenzie, 1970) shows crustal spreading is already taking place.

Structure of rift and Petro-chemistry of lava flows leads most geologists to doubts on the similarity in mechanism; and therefore structure, between the East African rift and Mid-ocean ridge. They are; (1) The volcanism associated with oceanic rifting is dominantly basaltic and tholeiitic. It occurs along an essentially linear system which produces the Mid-ocean ridges such as those of Carlsberg and the Mid-Atlantic, and is associated with the development of tectonic plate and with continental drift. Transverse faulting, tensional phenomena and the abundance of dykes also characterize this association (Irvine, 1966; Bullard, Cann and Matthews, 1969; McConnel, 1970; Murray, 1970).

In strong contrast, the volcanism associated with continental rift valleys is characteristically per-alkaline (that is, nepheline and aemite normative) with abundant alkaline basaltic rocks. Further, these per-alkaline igneous rocks group together in provinces in regions of crustal swelling (Holmes, 1965) or large domes which are often about 1,000 km in diameter (For example, East Africa, Lake Baikal) or sometimes smaller - about 500 km (For example, Rhine, Chilwa-Zambesi, Maimacha - Kotui). Transverse faults and dykes are rare, and despite the normal character of the rift faults none of the continental rift valleys show any sign of significant and continued opening (according to Harris, 1970; this

absence of any large horizontal movement of the East African rift walls away from each other is due to inward pressure towards Africa from the Mid-Atlantic and Mid-Indian ocean convective upwells). Further, over most of the lengths of the rift valleys, the volcanics are erupted in relatively small volume from single vents.

(2) The suggestion that the Ethiopia-Kenya-Tanzania-Malawi rift valleys form an essentially single fault structure is not accepted for several reasons. (a) Many of these are physically discontinuous, even the postulate of a structural feature joining the southern end of the Ethiopian rift valley with the northern end of the Kenya rift valley is not straight forward. Furthermore, Baker and Wohlenberg (1971) have shown that the Kenya rift valley is a physical unit with a dilation of about 10 km in the centre, decreasing to about 3 km or less at the northern and southern extremities. (b) The periods of rifting differ from province to province. The northern province rifted at different times in the Cainzoic; the more southerly ones chiefly in the Mesozoic. (c) Most of the rift valleys of eastern Africa have a West-South orientation as they are superimposed on the Mozambique belt which has a North-South "grain"; many of the other rift valleys also show orientations which reflect the "grain" of the basement. (d) Most of the rift valleys are seen in fact to be formed essentially from the centre of three or more branches which radiate from the centre of the province (For example, the tripartite rifts of Ethiopia, Kenya and the Rhine) or bifurcate from the main rift structures toward their ends (For example: in North Tanzania and Lake Baikal).

(3) It seems that the heat flow in the rift valleys (Von Herzen and Vacquier, 1967) is similar to that in the adjacent shield areas, except for local high values associated with current volcanic activity.

(4) With a single upwell it is difficult to see how the change from a double to a single rift zone, both north and south of East Africa, can be accommodated. Other difficulties arise if separate upwells are postulated beneath East African rift zone.

A Number of new theories ^{have} been put forward; the theory most popular among geologists (Gass, 1970; Bailey, 1964; Baker and Wohlenberg, 1971) is: Since coeval volcanism and rifting in East Africa are associated with major updoming, it is tentatively suggested that the African rift system may be the combined result of a number of litho-thermal systems, each with its own regional updoming and resultant axial fracturing which coalesces or overlaps at the dome margins. The mechanism for the formation of doming is the one of "Vertical tectonics" suggested by Magnitsky and Kalashrikova (1970); who show that a phase change from a dense to a less dense mineralogical assemblage can give vertical movement of the correct magnitude. Degassing of the mantle could also be associated with this phenomena.

(1.4) The Present Study

It is generally thought that the East African rift valley is an extension of Mid-ocean ridge into a continent and is in an embryonic state of ocean formation.

The study of the crust and upper mantle structure beneath this area should help us to understand the difference between the eastern - and western - rift valley and to verify the similarity between the Mid-ocean ridges and the rift valley system.

So far there is no geo-physical work undertaken to study the broad structure over this area, although there has been geo-physical work to study the local structures. With this view, analysis of surface - wave dispersion over this area is undertaken . This became possible, because since 1964 there has been a number of permanent World Wide Standard

Seismic stations and few local stations in operation in African continent.

This thesis presents results based on the dispersion of fundamental mode Rayleigh- and Love- waves. Both phase and Group velocity measurements will be presented. It can be shown that Rayleigh wave dispersion is in some ways more sensitive than Love wave dispersion to Upper-mantle structure, especially anomalous region.

To determine the phase velocity Fourier analysis method and to determine the group velocity, both multiple filter techniques, and Peak and Trough methods are used.

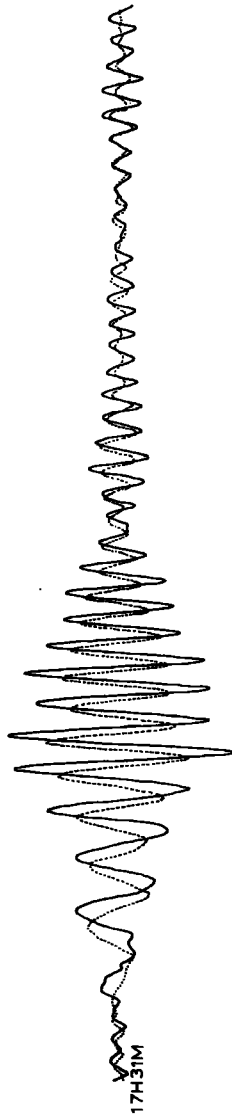
Problem of Non-Uniqueness has been investigated in greater detail and found that, in addition to the error of observation, it is due to the interaction of one layer's parameters with the ^{another's.} Non-Uniqueness can be overcome to a certain degree, when we are looking for mean structure over a depth, by correctly choosing the thickness of the layers and the active parameters.

Extensive use has been made of Non-Linear optimization techniques for inverting the surface wave dispersion. The crust and Upper mantle shear velocity models will be presented.

P- and S- wave delay times at Addis Ababa, Nairobi, Lwiro and Bulawayo are computed.

EVENT 19MARCH1966

STATION: BUL



NAI



AAE



COMPONENT
— VERTICAL
..... N-S

1 MIN

FIG. 7

CHAPTER 2

S U R F A C E W A V E S

(2.1) Review

Seismographic records of moderately distant earthquakes reveal many groups of waves. However, these individual groups normally fall into three more general time intervals which strike the eye at once in looking at a record. The first interval is occupied by waves of predominantly longitudinal character, the second mostly by transverse waves and the third by surface waves of large amplitude. This last set of waves usually runs for several minutes and the rate of decrease of period in the early part of the train is fairly large. Later in the records, the character of the surface wave changes to a series of wave trains (Coda Wave) separated from each other by waves of smaller amplitude and shorter period.

There are two types of surface waves. First, Rayleigh waves, whose particle motion is confined to the vertical plane containing the direction of propagation and describes a retrograde ellipse; In general the major axis of the ellipse is in the vertical direction. This type of wave is recorded by vertical and horizontal seismographs (Fig.7). Second, Love waves, whose particle motion is entirely in the direction perpendicular to the direction of propagation and therefore recorded by a horizontal seismograph aligned in a direction perpendicular to the direction of propagation. In fact Love waves are equivalent to SH waves reflected up and down within the upper layers with associated movement in the lower layer of the type that always arises in total reflexion.

The problem of the generation of Rayleigh waves from a source at a finite depth was studied by Lamb (1904). It is necessary that they should be generated in order to provide zero stress over the free surface; this condition cannot be fulfilled in any other way when the incident

wave front is curved. Rayleigh waves may be considered to be generated by the interaction of P or S waves with the free surface at some distance, X , from the epicentre. The distance, X , is governed by the depths of the source, H , according to the equation

$$X = Cr H / \sqrt{\gamma^2 - c_r^2}$$

where Cr is the Rayleigh wave velocity and γ is either the P- wave or the S- wave velocity. However, the travel times of the Rayleigh waves are the same whether they are considered to be generated at the epicentre or at X . The amplitudes of the generated waves depend on the depth of the source and on the wavelengths of the wave components. The expression for the amplitudes contains a factor of the form $\exp(-sH/\lambda)$, where λ is the wavelength and s is a constant which depends on the nature of the source, that is, whether it is shear or compressional (Jeffreys, 1962). (This is analogous to the way in which the components of the Rayleigh wave penetrate according to their wavelengths). Thus the generated waves contain proportionally less high-frequency energy as the focal depth increases (Jeffreys, 1962).

The depth of propagation of surface waves in a homogeneous medium remains effectively the same however far the wave travels and the energy is spread over an area proportional to r , therefore amplitude is proportional to $1/\sqrt{r}$ (whereas body wave amplitude is proportional to $1/r$).

Gutenberg was the first to attempt to infer crustal structure from observed surface wave dispersion in 1924 (Gutenberg, 1959). The early observations were very scattered and because of the complex theory the structural models calculated were very simple and unrealistic. The application of surface waves to studies of crustal and upper mantle structure has developed rapidly since the pioneering work of Ewing, Press

and their co-workers (Ewing, Jardetzky and Press, 1957). The full potential of surface wave studies, however, began to be realized only after the advent of the electronic digital computer. Theoretical dispersion curves for realistic models of the earth could now be calculated. The Thompson - Haskell matrix iteration theory (Haskell, 1953) and the numerical methods developed by Alterman, Jarosch and Pekeris (1961) have become the methods most widely accepted for computing surface wave dispersion. Computers have also made digital analysis of seismograms much more convenient. The development of instrumentation with improved long-period response was also an important factor, which contributed to the advance in knowledge from surface wave studies.

Two important results of the early interpretation of earth structure deduced from surface wave dispersion were the confirmation of the low velocity channel in the upper mantle, as has been suggested by Gutenberg (1926, 1954 and 1955) and Lehmann (1955) from body wave studies, and of the sharp velocity increase at a depth of about 400 km corresponding to the Jeffreys 20° discontinuity. The first inference from surface wave studies of the low velocity channel came from a comparison of the 4.4 km/sec G-wave velocity (the G wave is a long period non-dispersive portion of the fundamental oceanic Love mode, and is pulse like in character) with the 4.7 km/sec sub-Moho velocity obtained from refraction studies. Press and Ewing (1956), Landisman and Sato (1958), and Press (1959) suggested that this indicated a low-velocity channel in the upper mantle. A comparison of Rayleigh wave dispersion calculated for realistic earth models with the data of Ewing and Press (1954 a, b) was made by Takeuchi, Press and Kobayashi (1959). They suggested that both the upper mantle low velocity channel and the sharp increase in velocity at about 400 km were indicated. Dorman, Ewing and Oliver (1960) came to similar conclusions from comparisons of Rayleigh wave data with dispersion calculated from realistic models. Landisman, Satô and Ewing

(1959) and Dorman, Ewing and Oliver (1960) suggested also that the low velocity channel occurred at shallow depths beneath the oceans than under the continents. The early interpretations were based on flat earth models. Numerous later investigations with improved observational data, and using spherical earth or spherically corrected (Alterman, Jarosch and Pekeris, 1961; Bolt and Dorman, 1961; Kovach and Anderson, 1962; Anderson and Toksoz, 1963) flat earth models made the early interpretations more secure; these have been comprehensively summarized by Nuttli (1963), Bolt (1964), Kovach (1965) and Anderson (1965 and 1967).

Some of the principal advances of the later investigations were, the introduction of perturbation parameters (Jeffreys, 1961; Dorman and Ewing, 1962) which greatly facilitated the computations of earth models, the increased quantity and quality of data permitted more detailed interpretations, the extension of the data to longer periods and the use of free oscillations making possible interpretations to very great depths in the mantle. An earth model with two upper mantle discontinuities at depths of about 360 and 700 km, was derived from Love wave and Torsional oscillation data by Anderson and Toksoz (1963) and has since been confirmed by body wave studies (Niazi and Anderson, 1965; Johnson, 1967; Green and Hales, 1968; Julian and Anderson, 1968 and others). Differences in velocity distribution among shield, tectonic and oceanic areas were confirmed by Brune and Dorman (1963); Toksoz and Anderson (1966), Toksoz, Chinnery and Anderson (1967) and others.

The quality of dispersion curves determined from surface wave recordings has increased largely because of new and improved techniques for the digital analysis of seismograms. The peak and trough method which was used in the early studies of surface wave dispersion does not exploit much of the information contained in the surface wave train. It is obviously desirable that a large proportion of the available information

should be used. Satô (1955) pioneered the use of Fourier analysis in a series of studies, Satô (1955; 1956 a, b; 1958) and showed how particularly useful the method was in studying the non-dispersive G wave.

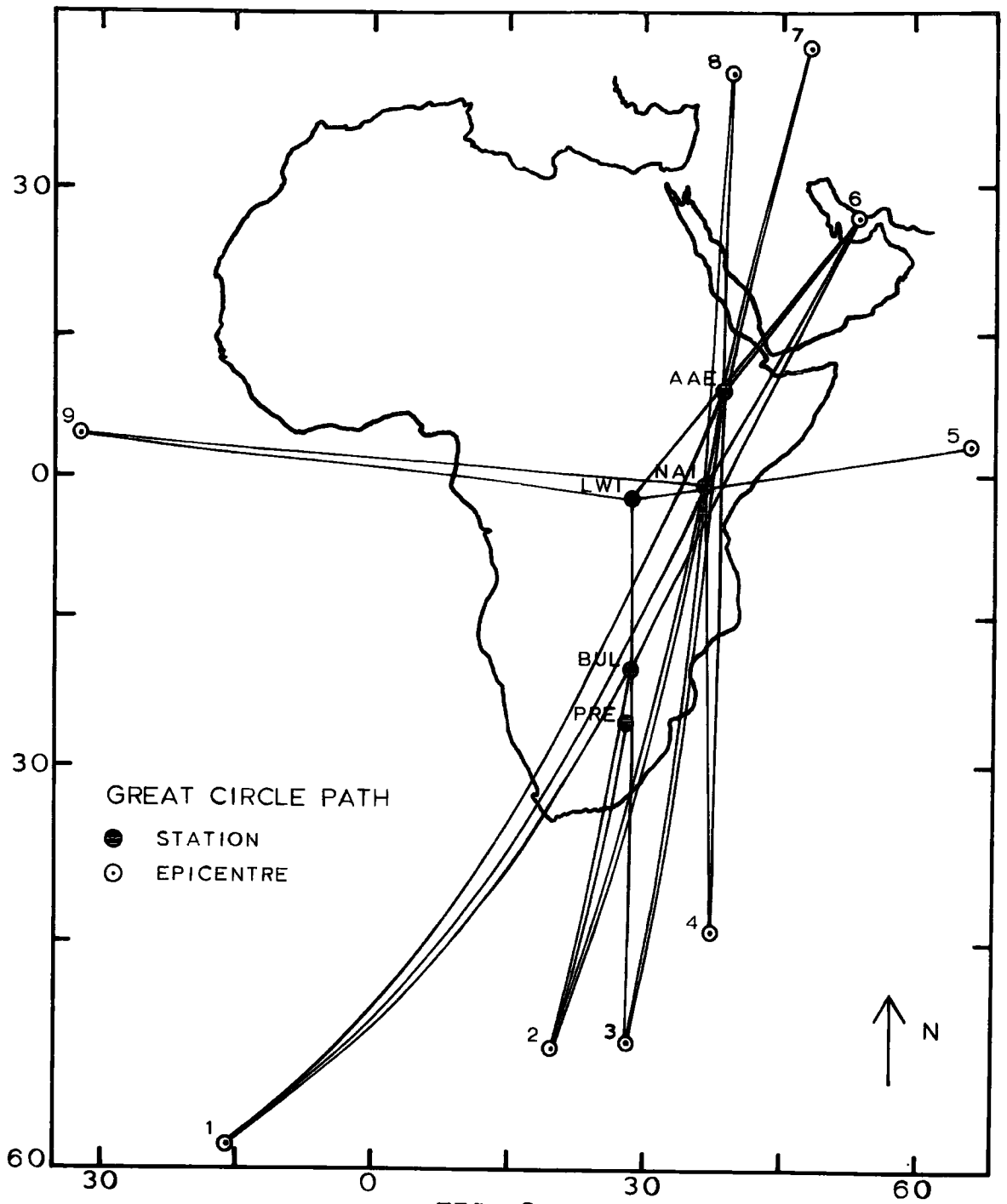
The early higher mode studies (Oliver and Ewing, 1957 and 1958; Brune and Dorman, 1963; Bath and Crampin, 1964; Crampin, 1964a, 1964b, 1966; Kovach and Anderson, 1964) used the peak and trough method on seismograms where it was possible to separate the modes visually. The main difficulty in studying higher modes is in delineating the various modes. Oliver's summary of observed dispersions indicates the difficulty in separating the different modes of propagation (Oliver, 1962). The various modes have different periods which travel at the same velocity and furthermore the same mode has different periods which also arrive at the recording station at the same time. Alexander (1963) introduced a number of digital methods of processing surface wave records in which it was possible to use more of the wave train in the analysis than the peak and trough method allowed. He was one of the first to use digital filters for mode delineation. Landisman, Dziewonski and Satô (1969) introduced a new technique called "Moving Window Analysis", for the determination of group velocity, which appears to be superior to either the peak and trough or Alexander's method. An improvement in data processing was made possible by the introduction of the time - variant digital filters (Pilant and Knopoff, 1964). The combinations of Fourier Analysis and time variant filtering of seismograms was used for the determination of phase velocity dispersion in limited geological regions ^{by} Knopoff, Mueller and Pilant (1966) and Berry and Knopoff (1967). Similar methods have been applied in the study of large scale structures by Toksoz and Anderson (1966).

It is worth noting some of the important advantages associated with surface wave methods as compared to body wave techniques. A single recording of surface waves, in principle, contains sufficient information

for a detailed structural interpretation. Group velocities from earthquake source to recording station, or phase velocities for waves circumscribing the earth (Brune, Benioff and Ewing, 1961; Toksoz and Anderson, 1966 and Others) can be studied. Body wave refraction or reflection studies, in general, require a large number of recording stations. Furthermore, aseismic regions can be studied by phase velocity methods while inaccessible regions can be studied with recording stations on their outskirts. Surface wave dispersion studies also have advantages over body wave studies for certain types of structures. For example, the existence of low velocity channels, velocity gradients or abrupt increases in velocities are in some cases difficult to establish by refraction and reflection. As surface waves sample the entire vertical profile, these types of structures do not ordinarily introduce complications into the analysis. They, in fact, introduce features into the phase and group velocity curves which are easily recognizable.

Crustal and Upper mantle shear velocity distributions have, in general, been very poorly determined by body wave travel time studies. Since the dispersion of surface waves is to a large degree controlled by shear velocity, one of their most important uses is in determining the shear velocity distribution. Surface wave dispersion is dependant on the density, and the compressional and shear velocities and therefore, one can directly infer density if the shear and compressional velocities are known. Density distributions for the earth have been determined in this manner by Anderson (1964), and Landisman, Satô and Nafe (1965).

The most difficult part in the interpretation of surface wave dispersion is the estimation of errors. The propagation of errors in complicated digital processing and filtering operations, inability to estimate the effects of lateral refraction, and lateral changes in the structure, and errors caused by instrumental phase shifts all contribute to the overall measurement error in varying and often unknown amounts.



| Stations | Interstation | |
|-----------|---------------|----------------|
| | distance - km | Azimuth degree |
| NAI - AAE | 1158.61 | 10.75 |
| BUL - NAI | 2267.31 | 202.62 |
| LWI - BUL | 1978.69 | 180.57 |
| AAE - LWI | 1664.09 | 222.04 |
| NAI - LWI | 895.93 | 263.05 |
| PRE - BUL | 621.97 | 3.47 |

Table 4

Further, because of the limitations of the data, readings for few modes within certain period range, there is always a certain lack of uniqueness, but it seems possible, nevertheless, to specify a mean structure and establish practical boundaries to this structure.

(2.2) Station Locations

The stations used in this study are shown on the outline map in Fig.8. Four of the five stations used in this study are World Wide standard seismic Network observatories. The fifth station, Iwiro, is run by Lamont - Doherty geological observatory (U.S.A.). At each station, there are six seismographs in operations. Three of them are long period instruments and the rest short period instruments. Of the three - long and three - short period instruments, one is a vertical seismograph and the other two are horizontal seismographs, aligned in E - W, N - S directions (Table 4).

(2.3) Instrumentation

The instrumentation of the World Wide Standard Seismic Network Observatories is well known (Handbook : World Wide Standard Seismic Network) and requires little description. From the time of installation of these stations in 1963 until the middle of 1965, the natural periods of the seismometers were adjusted to be 30 sec and the galvanometer period were 100 sec. In 1965 the seismometer periods of the entire network were reduced to 15 sec, the galvanometer periods were unchanged. The recording was photographic at a rate of 30 mm/min, with instrumental calibration pulses at the beginning and end of each twenty four hour record. The recorded clock time was checked daily with transmitted time (G.M.T.), and in general was accurate to a few milliseconds.

Iwiro station - the natural period of the seismometer is 15 sec and that of galvanometer is 75 sec. There is no calibration pulse

Earthquakes Used in Interstation Study

| Location | Date | Origin Time | | | Coordinates (Degrees) | Station Pairs | Data |
|--------------------------|-------------|-------------|----|------|--------------------------|-------------------------------------|----------------------------------|
| | | H | M | S | | | |
| South Africa | 5 Jan 1964 | 23 | 46 | 10.7 | 52.26S 28.3E | NAI - AAE- BUL - LWI- | Rayleigh Love |
| South Persia | 19 Jan 1964 | 09 | 13 | 53.5 | 26.79N 54.0E | NAI - BUL AAE - LWI | Rayleigh Rayleigh |
| Sunda Strait | 10 Feb 1964 | 17 | 27 | 58.2 | 6.15S 104.1E | NAI - LWI | Rayleigh |
| Prince Edward Islands | 25 Feb 1964 | 00 | 34 | 32.0 | 44.60S 37.34E | NAI - AAE | Rayleigh |
| S.W. Atlantic | 29 Apr 1964 | 17 | 37 | 43.1 | 58.6S 16.2W | BUL - NAI | Rayleigh |
| Central MA. Ridge | 28 Jun 1964 | 17 | 27 | 59.8 | 4.26N 32.56W | LWI - NAI | Rayleigh |
| Carlsberge Ridge | 18 Oct 1964 | 09 | 06 | 26.0 | 3.11N 65.87E | NAI - LWI | Rayleigh |
| Southern Persia | 22 Dec 1964 | 04 | 36 | 34.7 | 28.20N 56.91E | AAE - LWI | Rayleigh |
| South Africa | 19 Mar 1966 | 14 | 51 | 49.4 | 52.70S 19.8E | PRE - BUL BUL - NAI NAI - AAE | Rayleigh Rayleigh Rayleigh |
| | 19 Mar 1966 | 17 | 16 | 40.9 | 52.7 S 19.9E | BUL - NAI NAI - AAE | Rayleigh Rayleigh |
| Southern Iran | 20 Apr 1966 | 16 | 42 | 3.7 | 41.7N 48.2E | AAE - NAI | Rayleigh |
| Turkey | 26 Jul 1967 | 18 | 53 | 1.3 | 39.5N 40.4E | AAE - NAI | Love Love |

Table 5.

or clock error indication in the record. The recording was on a paper at a rate of about 20 mm/min.

(2.4) Data Selection

Knopoff, Mueller and Pilant (1966) showed that provided the angle between the earthquake and inter-station paths was small, the disturbance in azimuth, arising, for example from refraction at continental margins, would introduce only second order errors in phase velocity. If the angle between the earthquake and inter-station paths was large, errors in phase velocity could also arise because of possible variations of the initial phase at the source with azimuths. In addition, the different source to station paths are likely to have different phase velocities.

In the Brune and Dorman (1963) study of the Canadian shield, angles between the earthquake paths and the Great circle between the stations of up to 7° were used initially; but the final analysis was restricted to those earthquakes for which this angle was less than 4° .

In the present study, shallow focus earthquake records of the years 1964 - 1968 have been used. These records come from Long period instruments in operation at Addis Ababa, Nairobi, Bulawayo, Pretoria and Lwiro (Table 5). Earthquakes which have magnitudes greater than 5.5 and epicentres on or near to the interstation path between any two stations are chosen for initial analysis. A computer program is used to plot Great circle path from an epicentre to the recording stations. Since most of the events used in this study are from Mid-ocean ridges, they travelled partly through oceanic areas. Therefore in addition to the azimuths of the earthquake to the pair of stations which do not differ by more than few degrees (and to the Great circle path joining the stations), the length of the path travelled through oceans should be same along either path (Fig.8). The Jeffreys - Bullen travel time table has been used to

Earthquakes used in Single Station Group Velocity

| Location | Date | Origin Time | | | Coordinates Degrees | Station | Data |
|-------------------|-------------|-------------|----|------|------------------------|------------|----------------------|
| | | H | M | S | | | |
| Tanzania Coast | 26 Feb 1964 | 02 | 32 | 23.7 | 7.60S 39.60E | BUL | Rayleigh |
| Uganda | 17 May 1966 | 07 | 03 | 33.3 | 0.76N 29.95E | NAI AAE | Rayleigh Rayleigh |
| Sudan | 09 Oct 1966 | 10 | 28 | 27.8 | 12.60N 31.40E | AAE | Rayleigh |
| Red Sea | 15 May 1968 | 07 | 51 | 17.4 | 15.89S 25.94E | AAE | Rayleigh |
| Zambia | 13 Mar 1967 | 19 | 22 | 15.4 | 19.7 S 38.85E | AAE | Love Rayleigh |
| Gulf of Aden | 6 July 1967 | 18 | 58 | 39.7 | 13.4 N 50.8 E | NAI | Rayleigh |

Table 6

Initial Model for Partial Derivatives

| H km | α km/sec | β km/sec | ρ gm/cc |
|----------|-----------------|----------------|--------------|
| 7.0 | 5.90 | 3.35 | 2.67 |
| 10.5 | 6.15 | 3.55 | 2.77 |
| 18.7 | 6.60 | 3.72 | 2.98 |
| 30.0 | 7.4 | 4.3 | 3.24 |
| 50.0 | 7.4 | 4.3 | 3.24 |
| 100.0 | 7.4 | 4.3 | 3.30 |
| 100.0 | 8.30 | 4.65 | 3.53 |
| ∞ | 8.70 | 4.85 | 3.70 |

Table 7

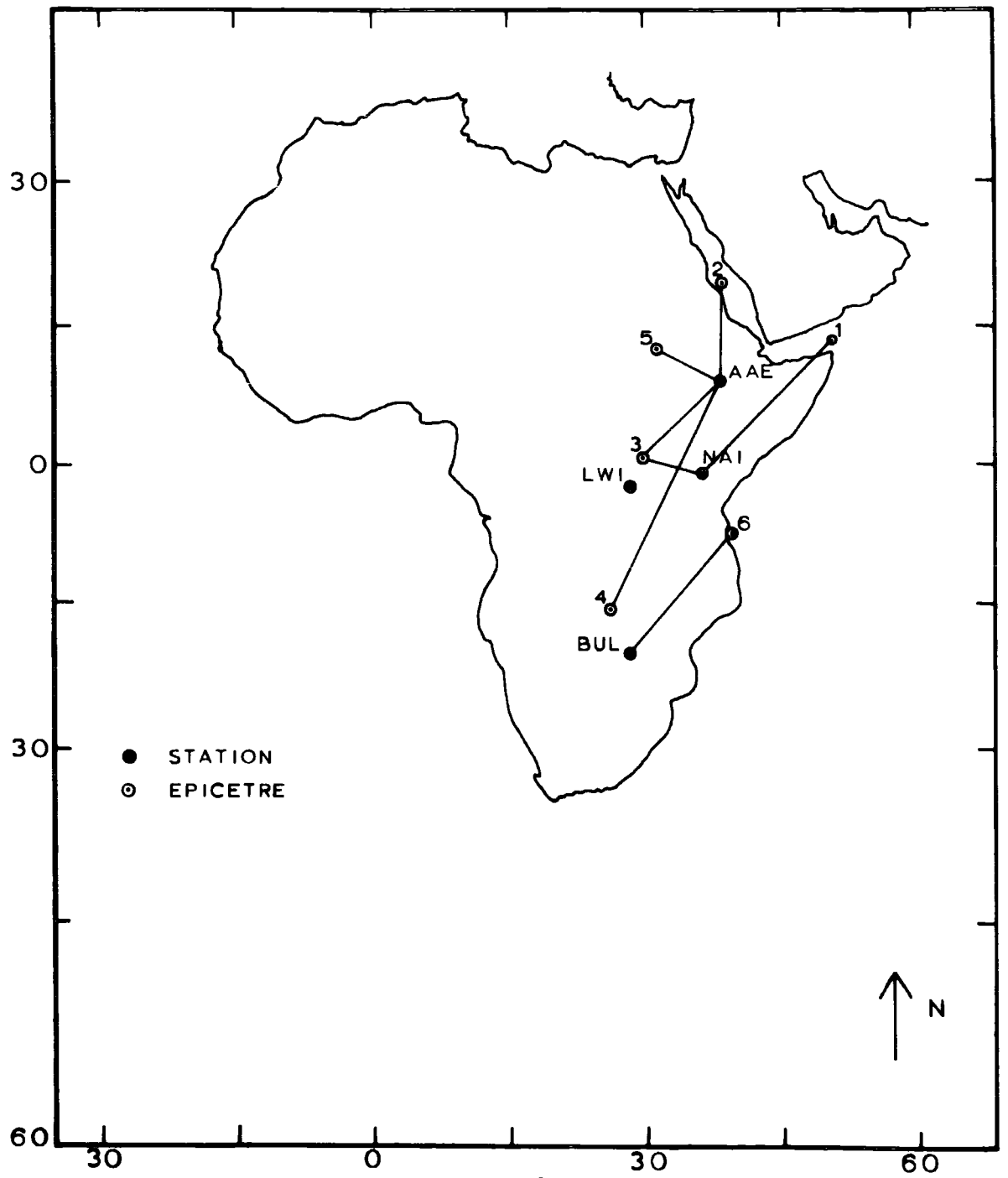


FIG. 9

calculate the expected arrival time of Rayleigh - and Love - waves. Then the quality of records was carefully studied and only those records which show well dispersed surface wave free from noise were selected. When studying interstation structure the general characteristic of the wave train should be almost the same in either record.

To make sure that the first long- period waves recorded are Rayleigh waves and are not mixed with long period SV - wave reflections, the phase difference between the vertical and longitudinal components are measured and found to be of the order of 90° and described a retrograde ellipse. Although for some angles of incidence, SV - waves produce retrograde elliptical orbits for simple particles, the criteria of travel time, orderly dispersion, duration and amplitudes leave no doubt that the waves measured are Rayleigh waves. Love waves arrive several minutes before the on-set of Rayleigh waves and their particle motion^{is} usually horizontal and transverse. The contamination of the Love wave by Rayleigh wave is a major problem in calculating Love wave dispersion curve.

Events in African continent (Table 6) recorded at stations within a few hundred to a few thousand km from the epicentre were selected to study regional group velocities for fundamental and higher modes; by single station method (Fig.9).

Knopoff and Schwab (1966) showed that the initial phase of a point source depends on the angle of inclination of the source to the vertical and that the effect is frequency dependent. They pointed out that corrections for this effect were important for source - to - station phase velocity determination. The effect on the group velocity is less significant.

CHAPTER 3

ANALYSIS OF SEISMOGRAMS

(3.1) Techniques for the determination of Group Velocities

Most of the early surface wave studies were concerned with measurement of Group velocity. There are number of methods of determining Group Velocity from a seismogram. They are:-

(3.1.1.) Peak and Trough method (Ewing and Press, 1952).

The arrival times of peaks and troughs of surface waves are read from the seismogram and the arrival time is plotted against the number of waves counted from an arbitrary chosen wave. A smooth curve is drawn through the points and the period of the arrival is given by the slope of this curve at that arrival time.

The group velocity (U) at any particular period (T) is ^{given by} the epicentral distance divided by the travel time for that period (T).

The peak and trough method often fails in group velocity studies at non-dispersive portions of the seismograms, when the signal - to - noise ratio decays or when the signal is contaminated by other arrivals. Difficulties are also encountered with seismograms containing both normally and inversely dispersed surface wave trains.

(3.1.2) Fourier Method:

The Group delay curve can be computed from the phase-delay curve resulting from a fourier analysis of the digitized surface wave train using the equation

$$Td = \frac{d\phi}{df}$$

where Td is the group - delay time with respect to the time of the first

digital sample, ϕ is the spectral phase in circles and f the frequency. This method of determining group velocities has some of the same difficulties encountered with the peak and trough method. Contamination of the signal by noise and non - least - time path arrivals often cause the phase delay curve derived from the records to be irregular (Pilant and Knopoff, 1964), jumps of up to half a cycle being common. Different modes of propagation are difficult to delineate and modes of vibration other than the one of interest can be considered as contributing to the noise.

Digital methods have been used previously in group velocity studies, such as the investigation by Alexander (1963), who used frequency and velocity windows to isolate portions of the observed modes. Crampin and Bath (1965) employed digital band-pass technique using the Fejer Kernel of Bartlett (1948) as described by Jansson (1964).

(3.1.3) Moving Window Analysis :

Landisman, Dziewonski and Sato (1969) describe a digital computer contouring technique which they have called "Moving Window Analysis". This technique produces a display of amplitudes and/or phases as functions of period and group velocity, and is in essence equivalent to the electrical analog method used by Ewing, Mueller, Landisman and Sató (1959). Similar digital computer techniques for producing frequency - velocity - energy diagrams, were used by Pfeffer and Zarichny (1963) and Iyer (1964). The moving window method allows the separation of different modes and can resolve transients of several different frequencies arriving simultaneously at the recording station.

This moving window process involves the multiplication of the digitized data time series by half a wave of a moving \cos^2 window centered at times corresponding to a series of steps in group velocity. At each step in group velocity the windowed data is Fourier analysed

and displayed as a matrix giving the amplitude as a function of group velocity and Period.

Due to the time-band width involved in Fourier analysis, the longer the COS^2 window is, the narrower the contours will be along the period axis (Frequency resolution). However, the longer the window the broader the contours will be along the velocity axis (time resolution). The optimum number of window lengths was found to be between 4 and 5 times the period of interest. A window length of 4.5 times each period of interest was generally used. Using a window length which varies but has a fixed relation to the period analysed results in a constant realistic frequency resolution at all periods. A Gaussian function window, which should theoretically have no side lobes after Fourier transformation from one domain to the other gives results almost exactly the same as the COS^2 window does.

A decided disadvantage of the moving window analysis method, which must be carefully taken into consideration when applying this technique, is the distortion introduced due to the truncation and modulation of the time series by the windowing function. Windowing the time series is equivalent to convolution of their frequency spectra, and result in a change of the original time series spectrum. The amount of error introduced depends on the type and time length of the windowing function (Bloch, 1969).

(3.1.4) Multiple Filter Techniques :

A new method for the determination of group velocity has been developed by Dziewonski, Bloch and Landisman (1969)^{and}, is called the "Multiple Filter Technique". This technique does not have the intrinsic period shift noted for the moving window analysis method, and the results are obtained with a much smaller expenditure of computer time.

Results produced by the multiple filter technique often show greater resolution, when compared with those calculated by the moving window process. The output of this method is similar to that of the "Moving Window Analysis" method, and is a plot of either linear or decibel amplitude as a function of group velocity and period. As in the moving window analysis method the multiple filter technique can resolve complex transient signals composed of several dominant periods that arrive at the recording station almost simultaneously.

The "multiple filter technique" requires the filtrations of the seismogram by a set of narrow-band filters and the determination of the amplitude envelopes of the resulting set of time series. Instantaneous spectral amplitudes, presented in either a linear or db scale may be interpreted in terms of multi-mode group velocity.

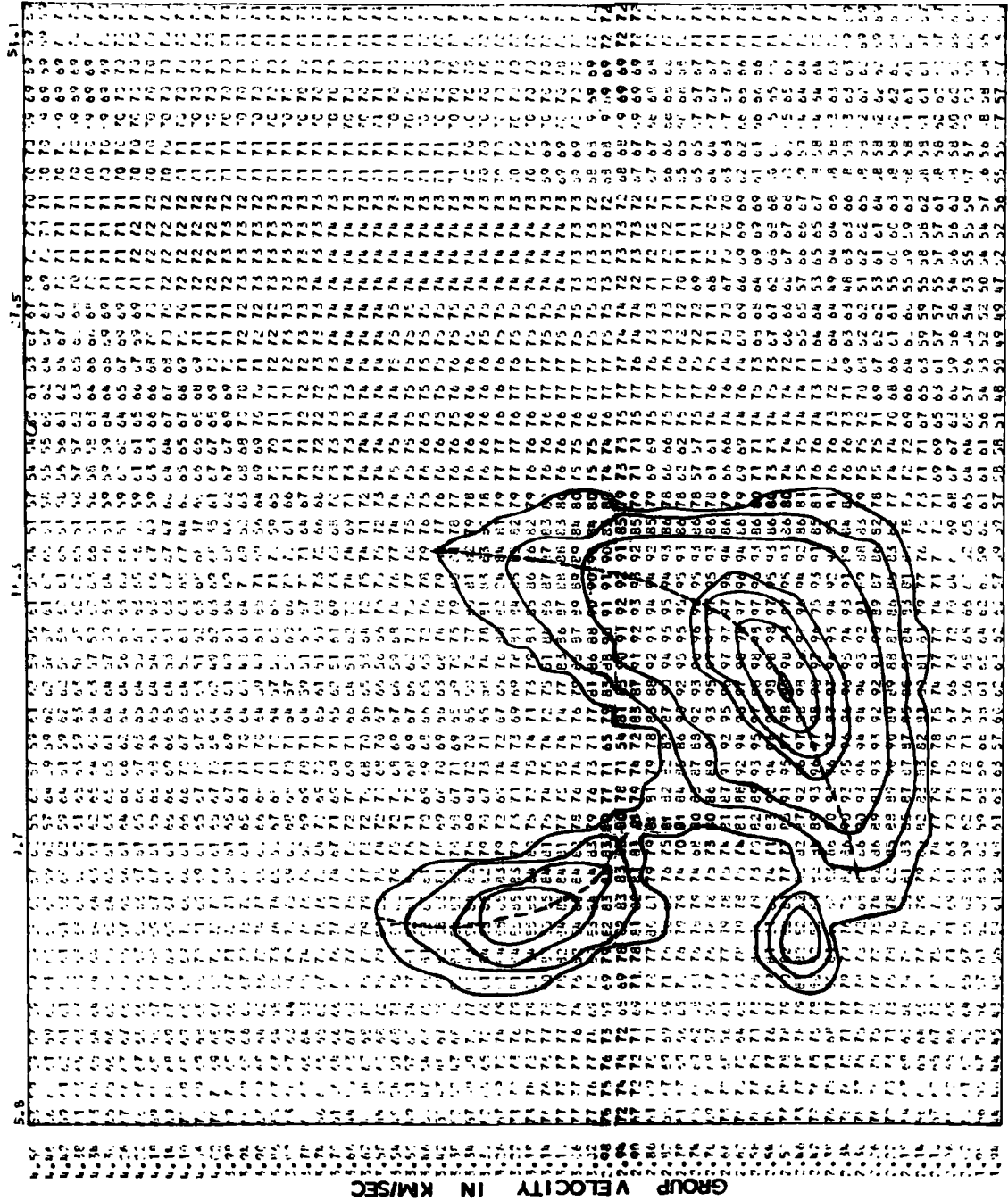
A full description of the multiple filter process is as follows:-

- 1) A seismogram digitized at a constant rate is entered into the computer and its mean and linear trend are removed. The digitization rate must be sufficient to prevent aliasing by the highest frequencies present in the seismogram.

- 2) The observed time series is expanded to a suitable power of 2, a requirement for Fast Fourier transform, by adding an appropriate number of zeros. The length of the expanded series is primarily determined by the requisite frequency resolution. The time function is then converted into a sine and a cosine series using the Cooley-Tukey algorithm for Fast Fourier transformation (1965).

- 3) Instrumental distortion of phase and amplitude may be removed in the complex domain at this stage, by correcting for the real and imaginary parts of the instrumental delays.

PERIOD IN SECONDS



EVENT: 26 FEB 64

STATION: NAI

RAYLEIGH WAVE

FIG. 10

4) The array of centre frequencies, which are related by a constant ratio, is evaluated for the filters which will be used in a later stage of processing. The periods which are used to label columns in the matrix output (Fig.10) correspond to the array of frequencies. The length of the time series and the sampling rate determine the frequency of the harmonic components obtained from the Fourier series. It is usually impossible to find the exact counterparts of the elements of the array among those harmonics. The peak of the Gaussian function may not, therefore, coincide with any of the Fourier coefficients. In general the maximum deviation of the harmonics from peak frequencies was always less than 1.5%.

5) An array of times is found for the presented values of group velocity (Row in Fig.10).

6) Filtration is accomplished by windowing the seismic spectrum with a filter function which is symmetric about the current centre frequency.

7) The quadrature spectrum is formed for calculation of the instantaneous spectral amplitude and phase.

8) The inverse Fourier transforms of the in-phase and quadrature spectra are computed with the same algorithm for Fast Fourier transformation, which was used in Step 2.

9) Instantaneous spectral amplitudes and phases are computed for each of the group arrival times.

The procedure described in points 6 through 9 must be repeated for each centre frequency.

(3.2) Techniques for the determination of Phase Velocities :(3.2.1) Peak and Trough Correlation Method :

Press (1956) was the first person to use phase velocities to determine the thickness of the crust. He determined the phase velocity together with the direction of propagation, from the difference in arrival times of individual crests and troughs recorded at three seismographs arranged in a triangular array.

It is important that the linear dimensions of the array be of the order of a wave length. If the separation is much smaller the arrival time difference cannot be determined with sufficient precision. A consequence of dispersion is the gradual increase of the period (hence phase velocity) associated with crest and trough. Therefore, if the separation of the elements of an array much exceeds a wave length the phase velocity cannot be considered uniform within the array. Another difficulty of large separation is the problem of identification of given crests and troughs at each of the stations.

A modified version of the above method is proposed by Brune (1960; 1961):

The arrival times of peaks and troughs of a dispersed wave train are recorded at a given station. Periods are assigned to each peak and trough by measuring the slope of a peak and trough number versus arrival time plot. A similar procedure is carried out at another station very nearly along the same direction of propagation from the source. Each peak and trough at one station is correlated with a peak or trough of nearly the same period at the other station, and phase velocity calculated from the formula,

$$c = \frac{X}{t - nT} ; \quad n = \frac{\phi_b - \phi_a}{2\pi} + N$$

where c is the phase velocity, X the distance $X_b - X_a$, t the difference

in time, $t_b - t_a$, T the average period and N is an integer which must be determined. $\phi_b - \phi_a$ is the phase difference between the times on the two wave trains used in the correlation. For smooth, well dispersed wave trains this method is experimentally equivalent to phase correlation of Fourier Analysis.

(3.2.2) Fourier Analysis Method :

Phase velocities can be determined by the Fourier analysis method, where the difference between the phase spectra of records at two different epicentral distances is used to determine the time delay of the phase. This method was introduced by Valle (1949) and Satô (1955) and applied by Satô (1955, 1956 a, b, 1958).

Fourier phase technique has the advantage of being applicable to the less well dispersed, or more impulsive, wave trains, where the time domain approximation is not satisfied.

Let us consider a cylindrically spreading wave, originated from an earthquake focus. As the signal spreads out on its way to the recording stations, its spectrum is modified by a number of factors, such as attenuation, geometrical spreading and dispersion.

Since, in the 2 - D propagation, the wave front increases proportionally to the epicentral distance, $f(t,r)$ must involve a factor $1/r$, where r is the epicentral distance. Consequently, if some wave train, whose amplitude at $r = r_1$ is A , is propagated and arrives at a point $r = r_2$, its amplitude becomes $A \sqrt{r_1/r_2}$.

Let us assume at first the movement at point $r = r_0$ which is situated near the origin can be expressed by :

$$f(t, r_0) = 1/\sqrt{2\pi} \int_{-\infty}^{\infty} f^{\text{re}}(p, r_0) \exp(ipt) dp \quad (1)$$

in which complex amplitude spectrum

$$f^{\mathbb{H}}(p, r_0) = 1/\sqrt{2\pi} \int_{-\infty}^{\infty} f(\tau, r_0) \exp(-i p \tau) d\tau \quad (2)$$

If a wave $A \exp(ip\tau)$ is propagated by the velocity $C(p)$, it takes the form $A \exp(ip(t - r/C(p)))$ at a distance r . Then the movement at a distance r , in time, becomes (Earthquake record at distance r)

$$\begin{aligned} f(t, r) &= 1/\sqrt{2\pi} \int_{-\infty}^{\infty} \sqrt{r_0/r} f^{\mathbb{H}}(p, r_0) \exp(ip(t - \frac{r-r_0}{C(p)})) dp \\ &= 1/\sqrt{2\pi} \int_{-\infty}^{\infty} \left[\sqrt{r_0/r} f^{\mathbb{H}}(p, r_0) \exp\left\{-ip \frac{r-r_0}{C(p)}\right\} \right] \exp(ip t) dp \quad (3) \end{aligned}$$

Now the Fourier transform (Complex Amplitude Spectrum)

of this function is :

$$f^{\mathbb{H}}(p, r) = 1/\sqrt{2\pi} \int_{-\infty}^{\infty} f(\tau, r) \exp(-i p \tau) d\tau \quad (4)$$

Substitute for $f(\tau, r)$ from equation (3)

$$\begin{aligned} f^{\mathbb{H}}(p, r) &= 1/\sqrt{2\pi} \int_{-\infty}^{\infty} \exp(-i p \tau) d\tau \cdot 1/\sqrt{2\pi} \int_{-\infty}^{\infty} \sqrt{r_0/r} f^{\mathbb{H}}(p^1, r_0) \\ &\quad \exp\left\{-i p^1 \frac{(r-r_0)}{C(p^1)}\right\} \exp(ip^1 t) dp^1 \\ &= \sqrt{r_0/r} f^{\mathbb{H}}(p, r_0) \exp\left\{-ip \frac{r-r_0}{C(p)}\right\} \quad (5) \end{aligned}$$

Since $f(t, r)$ is the wave-form observed at $r = r$ the function $f^{\mathbb{H}}(p, r)$ can be calculated from the seismogram of that station, namely (from equ. 4)

$$\begin{aligned} f^{\mathbb{H}}(p, r) &= 1/\sqrt{2\pi} \int_{-\infty}^{\infty} f(\tau, r) \cos(p\tau) d\tau - \frac{i}{\sqrt{2\pi}} \int_{-\infty}^{\infty} f(\tau, r) \sin(p\tau) d\tau \\ &= C(p, r) - i S(p, r) \quad (6) \end{aligned}$$

where $C(p, r) = 1/\sqrt{2\pi} \int_{-\infty}^{\infty} f(\tau, r) \cos(p\tau) d\tau$

and $S(p, r) = 1/\sqrt{2\pi} \int_{-\infty}^{\infty} f(\tau, r) \sin(p\tau) d\tau$

if $f^{\mathbb{H}}(p, r_0) = F(p) \cdot \exp(-i\beta(p))$

$F(p)$ the amplitude, and $\beta(p)$ the phase angle of the Fourier component p at $r = r_0$.

Then $f^{\mathbb{H}}(p, r) = F(p) \exp(-i\beta(p)) \exp(-ip \frac{r-r_0}{C(p)})$

$$F(p, r)^2 = C(p, r)^2 + S(p, r)^2$$

and phase $\phi(p) = -\arg f^{\mathbb{H}}(p, r)$

$$= \arctan\left\{ S(p, r) / C(p, r) \right\}$$

$$= \beta(p) + p \cdot (r-r_0) / C(p) \quad (7)$$

In general, seismographs introduce phase shift to each Fourier component. If we can express instrumental phase shift by $\theta(p)$, then,

$$\phi(p) = \beta(p) + \theta(p) + p \cdot \frac{r - r_0}{C(p)}$$

Let us consider two recording stations at a distance of r_1, r_2 from an epicentre. r_1, r_2 , do not differ by more than half the circumference of the earth (No polar phase shift). Then :

$$\phi_{r_1}(p) = \beta(p) + \theta_{r_1}(p) + p \cdot (r - r_0)/C(p)$$

$$\phi_{r_2}(p) = \beta(p) + \theta_{r_2}(p) + p \cdot (r_2 - r_0)/C(p)$$

Therefore, difference in phase angle

$$\phi_{r_2}(p) - \phi_{r_1}(p) = \left\{ \theta_{r_2}(p) - \theta_{r_1}(p) \right\} + p \cdot \frac{(r_2 - r_1)}{C(p)}$$

The above equation clearly shows that analysis of records at two distances yields a unique solution without assumption of the phases at the origin.

If the seismographs at the two stations are identical in behaviour,

Then

$$\theta_{r_1}(p) = \theta_{r_2}(p)$$

and

$$\phi_{r_2}(p) - \phi_{r_1}(p) = p(r_2 - r_1) / C(p)$$

$$C(p) = \frac{p(r_2 - r_1)}{\phi_{r_2}(p) - \phi_{r_1}(p)}$$

$$C(p) = \frac{p(r_2 - r_1)}{\text{Arc tan} \left\{ \frac{S(p, r_2)}{C(p, r_2)} \right\} - \text{Arc tan} \left\{ \frac{S(p, r_1)}{C(p, r_1)} \right\}}$$

In practice, we must introduce a term $2m\pi$ in the denominator, which arises from the multi-valued nature of the trigonometric function (where m is an integer and a function of p).

$$C(p) = \frac{p(r_2 - r_1)}{\text{Arc tan} \left\{ \frac{S(p, r_2)}{C(p, r_2)} \right\} - \text{Arc tan} \left\{ \frac{S(p, r_1)}{C(p, r_1)} \right\} + 2Mp\pi}$$

To add a correct number, M_p , of whole wavelength to the phase shift from Fourier analysis, M_p was first set at long periods, where its

effect is so large that only one of its values give^s reasonable velocities (within a geologically plausible region). When transferring to short periods, M_p was adjusted so that the phase velocities changed continuously.

The value of M_p can also be determined using group velocity values for the same pair of stations and^{the} value of the phase velocity at the longest period.

Suppose we Fourier Analyse each record with respect to a different initial point; say t_1 and t_2 .

$$C(p) = \frac{r_2 - r_1}{\text{Arc tan} \left\{ \frac{S(p, r_2)}{C(p, r_2)} \right\} - \text{Arc tan} \left\{ \frac{S(p, r_1)}{C(p, r_1)} \right\} + (t_2 - t_1) + \frac{2N\pi}{p}}$$

where N is an integer. In other words, $\frac{2N\pi}{p}$ is an integral multiple of period.

Computation of $C(p)$ as a function of period, $2\pi/p$, leads to a discrete set of possible phase velocity curves, according to the value of N , one of which must be correct. When station pairs^{are} separated by a distance less than few thousand km, only one curve falls within a geologically plausible region.

Since the spacing between possible inter station phase velocity curves, according to the value of N , is strongly dependent on the station spacing, the foregoing ambiguity may be resolved if data from additional station pairs is available.

For a fixed record length, the problem of aliasing can be substantially reduced by increasing the sampling rate. Therefore, it is necessary to digitally sample with a time interval, Δt , such that the Nyquist frequency $1/2\Delta t$ is at least as high as the highest frequency containing any energy in the records.

It is important to detrend the data since a non zero average or

a linear trend would introduce errors in the spectral analysis. A non-zero average or a linear trend could be introduced into the data by very long period signals, barometric or thermal instrumental noise or in the digitizing process. It is interesting to note that the amount of information we are able to obtain by digital analysis is always equal to or smaller than the number of digitized samples we fed in at the onset.

(3.2.3) Correlation Techniques :

A number of new correlation techniques have been developed (Bloch and Hales, 1968) for the determination of interstation phase velocities from the digitized seismogram for a pair of stations.

One of these techniques is to Fourier analyse the sum or difference of the two seismograms from earthquake recording stations after time shifting in two steps to correspond to steps in phase velocity. The amplitude of the summed seismogram is a maximum for a given period when both seismograms are in phase for that period (T). Similarly, on subtracting, the amplitude is a minimum when the two waves are in phase.

Suppose t_1 mark on one seismogram coincides with t_2 mark on the second seismogram. Then, the phase velocity at period (T) is given by

$$C_T = (r_2 - r_1) / (t_2 - t_1 \pm NT)$$

Another method is to pass both seismograms through a narrow - band pass digital filter centered at various periods and ^{form} the cross product of the filtered seismograms, after time shifting. The average of the resultant time series is a maximum, when the two signals are in phase.

The computer output is a matrix consisting of amplitudes or averages, as a function of phase velocity and period. The phase velocity dispersion is determined from the contoured matrix.

The practical significance of the cross-correlation method (Landisman, Dziewonski and Satô, 1969), as applied to seismograms contaminated by noise, is related to the fact that only a fraction of the entire cross-correlogram is needed for evaluation of the inter-station phase delay curve. The inter-station separation is always smaller than the epicentral distance to the further station, and it usually is also less than the distance to the closer one. The cross-correlogram then exhibits less dispersion than either of the individual recordings. The signal - to - noise ratio of the correlogram can always be greater than that which results from the summary effect of the noise contained in the individual recordings, if the time limits of cross-correlation are properly chosen. The improved signal - to - noise ratio results from the fact that the entire signal is correlated while only a portion of noise energy enters the cross-correlogram.

Phase velocities determined from seismograms contaminated with noise have been found to be more reliable if the cross-correlogram is smoothly windowed before Fourier transformation, because the noise usually is widely distributed in apparent inter-station velocity. The window function is designed to enhance the signal - to - noise ratio by emphasizing those portions of correlogram associated with the signal at the expense of portions contaminated with noise.

The spread of the lags used in the cross-correlogram operation should be chosen such that the temporal length of the correlogram is about five times as great as the longest period of interest. Also, for best results the signal should be located near the centre of the cross-correlogram. The requirements represent an attempt to minimize the distortions introduced by modulation of the signal.

(3.3) Data Reduction

(a) The records are digitized over a total time length which

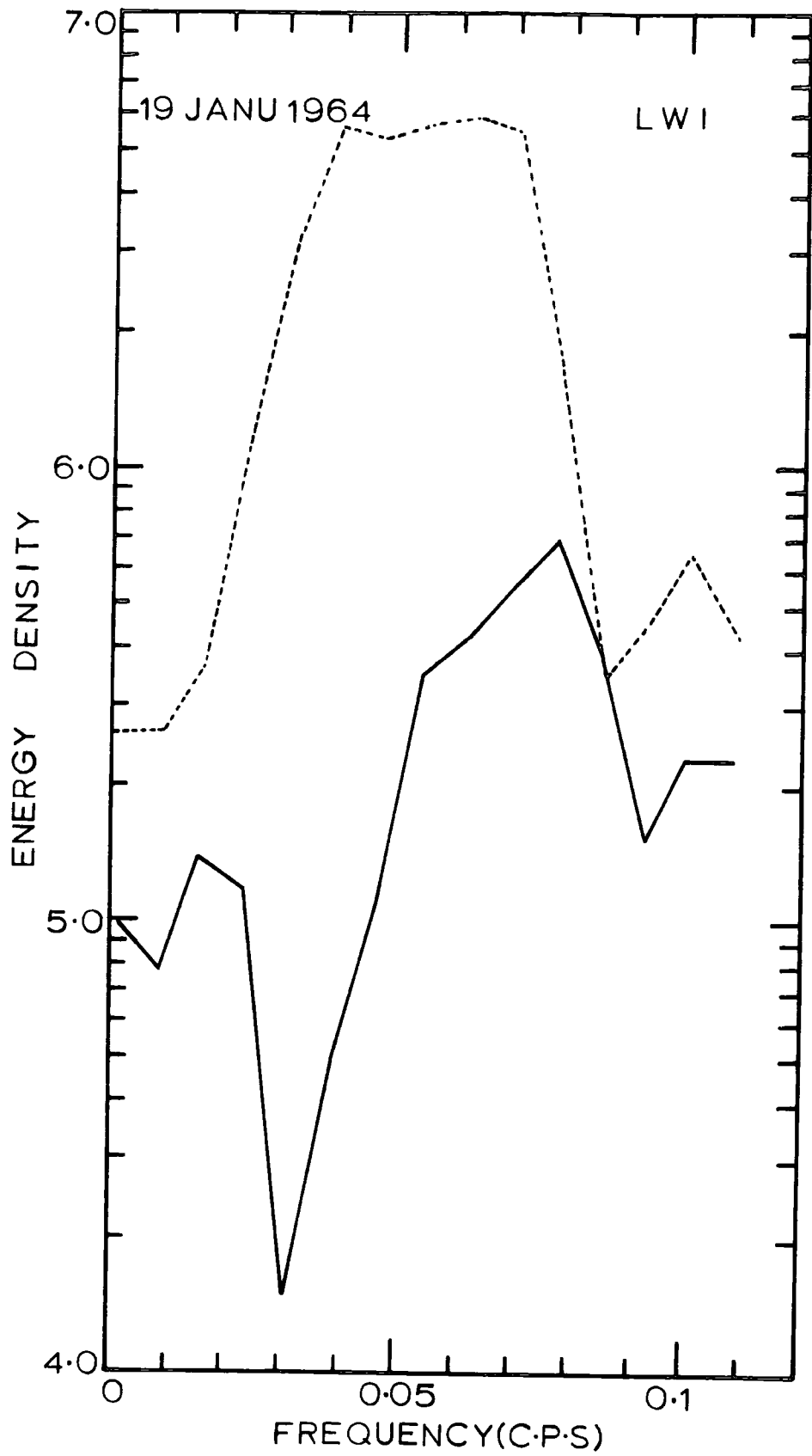


FIG. II

include the significant part of the Rayleigh (or Love) wave-train. To get adequate frequency resolution the total length of records digitized should be about five times the longest period in the seismogram and sampling interval should be as short as possible. But at the back, we should try and avoid any multiple arrivals.

A piece of transparent graph paper, in few cases a Pen-follower, graduated in mm is used for the purpose of digitization. The base line should be symmetrical about the wave train and parallel to the time axis. The first and the last digitized data points should be on the base line. Since the trace on a record is about a mm thickness, one side of the trace is always followed in taking the amplitude but it may introduce an error by increasing the sharpness of negative peaks in comparison with positive peaks or visa versa.

To understand the exact frequency content of the surface-wave a portion of record equal in length to the above case, its first digitized data same as last digitized data of the first set, has been digitized (there should be no new arrivals in this portion) and Amplitude spectrum for these two cases is compared (Fig.11).

The behaviour of the record for the same earthquake from the second station is studied carefully and a portion identical in frequency content to the first record is chosen for digitization (that is, same packet of energy is correlated).

The wave form is traced using the digitized data, the traced wave form is then compared with the original record.

To study the phase and group delay introduced by the seismographs, the calibration pulses on both records were compared visually. If

there was any difference, then corrections for instrumental distortions of phase were evaluated after determining the seismograph constants, by a comparison of the recorded calibration pulses with a set of theoretical pulses. The following steps are to be observed with care :

(1) When the experimental transient is traced on a piece of paper obtain a good zero-line (DC line) at the beginning and at the end of the transient.

(2) When superimposing the traced, experimental transient of the standard, set the zero-line of the former to the latter.

(3) Observe and compare the locations of the maximum amplitude of the experimental transient with that of the standard. If the experimental transient has the maximum amplitude to the right or to the left of the standard it will indicate that the chosen case (for the standard) is not the proper one. Try another case.

(4) When the location of the maximum amplitude of the experimental transient falls close to that of the standard transient one should check the slope of the rising (beginning) part of the experimental transient and the slope of the decaying part of the corresponding slopes of the standard transient. If the rising slope matches, but the decaying part does not, one should try another case which has similar period of seismometer and galvanometer but with different ho or hg. Repeat the last step until a closer fit is obtained.

A computer program is used to calculate the phase delay introduced by the seismograph from ^{the} free period ^{of the} seismometer ^{and} galvanometer; ^{and} damping constants and coupling factor.

Inter-station ^{are} group velocity values ^{are} determined using both Peak and Trough ~~M~~ethod and Multiple Filter Technique (SWAP - Blacknest).

A simple harmonic analysis is performed on a digitized data, using

Fast Fourier analysis (Cooley-Turkey algorithm) computer program, resulting in a preliminary energy density and phase spectrum.

A computer program is used to calculate the phase angle and phase velocity from the observed group velocity spectrum and phase velocity at the longest period. The mathematics behind this program is :

The group velocity, U , is related to the phase velocity, C , by the equation

$$U = C - \frac{dC}{d\lambda} \cdot \lambda$$

where λ is the wave length and $\lambda = CT$ (T - period)

$$\left(\frac{dC}{dT}\right)_T = \frac{C_T(C_T - UT)}{UT}$$

If the variation in phase velocity with period is very gentle. Then

$$C_{T-1} = C_T - \left(\frac{dC}{dT}\right)_T$$

and phase angle $\phi_{T-1} = \left\{ \left(\frac{\Delta}{CT-1} - t \right) \cdot 2\pi \right\} / T$

The phase angle from the above computer program is used to assign integer number of cycles to interstation phase angle to achieve a smooth variation in phase with period.

The smoothness of the phase angle (that is, value of M_p) is further checked by correlation techniques.

It can be shown very clearly that to get a very slow variation in the phase angle with period, the first digitized data points should coincide with the arrival time of the longest period in the record. Further, epicentral distance should not be too great.

High frequency irregularities in the interstation phase spectrum are smoothed out by fitting a polynomial of degree five with the aid of a computer. The reliability of the smoothed phase spectrum is

checked by differentiating with respect to frequency and comparing the result with the group velocity obtained from Multiple Filter Techniques.

Finally the phase spectrum is used to determine the phase velocity spectrum from equation (8).

(3.4) Errors

(a) The effect of lateral refraction due to different phase velocities in continental, oceanic or other types of crust may introduce error into a phase velocity measurement, because the wave-fronts may not have travelled along a Great circle path between the source and the receiver. Such errors will usually cause the interstation phase velocities to be too high.

Evernden (1953) and Capon (1970) observed that the multi-path propagation in the period range 20- to 40- sec is caused primarily by the phase - velocity contrast between the oceanic and the continental region. Consideration of the ratio of oceanic to continental phase velocities shows that the biggest ratio occurs at 20 sec period for both Love - and Rayleigh - waves and is about 1.15. The corresponding change in the angle of incidence is about 6° , for this angle which introduces an error of about 0.02 km/sec. At longer periods the error is smaller. There could be additional error due to different source to station path for the pair of stations, if there is large variation in structure.

It may be suggested that this problem could be overcome by using the tripartite method. But, with the set of stations we used in this study, we cannot use the tripartite method. Because the separations between the stations are very much greater than the wavelength of the wave under consideration and it is known from regional gravity anomaly map (Wohlenberg, 1970; Khan and Mansfield, 1971) that there is large variation in the crust and Upper mantle structure ^{under} East Africa.

(b) Errors in the epicentre and origin time should not affect interstation phase - and group - velocity measurement, because of the way we selected the events. But it will certainly have some effect on the single station group velocity measurement.

This error in the observation of epicentral distance is between 10 - 20 km and in the origin time is between 0.5 - 1.5 sec. Therefore error in the single station group velocity measurement is $\pm \frac{\Delta + 15t}{t^2 - 1}$ km/sec

Where Δ is the epicentral distance and t is the travel time for a given period.

(c) The average distance between the two adjacent minute marks on the record is about 42 mm and the minute mark, itself, is about a mm in length. Therefore, error in the time of the first digitized data could be about ± 0.71 sec.

When studying interstation phase - and group - velocity, this error can be reduced to a great extent by always taking one end of the minute mark as time corresponds to that mark.

For the reasons mentioned in the above case, there could also be an error in the value assumed for sampling interval. This error can be reduced to a very great extent by measuring the length of the record cover longer time length; provided no fluctuation in the speed of the drum. It is difficult to estimate the percentage of error introduced in the phase angle measurement due to error in the sampling interval. But it is certain that this error is large at long periods and becomes negligible at the short period end of the spectrum.

(d) Mitchell and Landisman (1969)^{have} shown by comparison of calibration pulses from several instruments of the World Wide - Standard Seismic Network of the United States Coast and Geodetic Survey that

there are differences in phase and amplitude response between instruments, sometimes even at the same station. This may result from deviation of any of the instrumental constants from standard values. Values for the free period of the seismograph are usually listed on the seismogram. Further, they have found that the galvanometer period differed from its listed value by almost 5 sec. Departures of instrumental parameters from their assumed values can cause errors in corrections for instrumental phase delay, group delay and magnification.

We have used in our study, a list of standard curves to determine the constants of the seismograph. When using standard curve it has been observed that the damping constants of galvanometer and seismometer can be determined within ± 0.2 and the free period of the galvanometer and the seismometer can be determined within ± 2 sec. Therefore the corresponding error in the phase delay is about 1.2 sec.

(e) In the case of Love waves, if the direction of propagation does not coincide with either N - S or E - W direction, then there can be an error due to interference of Rayleigh waves.

If Fourier amplitudes and phases obtained from Fourier analysis of the North and East components of motion is designated by the symbol A_N , ϕ_N , A_E , and ϕ_E , then the Longitude and Transverse, amplitudes and phases may be expressed in terms of these quantities and the great circle azimuth θ from the receiver to the source as :

$$A_L = \left[A_E^2 \sin^2 \theta + A_N^2 \cos^2 \theta + 2A_E A_N \sin \theta \cos \theta \cos (\phi_N - \phi_E) \right]^{\frac{1}{2}}$$

$$\phi_L = \tan^{-1} \left[\frac{A_E \sin \phi_E \sin \theta + A_N \sin \phi_N \cos \theta}{A_E \cos \phi_E \sin \theta + A_N \cos \phi_N \cos \theta} \right]$$

$$A_T = \left[A_E^2 \cos^2 \theta + A_N^2 \sin^2 \theta + 2A_E A_N \sin \theta \cos \theta \cos (\phi_N - \phi_E) \right]^{\frac{1}{2}}$$

$$\phi_T = \tan^{-1} \left[\frac{A_E \sin \phi_E \cos \theta - A_N \sin \phi_N \sin \theta}{A_E \cos \phi_E \cos \theta - A_N \cos \phi_N \sin \theta} \right]$$

In all the events considered in this study, $A_E \geq A_N$ for all period T. The

largest error that occur at the longest period, 60 sec, is 2.0 sec, corresponds to $\Theta = 12.5^\circ$.

Taking into consideration all the errors mentioned above, the overall error in the Rayleigh wave phase velocity measurement is about 0.03 km/sec and in the group velocity about 0.04 km/sec. Love wave velocity will have little greater error, depending on the value of Θ .

CHAPTER 4

INVERSION OF SURFACE WAVE DISPERSION CURVES

(4.1) Theoretical Study on Inversion problems

Theoretically it has been observed that (Knopoff, 1961; Gilbert and Backus, 1967, 1968 a, b) the direct inversion of surface wave dispersion curves into unique density - modulus - depth distribution is impossible; a further relation specifying one or both of these is necessary. In the absence of such additional information one can only construct a suite of inter-related density and modulus perturbations, all of which exactly yield the same dispersion curve. This set can be limited by certain physical arguments, such as geologically plausible range of values. Further, as we accumulate measurements of more gross earth data, the infinite - dimensional manifold of acceptable earth models shrinks. If there are more data, there are fewer earth models which can satisfy them all.

If the data are admittedly inaccurate, then the number of permissible solutions is augmented by another parameter. This parameter describes the latitude that a permissible exact solution be given in view of a known inaccuracy in the measurement.

Dziewonski (1970) based on the Auto - correlation function of shear velocity partial derivatives ^{has} shown a poor resolution for shear velocity in the first 350 km of the upper mantle; Further it is impossible to determine from the Love wave data alone whether there is a low velocity channel in the depth interval from 33 to 240 km and therefore, appearance of a double low-velocity channel in a model obtained from the inversion of Love wave data is a highly non-unique feature.

Der, Masse and Landisman (1970) by studying the effects of observational errors on the resolution of surface waves at intermediate distances made the following conclusions : The partial derivatives of the observed quantities (phase and group velocities) with respect to the parameters of interest (for example, shear velocity) in a layered medium can be used in combination with the errors of observation to estimate the resolution of a given set of data ^{as} a function of depth, as well as the uncertainty of the resulting velocity distribution. The shear wave velocity determinations and the resolution decreases with increase of depth and Love wave observations yield much less information about the shear-velocity distribution than Rayleigh waves. Further, if the errors of phase - and group - velocity measurements are set equal, the resolution gained from phase velocity is found to be inferior to that obtained from group velocities.

Higher mode observations increase the accuracy and the resolution that may be attained. For regional studies of surface waves based on fundamental mode observations that ordinarily extend only to periods of 80 sec, and for higher mode data for periods below 15 sec, any deductions about the upper mantle are apt to be rather inaccurate.

Pilant and Knopoff (1970) ^{have} shown that there exists an additional degree of non-uniqueness in the inversion of group velocity data compared with the inversion of phase velocity data, independent of the other points of Non-uniqueness that apply uniformly to inversion of dispersion data of both types. This is most easily illustrated by noting that the group slowness $1/u$ and phase slowness $1/c$ at frequency w are related by the familiar relation

$$\frac{1}{u} = \frac{d}{dw} \left(\frac{w}{c} \right) \quad (1)$$

Consider two different hypothetical structures with corresponding

theoretical phase slowness dispersion relations $1/c_1(\omega)$ and $1/c_2(\omega)$.

If these are related by the expression.

$$\frac{\omega}{c_1} = \frac{\omega}{c_2} + A \quad 0 < \omega_a \leq \omega \leq \omega_b \quad (2)$$

over a finite band of frequencies, with A a constant, then the two structures have the same group slowness

$$\frac{1}{u_1} = \frac{1}{u_2} \quad 0 < \omega_a \leq \omega \leq \omega_b$$

over the same band.

We suppose that data of $u(\omega)$ are available over this band of frequencies excluding $\omega = 0$. The conclusion above leads to the following observations. (a) There exists an infinite number of structures generated by the parameter A , all of which have the same group velocity. The class of solutions to the inversion of group velocity dispersion can be restricted by determining the parameter A by knowing the phase velocity at least one frequency. (b) If the group velocities for two regions are the same, it does not follow that the two structures are the same, unless the values of A are the same. (c) If the group velocities for two regions are different, the two structures are different.

In view of the present accuracy of observations of surface wave dispersion data and in view of the non-uniqueness of the inversion of exact dispersion data, it may be concluded that the fine structure of the earth's interior as determined from surface waves remains in doubt.

(4.2) Methods of Inversion

(4.2.1) Trial and Error Method :

Even though trial and error method is a very old and very subjective method of interpretation, it is still widely used in the surface wave interpretation. In this method few parameters (In general, either β or H)

are selected as active parameters and the values of these parameters are varied one by one until the calculated dispersion curve for a model fits with the observed dispersion curve within a certain reasonable deviation. Then the model is accepted as representing the elastic wave velocity structure of the region under investigation. This method of interpretation becomes very difficult when one tries to interpret more than one set of dispersion curve.

(4.2.2) Monte Carlo Inversion :

Monte Carlo Inversion method is a special type of Trial and Error method. This method (Press; 1964, 1968 a,b; Keilis-Borok and Yanovskana, 1967) offer the advantage of exploring the range of possible solutions and indicate the degree of uniqueness achievable with currently available geophysical data.

This method uses a high speed digital computer to generate, purely at random, literally millions of structure models, each active parameter is constrained to lie within a certain bound of physical reasonability. For each of the models, surface wave dispersion data and other geophysical data are calculated and compared with the observed data. The models which satisfy all the observed data within certain degree of accuracy are printed out.

(4.2.3) Least Squares Inversion Techniques :

In 1962, Dorman and Ewing interpreted the fundamental mode Rayleigh - and Love - wave phase velocities measured in the New York - Pennsylvania area; using the concept of constant partial derivative of phase velocity with respect to layer parameters in a least square inversion scheme. This method is investigated in greater detail by Brune and Dorman (1963) when interpreting surface wave dispersion

over Canadian shield and by McEvilly (1964) when studying the crust and Upper mantle structure of central United States. The method is as follows:

It is possible to express the difference between the observed phase velocities C and the phase velocities calculated from a trial model (to first order) as follows:

$$\Delta C(T_j) = \sum_{i=1}^N \frac{dC(T_j)}{dP_i} \cdot \Delta P_i \quad (1)$$

where N is the number of parameters, P_i are the physical parameters, and ΔP_i are perturbations to the parameters. The period at which the phase velocities have been obtained are T_j .

If there are more data $\Delta C(T_j)$ than parameters, the redundancy can be removed by requiring a least mean square fit: We choose the quantities ΔP_i in such a way that we minimize

$$\sum_{j=1}^M W_j (\Delta C(T_j) - \sum_{i=1}^N \frac{dC(T_j)}{dP_i} \Delta P_i)^2 \quad (2)$$

Where M is the number of data points and W_j are weighting functions. The weighting functions could be made proportional to the spectral amplitudes (or error of observation at T_j). The result of the minimization is

$$\sum_{i=1}^N \sum_{j=1}^M \Delta P_i \cdot \frac{dC(T_j)}{dP_i} \cdot \frac{dC(T_j)}{dP_n} = \sum_{j=1}^M \Delta C(T_j) \cdot \frac{dC(T_j)}{dP_n} \quad n = 1, 2, \dots, N. \quad (3)$$

This is a set of N simultaneous equations in the unknowns ΔP_i of the form

$$\sum_{i=1}^N A_{ni} \Delta P_i = b_n \quad n = 1, 2, \dots, N.$$

In principle, we can invert equation (3) to solve for the values of ΔP_i . This inversion can only be made, however, when each of the parameters in the perturbation has a different and measurable effect on the phase - velocity curve in the range of observation.

The result of the study shows that this method produces results

which are exact in the sense that the earth parameters used in an exact theoretical calculation of dispersion data can be recovered from a knowledge of the dispersion data alone; provided the structural detail in the initial model should be sufficient to give a model which will satisfactorily match the observational velocities in the absence of such factors as extreme velocity gradients or reversals or anisotropy. Further, in interpreting fundamental mode data, the use of layers having distinct - zones of influence along the dispersion curves guided by reasonably valid additional data especially for total crustal thickness, will yield the most unique interpretation in the sense of average properties in the given zones.

The method permits a survey of the possible interpretation of a given set of data which is more rapid, precise, and complete than can be made by trial and error^{method.} Also, by observing the performance of the calculation under various sets of constraining conditions, a practical evaluation of the uniqueness question in each case can be made. The number of variables that can be evaluated simultaneously depends on the quality of the data. The number of modes observed, the breadth of the observed spectrum in each mode, and the scatter of the data points are quality factors which strongly affect the performance of the calculation.

With this method, the depth to interfaces between layers where the change in shear velocity is small could not accurately determined and if the number of layers in any depth range is too great, large and unreasonable variations in shear velocity and layer thickness could occur, with adjacent layers developing unreasonably low and unreasonably high shear velocity. Further the inversion process becomes unstable if density and shear velocity are allowed to vary concurrently in the same depth range or compressional velocity is allowed to vary in any of the layers except the upper two. The comparison of the shape of the

density and shear velocity derivatives shows that in general a small increase in the density of a particular layer can be counteracted by a small decrease in shear velocity in this layer along, with a small increase in the shear velocity in the underlying layer.

In many cases it will be useful to assume that the earth consists of n layers of fixed thickness, compressional velocities and densities and to attempt to evaluate layer shear velocities only. The final result depends on the constraints used. They are (a) The number of layers chosen for the problem (b) The particular division made between active and passive parameters, and (c) The fixed values adopted for the passive parameters.

Berry and Knopoff (1967) questioned the confidence limits that should be assigned to the derived shear velocity structure and they put forward the following method.

Assume that the experimental data have been fit perfectly by the model. For physically reasonable data, this is always possible if one introduces a sufficient number of parameters. We now inquire what significance a shift dc of the entire phase velocity curve has for each parameter considered separately. For the purposes of this assumption, we take $dp_i = 0$, $i = 1, 2, \dots, M$, $i \neq k$, where p_k is one of the parameters in the set. The function to be minimized is

$$\sum_{j=1}^M \left\{ dc(T_j) - \frac{dC(T_j)}{dp_k} dp_k \right\}^2 \quad (1)$$

The result of the minimization is

$$dp_k = dc(T_j) \cdot \frac{\sum_{j=1}^M \frac{dC(T_j)}{dp_k}}{\sum_{j=1}^M \left(\frac{dC(T_j)}{dp_k} \right)^2} \quad (2)$$

where we assume that $dc(T_j)$ is a constant for all T_j . Qualitatively from equation (2), we see that the uncertainty in any parameter is inversely

proportional to the area under the (dC/dp) versus T curve.

(4.3) New Techniques.

When studying mean velocity - depth structure, the Least squares Inversion techniques have ^a number of advantages over trial and error method. It provides us with information, which enables us to separate all the parameters into two groups, active and passive. Each of the active parameters would be altered according to the partial derivative and all the active parameters at the same time. Therefore time involved in this process would be shorter, and is more of objective method than trial and error method. But the main weak point of this method is that it uses constant partial derivative, partial derivative with respect to a set of active parameters for an initial model, to fit a structural model to the observed dispersion curve. Further, even though in this method it is said that layers having distinct zones of influence along the dispersion curves should be considered for alteration, it did not give any objective method of constructing such layered structure. The answer to this last problem is given by Der, Masse and Landisman (1970). To overcome constant partial derivative problem, we have developed number of Non-linear optimization techniques and is applied for the interpretation of surface wave data.

It is necessary for all the techniques we used in the interpretation, to calculate partial derivative for an initial model with respect to compressional velocity (α), shear velocity (β), density (ρ) and thickness (H). Since the initial structure should have all the characteristics of the final structure, and the thickness of the layers should be as such. each layer has distinct effect on the dispersion curve (resolution). AFRIC model with an anomalous mantle, as indicated by the gravity studies, is used for this purpose (Table 7).

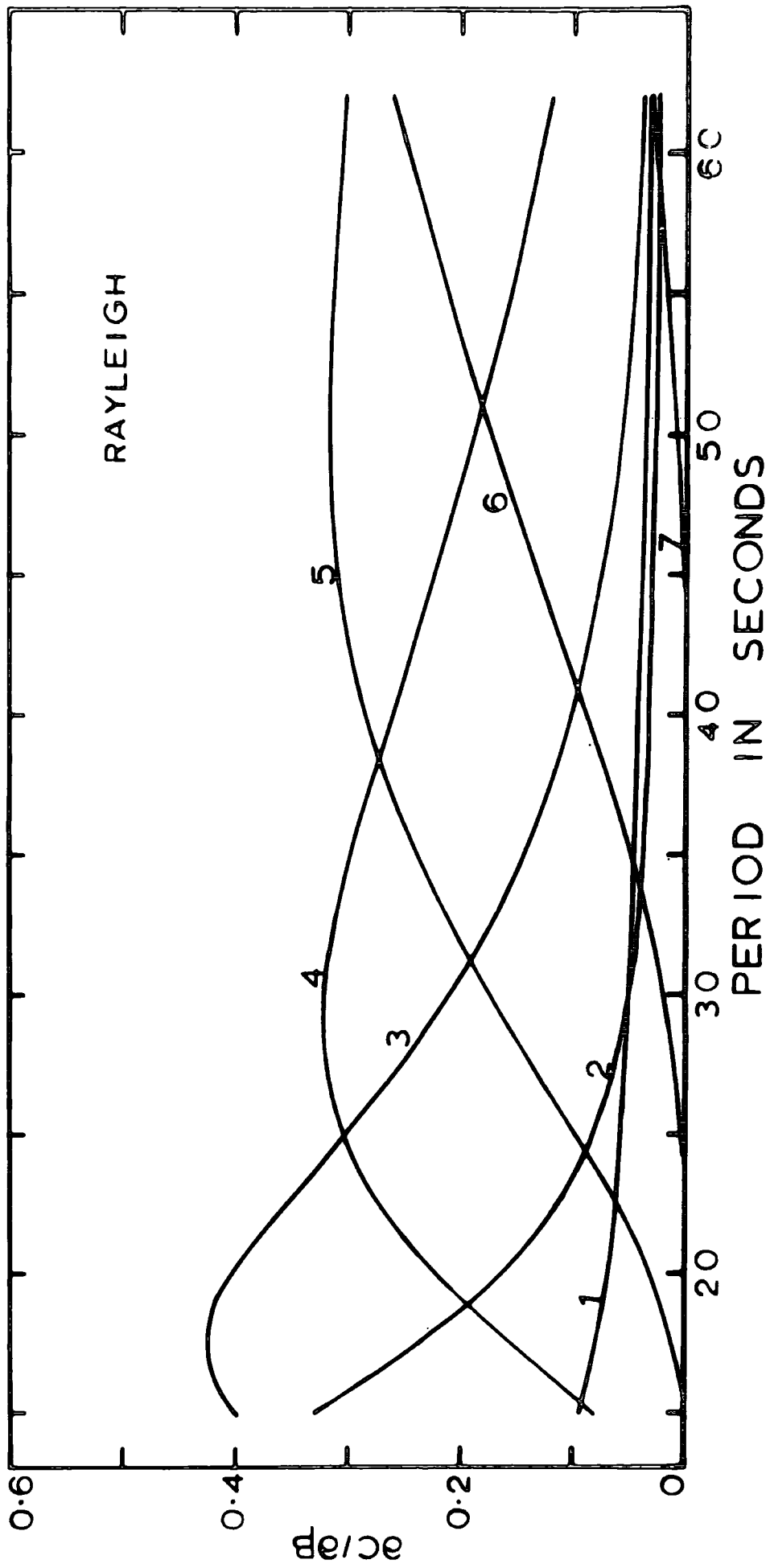


FIG. 12a

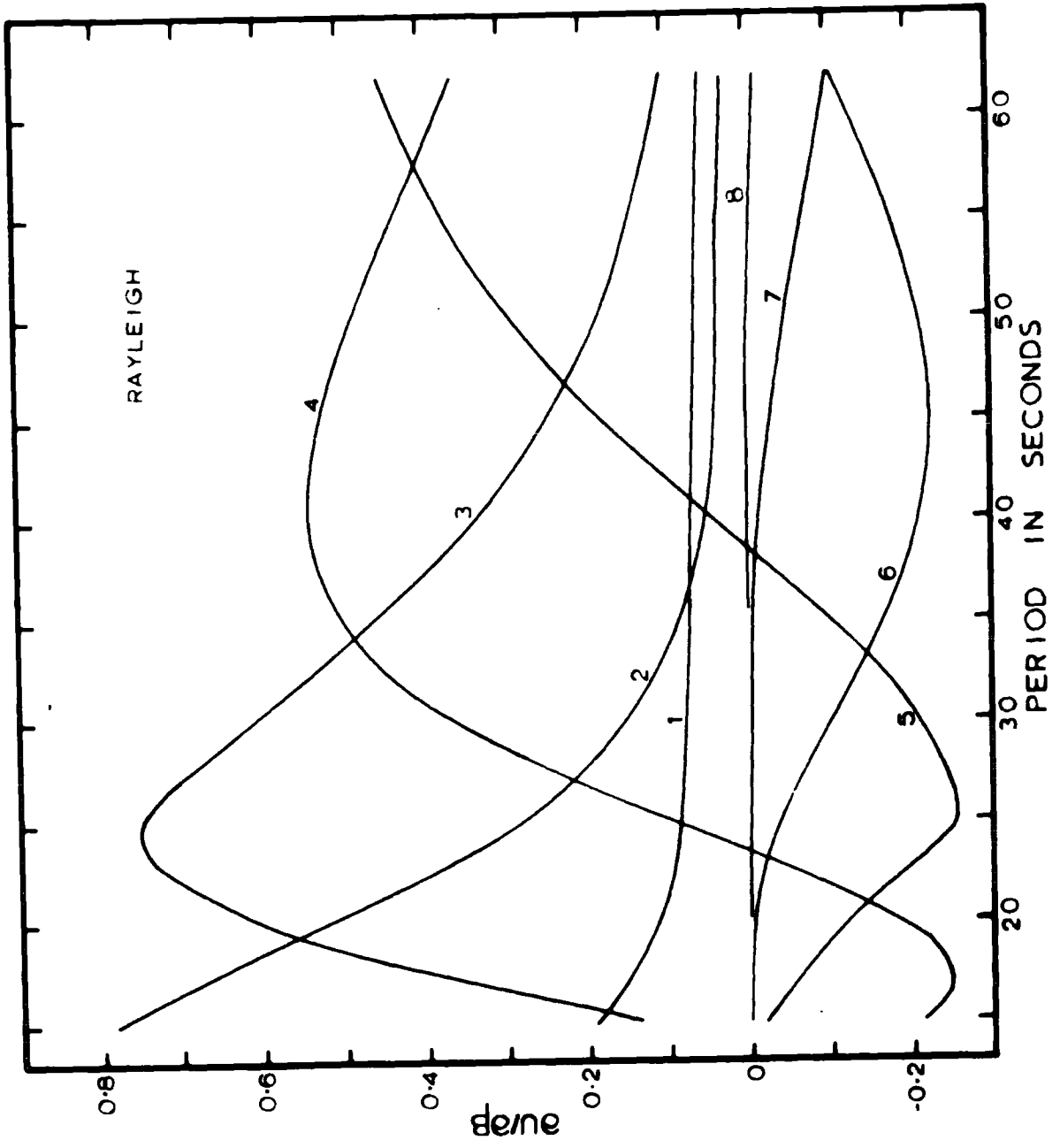


FIG. I2b

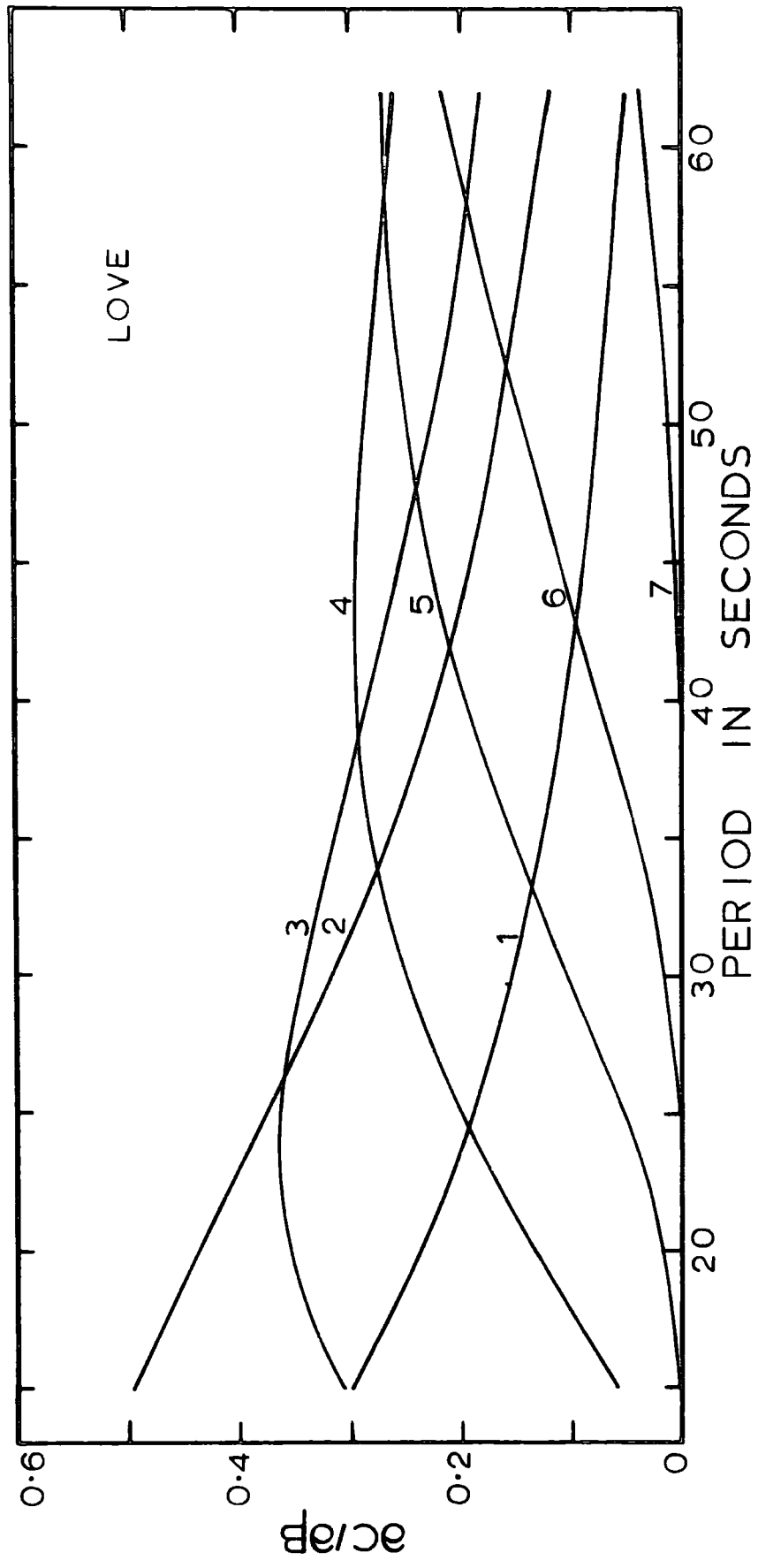


FIG. 12c

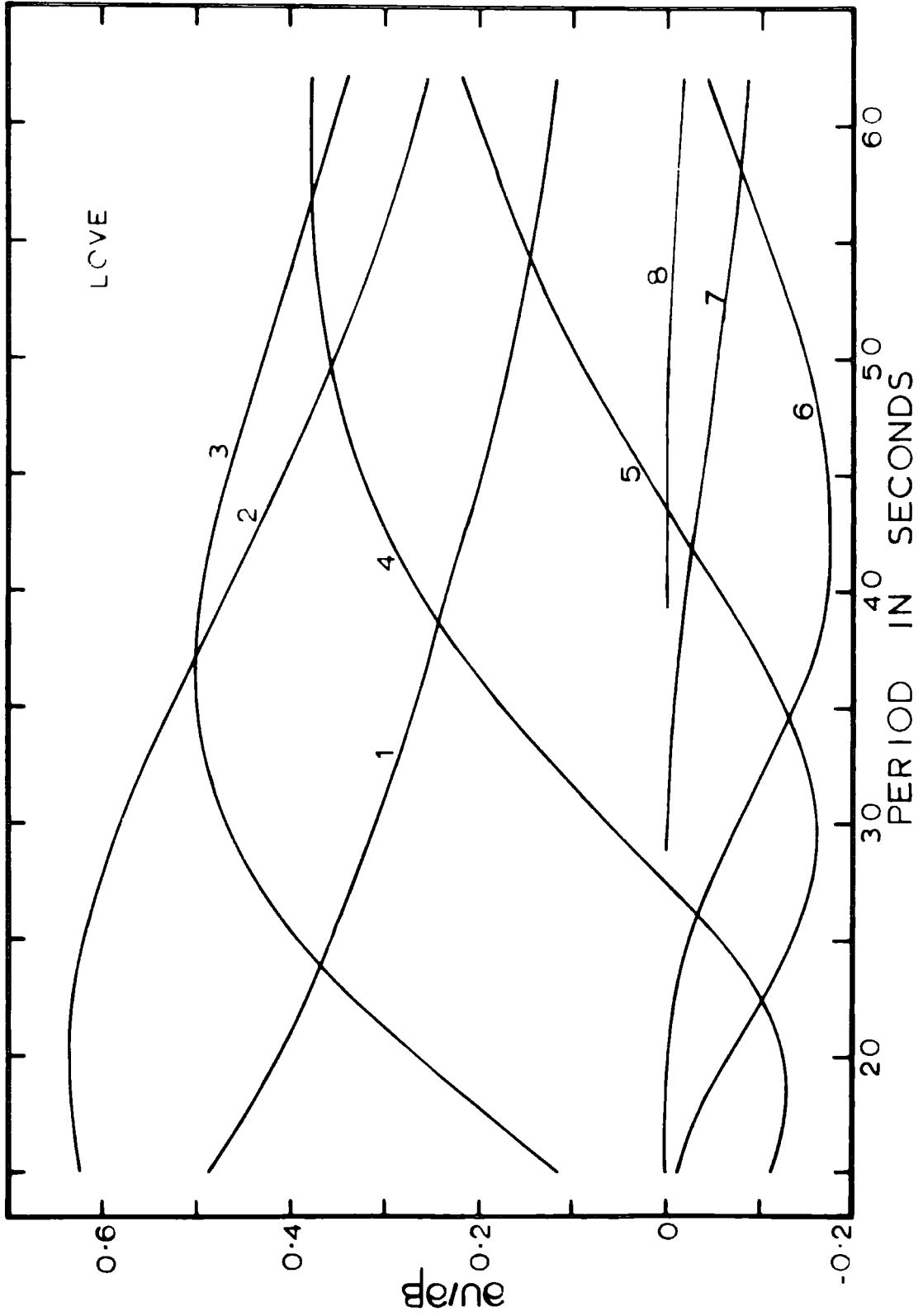


FIG. 12d

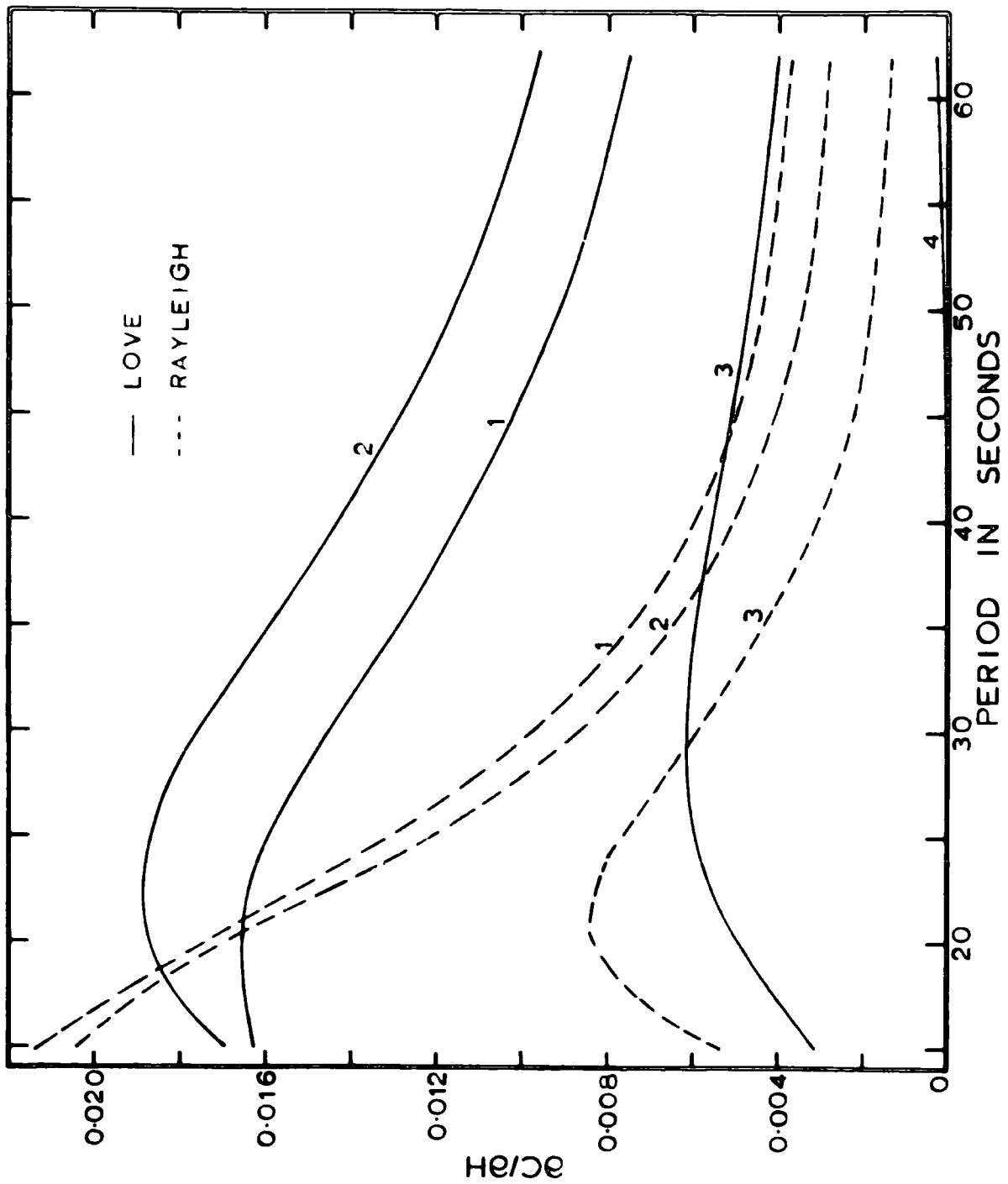


FIG. 12e

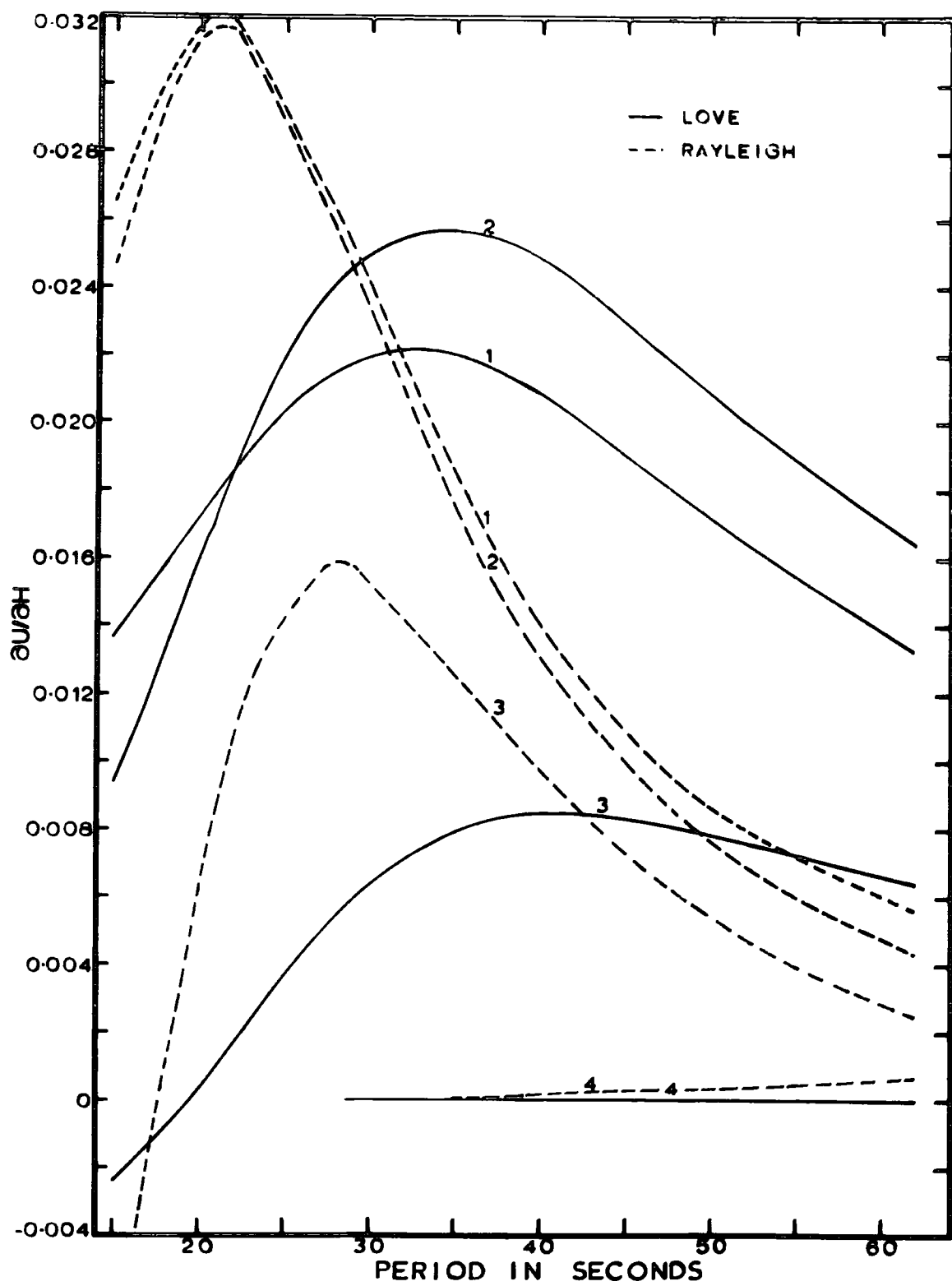


FIG. 12f

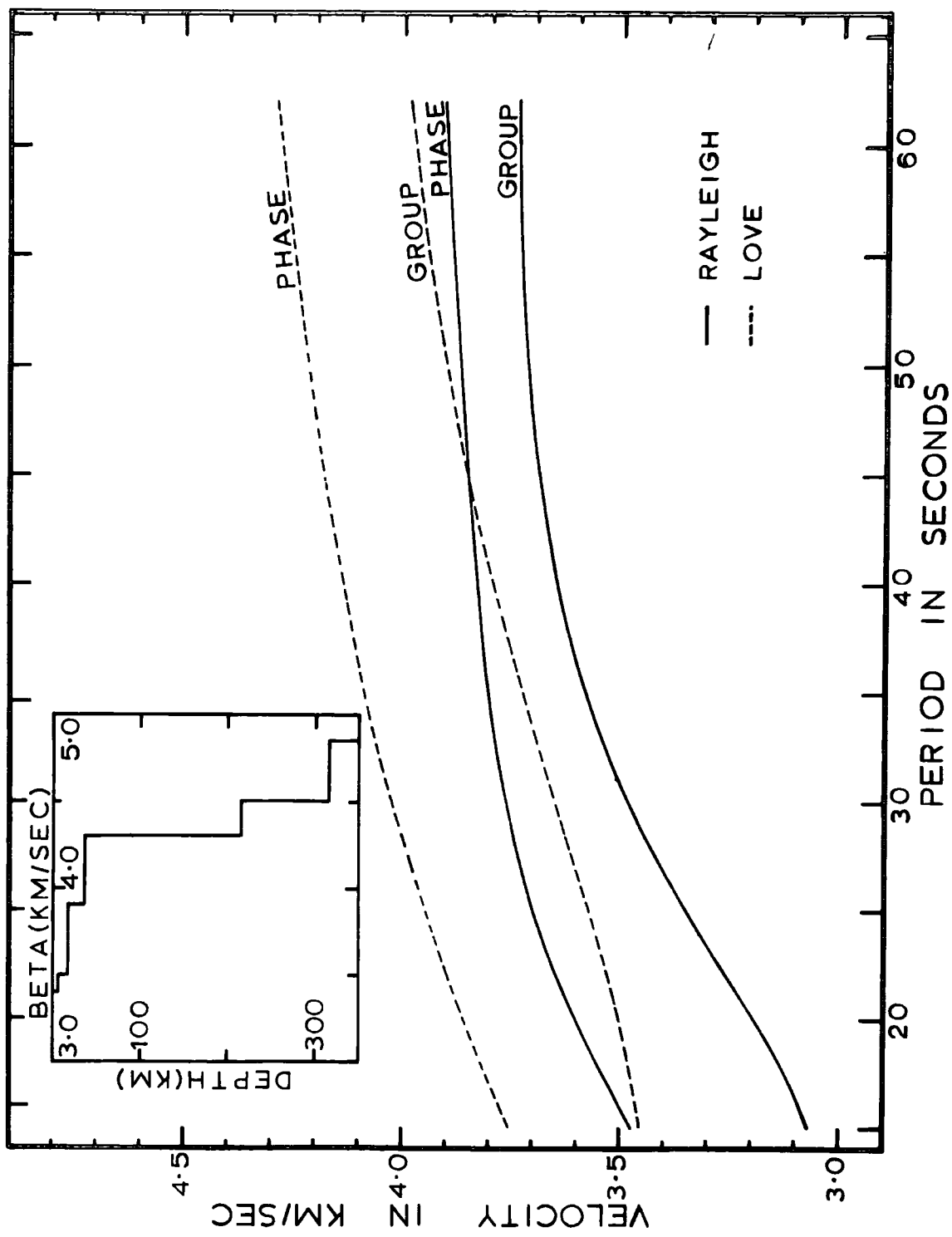


FIG. 13

Root Mean Square Deviation

km/sec

| Layer | Rayleigh | | Love | |
|-------|---------------------------------|---------------------------------|---------------------------------|---------------------------------|
| | $\frac{\partial c}{\partial h}$ | $\frac{\partial u}{\partial h}$ | $\frac{\partial c}{\partial h}$ | $\frac{\partial u}{\partial h}$ |
| 1 | 0.0105 | 0.0194 | 0.0125 | 0.0182 |
| 2 | 0.0097 | 0.0186 | 0.0148 | 0.0207 |
| 3 | 0.0048 | 0.0091 | 0.0050 | 0.0065 |
| 4 | 0.0002 | 0.0003 | 0.0001 | 0.0002 |
| 5 | 0.0002 | 0.0003 | 0.0001 | 0.0002 |
| 6 | 0.0001 | 0.0003 | 0.0001 | 0.0002 |
| 7 | 0.0000 | 0.0000 | 0.0000 | 0.0000 |
| 8 | - | - | - | - |

| Layer | Rayleigh | | Love | |
|-------|---------------------------------|---------------------------------|---------------------------------|---------------------------------|
| | $\frac{\partial c}{\partial e}$ | $\frac{\partial u}{\partial e}$ | $\frac{\partial c}{\partial e}$ | $\frac{\partial u}{\partial e}$ |
| 1 | 0.060 | 0.123 | 0.033 | 0.045 |
| 2 | 0.058 | 0.111 | 0.032 | 0.040 |
| 3 | 0.063 | 0.140 | 0.024 | 0.051 |
| 4 | 0.053 | 0.142 | 0.030 | 0.053 |
| 5 | 0.065 | 0.119 | 0.019 | 0.027 |
| 6 | 0.046 | 0.046 | 0.013 | 0.010 |
| 7 | 0.005 | 0.018 | 0.003 | 0.008 |
| 8 | 0.000 | 0.002 | 0.000 | 0.002 |

Table 8a

Root Mean Square Deviation

km/sec

| Layer | Rayleigh | | Love | |
|-------|-------------------------------------|-------------------------------------|-------------------------------------|-------------------------------------|
| | $\frac{\partial c}{\partial \beta}$ | $\frac{\partial u}{\partial \beta}$ | $\frac{\partial c}{\partial \beta}$ | $\frac{\partial u}{\partial \beta}$ |
| 1 | 0.051 | 0.089 | 0.154 | 0.283 |
| 2 | 0.112 | 0.299 | 0.290 | 0.486 |
| 3 | 0.217 | 0.413 | 0.286 | 0.402 |
| 4 | 0.227 | 0.400 | 0.248 | 0.262 |
| 5 | 0.241 | 0.253 | 0.187 | 0.125 |
| 6 | 0.137 | 0.151 | 0.116 | 0.109 |
| 7 | 0.013 | 0.047 | 0.016 | 0.044 |
| 8 | 0.001 | 0.005 | 0.001 | 0.008 |

| Layer | Rayleigh | |
|-------|--------------------------------------|--------------------------------------|
| | $\frac{\partial c}{\partial \alpha}$ | $\frac{\partial u}{\partial \alpha}$ |
| 1 | 0.047 | 0.080 |
| 2 | 0.041 | 0.056 |
| 3 | 0.036 | 0.036 |
| 4 | 0.015 | 0.006 |
| 5 | 0.004 | 0.006 |
| 6 | 0.000 | 0.002 |
| 7 | 0.000 | 0.000 |
| 8 | 0.000 | 0.000 |

Table 8h

Phase as well as group velocity partial derivatives were computed for the fundamental Rayleigh and Love waves for this simplified tectonic model ^{and} is shown in Fig.12. The group - and phase - velocities for this model are also shown in Fig.13. The partial derivatives of phase - and group velocity for each layer were calculated numerically for a span of periods (15 - 62 sec) appropriate to the observations, by alternation of the velocity in each layer by 0.1 km/sec, density by 0.1 gm/cc and thickness by 1 km. The root mean square deviation (RMSD) between the initial dispersion curve and the one after altering the respective parameters by 1 unit is also computed (Table 8).

The computer program used in ^{this study to calculate} dispersion curves is Dorman's FV7 program. The earth flattening approximation by Bolt and Dorman (1961) was used to correct for fundamental Rayleigh wave phase velocity C_s , for the spherical earth is related to that computed for a flat half space, C_h , by

$$C_s = C_h (1 + 0.00016 \times T)$$

where T is the period.

The corresponding corrected group velocity is given by Knopoff and Schwab (1968) as

$$U_s = U_h \left[1 + (0.00016 \times T) \left(1 - \frac{U_h}{C_h} \right) \right]$$

For Love waves, Earth - flattening calculation of Biswas and Knopoff (1970) was used.

From the partial derivative with respect to shear and thickness, curves shown in fig.12 and RMSD values given in Table 8, the following conclusions can be made. The compressional velocity and density do not have greater effect on the dispersion curve, when compared with that due to shear velocity. Rayleigh waves are much more sensitive to density than Love waves and density has greater effect on Rayleigh wave dispersion than compressional velocity

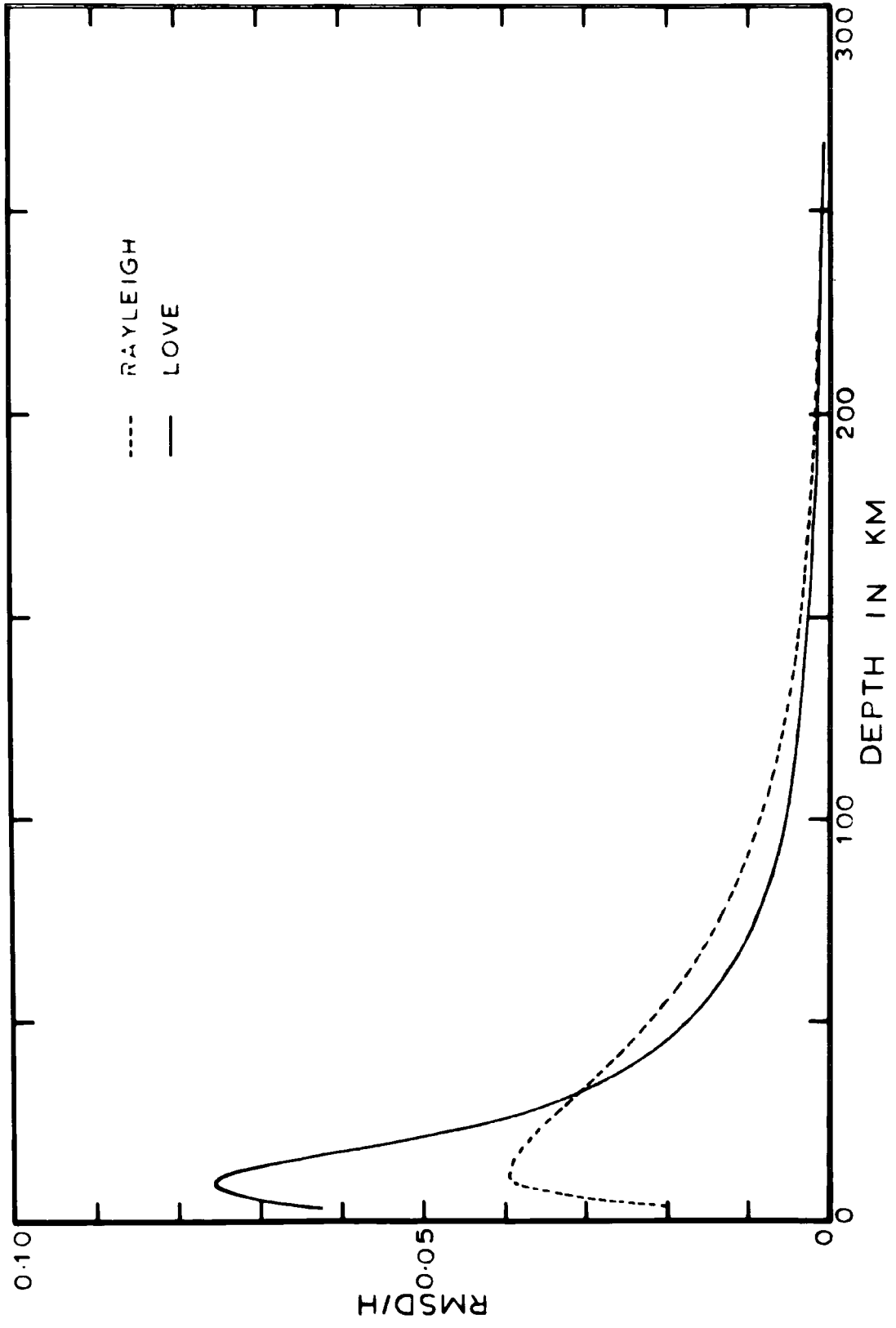


FIG. 14

(Table 8). For the initial model we used, the thickness of the crustal layers has greater effect on the dispersion curves. Near-surface layers have greater effect than deep layers. To a large extent a small variation in thickness of one layer could be compensated by a corresponding change in the thickness of the neighbouring layer. Therefore if there is a sedimentary layer and if we do not take into account its presence, then we may end up with thicker crust.

From the partial derivative for shear velocity, we can see clearly that in the period range we have considered (15 - 62 sec) the fundamental Love mode partial derivative curves (β), particularly for the upper layers, are broader than the corresponding Rayleigh mode curves and, therefore, much more sensitive to crustal shear velocities than Rayleigh waves. Rayleigh - mode curves have larger maxima and for the uppermost upper mantle shear velocities, it is much more sensitive than Love waves. The above statement can be quite clearly proved by plotting $(\text{RMSD})/H$ as a function of the depth to the mid-point of the layers (Fig. 14). Increases (or decreases) in β causes only increases (or decreases) in the phase velocity, whereas changes in β cause both increases and decreases in group velocity. It is therefore possible to increase (or decrease) the group velocity by increasing (or decreasing) the shear velocity at an appropriate depth by decreasing (or increasing) the shear velocity at some other depth in the model.

Rayleigh waves at any period are influenced by the shear velocities at greater depths than the Love waves for the corresponding periods and for Rayleigh wave the effective depth of penetration is about 0.45λ and for Love wave is about 0.3λ .

For the initial model we considered, 15 sec period Love wave will have wave length of 56.2 km and therefore have effective depth of

penetration of about 16.8 km. A 62 sec period Rayleigh wave will have wavelength of 240.0 km and therefore have effective depth of penetration of about 108 km. Therefore with the phase and group velocity values in the period range 15 - 62 sec, we can study with the great precision the shear velocity - depth structure in the depth range 16.8 - 108.0 km. The layers should be constructed in such a way that the boundary of a layer should coincide with the above depth. Further layer thickness within this depth range should be selected with the knowledge of RMSD value and error of observation to achieve a certain accuracy, say ^{about} $\Delta 0.1$ km/sec, in the shear velocity values; In other words the thickness of the layer as such RMSD value corresponds to change in shear velocity of 0.1 km/sec should be ^{roughly} Δ equivalent to error of observation. It has been found that layer thicknesses used in the initial model are of the correct order. Further, if the value of the thickness of the layers are of correct order, then the auto correlation function of phase and group velocity partial derivative with respect to shear velocity should be very low. With the Love wave data alone we can determine the shear velocity of second, third and fourth layers with an accuracy of ^{about} $\Delta 0.1$ km/sec and with the Rayleigh wave we can determine the shear velocity of third, fourth and fifth layers with the same degree of accuracy.

We can also determine the shear velocity of first layer using Love wave data and that of sixth layer using Rayleigh wave with an accuracy of about 0.2 km/sec.

As a result of information gained from partial derivative, we have divided all the parameters (α_i , β_i , G_i and H_i ; $i = 1, 2, 3, \dots, N$, where N - number of layers) into two groups Active - and passive - parameters. The active parameters are the shear velocity of second to sixth layers and the thickness of sedimentary and lower crustal layers.

(4.3.1) The Alternating Variable Search Method :

Each active parameter is considered in turn and altered until a minimum of the RMSD value; the value between the observed dispersion data and the calculated data for the present model, is located, the remaining parameters remained fixed. The current best point therefore moves parallel to each axis in turn, changing direction when a minimum in the current direction of search is reached. In this present work step length is selected to coincide with the accuracy we are looking for each of these active parameters (In case of β , step length = ± 0.1 km/sec).

In most cases this method is extremely inefficient for the interpretation of surface wave data, when the number of active parameters is large and/or phase - and group - velocity data for Love - and Rayleigh - wave is used. Inefficient in the sense that very large number of iterations (in other words, trial models) and therefore longer computing time is required.

A modification of the above method, using the fact that increases (or decreases) in β causes only increases (or decreases) in the phase velocity, can be used to fit the phase velocity dispersion with an improved efficiency.

In this method, difference in phase velocity value between the observed and the calculated data for an initial model at the period T_1 , where T_1 corresponds to the maxima in the plot of $\left(\frac{dG}{d\beta_i}\right)_T$ versus T curve, divided by the value of $\left(\frac{dG}{d\beta_i}\right)$ at T_1 is taken as the amount through which active parameter β_i would be altered.

Each active parameter is considered in turn and the whole

procedure is repeated several times until a theoretical curve fits with the observed curve within the experimental error.

A third form of this method is that the active parameters are selected two by two and their values varied by fixing one value alternately and varying the other by discrete increments, within upper and lower bounds defined by geological plausibility. The RMSD value is contoured and the values correspond to a minimum value of RMSD is taken down. This procedure is repeated for all combination of active parameters, until we have a minimum for all the active parameters. This method requires very large number of computations, therefore requires longer computer time. We used this method extensively at the beginning of our studies and found that there was always one minimum in the space we explored.

(4.3.2) The Steepest Descent Method :

This is the simplest gradient method and is based on a local linearization of the objective function (RMSD) by neglecting the second order and higher terms. This method is first used in seismology by Pekeris (1966) in the determination of the internal constitution of the earth.

A form of this method we programmed is starting from an initial model; $(RMSD)_I$ is the root mean square deviation between the observed data and that for the initial model, each active parameter is altered in turn through + 0.1 km/sec or - 0.1 km/sec according to bring the RMSD value down that is, less than $(RMSD)_I$ and the change in RMSD value is computed. The active parameter which introduces ^{the} largest change in RMSD value is chosen for alteration (Program 1).

The value of this active parameter is altered in steps (0.05 km/sec)

until a minimum of RMSD value is reached. Then the whole procedure is repeated several times until it reaches a global minimum (Minimum for all the active parameters). The confidence limit on each active parameter (Berry and Knopoff, 1967) is then determined.

Theoretical studies using the steepest descent method shows that, (a) provided we select the thickness of the layers to satisfy the resolution, shear velocity of the layers can be recovered within ± 0.1 km/sec, whatever the starting model may be. Further this method is found to be reasonably fast. (b) For a given dispersion curve, we need a structural model with a definite number of layers, depending on the shape of the curve, to satisfy it. No model can fit satisfactorily if the number of layers is reduced below this value. (c) Using this method one cannot recover the velocity of a thin layer even if it is known to exist. (d) If the number of layers is too great, large and unreasonable variations in shear velocity could occur, with adjacent layers developing unreasonably low and unreasonably high shear velocity.

(4.3.3) Powell - Conjugate direction Method :

Powell's method (Powell, 1964 and 1965) is probably the most effective of currently available direct search techniques, with its convergence being particularly impressive in the region of the optimum where the function can be well approximated by a quadratic.

Before any detail description of the Powell's method, let us first derive the mathematics for the generalized least square method :

It is required to find x_1, x_2, \dots, x_n , (x , say), to minimize

$$F(x) = \sum_{k=1}^m \left[f^{(k)}(x) \right]^2, \quad m \geq n \quad (1)$$

It is hoped that using a superscript to distinguish the m different functions that appear in the sum of squares will not be found confusing -

derivatives will be written out explicitly. In addition the notations

$$g_i^{(k)}(x) = \frac{d}{dx_i} f^{(k)}(x) \quad (2)$$

and

$$G_{ij}^{(k)}(x) = \frac{d^2}{dx_i dx_j} f^{(k)}(x) \quad (3)$$

will be used.

The method is iterative, and an iteration requires an approximation ξ to the position of the minimum. If the actual minimum is at $(\xi + \delta)$ then, by differentiating (1)

$$\sum_{k=1}^m g_i^{(k)}(\xi + \delta) \cdot f^{(k)}(\xi + \delta) = 0; \quad i = 1, 2, \dots, n. \quad (4)$$

By approximating the left hand side of (4) by the first two terms of the Taylor series in δ about ξ , equation (5) is obtained.

$$\sum_{k=1}^m \left[g_i^{(k)}(\xi) \cdot f^{(k)}(\xi) + \sum_{j=1}^n \left\{ G_{ij}^{(k)}(\xi) \cdot f^{(k)}(\xi) + g_i^{(k)}(\xi) \cdot g_j^{(k)}(\xi) \right\} \delta_j \right] \approx 0 \quad (5)$$

The least squares method hinges on the further approximation that the term $G_{ij}^{(k)}(\xi) \cdot f^{(k)}(\xi)$ can be ignored. This term is of order (k) if $f^{(k)}(\xi)$ is zero at the minimum, and it vanishes if f is linear in the variables. In all other cases the convergence of the procedure will be only linear, the correction to ξ being calculated by solving

$$\sum_{j=1}^n \left\{ \sum_{k=1}^m g_i^{(k)}(\xi) g_j^{(k)}(\xi) \right\} \delta_j = - \sum_{k=1}^m g_i^{(k)}(\xi) f^{(k)}(\xi), \quad (6)$$

$i = 1, 2, \dots, n.$

Note that the matrix of these equations is in general positive definite so that

$$\frac{d}{d\lambda} F(\xi + \lambda\delta) \Big|_{\lambda=0} < 0 \quad (7)$$

unless all the derivatives of $F(x)$ at ξ are zero. Therefore, unless ξ happens to be a stationary point of $F(x)$, extending the iteration to calculate a positive value of λ , λ_m say, which minimizes $F(\xi + \lambda\delta)$, provides a theoretical guarantee that the least squares method will converge. Of course $(\xi + \lambda_m\delta)$ is chosen as the new approximation to the minimum.

If the second derivatives $G_{ij}^{(k)}(\xi)$ are not zero, the quadratic convergence depends on the functions $f^{(k)}(\xi)$ being of the same order as the correction δ . In this case numerical estimates of the derivatives $g_i^{(k)}(\xi)$ in (6) that are in error by δ are acceptable. On the other hand, if the second derivatives are zero, one expects numerical estimates of the derivatives to be exact. It is for these reasons that the procedure to be described has convergence comparable to the generalized least squares method.

The procedure without derivatives :

The new method is iterative, and at the start of an iteration n linearly independent directions in the space of the variables, $d(1)$, $d(2), \dots, d(n)$, say, are required together with estimates of the derivatives of the $f^{(k)}$ along the directions. The notation that will be used for the estimated derivative of the k^{th} function along the i^{th} direction is $\gamma^{(k)}(i)$, so

$$\gamma^{(k)}(i) \approx \sum_{j=1}^n g_j^{(k)}(x) \cdot d_j(i); \quad \begin{array}{l} i = 1, 2, \dots, n; \\ k = 1, 2, \dots, m. \end{array}$$

To equilibrate the matrix of equation (11), the directions should be scaled so that

$$\sum_{k=1}^m \left[\gamma^{(k)}(i) \right]^2 = 1; \quad i = 1, 2, \dots, n. \quad (9)$$

It is intentional that the notation does not allow for the dependence of $\gamma^{(k)}(i)$ on x , because the approximation to the derivative is a number which is calculated when $d(i)$ is chosen. If x is changed by δ , the resultant error in $\gamma^{(k)}(i)$ will be of order δ multiplied by a second derivative term, and it has been pointed out that this can be tolerated.

As in the least squares method, an approximation to the position of the minimum, ξ , is required and a correction to it, δ , is calculated. The correction is worked out by substituting the approximate derivatives in (6), if

$$\delta = \sum_{i=1}^n q(i) \cdot d(i) \quad (10)$$

$$\sum_{j=1}^n \left\{ \sum_{k=1}^m \gamma^{(k)}(i) \gamma^{(k)}(j) \right\} q(j) = - \sum_{k=1}^m \gamma^{(k)}(i) f^{(k)}(\xi);$$

$$i = 1, 2, \dots, n. \quad (11)$$

It is convenient to define

$$p(i) = - \sum_{k=1}^m \gamma^{(k)}(i) f^{(k)}(\xi) \quad (12)$$

The iteration is extended to find λ_m to minimize $F(\xi + \lambda\delta)$ but, because (8) is an approximation, λ_m is not necessarily positive. The procedure used for finding the minimum along a line is as follows :

The function is evaluated at a base point x_1 and at $x_2 = x_1 + S$, S being the step-size, and we suppose that the two function values so obtained are f_1 and f_2 respectively.

The point x_3 is chosen to be

$$x_1 + 2S \quad \text{if } f_1 \geq f_2$$

$$\text{but } x_1 - S \quad \text{if } f_1 < f_2$$

The function is then evaluated at x_3 to give a value f_3 .

The optimum x_m of the quadratic passing through these three points is given by

$$x_m = \frac{1}{2} \frac{(x_2^2 - x_3^2) f_1 + (x_3^2 - x_1^2) f_2 + (x_1^2 - x_2^2) f_3}{(x_2 - x_3) f_1 + (x_3 - x_1) f_2 + (x_1 - x_2) f_3} \quad (13)$$

If x_m and whichever of x_1 , x_2 and x_3 corresponds to the smallest function value differ by less than the required accuracy, the minimum is assumed to have been located. Otherwise the function is evaluated at x_m , and one of the three points x_1 , x_2 and x_3 is discarded. The discarded point is that which corresponds to the greatest function value, unless by discarding some other point, we can achieve a bracket on the minimum which would not be obtained otherwise. The process of quadratic interpolation is then continued.

Two undesirable possibilities exist, however. First, if too large an extrapolated step is allowed, this can introduce a point distant from the minimum, which can be detrimental to the search, as for example when this wayward point returns to the vicinity of the minimum only slowly. Secondly, the turning point predicted by equation (13) will be a maximum instead of a minimum if

$$\frac{(x_2 - x_3) f_1 + (x_3 - x_1) f_2 + (x_1 - x_2) f_3}{(x_1 - x_2)(x_2 - x_3)(x_3 - x_1)} \geq 0$$

If either of these circumstances does arise, a specified maximum permissible step is taken in the direction of decreasing f , and the point so obtained is used to replace one of x_1 , x_2 , and x_3 as before.

In the meantime, the estimates of the derivatives of the function $f^{(k)}$ in the direction δ are worked out in the following way :

The function values $f^{(k)}(\xi + \lambda_1 \delta)$ and $f^{(k)}(\xi + \lambda_2 \delta)$, $k = 1, 2, \dots, m$, which yield the lowest and next lowest values of

$F(\xi + \lambda\delta)$ are noted. These are differenced to provide the approximation

$$\frac{\partial}{\partial \lambda} f^{(k)}(\xi + \lambda\delta) \approx \frac{f^{(k)}(\xi + \lambda_1\delta) - f^{(k)}(\xi + \lambda_2\delta)}{(\lambda_1 - \lambda_2)} = U^{(k)}(\delta) \quad (14)$$

The approximation is improved by

$$V^{(k)}(\delta) = U^{(k)}(\delta) - \mu f^{(k)}(\xi + \lambda_m\delta) \quad (15)$$

where

$$\mu = \frac{\sum_{k=1}^m \left[U^{(k)}(\delta) \cdot f^{(k)}(\xi + \lambda_m\delta) \right]}{\sum_{k=1}^m \left[f^{(k)}(\xi + \lambda_m\delta) \right]^2} \quad (16)$$

because it is known that the derivative of $F(x)$ along δ at $\xi + \lambda_m\delta$ must be zero. Finally $V^{(k)}(\delta)$ and δ are scaled so that the Euclidean norm of the derivative vector is unity, in accordance with (9).

Of course the derivatives along δ have been calculated in order that δ may replace one of $d(1), d(2), \dots, d(n)$. $d(t)$ is replaced, where t is the integer such that

$$\left| p(t) \cdot q(t) \right| = \max \left| p(i) \cdot q(i) \right| \quad 1 \leq i \leq n \quad (17)$$

$\xi + \lambda_m\delta$ replaces the original value of ξ , and then the next iteration may be commenced.

An important point to notice is that, apart from calculating function values, the most laborious stage of the iteration is solving the equations (11). After each iteration just one row and one column of the left-hand side matrix are changed so that, if the inverse of the old matrix is stored, that of the new can be worked out by partitioning in an n^2 rather than an n^3 process.

For the first iteration, $d(1), d(2), \dots, d(n)$ are chosen to be the coordinate directions. A starting value of ξ has to be

provided; and then values of $\gamma^{(k)}(i)$ must be worked out. This calculation requires increments E_1, E_2, \dots, E_n to be specified which will yield reasonable estimates of the first derivatives.

They are calculated from

$$\gamma^{(k)}(i) = S_i \cdot \frac{f^{(k)}(E_1, E_2, \dots, E_{i-1}, E_{i+1}, E_{i+1}, \dots, E_n) - f^{(k)}(E)}{E_i} \quad (18)$$

where S_i is a scaling factor, introduced so that (9) may be satisfied.

In accordance with (18), for the first iteration,

$$d(i) = (0, 0, \dots, 0, s_i, 0, \dots, 0) \quad (19)$$

the only non-zero element being the i^{th} component.

The subroutine VAO4A, which contains the Powell Conjugate direction method, is used together with the Dorman's PV7 computer program, to develop a new Non-Linear optimization technique. This technique would be used to invert the observed surface wave dispersion data (Program 2).

In such case

$$f^{(k)}(x) = (C_0 - C_c) = \Delta C$$

where C_0 is the observed velocity value at period k ;

C_c is the calculated velocity value at period k for a model;

x_i is an active parameter;

n the number of active parameters;

m the number of data points.

$$F(x) = n \cdot (\text{RMSD})^2$$

Unlike Least square inversion techniques this program has the facility of imposing constraints on the active parameters. Constraints in geophysical work are usually some upper - and Lower - bounds on each active parameters serving as a guard against the geologically or physically unfeasibility.

The constraints will, therefore, be of a very simple form

$$X = z + (Z - z) \cdot \sin^2 Y$$

where,

X is the current value for the active parameter;

z the lower bound;
 Z the upper bound;
 and Y the initial value;

Further, the program is written in such a way that we can fit, in addition to phase - and group - velocity of Rayleigh - and Love - waves, the P- and S- wave delay time as well. After each iteration the best model, its dispersion curve together with RMSD value between the observed and the calculated dispersion curve would be printed out.

Theoretical studies using the above method shows that (a) If we fixed the thickness, compressional velocity and density of the layers, then whatever the starting model may be the shear velocities can be recovered to within ± 0.1 km/sec. Usually the neighbouring layers have ^{or} larger and smaller values than they ought to be.

If we assume that there is no experimental error, then shear velocities can be recovered to a very great accuracy. But, it may take large number of iterations.

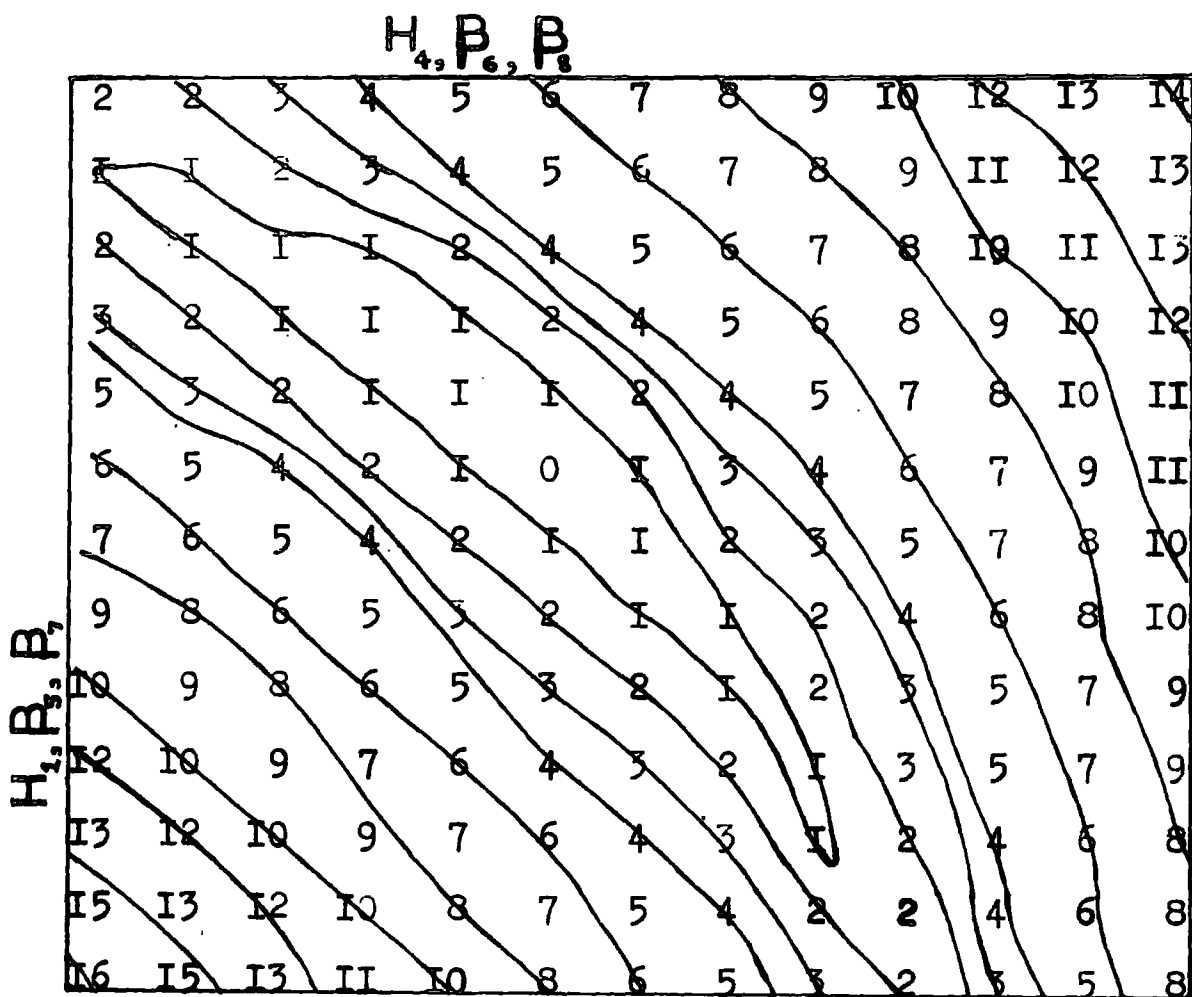
(b) If we allow the thickness and the shear velocity of certain layers to vary, then we may fail to recover the shear velocity with the same degree of accuracy as in the first case. But this would be compensated by proportional change in the thickness of the layers. Therefore it may be a good idea to keep the total thickness of the layer parameters fixed but vary the individual thickness of the layers.

(c) If the number of layers is too great, large and unreasonable variations in shear velocity could occur, with adjacent layers developing unreasonably low and unreasonably high shear velocity.

(d) This method break down when one try to vary shear velocity and density at the same time.

We can see clearly from the facts mentioned in this chapter that Powell - Conjugate direction method ^{is} the more powerful and flexible

Event: 20 April 1966 AAE-NAI Rayleigh Wave



RMSD value of first point(3,3) = 0.039
 RMSD value of ~~first~~ second point(10,10) = 0.097
 First point corresponds to Optimized model
 Second point corresponds to AFRIC model

FIG. 15

method for the interpretation of surface wave data.

In actual practice, the starting model should have almost all the characteristics of the final model. In case such a model cannot be constructed because of unavailability of other geophysical information then starting from a typical continental structural model, a model can be constructed using the information gained from the partial derivatives curves; this model is altered in shear velocity, using steepest descent method, to have an optimized model for the observed dispersion curve. Then this optimized model is treated as an initial model and the whole process is repeated.

To investigate the case of having more than one acceptable model in the hyperspace, which is formed by all the active parameters, A computer program is developed (Program 3) to take two dimensional section of the hyperspace. Each section can be varied at will. An extensive use of this program shows that whatever the section may be there is always one minimum; but the shape of this minimum is highly variable (Fig.15).

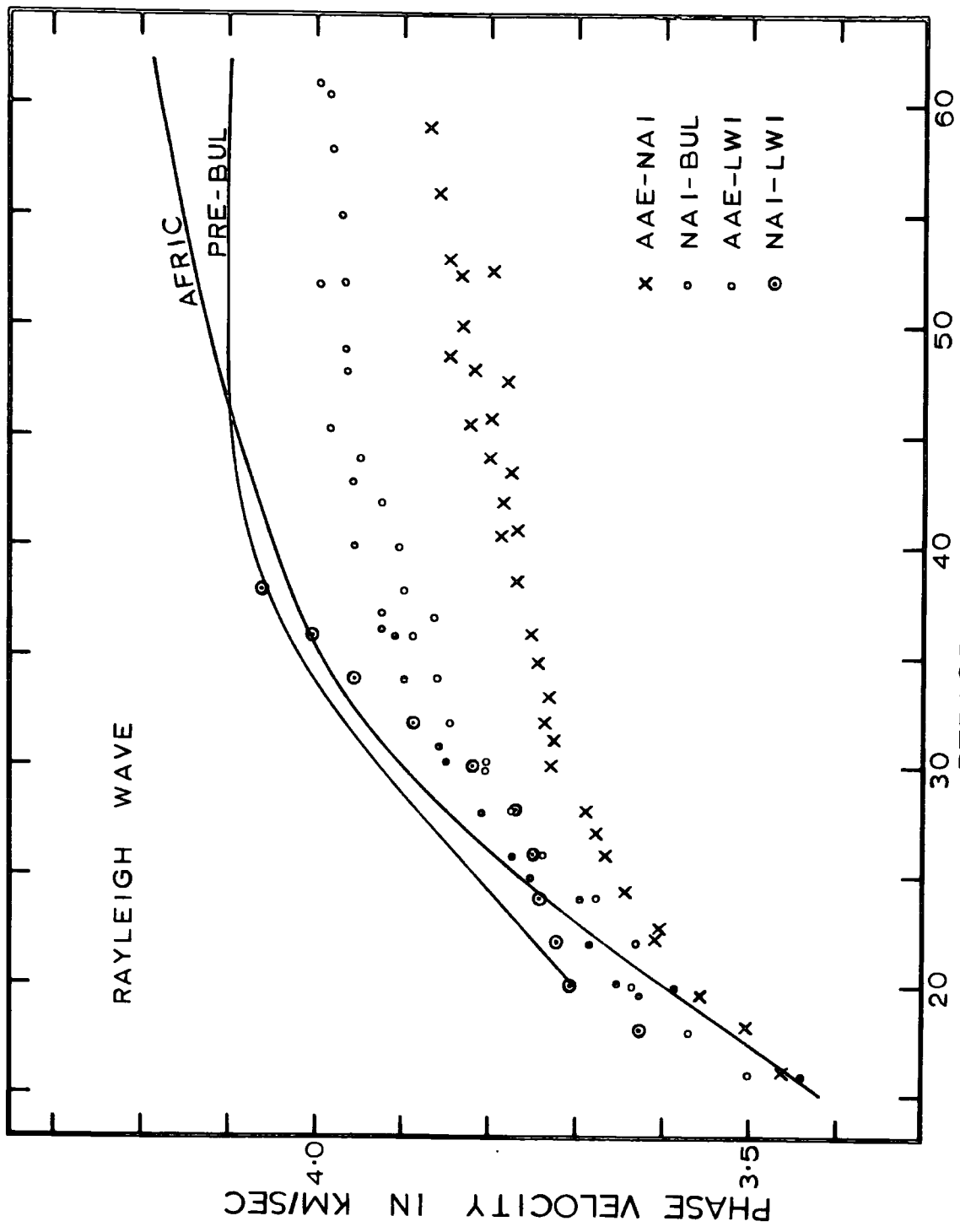


FIG. 16

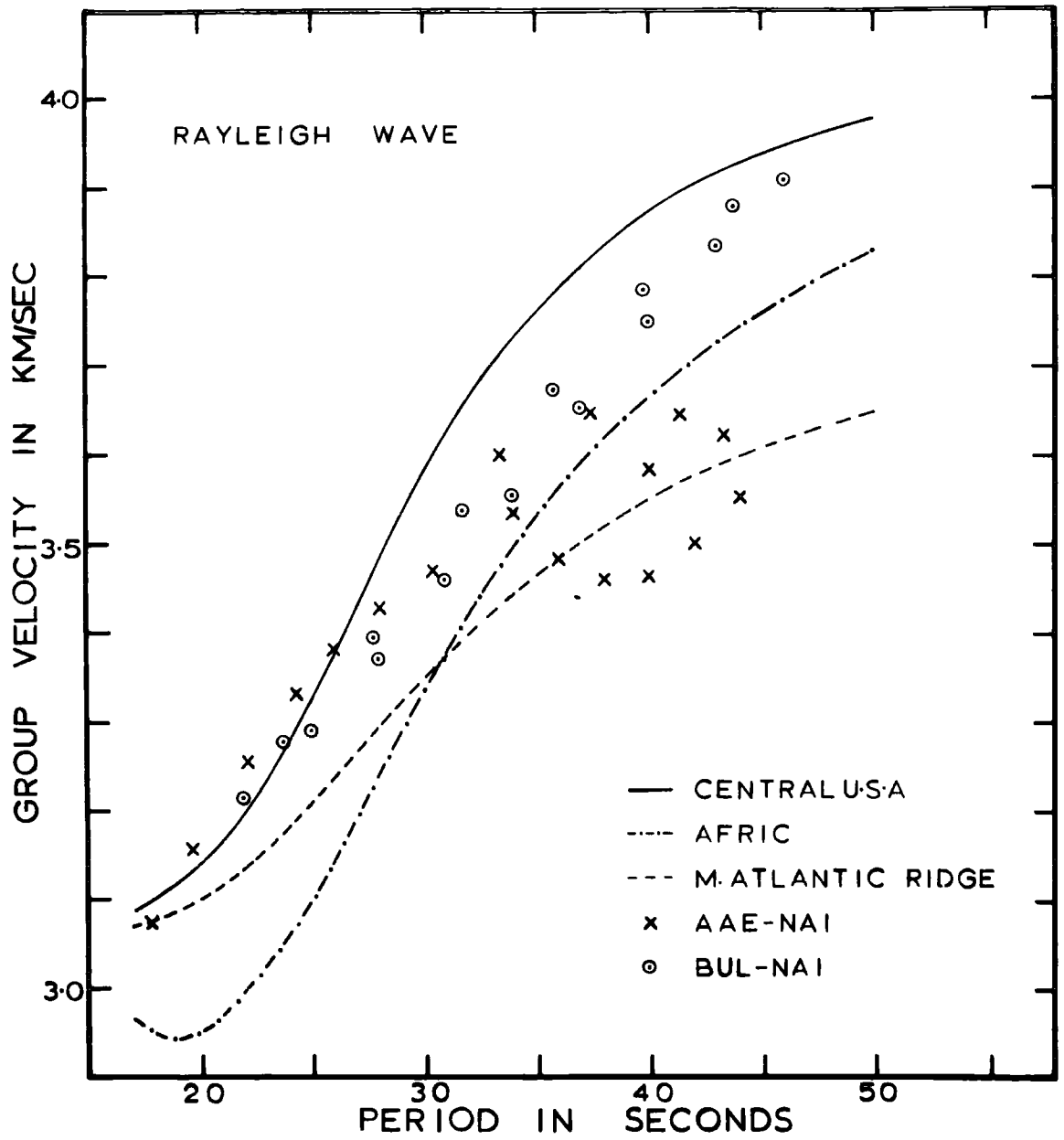


FIG. 17

CHAPTER 5

RESULTS AND INTERPRETATION

(5.1) Results and Regional Comparisons

The interstation Rayleigh wave phase velocities for the various station pairs; together with the dispersion curve for the AFRIC model (Gumper and Pomeroy, 1970) and that for the path PRE - BUL (Bloch, Hales and Landisman, 1969) were shown in Fig. 16 and interstation group velocities for the same station pairs together with that for AFRIC, central United States and Mid-Atlantic ridge type model were shown in Fig.17.

The refraction of surface waves, for example at the continental margins, can cause interstation phase velocity determination to be too high, if both the epicentre and a pair of stations are on a great circle. As we said earlier, ^{the} error, arise from this cause is only about 0.02 km/sec at 20 sec; at longer periods the error is smaller. Therefore the low velocity values at longer periods, especially along the AAE - NAI path, cannot be explained in terms of refraction. The other phenomenon which could take place between AAE - NAI stations is that of Guided wave (Capon, 1970). Guided along the rift valley between the two stations. In such case, ^{the} effective path difference between the stations become greater; and interstation velocity become almost in line with that of AFRIC model, which contradict the very necessary condition for the existence of Guided wave. Further, a possible break in the surface rift structure near Lake Rudolf, create problem for the existence of such a wave.

Diffraction phenomena (McGarr, 1969 a, b) which could take place outside the region of interest may introduce some error in the calculated velocity value. But the fact that we had, for several interstation paths,

events from either direction and the velocity values for these events are found to be the same within the experimental error; shows that the measured velocity dispersion does represent the structure beneath this path. Since it is very unlikely that the region outside, that bound the interstation path is the same on either side.

For the path NAI - LWI, the interstation phase and group velocities for the event from the west (28 June 1964) were found to be low and have energy only in the period range 20 - 30 sec. For the same path, the interstation phase and group velocities for the event from the east (18 Oct 1964) were found to be very high, higher than that for the AFRIC model. This difference in the velocities for the paths NAI - LWI and LWI - NAI could be due to lateral variation in the structure between the two stations (Abe, Suzuki, 1970). Since the record from the event 28 June 1964 is not a good one and for this event great circle path differ from the interstation path by about 12° , we need to have at least one good event from west to verify the theory of lateral variation along the path NAI - LWI (no such record available in our study).

We have used only records from the event 18 Oct 1964 to calculate the interstation velocities between NAI - LWI, path. The shape of the continental margin at which the great circle path intersected (Fig.8) created some doubt on this high velocity values; and indicated the possibility of refraction. Using AAE as third station, we calculated the direction of propagation of Rayleigh wave spectrum (Tripartite Method) and then the interstation phase - and group velocities. In actual fact, the application of Tripartite method over this area is not fully justified: because we are assuming that the structure is uniform throughout this area (North of East Africa). The calculated phase - and group velocities are shown in Fig. 16 and 17 respectively. These velocities now seem to be in line with that for a shield

type area.

Knopoff (1969) has shown that the phase and group slowness in inhomogeneous media can be represented by

$$\frac{1}{c} = \int_{x_1}^{x_2} \frac{dx}{c(x)} \Big/ \int_{x_1}^{x_2} dx; \quad \frac{1}{u} = \int_{x_1}^{x_2} \frac{dx}{u(x)} \Big/ \int_{x_1}^{x_2} dx$$

where c is the interstation phase velocity;

u is the interstation group velocity;

$x_1 - x_2$ is the interstation distance;

$c(x)$ is the phase velocity at co-ordinate x
(between the two stations);

$u(x)$ is the group velocity at co-ordinate x .

It follows that the apparent phase slowness is the distance average of the phase slowness and the apparent group slowness is the distance average of the group slowness. Therefore, whatever the deduction we make about the structure from the interstation phase and group velocities is the mean one.

For the purpose of regional comparison, phase velocities are more suitable than group velocities. Because increase (or decrease) in shear velocity causes only increase (or decrease) in phase velocities, whereas changes in the shear velocity cause both increase and decrease in group velocities. Therefore higher (or lower) phase velocities over a period range, say $T_1 - T_2$, would indicate high (or low) shear velocity at certain depth range, say $H_1 - H_2$, appropriate to that period range. On the other hand higher (or lower) group velocities over the same period range, $T_1 - T_2$, do not necessarily mean higher (or lower) shear velocity in the depth range, $H_1 - H_2$. It could be the result of abnormal shear velocity at certain other depth range.

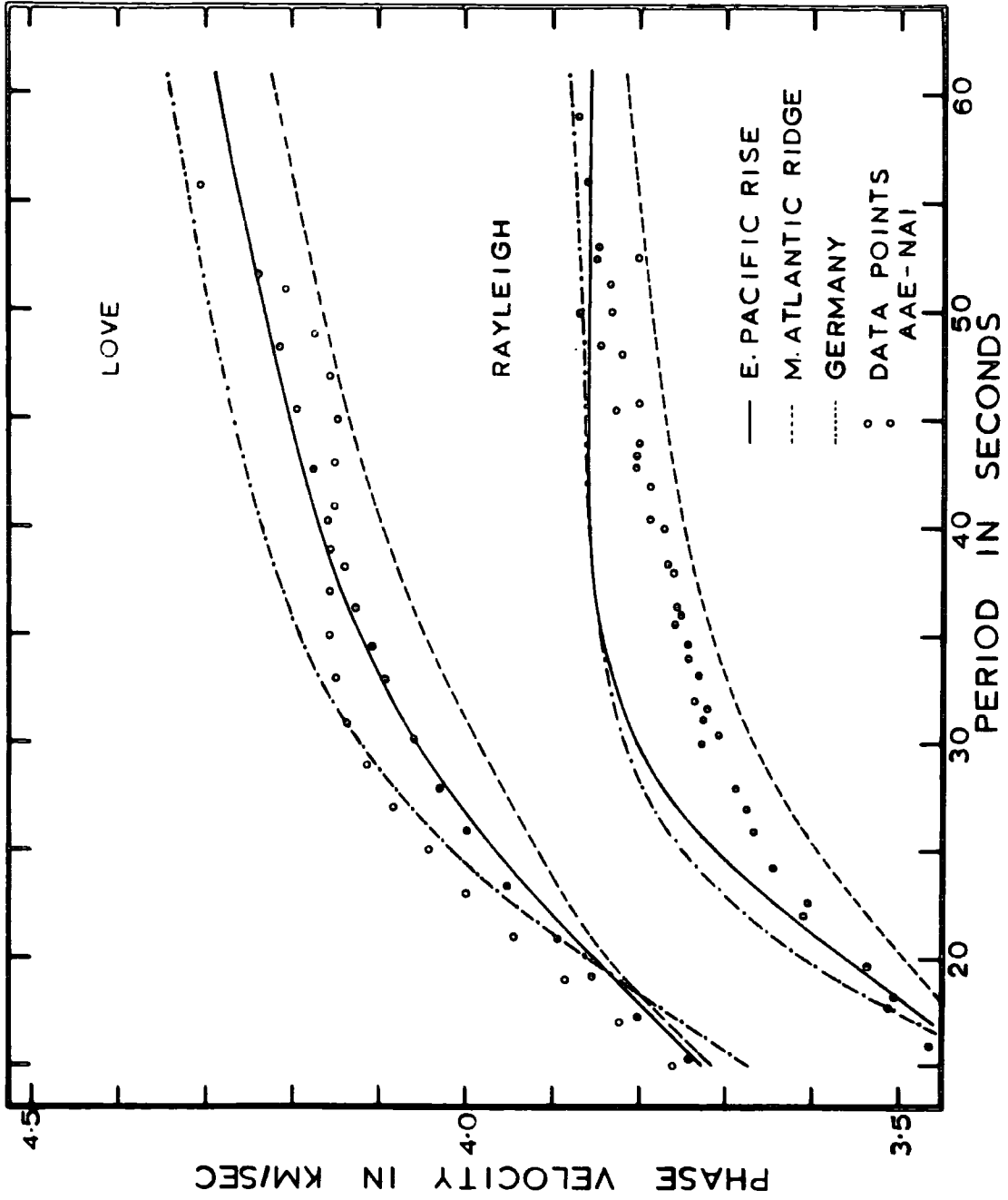


FIG. 18

The most characteristic feature of this set of Rayleigh wave phase velocity curves (Fig.16) is that there is a definite merging of phase velocities from longer to shorter periods. The spread at 60 sec period is 0.33 km/sec whereas at 20 sec period this is reduced to 0.1 km/sec. This seems to indicate that there is a large degree of lateral inhomogeneity in the upper mantle under East Africa; maybe in the lower crust as well. The regional gravity map over this area would certainly be in agreement with the above conclusion.

Pilant (1967) studied the regional differences in phase and group velocities of long period Rayleigh waves using that portion of the network of World Wide Standard Seismic Stations located on the North American continent. Waves have been analyzed that traverse the continent from many azimuths. One major trend appears : there is a definite merging of phase velocity values as one goes from longer to shorter periods, at 50 sec period spread is 0.35 km/sec whereas at 20 sec period it is reduced to 0.18 km/sec.

Rayleigh wave phase velocity determinations for the path AAE - NAI have the lowest velocity values. For the paths BUL - NAI and AAE - LWI the velocity values lie between those for the AFRIC and for the AAE - NAI path. From this, it seems mean upper mantle shear velocity drops from south to north along the path PRE - BUL - NAI - AAE. The phase velocity values for the path NAI - LWI seem to be, roughly, in agreement with the PRE - BUL dispersion, except the detail characteristic of the curve.

A comparison of Rayleigh - and Love wave phase velocity dispersion curves for different areas with that for AAE - NAI is shown in Fig.18. The curves plotted are those for the Mid-Atlantic Ridge (Francis, 1969) and the East - Pacific rise (Knopoff, Schlue and Schwab, 1970) type

GERMANY MODEL

| | H | ALPHA | BETA | RHO |
|----------|-------|-------|------|------|
| Crust : | 1.5 | 3.5 | 2.0 | 2.50 |
| | 5.0 | 5.6 | 3.3 | 2.75 |
| | 13.5 | 6.0 | 3.5 | 2.85 |
| | 10.0 | 6.7 | 4.0 | 3.00 |
| Mantle : | 50.0 | 8.15 | 4.5 | 3.30 |
| | 140.0 | 8.20 | 4.15 | 3.40 |
| | 100.0 | 8.49 | 4.77 | 3.53 |
| | | 8.70 | 4.85 | 3.70 |

CENTRAL UNITED STATES

| | H | ALPHA | BETA | RHO |
|----------|----------|-------|------|-----|
| Crust : | 11.0 | 6.10 | 3.50 | 2.7 |
| | 9.0 | 6.40 | 3.68 | 2.9 |
| | 18.0 | 6.70 | 3.94 | 2.9 |
| Mantle : | 24.0 | 8.15 | 4.75 | 3.3 |
| | 40.0 | 8.20 | 4.61 | 3.3 |
| | 180.0 | 8.20 | 4.45 | 3.3 |
| | ∞ | 8.70 | 4.80 | 3.6 |

EAST PACIFIC RISE

| | H | ALPHA | BETA | RHO |
|----------|----------|-------|------|------|
| Mantle : | 86.0 | 8.00 | 4.45 | 3.44 |
| | 46.0 | 7.95 | 3.50 | 3.44 |
| | 47.0 | 8.23 | 4.54 | 3.44 |
| | 100.0 | 8.49 | 4.77 | 3.53 |
| | ∞ | 8.81 | 4.89 | 3.60 |

MID - ATLANTIC RIDGE

| | H | ALPHA | BETA | RHO |
|----------|----------|-------|------|------|
| Mantle : | 240.0 | 7.4 | 4.20 | 3.24 |
| | 100.0 | 8.2 | 4.50 | 3.53 |
| | ∞ | 8.7 | 4.85 | 3.70 |

Table 9

upper mantle structure with AFRIC crust (Table 9), and that for the path between Stuttgart and Oropa, along a continental graben and taphrogenic fracture zone, in S.W. Germany (Seidl and Knopoff, 1965).

For the station pairs AAE and NAI, the interstation Love wave velocity values for the event 26 July 1967 are different from that for the event 20 April 1966. This difference must be due to difference in the interstation paths; for the event 26 July 1967 about one-half to two-third of the interstation path runs along the rift valley system, whereas for the other event the interstation path on an average about 100 km away from the rift valley system. Therefore this Love wave phase velocity data indicates lateral variation in the structure across the eastern rift.

The East-Pacific rise Love wave phase velocities are closely in agreement with AAE - NAI Love wave phase velocities (black dot); but there is a substantial difference between AAE - NAI Rayleigh wave phase velocities and those for the East-Pacific rise in the period range 25 to 50 sec. Love - and Rayleigh wave phase velocities for the Germany model are higher than those of the observed corresponding velocities for periods above 20 sec. The shape of the Rayleigh and Love wave phase velocity dispersion curves for Mid-Atlantic ridge type model are similar to that of the observed data; but have lower values. Since the major difference between the three structural models used for comparison is that two of those, Germany and East Pacific rise; have higher velocity lid (uppermost upper mantle) of about 50 - 86 km thickness above the low velocity channel, and that Rayleigh wave phase velocity for Germany and East Pacific rise model is higher than that of observed velocity values in the period range 25 - 50 sec (corresponds to depth range of 40 - 85 km) shows that if a higher velocity lid exist above the low-velocity channel, for the path AAE - NAI, then it must be fairly thin. The comparison of

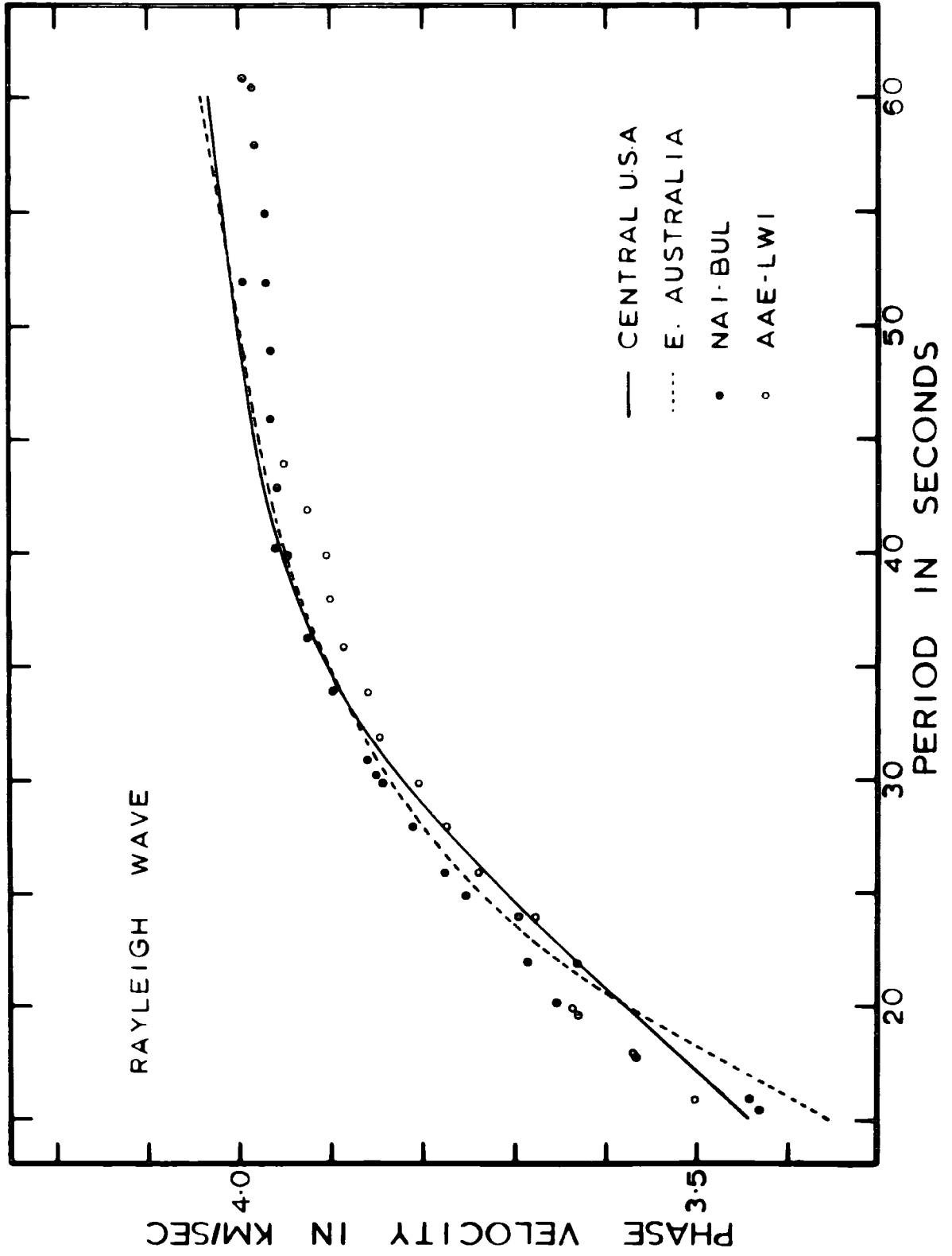


FIG. 19

group velocities for the path AAE - NAI with that for AFRIC model would support this conclusion.

A comparison of Rayleigh wave phase velocity values for the central United States (McEvelly, 1964) and that for the Charters Towers - Adelaide path in eastern Australia (Landisman, Dziewonski and Sato, 1969) with the Rayleigh wave phase velocities observed for the paths BUL - NAI and AAE - LWI are shown in Fig. 19.

The difference between the Rayleigh wave phase velocities for the central United States and that for the eastern Australia from our observed Rayleigh wave velocities for AAE - LWI and BUL - NAI paths are less than about 0.05 km/sec in the period range 15 - 60 sec. Slightly lower velocity values at longer periods may indicate a lower shear velocity in the upper mantle beneath BUL - NAI and AAE - LWI, when compared with that beneath central United States. The comparison of group velocity for the BUL - NAI path with that for AFRIC model and central United States would support the above conclusion.

An attempt to interpret the Rayleigh wave phase velocities for the BUL - NAI path as a mixed path; mixture of those for the AAE - NAI path and for those for PRE - BUL path (Bloch, Hales and Landisman, 1969) shows that in the period range 20 to 60 sec, the ratio 0.45 (approximately) of the total interstation path BUL - NAI^{is} equivalent in dispersive character (therefore presumably in the structure) to AAE - NAI and the rest, 0.55, equivalent to PRE - BUL. Such division along the BUL - NAI path coincide with the point of intersection of this path with the western rift. The regional gravity map (Fig.5) ^{of} East Africa would support this finding.

The application of the same technique for the Rayleigh wave phase velocities along the AAE - LWI path; as a combination of AFRIC type and AAE - NAI type dispersion, shows in the period range 28 to 44 sec,

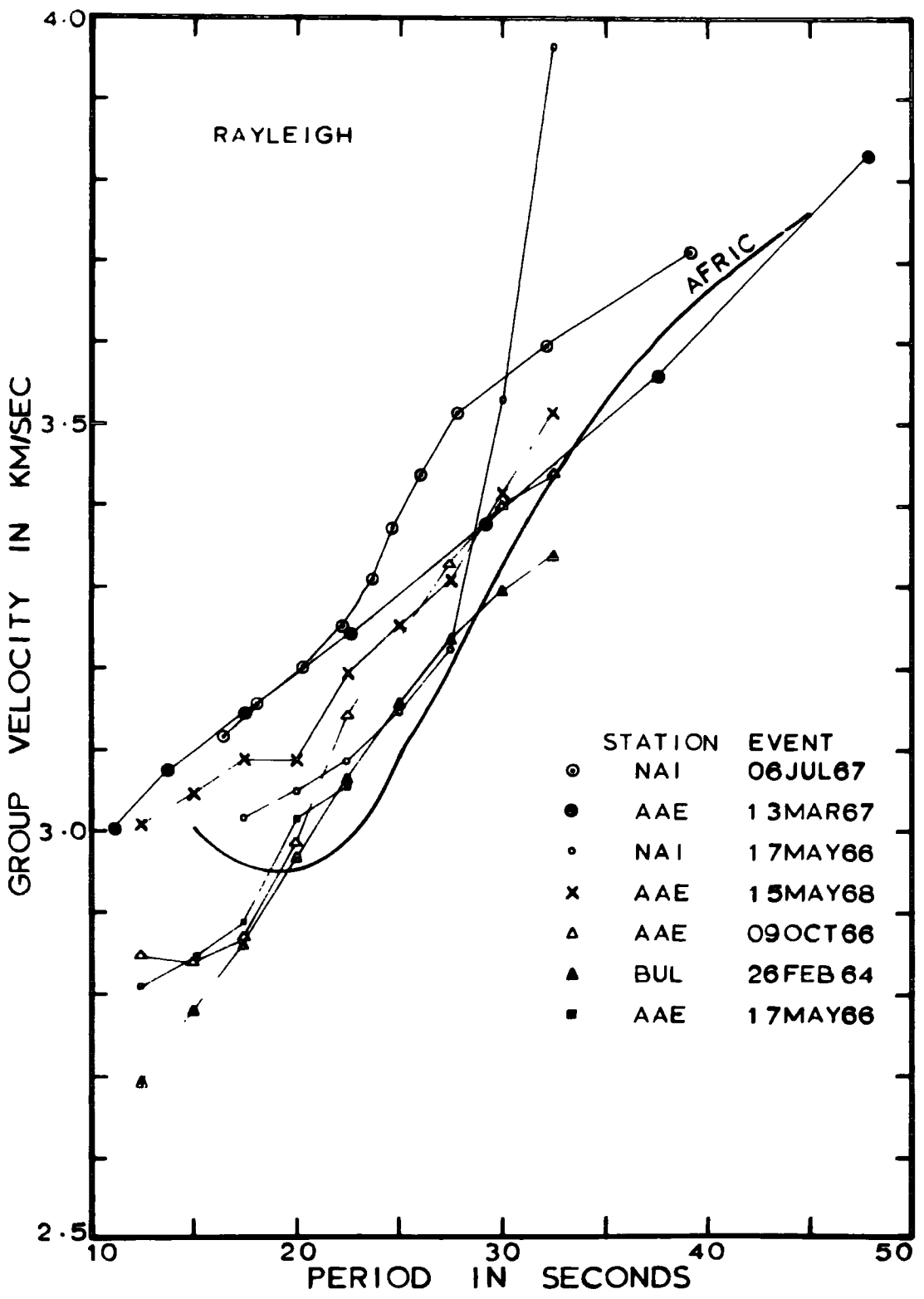


FIG. 20

corresponds to a depth of 47 - 77 km, the ratio 0.46 of the total path^{is} equivalent to AAE - NAI dispersion and the rest, 0.54, equivalent to AFRIC, below 28 sec period this does not hold.

The combination of this finding with the regional gravity map (Fig.5) ^{of} East africa suggests that a small portion of the path near LWI station, about one-sixth, and the rest, about one-third, of the path near AAE combine to form the ratio 0.46 of AAE - NAI path and the portion in between, ratio 0.54, is of AFRIC type.

The fact that the phase velocities along the path BUL - LWI are almost the same as that for the AFRIC model (Fig.16), which is a typical shield structure, and that about one-third of the interstation path runs on an average 150 km westwards of western rift shows that, if there is an anomalous region beneath the western rift (as indicated by P- delay beneath LWI) then the westward extension of it must be limited. This picture would be in agreement with regional gravity anomaly over this area.

Single station group velocity measurements for events in the African continent (Fig.9) together with that for AFRIC model are shown in Fig.20. In computing the group velocities from seismogram correction have been applied for the instrumental distortion, but no attempt was made to correct for source effects. In the case of major earthquakes, the finiteness effect could be significant and is given by the following expression.

$$u^1 = \frac{u}{1 - \frac{b}{2\Delta} \left(\frac{u}{Vf} - \cos \theta_0 \right)}$$

where $u = \frac{d\omega}{dk}$

$u^1 = \frac{\Delta}{t}$; measured from the seismogram.

$b =$ fault length.

V_f = rupture velocity along the fault
and θ_0 = Azimuth angle.

For most of the paths, group velocities in the period range 20 - 30 sec are higher than that for AFRIC model. These higher values are, probably, due to higher crustal shear velocities and/or lower velocities at a greater depth in the upper mantle.

(5.2) Interpretation

The phase velocity measurements in our study extend from 15 - 62 sec period. Therefore, as we have shown in chapter 4, we can study in greater detail only shear velocity - depth structure in the depth range 16.8 - 108.0 km. But it does not mean that phase and group velocity values in the period range 15 - 62 sec ^{are} independent of elastic wave velocities for layers above 16.8 or below 108.0 km. We should either give exact values for those elastic velocities if available from other geophysical studies or must assume certain values with the knowledge of geology. The accuracy to which elastic wave velocities ^{can} be assumed decreases as one goes further away from those boundaries, 16.8 and 108.0 km; this is clear from the partial derivative curves given in Fig.12 a, b, c and d. But crustal shear velocity has greater effect on the dispersion curve than the mantle shear velocity (Fig.14).

In our study, we dealt with large number of interstation paths and these paths run through various geological regions. For these paths we do not know accurately the elastic wave velocities of the layer beyond these boundaries, especially below 108.0 km. Therefore we have decided to allow one layer below and one layer above these boundaries to be ^{varied}. As we said in chapter 4, with the accuracy of our velocity data we can determine the elastic velocity of these layers within

an accuracy of about 0.2 km/sec. For the layers below about 200 km, and for the upper crustal layer we have assumed elastic wave velocities from AFRIC model; which represent the western part of East Africa.

The density of the layers used in this study are those used for gravity interpretation (R.C. Searle, 1970) and the following relation is used between the shear and the compressional velocity (Anderson, 1965).

$$\alpha = 1.74 \beta$$

McEvelly in 1964 and others (Ref : Chapter 4) show that if we have large number of layers within a certain depth range (that is, thin layers), then we may have unreasonable variations in shear velocity with adjacent layers developing unreasonably low and unreasonably high shear velocity. Even though this is mainly due to interference (Ref : Non-Uniqueness), that is the change in the phase and the group velocities over the period range due to a change in the shear velocity in one layer is to a great extent compensated by change in the shear velocity in the neighbouring layer or layers (within the experimental error). We cannot completely deny that such a layered structure could exist in real earth structure. Therefore what we will recover from dispersion curves is a mean shear velocity value over the depth range appropriate to each layer, further the boundaries of our final model may not have direct bearing on the actual structural boundaries. The importance of a minimum number of layers over a depth range appropriate to our observational data, required to fit a dispersion curve within the experimental error should be realised.

(5.2.1) Application of the Steepest Descent Method :

During the early attempt at deriving a shear velocity - depth structure from dispersion data, a Steepest descent method was employed

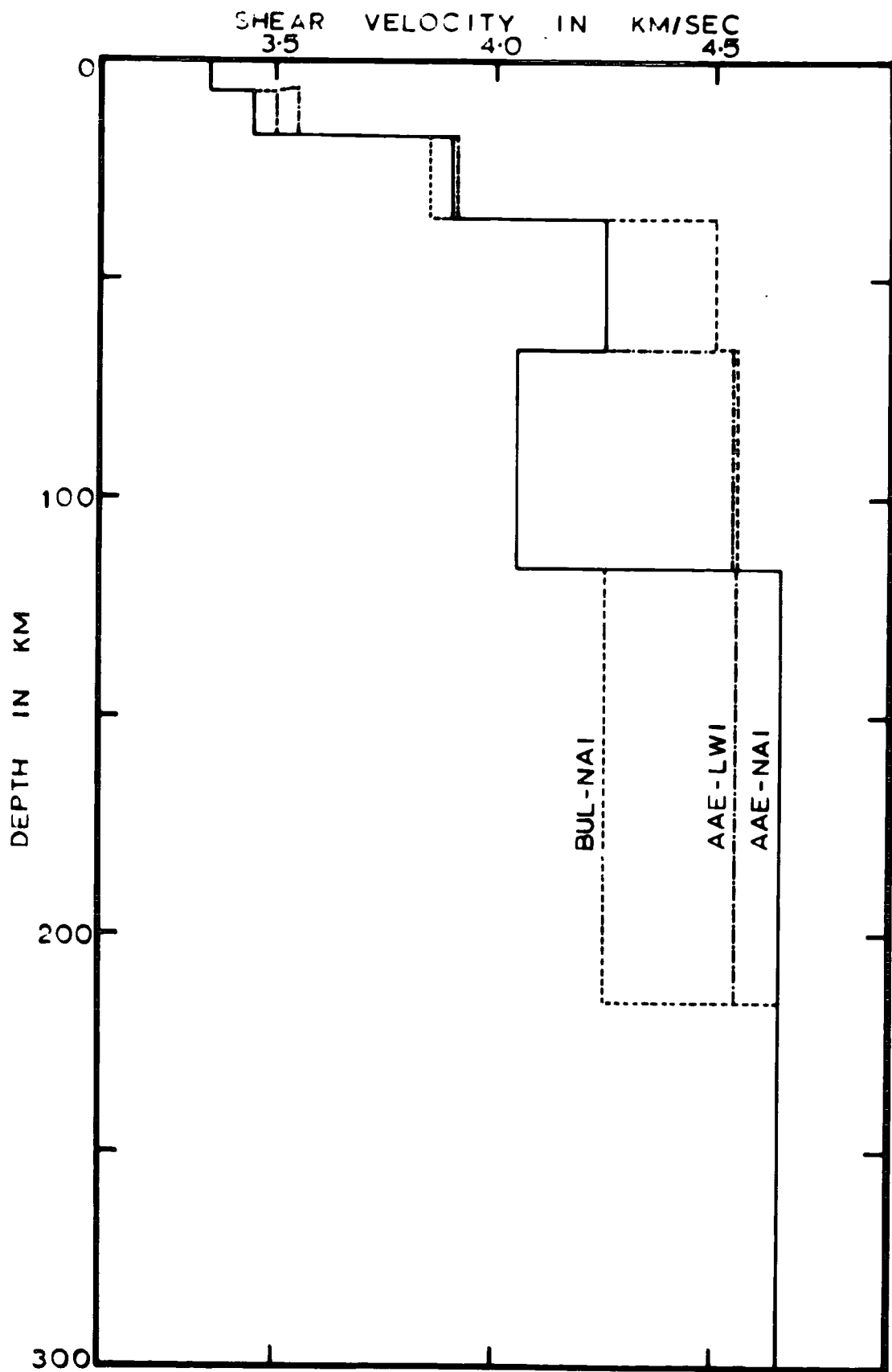


FIG. 2I

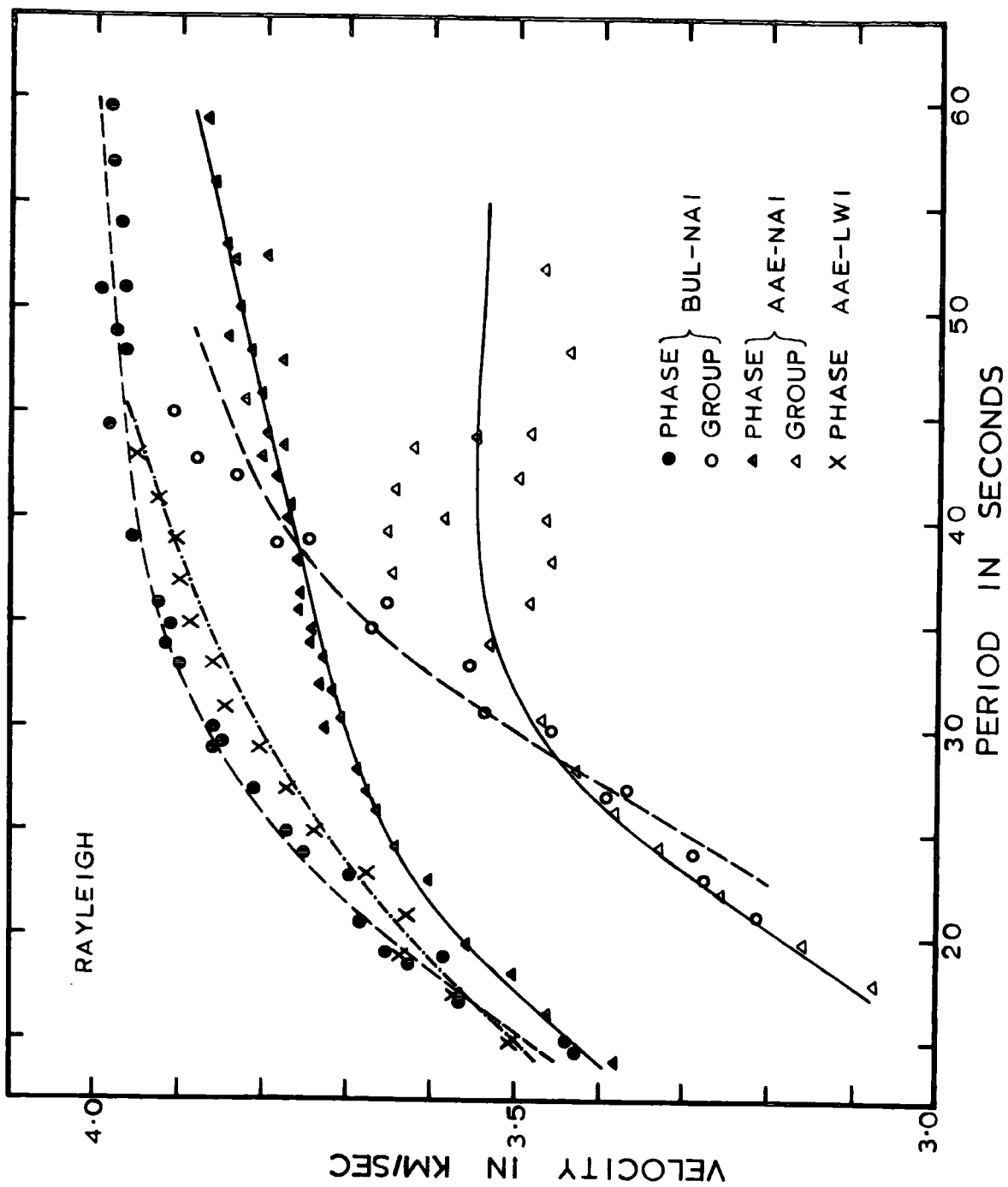


FIG. 22

for a few cases. The application of this method to these few real, observed cases would show not only that this method works very efficiently for such cases, but also helps to verify the structural model obtained by the application of other techniques (Powell - conjugate direction method).

As we said in Chapter 4, the layer thicknesses are taken according to the error of observation and the partial derivative to achieve an accuracy of about 0.1 - 0.15 km/sec in the shear velocity for those layers in the depth range appropriate to the period range considered. The velocities of the second to the sixth layers are considered as active parameters.

The shear velocity - depth structures obtained by using Steepest descent method for the paths BUL - NAI, NAI - AAE and AAE - LWI are shown in Fig.21. The computed Rayleigh wave phase - and group velocities are compared with the observed data in Fig.22 and ^{it is} found that the fit between the two is well within the experimental error (The possibility of a low velocity sedimentary cover is not considered and the only models used were those having high velocities at the surface).

It is interesting to note that the model obtained for the path AAE - NAI shows when compared with the AFRIC model, higher shear velocity for the lower crustal layer and substantially lower shear velocity for the upper mantle. This higher shear velocity for the lower crustal layer may be a real one, because such higher values are observed beneath NAI station from Spectral response ratio studies (Bonjer, Fuchs and Wohlenberg, 1969); and the total thickness of the crustal layers, 36.2 km, is less than that observed beneath NAI, 43 km, and beneath AAE, 39 km.

Since the structural model derived from a dispersion curve is the mean shear velocity over a depth range, it seems that the upper mantle

shear velocity beneath the path AAE - NAI drops from a normal mantle velocity or a low velocity value, greater than 4.25 km/sec and less than 4.63 km/sec, beneath the Moho to an even lower value (≤ 4.05 km/sec) between the depth of 66 - 116 km and then increases gradually to a normal value. This region of very low velocity may be where the formation of magma takes place (An optimized model for the above set of dispersion data, which has ^{an} ultra - low velocity layer at a depth of about 61 km is shown in Fig. 25).

For the path BUL - NAI, shear velocity of the lower crustal layer is slightly higher than that for AFRIC model. For the same path the shear velocity for the first two uppermost upper mantle layers is found to have almost the same value, 4.5 km/sec, therefore it is very likely that in the depth range 36 - 116 km shear velocity of the upper mantle is nearly uniform and is about 4.5 ± 0.1 km/sec. The velocity of the layer beneath this (that is, the sixth layer) is found to be 4.25 km/sec. Which may correspond to the low-velocity channel and can have shear velocity value of about 4.25 ± 0.25 km/sec.

If we extend the surface wave dispersion studies in South Africa by Bloch, Hales and Landisman (1969), to the north of East Africa through BUL, NAI to AAE, we can see clearly that not only the shear velocity values of the low velocity channel and the lid above it fall, but also the low velocity channel rises closer to the Moho discontinuity. This is in agreement with conclusion made from Sn-wave propagation study (Molnar and Oliver, 1969).

It is interesting to note that the structural model obtained for the AAE - LMI path shows for the third and the fourth layers the same velocity as that for the AAE - NAI path ($P_3 = 3.90$ km/sec and $P_4 = 4.25$ km/sec). The fifth and the sixth layers have the same velocity and equivalent to

4.55 km/sec. The absence of 4.05 km/sec layer beneath this path may indicate that there is large lateral variation in the mantle anomaly across the eastern rift; because the path AAE - NAI is much closer to the eastern rift than the path AAE - LWI, and/or more mantle anomaly^{is} on the eastern side of the eastern rift valley system than on the western side.

(5.2.2) Application of the Powell - Conjugate Direction Method :

The main handicap of the form of Steepest descent method we used are that no constraints can be imposed on the active parameters and it is difficult to vary more than one set of parameters, say ρ and H , at the same time. Further, one variable would be varied at a time in seeking for minimum.

As said in chapter 4, since Powell - conjugate direction method can overcome all these problems, it is widely used in this study for inversion of surface wave data.

At the beginning of the interpretation, using Powell - conjugate direction method, we used three upper mantle layers in the depth range from Moho to about 216 km and found that either the velocity of the two neighbouring layers turns out to be almost the same or the thickness of one of the layers became too thin. Therefore two upper mantle layer model in the depth range from Moho to about 216 km, is used to fit the observed dispersion data.

When using the Powell - conjugate direction method, the thickness of the sedimentary layer, the thickness and the shear velocity of the lower crustal layer and the first two upper mantle layers are all varied. Where Love wave data is used (AAE - NAI) the shear velocity of the second crustal layer is also allowed to vary.

The shear velocity of the sedimentary layer is assumed to be 2.0 km/sec and the total thickness of the first two upper mantle layers is kept fixed at 180 km. The upper and the lower limits used for the thickness of the sedimentary layer are 3.0 and 0.0 km (that is, when looking for a best model thickness of the sedimentary layer would be varied only in the range 0.0 to 3.0 km); and for the lower crustal layer 25.0 and 10.0 km respectively. For the limits of the shear velocities, extreme shield and tectonic values appropriate to the depth range are used.

Theoretical studies using an above type of structure and Rayleigh - and Love - phase and group velocities in the period range 15 to 60 sec show that, in fact, shear velocities can be recovered within 0.2 km/sec and the thickness of crustal layer within about 6 km. As said in chapter 4, the depth to interfaces between ^{the two} layers (In our studies, between two uppermost upper mantle layers) where the change in shear velocity is small could not accurately (within few km) be determined. Furthermore we have observed that the optimized model when using both phase and group velocity dispersion data is much closer to the actual model than when using, only, phase velocity dispersion data (after same number of iterations). This finding clearly demonstrates the importance of group velocity data in inverting surface wave dispersion data.

Since the single station group velocity measurements are made in the period range 12 to about 33 sec, it is suitable to study the shear velocities of last two crustal layers and the uppermost upper mantle layer. A Theoretical study using Rayleigh wave group velocities in the period range 12 - 33 sec show that we can, in fact, recover the shear velocities of the lower crustal layer within 0.2 km/sec and its thickness within 8 km. The shear velocities of the second and the uppermost upper mantle layer can be recovered within 0.05 km/sec and 0.15 km/sec

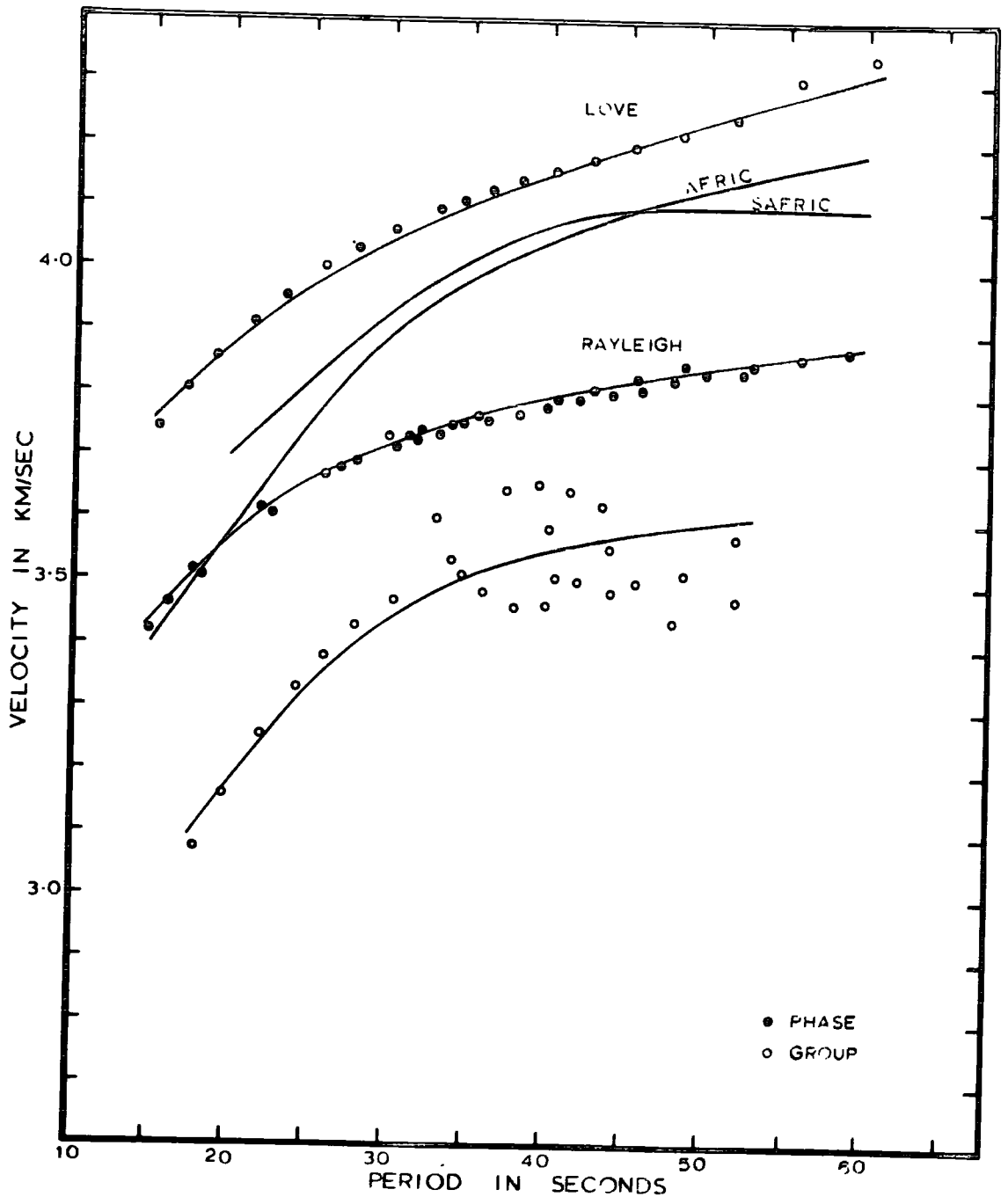


FIG. 26

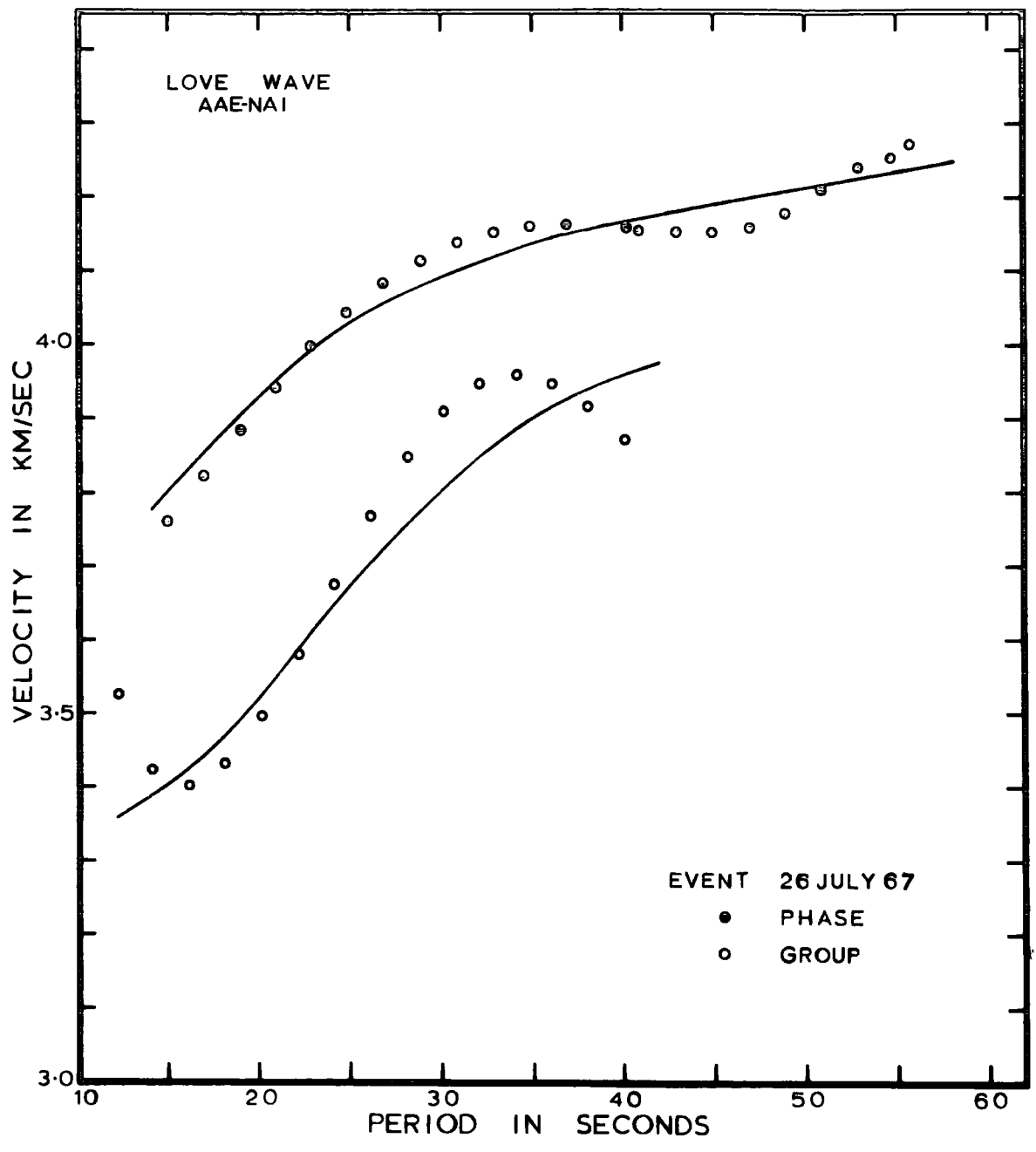


FIG. 27

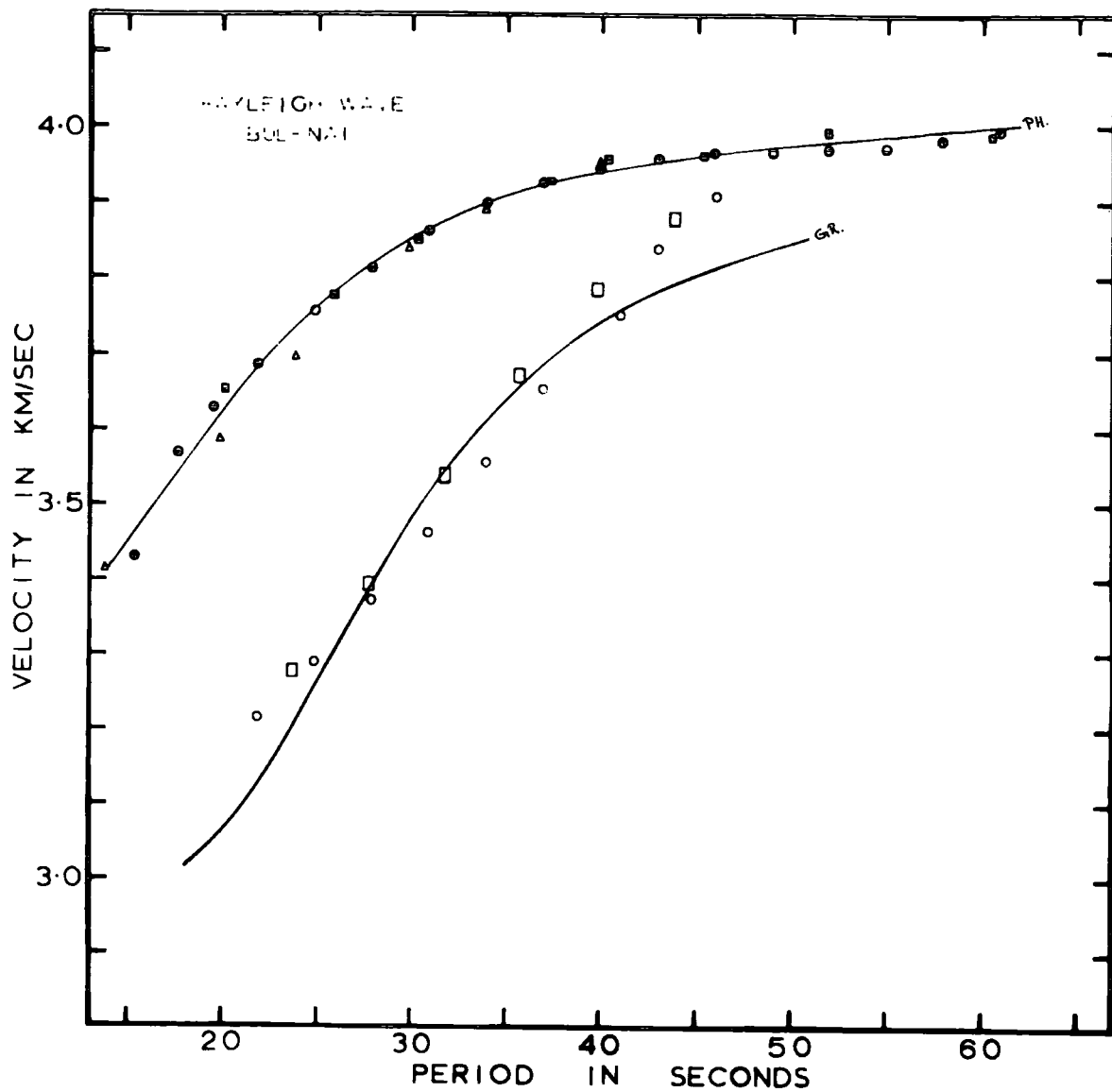


FIG. 28

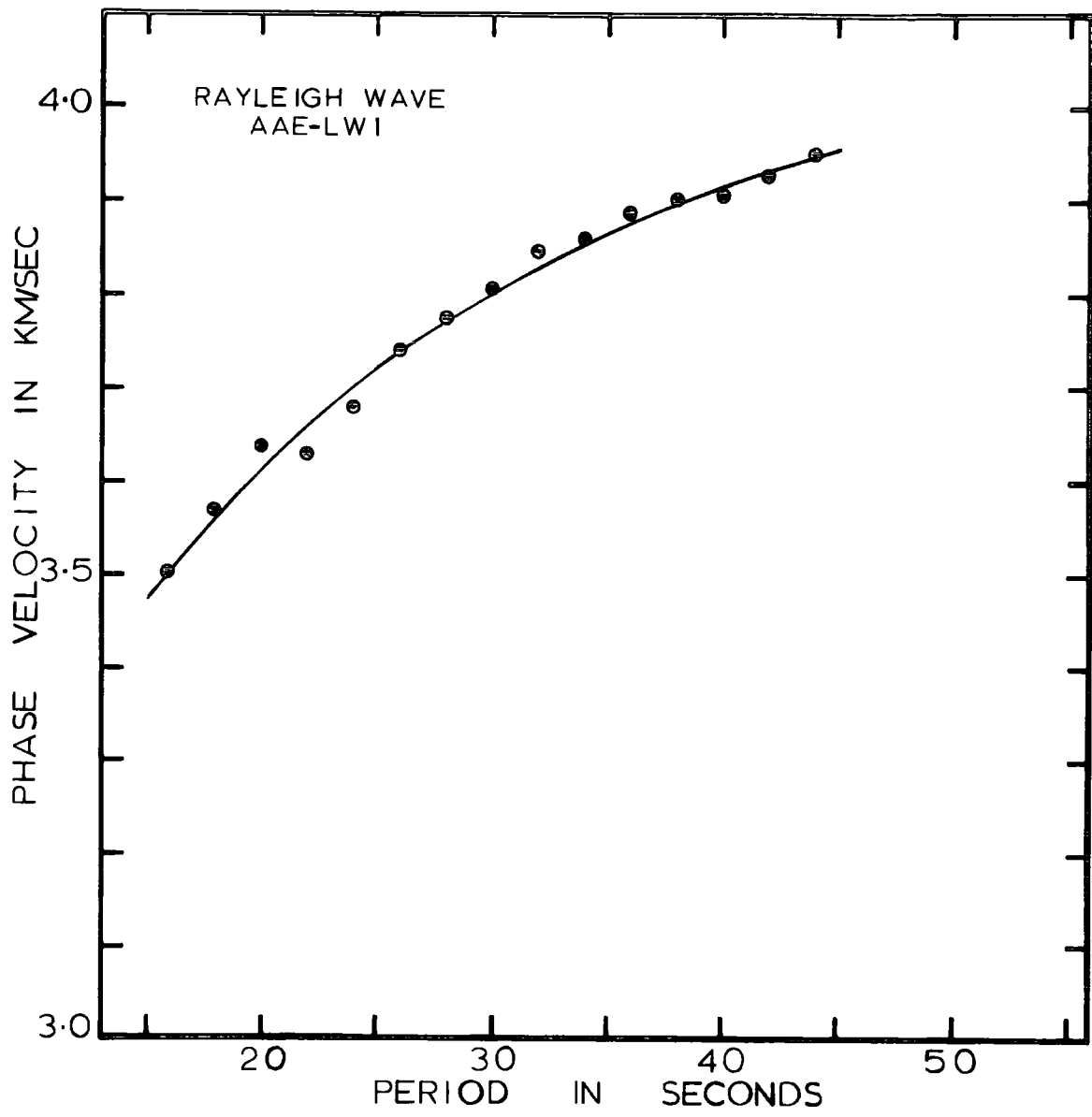


FIG. 29

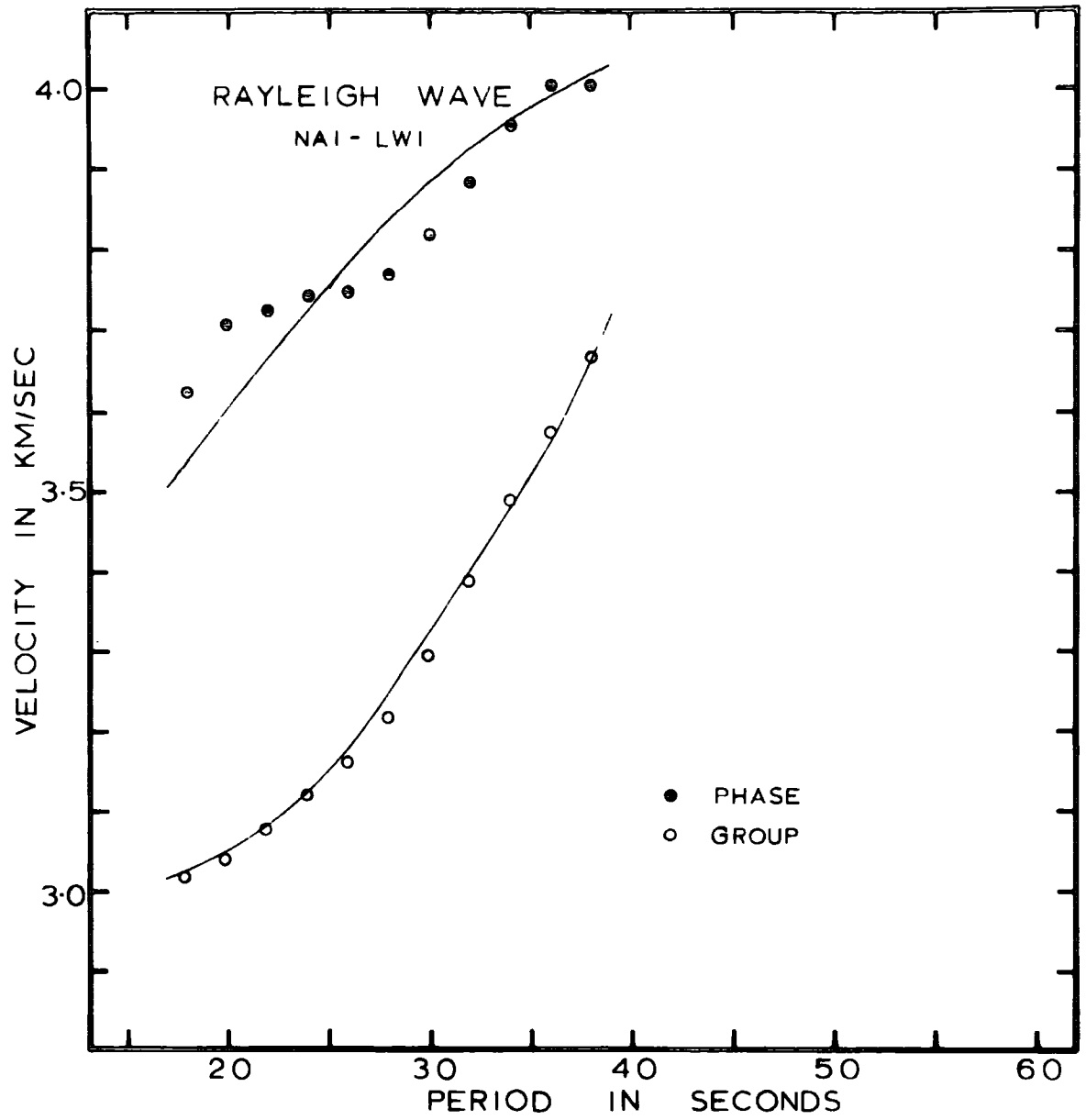


FIG. 30

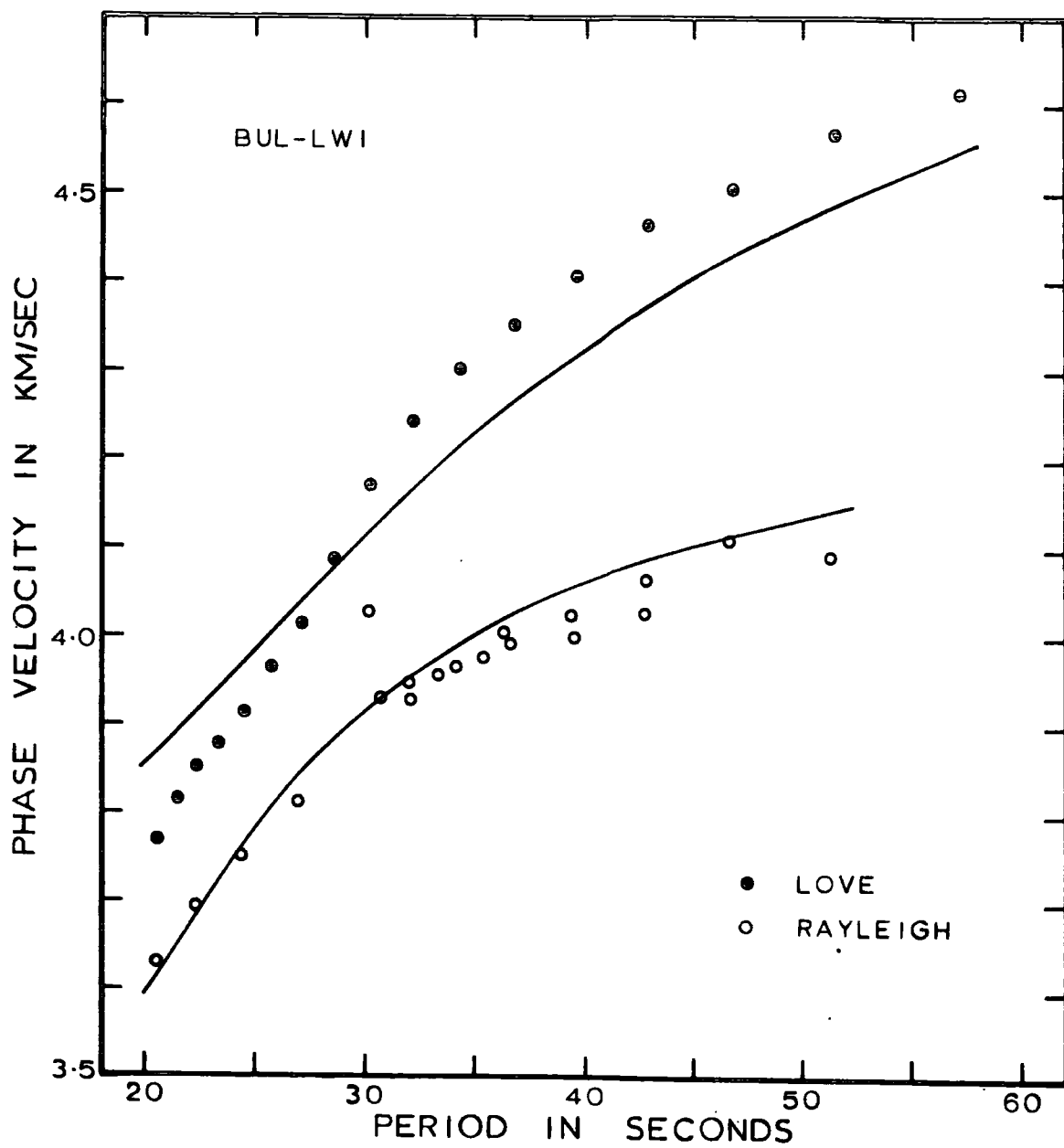


FIG. 3I

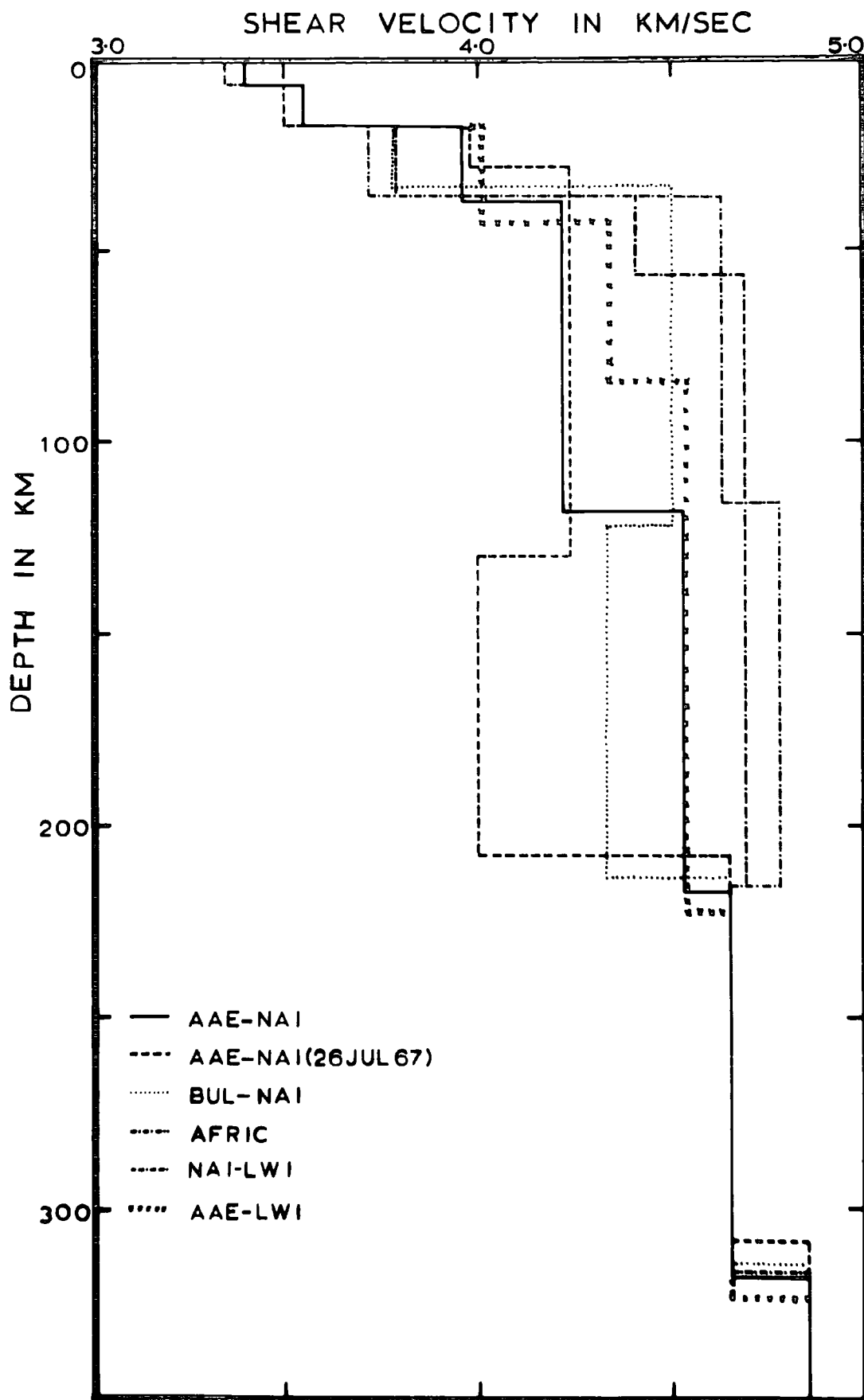


FIG. 32

3.

BUL - NAI

| | H km | α km/sec | β km/sec | ρ gm/cc |
|----------------|-----------------|--------------------|-------------------|-----------------|
| Crust : | 0.11 \pm 0.7 | 3.50 | 2.00 | 2.27 |
| | 7.00 | 5.90 | 3.40 | 2.67 |
| | 10.50 | 6.15 | 3.50 \pm 0.15 | 2.77 |
| | 16.58 \pm 5.0 | 6.58 | 3.78 \pm 0.11 | 2.98 |
| Upper Mantle : | 88.62 | 7.84 | 4.50 \pm 0.07 | 3.24 |
| | 91.37 | 7.45 | 4.33 \pm 0.20 | 3.30 |
| | 100.00 | 8.30 | 4.65 | 3.53 |
| | | 8.70 | 4.85 | 3.70 |

P- delay with respect to AFRIC model = 1.43 sec.

4.

AAE - LWI

| | H km | α km/sec | β km/sec | ρ gm/cc |
|----------------|-----------------|--------------------|-------------------|-----------------|
| Crust : | 1.06 \pm 0.7 | 3.5 | 2.00 | 2.27 |
| | 7.00 | 5.9 | 3.40 | 2.67 |
| | 10.50 | 6.15 | 3.55 \pm 0.15 | 2.77 |
| | 24.70 \pm 5.0 | 7.11 | 4.09 \pm 0.08 | 2.98 |
| Upper Mantle : | 41.57 | 7.56 | 4.35 \pm 0.10 | 3.24 |
| | 138.43 | 7.90 | 4.54 \pm 0.15 | 3.30 |
| | 100.00 | 8.30 | 4.65 | 3.53 |
| | | 8.70 | 4.85 | 3.70 |

P- delay with respect to AFRIC model = 1.00 sec.

Table 10

5.

NAI - LWI

| | H km | α km/sec | β km/sec | e gm/cc |
|----------------|-----------------|--------------------|-------------------|--------------|
| Crust : | 0.18 \pm 0.7 | 3.50 | 2.00 | 2.27 |
| | 7.00 | 5.90 | 3.40 | 2.67 |
| | 10.50 | 6.15 | 3.55 \pm 0.15 | 2.77 |
| | 18.70 \pm 5.0 | 6.59 | 3.79 \pm 0.10 | 2.98 |
| Upper Mantle : | 120.08 | 7.68 | 4.41 \pm 0.15 | 3.30 |
| | 159.91 | 8.17 | 4.69 \pm 0.15 | 3.40 |
| | 100.00 | 8.30 | 4.65 | 3.53 |
| | | 8.70 | 4.85 | 3.70 |

P- delay with respect to AFRIC model = 0.1 sec.

6.

BUL - LWI

| | H km | α km/sec | β km/sec | e gm/cc |
|----------------|---------|--------------------|-------------------|--------------|
| Crust : | 7.0 | 5.90 | 3.35 | 2.67 |
| | 10.5 | 6.15 | 3.55 \pm 0.15 | 2.77 |
| | 18.7 | 6.70 | 3.66 \pm 0.10 | 2.98 |
| Upper Mantle : | 80.0 | 8.05 | 4.67 \pm 0.07 | 3.33 |
| | 100.0 | 8.20 | 4.72 \pm 0.20 | 3.44 |
| | 100.0 | 8.30 | 4.65 | 3.53 |
| | | 8.70 | 4.85 | 3.70 |

(Similar to AFRIC model)

Table 10

respectively (The only mantle layer used is a half-infinite one). Further, if a model with thicker (or thinner) crustal layer; thicker (or thinner) than the model to which dispersion curve computed, could satisfy the dispersion curve within the experimental error; then the shear velocity of the lower crustal layer is found to be higher (or lower) than that for the original model. Therefore it is unsatisfactory for the measurement of Moho depth.

(5.2.3) The Models :

The observed dispersion data points and the theoretically best fit dispersion curves for the optimized model, for various interstation paths in East Africa, are shown in Fig. 26 - 31. The relevant optimized models are shown in Fig. 32 and in Table 10 with confidence limit on each of the active parameters.

A comparison of the structural models obtained for the paths BUL - NAI, AAE - NAI and AAE - LWI using the Powell - conjugate direction method with the models obtained for the corresponding paths using the Steepest descent method shows that the mean shear velocity - depth structures are approximately the same since these optimized models are the same whatever the starting structure may be the structures obtained are unique; in this context uniqueness is taken to mean the existence of only one solution (a set of parameters satisfying the least squares condition) within the framework of layering provided in the initial case and within a considerable range of values of the parameters.

In general the agreement between the observed dispersion data points and that for the optimized model is good, except few cases where the shape of the observed data points differ from that for the optimized model. In such cases, phase velocity of NAI - LWI path; and phase - and group velocity of AAE - NAI (LOVE) path, if we increase the number

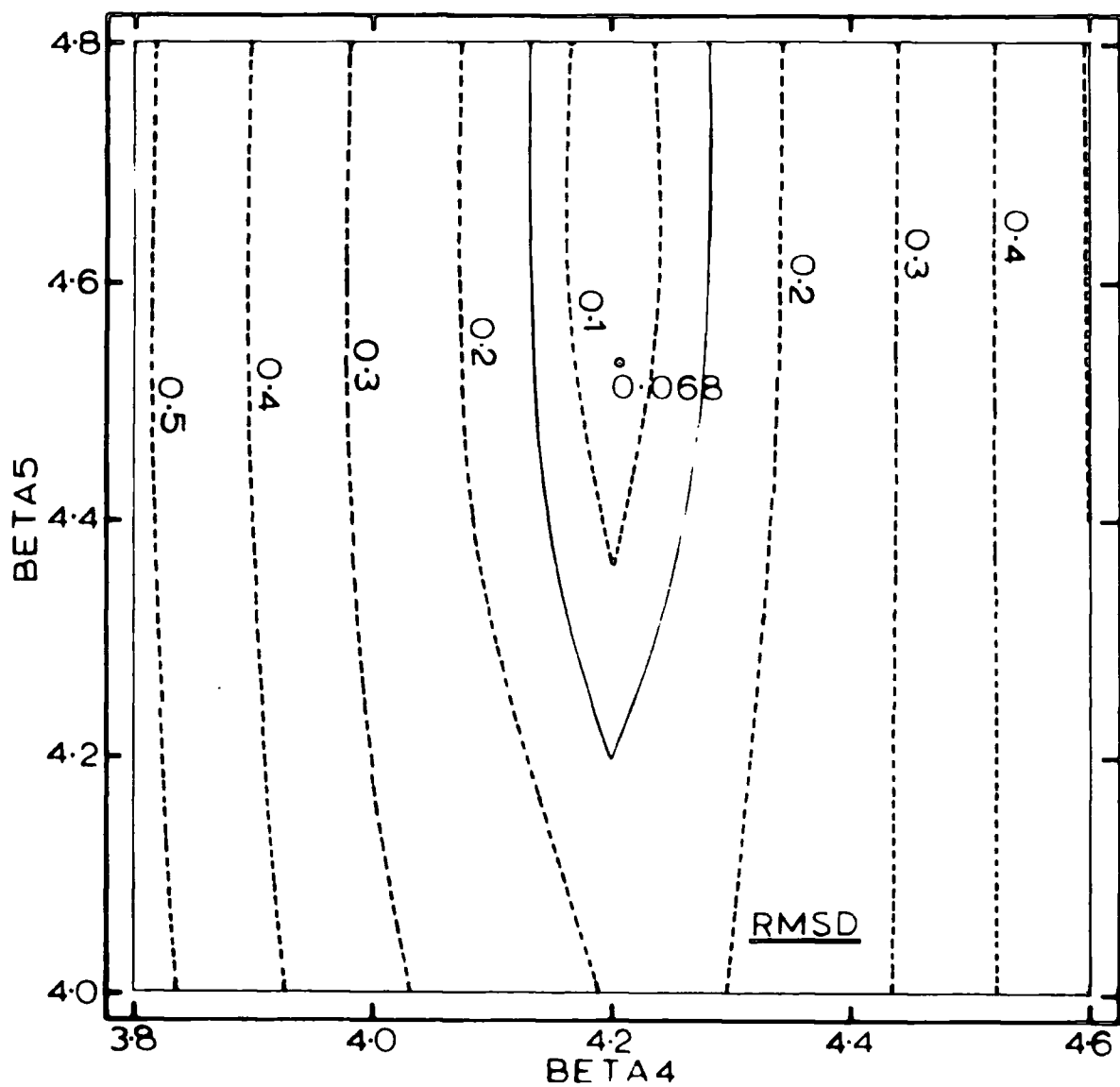


FIG. 33

of layers we may be able to get a better fit. Since the phase and group velocity values for the above paths come from only one event, the reliability of the values require further check. In the case of BUL - LWI path, as observed in central United States and in Japan (Aki, 1968), the Love wave velocities are too high for a model that can explain Rayleigh wave dispersion. This high Love wave velocity may be either due to anisotropy or due to higher mode interference (Thatcher and Brune, 1969).

The large spread of Rayleigh wave group velocities along the path, AAE-NAI, at long periods may be due to lateral variation in the upper mantle in East Africa.

To estimate the reliability of the inversion results, it is a good practice to study the variation in RMSD value while varying the value of each active parameter through geologically plausible region. One of such studies is shown in Fig. 33. In Fig. 33 shear velocity of the first two uppermost upper mantle layer of the optimized model, AAE - NAI, is varied and the RMSD value is contoured. We can see clearly that, in general, the contour lines are parallel to the axis, BETA 5. Therefore, a change in the BETA 4 value associated with a given change in the RMSD value, say X, is very small when compared with a change in the BETA 5 value associated with the same change (X) in the RMSD value. Further, from the shape of the contour lines we can say that (Refer : Non-uniqueness) there is no interference between these two layers.

In the case of event, 26 July 1967, from one-half to about two-third of the interstation, AAE - NAI, path runs almost along the centre of the rift valley system. A structural model obtained for this path by fitting phase - and group - velocity of Love wave is shown in Fig. 32. This model has much thinner crust and lower shear velocity in the depth range from 130 - 200 km, than the structural model obtained for the same

pair of stations using Love - and Rayleigh wave velocity data from the event 20 April, 1966 (For this event interstation path_A^{was} at an average distance of about 100 km from the rift valley system). In this case, the thickness of the crust is almost as that for the AFRIC model, but have higher shear velocity for the lower crustal layer.

It seems that the low velocity channel beneath AAE - NAI path is very close to the Moho, whereas that beneath BUL - NAI path probably below a depth of about 122 km. This would explain the reason for the attenuation_A^{of} Sn- wave to the North of East Africa; and may be in agreement with the conclusion made from Sn- wave propagation studies that under the northern part of the rift zone there exists a gap in the mantle portion of the lithosphere and which closes as_A^{we} move towards the southern part of the zone.

It has been shown that the structures beneath PRE - BUL (Bloch, Hales and Landisman, 1969) and that beneath BUL - LWI (Pomeroy and Gumper, 1970) are of shield type. The structure beneath the LWI - AAE path shows a mean low velocity value for the mantle beneath the crust (41 km thick), and the velocity is about 4.4 km/sec.

The combination of structural models obtained for the paths BUL - LWI, LWI - AAE with that along the paths BUL - NAI, NAI - AAE shows that, in general, there is lateral variation in the upper mantle shear velocity along the E - W direction, between these two profiles. The anomaly is greater along the eastern profile.

Let us first consider the triangular portion formed by BUL, LWI and NAI and study the variation in structure within this and in terms of the mean shear velocity - depth structure observed along the paths BUL - NAI, NAI - LWI and LWI - BUL. The comparison of structural model obtained for

the path BUL - LWI with that of BUL - NAI and LWI - NAI shows that the mean crustal shear velocity - depth structure over this area is almost identical, except slightly low shear velocity for the lower crustal layer along the path BUL - LWI. The thickness of the crust is about the same as that for the AFRIC model (About 36 km).

Between the structural models for paths BUL - LWI and BUL - NAI, the difference in the mean shear velocity for the layer beneath the Moho is about 0.17 km/sec and that for the layer in the depth range 120 - 200 km is about 0.45 km/sec.

But, if we accept the fact that the path BUL - NAI is a mixed path, then the difference in the upper mantle shear velocity becomes even greater for the portion of the BUL - NAI path, between NAI and northern part of Lake Nyasa; and becomes less for the portion from Lake Nyasa to BUL. In any case, if we combine this finding with regional gravity anomaly over this area, we can see clearly that there is lateral variation in the upper mantle velocity from west to east in the southern part of East Africa.

Now let us consider the triangular portion formed by NAI, LWI and AAE. We can see clearly that, especially along the paths AAE - NAI and AAE - LWI the shear velocity - depth structure for the crust is fairly uniform; the shear velocity value for the lower crustal layer (3.96 ± 0.1 km/sec) is little higher than that for shield type area (3.66 km/sec). We believe that this higher shear velocity is really representing shear velocity of the lower crustal layer and not influenced by the upper mantle velocity, because the thickness of the crustal layer obtained from the optimized model is of the same order as that obtained beneath NAI and AAE by the Spectral response ratio method. Since the eastern rift valley system is subtended by these two paths and the crustal layer beneath

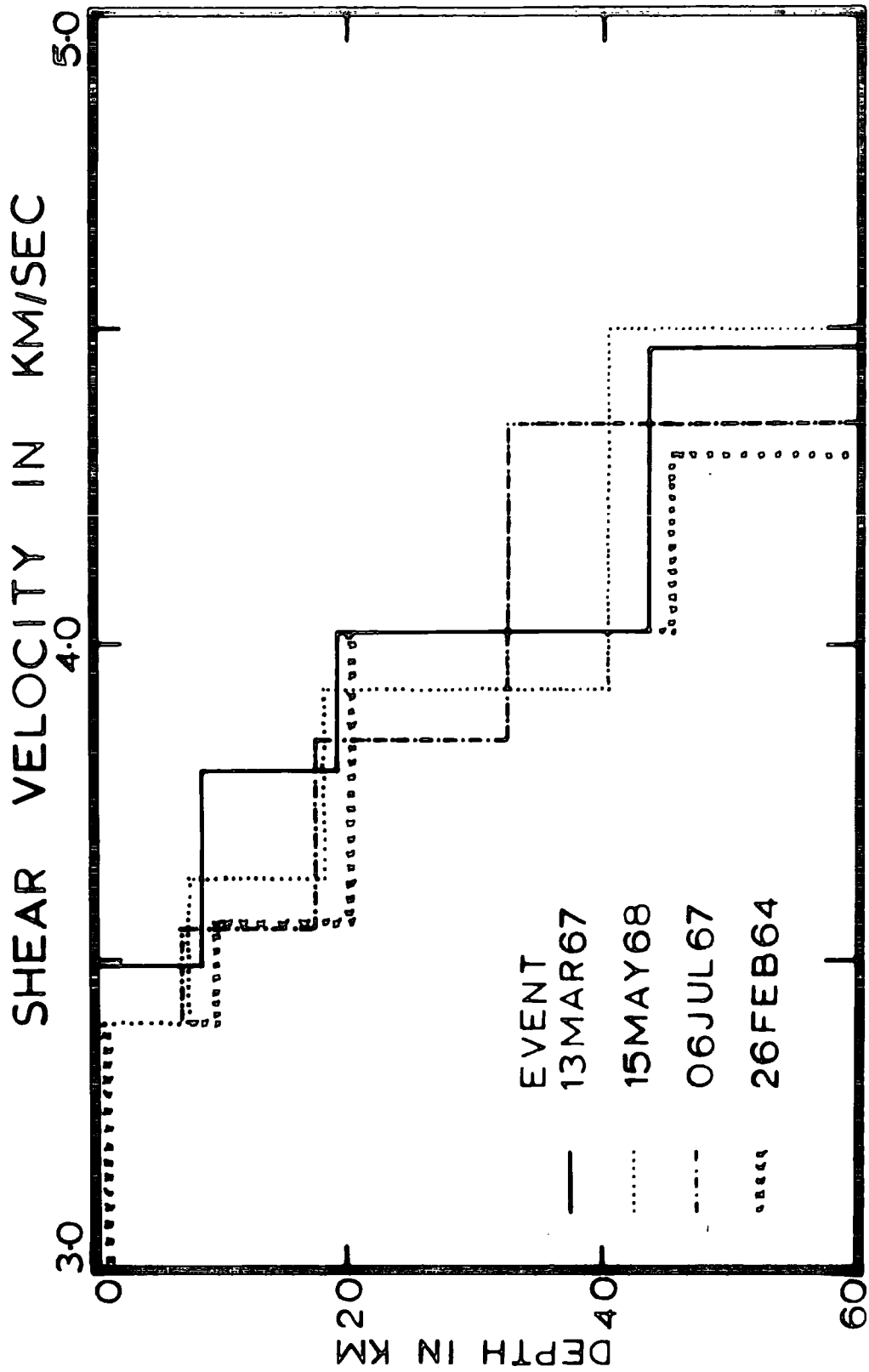


FIG. 34

the centre of the Gregory rift is found to be about 20 km (Griffiths, King, Khan and Blundall, 1971) we cannot assume that ^{the} crust is uniform in this area, but may be uniform outside the floor of the rift valley. The mantle layer beneath the Moho has a difference in mean shear velocity of about 0.13 km/sec; further, beneath the path AAE - NAI the uppermost upper mantle low velocity layer ^{is} much thicker than that beneath the path AAE - LWI. The mean shear velocity for the lower upper mantle layer is found to be the same (4.5 ± 0.2 km/sec). For the path NAI - LWI, the mean shear velocity - depth structure for the upper mantle is different from other two paths, AAE - NAI and AAE - LWI. The shear velocity of the uppermost upper mantle layer is 4.4 km/sec and for the second upper mantle ^{layer} is 4.69 km/sec.

The shear velocity - depth structure obtained from the interpretation of single station group velocity measurements are shown in Fig.34.

The comparison of shear velocity - depth structures obtained for the interstation path AAE - NAI and AAE - LWI with that obtained for single station group velocity measurement at NAI for the event from Gulf of Aden indicates that there is general decrease in the crustal thickness from west to east (except in the centre of the rift valley system). Further, there is some indication of non-symmetry in the mean uppermost upper mantle shear velocity about the centre of the eastern rift, the anomalous uppermost upper mantle extending to a greater distance on the eastern side.

The structural model obtained from Rayleigh wave group velocities for an event in Zambia recorded at AAE shows a shear velocity of 3.94 km/sec for the lower crustal layer and 4.5 km/sec for the half-infinite upper mantle layer. The thickness of the crust is about 39 km. For this event about one-half of the path to AAE runs closer (within a few km) and on the

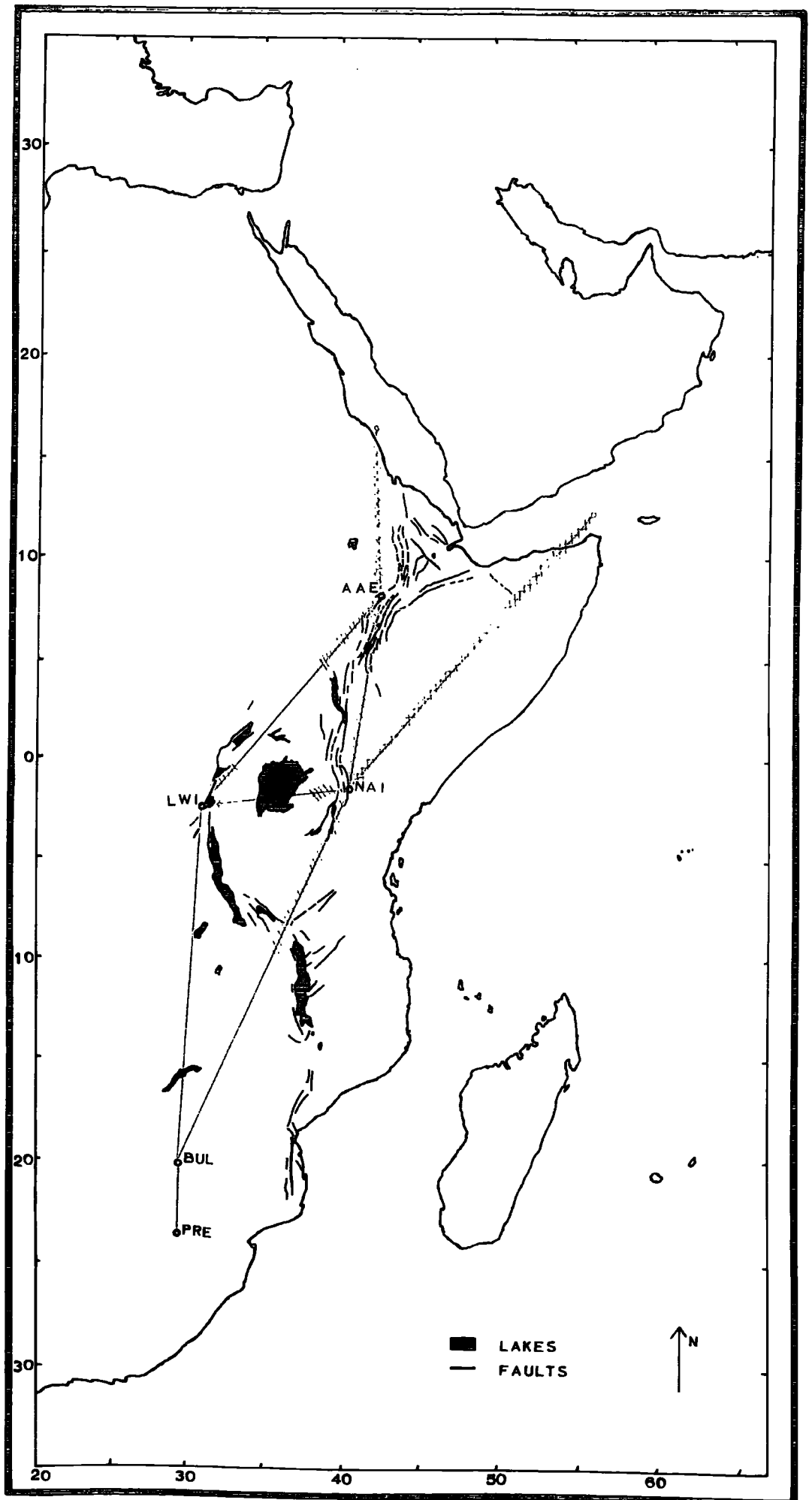


FIG. 36

western side of the eastern rift valley system, and the other one-third through an area bounded by the eastern and the western rift valley system. Therefore comparison of this structural model with that^{which} _Aone would expect by the combination of structures BUL - NAI and AAE - NAI indicates crust is uniform over this area and there may be some lateral variation in the uppermost upper mantle from west to east direction.

An event in Uganda recorded at NAI_A^{is} in agreement with shield type structure along the NAI - LWI path; uppermost upper mantle shear velocity _A^{is} about 4.7 km/sec.

The structural model obtained from Love and Rayleigh wave group velocities for an event from Red Sea recorded at AAE and about 300 km away from the part of Red Sea rift cutting across the north of East Africa indicates a thicker crust (43.8 km) and very high shear velocities for the second (3.80 km/sec) and the third layers (4.02 km/sec). The uppermost upper mantle beneath the Moho has an anomalously low value (4.47 km/sec). We can see clearly that this structural model differs from that for AAE - NAI path in particular in the shear velocity of the second crustal layer; even though both profiles run closer to a rift system.

In conclusion, we can say that the total thickness of the crustal layers seem to be roughly the same throughout East Africa and is between 34 to 42 km, except along the centre of the eastern rift valley system where crustal thinning is indicated by refraction and gravity studies. There is some indication of modification of the lower crustal layer, to higher shear velocity, along the flanks of the eastern rift valley system. Thinning of the crustal layer towards the coast of Indian Ocean is also revealed, in agreement with the gravity data (Khan and Mansfield, 1971).

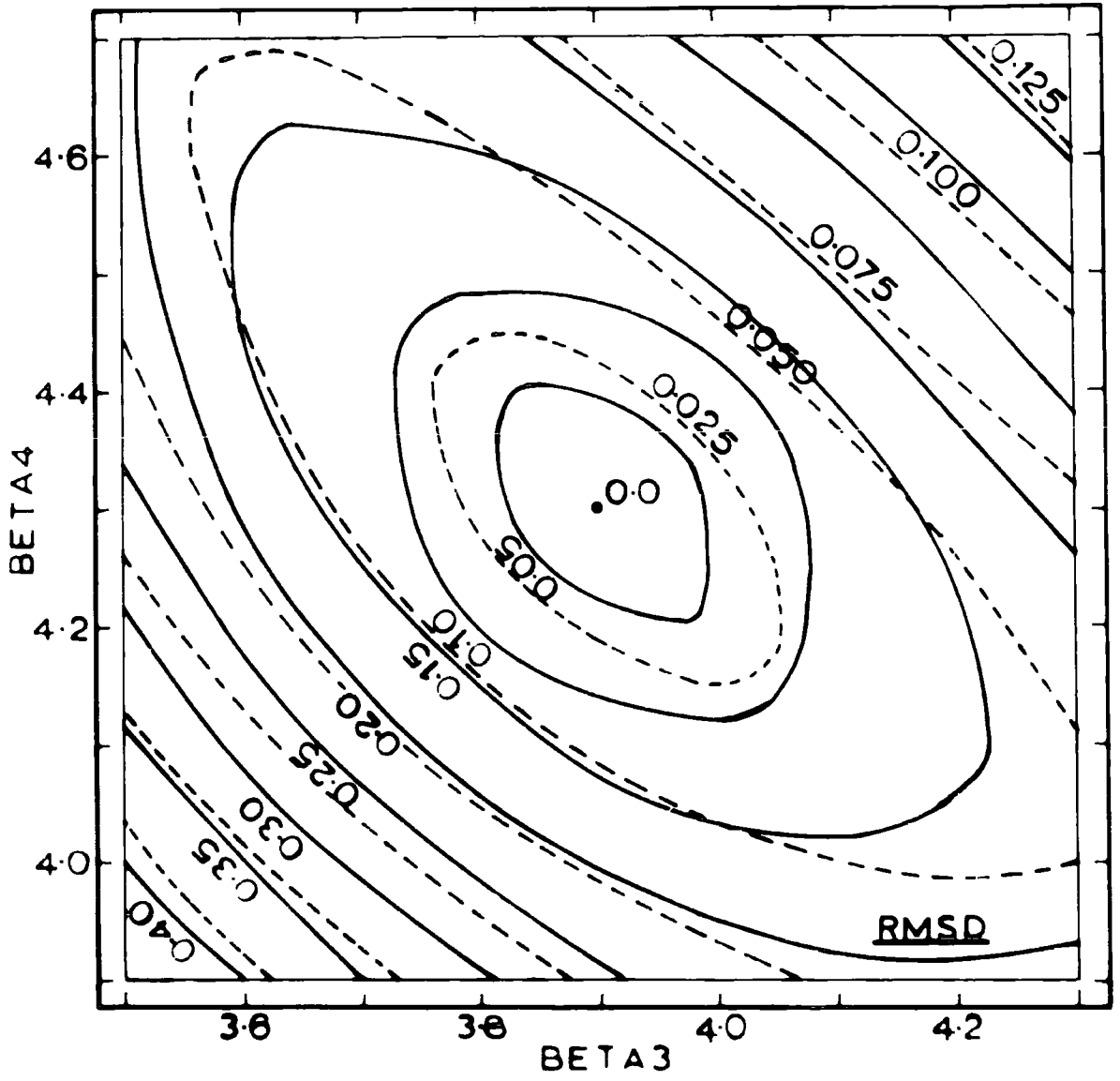


FIG. 23

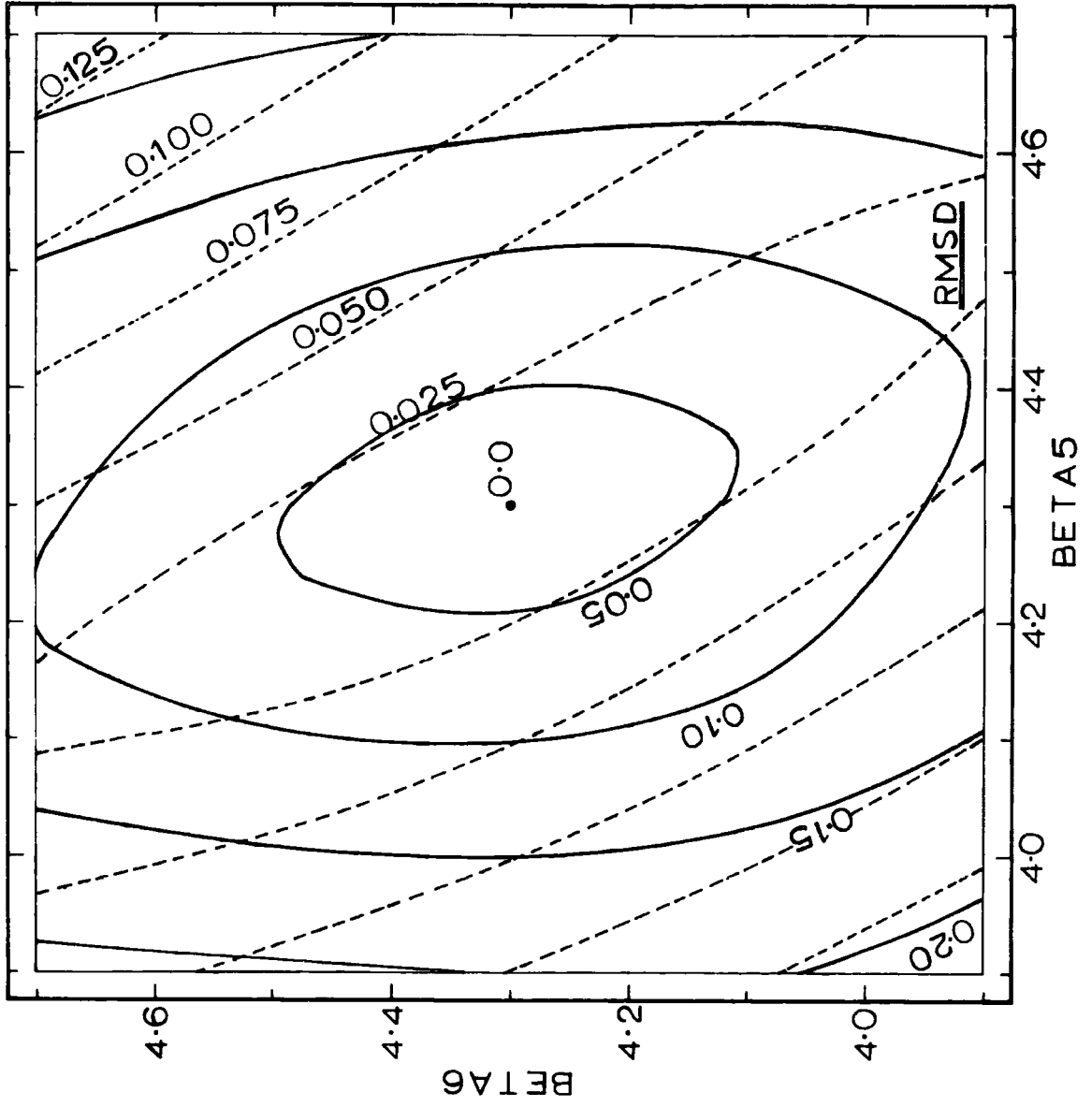


FIG. 24

The profiles (the red lines) along which we have information about the upper mantle structure ^{are} shown in Fig. 36. The red-dashed portion of the profiles are the places beneath which we believe there is large anomaly in the upper mantle; the mean Bouguer - anomaly for this part of the profiles is about 160 mgal (The background anomaly is about 100 mgal) and the undashed portion of the interstation paths are the places where the upper mantle structure is likely to be similar to that for a shield type area (for example, AFRIC model).

The red-hatched profiles are the places where anomalous uppermost upper mantle velocity is derived from single - station group velocity measurement.

(5.2.4) Non - Uniqueness :

The existence of Non-uniqueness and the degree of Non-uniqueness can be clearly demonstrated by contouring the RMSD value in a two dimensional space. The axes of the space can be any two of the active parameters.

A theoretical study, using the structural model used to derive the partial derivative is illustrated in Figs. 23 and 24. In Fig. 23 the shear velocities for the third and the fourth layers are varied and the RMSD value for Rayleigh wave phase and group; and phase are contoured. In this case the change in the RMSD value for a unit change in the shear velocity is the same for the third and the fourth layers (that is, $\partial(\text{RMSD})/\partial\beta$ same). Therefore one would expect that the contour lines should be more or less circular, ^{ular} but in actual fact the contoured lines are inclined to the axes. The inclination is more or less the same for both cases; but in the case of phase the contours are much more elongated.

The auto correlation (Dziewonski, 1970) between the shear velocity of the third and the fourth layers is 57.9 % when using the Rayleigh

wave phase and group, and is 75.6 % when using Rayleigh wave phase only. That is, 57.9% of the change in the Rayleigh wave phase and group velocities over a period range associated with unit change in the shear velocity of one layer, say third, can be compensated by a change in the shear velocity of the fourth layer. We can see this very clearly by looking at the partial derivative curves, Fig. 12a and Fig. 12b, that by just shifting the one curve (say, 3) up and down, corresponding^{ing} to different value of $\rho\beta$, one cannot bring the two curves (3 and 4) together (the higher the auto correlation functional value^{the}, more closely the curves can be brought together).

In Fig. 24 shear velocities for the fifth and the sixth layers are varied and the RMSD value for the Rayleigh wave - phase and group₃ and phase are contoured. In this case the change in the RMSD value for a unit increment in shear velocity of the sixth layer is half as that for the same increment in the shear velocity of fifth layer. We can see clearly that the inclination of the contour lines to the axes is different in each case and that the contour lines are very much elongated in the case of Rayleigh wave phase.

The auto correlation between the shear velocity of the fifth and the sixth layers is 17.8% when using the Rayleigh wave - phase and group, and is 90.8% when using Rayleigh wave phase only.

We believe that the inclination of the contour lines to the axes, together with the narrow elongated shape, is a characteristic of the Non-uniqueness; that is, it can be considered as a pictorial representation of the auto-correlation function. Further, it is clear that when the auto-correlation function is very high, a change in shear velocity of one layer could be more or less completely compensated by a change in the other layer; without altering the RMSD value. In such cases the contour lines may not close at all. The angle of

inclination of the contour lines should be related to the ratio of the (RMSD) partial derivative with respect to shear wave velocity for the layers considered.

We have shown that there is only one minimum in the shear velocity space we explored. The acceptable solutions within this minimum is dependent on the error of observation and if the error of observation is, say E , then all the combination of values within the contour line whose value, E , are acceptable. But some of these models could be rejected on the basis that within a certain period range the difference in velocity values between the observed and that for a model were very much greater than the error of observation. Further, we can see clearly that whenever the auto-correlation function is large, the contour lines are inclined to the axes and the variables may take a large range of acceptable combination of values (larger than when there is no correlation). Therefore, in an ideal case, when there is no error of observation and no correlation between the partial derivatives, there can be one and only one solution which could satisfy a given dispersion curve. But, in the above cases, if there is perfect correlation between the variables then all the acceptable set of values would fall on a straight line inclined to the axes.

Finally we can make the following conclusions :

(1) If the thicknesses of the layers are chosen in such a way that the change in RMSD value is the same for a unit change in shear velocity and if there is no correlation between the phase and group velocity partial derivatives with respect to shear velocity, then the contour lines should be perfect circles.

(2) If the change in the RMSD value for a given change in the shear velocity is not the same for the layers considered and if there is no correlation between the phase and group partial derivatives

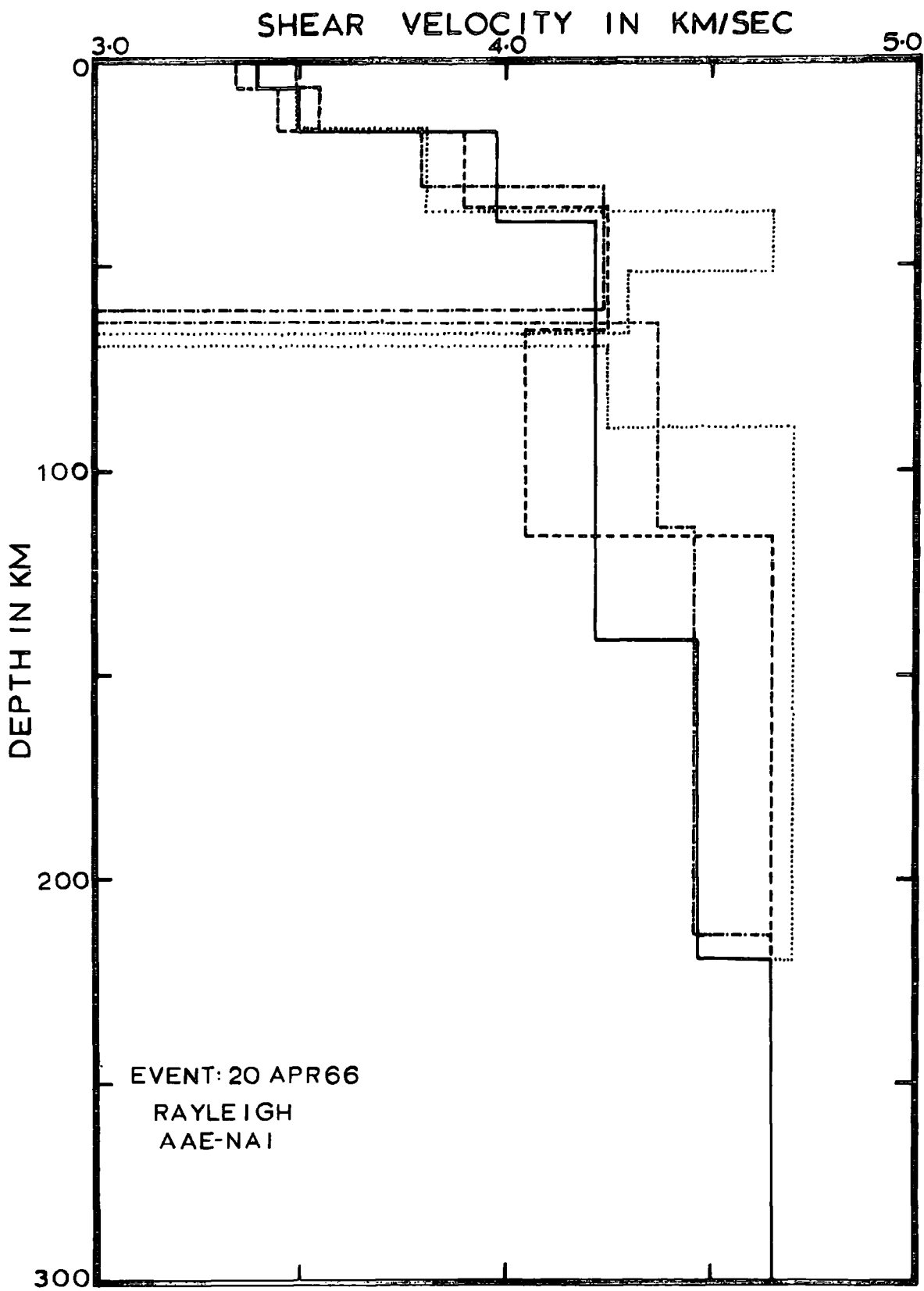


FIG. 25

with respect to shear velocity for these two layers, then the contour lines should be more like an ellipsoid with its axes parallel to the axes of the co-ordinates. The major axis of the ellipsoid should be parallel to the shear velocity axis, which has smaller effect on the RMSD value.

(3) If there is a very good correlation between the two shear velocities, then the contour lines should be inclined to the axes of the co-ordinates and must be very elongated.

In general, Love wave seem to be inferior to Rayleigh wave in the structural studies. In other words, they tend to have higher auto-correlation function than that for Rayleigh wave for the same pair of layers.

In order to demonstrate the presence of more than one structural model which satisf^{ies} the same dispersion curve, we have fitted several models to Rayleigh wave - phase and group velocities from the event 20 April 1966 for the interstation path AAE - NAI. In fitting the models we have made use of mapping techniques, Steepest descent method and Powell - conjugate direction method. The structural models obtained are shown in Fig. 25. It is interesting to note that over a certain depth range, arithmetic mean of shear velocity value from one model is not always equivalent to that from the other model. The difference depends on the thickness over which we calculate the mean velocity. This difference may be partly due to interference of parameters, but it may also indicate the fact that when we say mean structure, it does not simply mean an arithmetic mean of the shear velocities over a depth range. It is the mean shear velocity over that depth range felt by the surface wave : In practice, when there is smooth variation in shear velocity with depth, the shear velocity - depth structure obtained from the surface wave studies very well approximate the real one.

Further we can see clearly that the uppermost upper mantle layers have different velocities.

ADDITIONAL GEOPHYSICAL STUDIES(6.1) Delay Time

The delay time, T_s , arising from the anomalous structure beneath the recording station, is incorporated in the travel time residual, R . We define the travel time residual as the difference between the observed and the expected travel times, that is,

$$R = \text{Observed travel time} - \text{Expected travel time} \dots\dots\dots(1)$$

We may express the residual, R , in more detail as the sum of five terms:

$$R = T_s + T_o + T_e + T_t + E + T_i \dots\dots\dots (2)$$

where

T_o , arises from errors in the assumed focal data. Incorrect focal data, particularly incorrect epicentres, arise from a non-symmetrical distribution of the stations used in the event location, combined with errors in the travel time tables used in the location. Further errors may arise from station delay times. These may both lead to systematic errors in R since most earthquakes in a given distance range from any station tend to come from a single seismic region. The term T_o may differ for two earthquakes from the same epicentre if they originate at different depths or if they are of different magnitudes, since they may then be recorded by a different selection of stations.

T_e is the effect of anomalies in the crust and upper mantle in the region of the earthquake.

T_t is the error in the calculated travel times resulting from errors in the travel time tables.

E represents errors which may arise from poor timing and misreading of the seismogram. This error could be at least 0.1 sec.

T_s - delay time at the station due to anomalies in the crust and upper mantle beneath the station.

and T_i - is the instrumental delay for which correction may be made.

We make direct measurement of relative delay which is the difference between residuals for a given event at a station pair, and is therefore the sum of sets of difference terms in the above parameters expressing the difference in path from an event to the two stations.

Assuming that lateral velocity variations are not rapid, and the stations are close together compared with their distance from the epicentre, the two paths are sufficiently similar to conclude that the difference terms largely cancel with the exception of those arising from differences immediately below the stations ($T_s - T_s^1$). Then the relative delay is a true measure of the crust and upper mantle differences between the two stations but is contaminated by a systematic error arising from the non zero value of the several difference terms.

Long and Mitchell (1970) concluded that the direct measurement of the relative delay gives a reliable measure of the differences in crust and upper mantle structure beneath the stations, with a systematic error arising principally from the uncertainty in the focal positions, and probably not exceeding 0.4 sec (value for Iceland).

The average delay differences between station pairs were corrected, where necessary, for the effects of station elevation according to the equation:

$$dt = dh \left[\frac{1}{V_c} \cdot \frac{1}{\cos(i_c)} - \text{Tan } (i_c) / V_a \right] \dots\dots\dots (3)$$

Where dt is the extra travel time due to the station elevation dh ,
 i_c is the angle made by the ray at the base of the crust,
 V_a is the apparent surface velocity of the ray and
 V_c is the crustal velocity.

Since we interpret delay time in terms of plane parallel layered structure, the delay time should be corrected for the angle of emergence.

Delay time with respect to BUL

| Station | P Sec | S Sec |
|---------|-----------|------------|
| AAE | 2.7 ± 0.3 | 3.8 ± 5.8 |
| NAI | 2.3 ± 0.3 | — |
| LWI | 1.1 ± 0.3 | 1.2 ± 13.5 |

Table 11

If θ is the average angle of emergence of all the events we considered, then real delay time is equal to $(T_s - T_s^1) \cdot \cos \theta$.

(6.1.1) Present Study :

Delays relative to Bulawayo (BUL) were measured for stations at Addis Ababa (AAE), Nairobi (NAI), and Lwiro (LWI). The data for these measurements were taken from the Bulletin of the International Seismological Centre (Edinburgh) for the years 1964 - 1967. Only those earthquakes whose epicentral distance lies within 28° to 90° are considered. Because Earth's structure is complicated, and has large-scale regional variations in the crust and upper mantle, it is not practical to estimate a world - mean travel time curve for distances less than 20° and possibly even less than 30° .

Herrain's (1968) travel time table is used to calculate P- wave delay time and Jeffreys - Bullen (1948) travel time table is used to calculate S- wave delay. The result of the calculation is shown in Table 11.

Number of events used to calculate P- delay is 66 and of S- delay is only 16. A plot of delay time against azimuth (not shown) for a small range of epicentral distances does not show any definite variation of delay time with azimuth. This may be partly due to the fact that most of the events ^{are} concentrated within $170^\circ - 180^\circ$ and $215^\circ - 230^\circ$ azimuth (that is, insufficient data points).

If we accept the crustal models suggested by Bonjer, Fuchs and Wohlenberg (1969) we would be in a position to derive some information about the mantle beneath AAE, NAI and LWI.

From the travel time through the crustal models for a P- wave incident

Refracted Body Wave

| Date | Origin Time | | | Epicentre | Epicentral Distance - Degree | | Travel Time Sec | | Phase |
|-----------|-------------|----|------|-------------|------------------------------|-------|-----------------|----------------|----------|
| | H | M | S | | BHA | BUL | BHA | BUL | |
| 19 Oct 67 | 01 | 22 | 42.4 | 8.35S 29.5E | 6.1 | 11.8 | 92.6 | 166.6 | Pn |
| 22 Sep 67 | 10 | 40 | 15.4 | 5.13S 35.1E | 11.4 | 16.2 | 161.6 | 226.6 | Pn |
| 10 Jun 67 | 15 | 52 | 25.5 | 23.4S 26.7E | 9.0 | 3.7 | 130.5 | 59.5 | Pn |
| 27 Aug 65 | 18 | 40 | 1.0 | 10.0S 32.0E | 5.61 | 10.60 | 86.0 | 157.0 | Pn |
| 19 Nov 64 | 16 | 34 | 36.0 | 7.0S 31.0E | 7.8 | 13.27 | 115.0 244.0 | 191.0 419.0 | Pn Sg |
| 12 May 64 | 8 | 50 | 56.9 | 4.7S 34.8E | 11.50 | 16.43 | 163.1 | 226.1 | Pn |
| 11 May 64 | 12 | 34 | 15.0 | 8.0S 31.0E | 6.82 | 12.17 | 110.0 189.0 | 180.0 394.0 | Pn Sg |
| 9 May 64 | 12 | 35 | 20.0 | 26.3S 27.3E | 11.84 | 6.25 | 164.0 389.0 | 89.0 196.0 | Pn Sg |
| 7 May 64 | 17 | 14 | 18.0 | 9.0S 28.0E | 5.34 | 11.15 | 84.0 173.0 | 160.0 355.0 | Pn Sg |
| 3. May 64 | 2 | 59 | 31.0 | 5.9S 29.4E | 8.54 | 14.18 | 125.0 | 197.0 | Pn |

BUL . 20 08 36 S 28 36 48 E

BHA . 14 26 30 S 28 28 06 E

BUL - BHA ; $\Delta = 631.23 \text{ km}$, $AZ = 358.58^\circ$

Table 12

vertically at the crust - mantle boundary, we find $t_p = 6.24$ sec in AAE, $t_p = 6.69$ sec in NAI and $t_p = 5.61$ sec in LWI. The difference in crustal travel times at AAE and LWI amounts to 0.14 sec, after correcting for difference in crustal thicknesses. Therefore, the remaining 1.43 sec has to be attributed to the mantle and indicating the presence of more material with a lower velocity in the mantle beneath AAE as compared to LWI.

The same quantity calculated between the stations NAI and LWI shows a difference of 1.11 sec in the mantle travel time and, therefore more material with a lower velocity in the mantle beneath NAI as compared to LWI.

It is very likely that mantle beneath AAE and NAI is similar. It does not mean that the anomalous mantle is uniform and continuous along the interstation path AAE - NAI, because the regional gravity anomaly map of Khan and Mansfield (1971) shows^a decrease in the gravity anomaly value from NAI to Lake Rudolf.

If we assume the structure of the crust given in AFRIC model (Gumper and Pomeroy, 1970) is that beneath BUL, then P- delay time attributed to upper mantle beneath LWI with respect to BUL is about 1.1 sec. This assumption would be justified in view of surface wave dispersion reported along PRE - BUL path and some refraction studies in Transvaal. Further, from the refracted arrivals time of the Pn- and Sg- wave to the BUL and BHA stations, for those events in the African continent (Table 12) and closer to the great circle path containing BUL and BHA stations the following measurement has been made by us.

$$P_n = 8.36 \pm 0.18 \text{ km/sec}$$

$$S_g = 3.28 \pm 0.25 \text{ km/sec}$$

(95 percent confidence)

This is in agreement with shield type structure around BUL station.

To determine the approximate thickness of the anomalous region, let us first assume that the anomalous mantle beneath each of these stations has a P- wave velocity of 7.4 km/sec (beneath western United States $P = 7.2$ km/sec, beneath Iceland $P = 7.4$ km/sec, beneath Rhine graben $P = 7.4$ km/sec and beneath Baikal rift $P_n = 7.1 - 7.5$ km/sec).

The mantle P- wave delay at AAE with respect to BUL is about 2.53 sec. The surface wave studies and gravity studies shows that the low velocity channel is, in fact, almost beneath the Moho at AAE and NAI. Therefore, if we accept that the anomalous mantle extends from Moho to a certain depth (with a thickness = H .) then the value of H below AAE is about 204 km. The mantle P- wave delay at NAI with respect to BUL is about 2.21 sec and therefore the value of H below NAI is about 182 km. The rough order of the thickness of the low velocity channel found beneath AAE & NAI is same as that found beneath western United States (Nuttli and Bolt, 1969) or that beneath the axis of the Mid-Atlantic ridge, near Iceland (Francis, 1969).

The P- delay for the optimized model, AAE - NAI, is only 1.53 sec with respect to AFRIC model. The difference, about 1.0 sec, between the observed (Table 11) and that for the optimized model could be due to a number of reasons:

(i) Lateral variation in the regional gravity anomaly along the interstation path AAE - NAI; the Bouguer gravity anomaly at NAI is about - 180 mgal and at AAE is about - 200 mgal, in between the value drops to about - 140 mgal near Lake Rudolf. Therefore the extent of the mantle anomaly beneath the stations NAI or AAE does not represent the

mean mantle anomaly beneath the path AAE - NAI. The mean mantle anomaly must be less than the mean mantle anomaly beneath AAE and NAI.

(ii) Surface wave data do not extend to sufficiently long periods to study the shear velocity - depth structure to an accuracy less than 0.1 km/sec, for layers deeper than about 108 km. Whereas part of the delay time could be due to mantle beneath this depth, 108 km.

(iii) We have assumed constant ratio, 1.74, between the P- and S- wave velocities. This assumption may not hold for the entire depth structure we studied using surface wave dispersion data. For the crust, (P/S) ratio is, normally, found to be 1.73 and for the upper mantle it varies from 1.74 beneath the Moho to about 1.9 at a depth of about 200 km. If we increase the value of (P/S) ratio from 1.74 to some higher value, we would be increasing the value of P (keeping the shear velocity - depth structure obtained from the surface wave studies the same); therefore decreasing the P- delay time. This makes the difference in P- delay time between the observed case and that for the optimized model greater than 1.0 sec.

The mantle P- delay at LWI with respect to BUL is 1.1 sec. At LWI it is very difficult to say where the low velocity channel begins. If it begins near Moho, then the value of its thickness is about 97 km.

Now, let us consider the path AAE - LWI. The P- delay for the optimized model AAE - LWI is 1.0 sec with respect to AFRIC model. The observed mean P- delay is 1.9 sec. The difference (0.9 sec) is almost certainly due to structural variation along this path.

If we look into this problem in terms of mixed path, then as we have already said, about 45% of the path AAE - LWI ^{is} equivalent to AAE - NAI and the rest to AFRIC. The calculated P- delay on this assumption, using mean

delay from AAE and NAI, is about 1.1 sec which is closer to that for the optimized mean model.

The P- delay time for the optimized model, NAI - LWI, is 0.1 sec with respect to AFRIC model whereas observed mean P- delay time between the stations NAI and LWI is 1.7 sec. The difference, 1.6 sec, between the observed P- delay and that for the optimized model cannot be accounted^{for} by allowing the layers beneath, say, 108 km depth to have low P- wave velocity value known for other tectonic regions. It is certain that this difference is mainly due to lateral variation in the structure between the two stations and that anomaly does not extend very far from the stations along this profile (especially at LWI station refer : Fig.5).

The P- delay time for the optimized model, NAI - BUL, is 1.43 sec with respect to AFRIC model, whereas observed mean P- delay time is 1.15 sec. If we assume that 45% of the path BUL - NAI is equivalent to AAE - NAI and the rest equivalent to PRE - BUL type, the P- delay works out to be 1.12 sec. Therefore, the difference between the observed mean P- delay along the path BUL - NAI and that for the optimized model, BUL - NAI, is 0.31 sec, which is about the same value as the confidence limits.

The overall picture emerged from the P- delay time measurement is in agreement with that from surface wave dispersion.

Not much weight is given to S- delay, because of large confidence limits. The (P/S) delay do not show such high value as 3.72 observed in the western United States.

We have said that there is definitely low velocity mantle beneath the Eastern rift and in few places along the western rift. The general explanation for the anomalous mantle beneath various tectonic regions is the rising isothermals and partial fusion. If that is the case in East

Africa, as in Iceland, then Rayleigh and Love waves should be attenuated by a factor greater than that for a shield area. The measure of attenuation is called Q .

(6.2) Q - Measurement

The classical seismological approach is to measure and correlate amplitudes of body waves from place to place on the earth's surface, a notoriously difficult task involving corrections for source, reflection and refraction and, since measurements are restricted to the surface of the earth, the decrease in amplitude along a given ray generally cannot be measured. The presence of a low - velocity region also complicated the extractions of useful amplitude information from the affected rays.

The most of the difficulties mentioned in the above paragraph could be overcome by using both Love and Rayleigh waves.

The equation used for the calculation of interstation Q - spectrum is as follows:

$$Q_T = \frac{(r_2 - r_1)}{U \cdot T} \left\{ \frac{A_1}{\text{Log } A_2} + \sqrt{\frac{(\text{Sin } A_1)}{\text{Log } (\text{Sin } A_2)}} \right\}$$

where r_1 and r_2 are the epicentral distances in km,

Δ_1 and Δ_2 are the epicentral distances in radians,

A_1 and A_2 are the amplitude values at T sec. period,

U the interstation group velocity at T sec period.

The advantages of surface wave method are (Anderson, 1967):

(a) The long period waves suffer less degradation due to inhomogeneities, that is, Rayleigh - type scattering.

(b) A given bundle of energy can be sampled at several points along its own ray, that is, ^{at} the surface of the earth.

(c) The geometric spreading factor can be calculated more accurately or cancelled out completely.

(d) Velocity reversals and horizontal discontinuities lead to no particular difficulty.

(e) Successive passages of lower - period surface waves from large earthquakes past a given instrument can be analysed, removing completely the effects of source asymmetry, instrument, local geology and geometric spreading.

(f) A single seismogram contains sufficient information for a fairly detailed interpretation.

The disadvantages of this method are the limited depth resolution, the restriction to large earthquakes, and the masking of any intrinsic frequency dependence by the variation of anelasticity with depth.

Results to date show that the upper mantle is more attenuating than the lower mantle, the maximum attenuation is in the vicinity of the low - velocity zone.

A frequency dependence of Q has not yet been discovered. The Rayleigh wave Q is systematically higher than the Love wave Q . Rayleigh wave Q for the upper mantle is about 350 - 500. Since Rayleigh wave motion involves both compression and shear, and Love wave involves only shear motion, this immediately suggests that losses in shear are greater than losses in compression. This situation is complicated by the fact that Rayleigh - and Love waves sample the earth differently and to different effective depths. The observed Q values of Love - and Rayleigh waves as

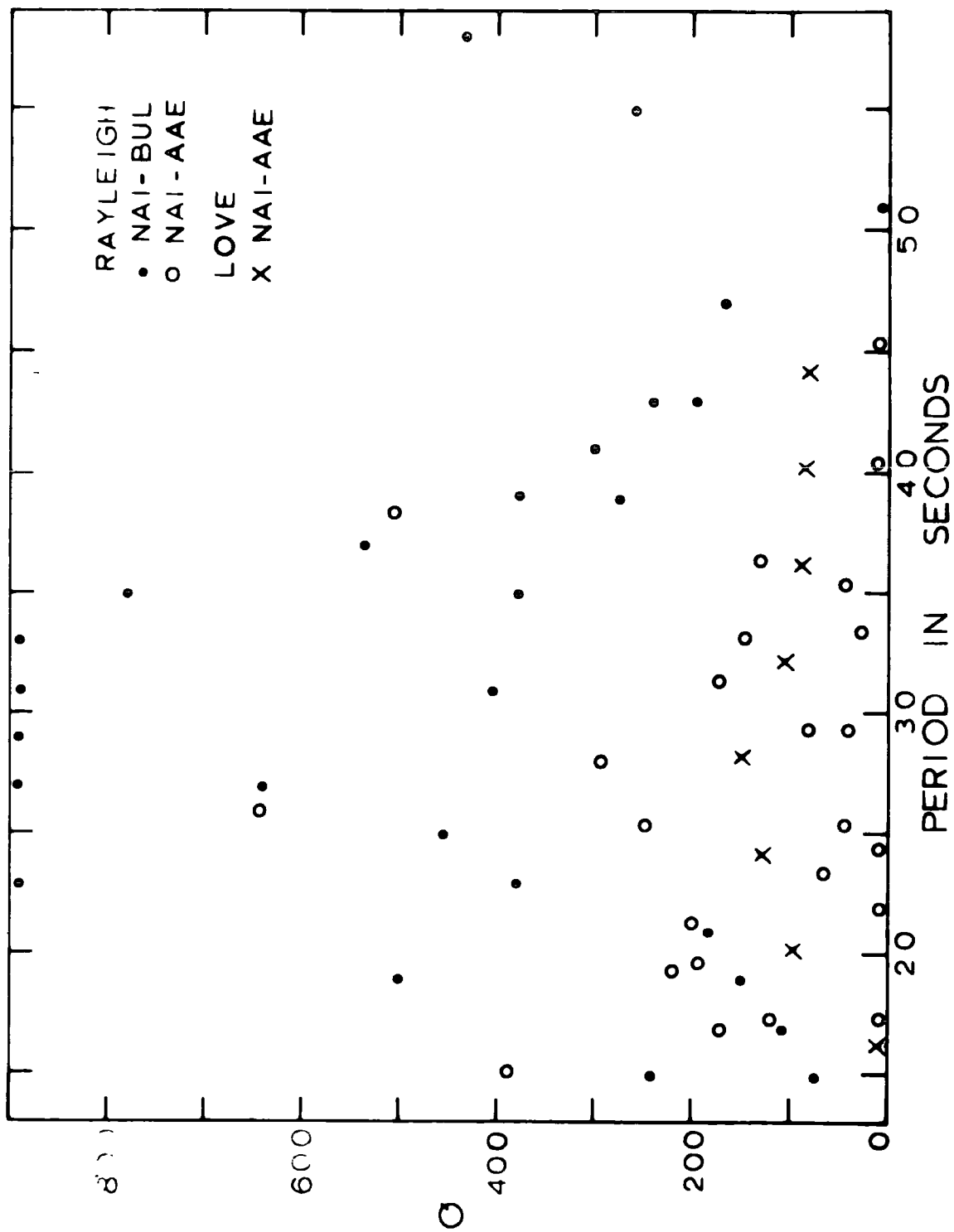


FIG. 35

LIBRARY
 NOV 1971

a function of period can be converted to the intrinsic Q and Q -distribution as a function of depth by using Anderson's method (Anderson and Archaubeau, 1964) if the intrinsic Q 's are assumed to be frequency independent.

The error involved in the calculation of Q is very high, as much as 30%, and the values are usually scattered in Q against period space.

Q values are calculated for the paths AAE - NAI and NAI - BUL, and are shown in Fig. 35. The events used in this study are same as those for interstation surface wave dispersion studies.

In a few cases, especially when the event is from south, the amplitude at the farther station (AAE) was found to be greater than that for the near station (NAI). Therefore, the Q - value becomes negative. This may either be due to interference or focusing (McGarr, 1969 a,b). Since there was no visual modulation in the amplitude envelope of the wave train, it seems this effect is due to focusing rather than interference. The term "focusing" means the convergence or concentration of waves that have travelled nearly the same path from epicentre to station (and therefore do not affect phase velocity value). Focusing results in an increase of amplitude but has almost no effect on the wave form. Interference, on the other hand, is the effect of simultaneous arrival of waves that travel two or more distinct paths from epicentre to station. Interference generally alters the amplitude modulation of the dispersed wave train considerably because the phase relationships between waves that have travelled different paths vary with period; this produces "beats" on the seismogram.

The interstation Q values for the station pair BUL, NAI, has a maximum value of about 900 in the period range 25 - 40 sec and minimum value of about 100 - 200 in the period ranges 15 - 20 sec and 40 - 55 sec. The comparison of interstation Q - values for the path AAE - NAI with that

of NAI - BUL path shows generally the former has low values. The Love wave Q- values for the path AAE - NAI, also show very low values throughout the entire period range 15 - 45 sec.

This low value, less than about 200, may be taken as indicating attenuation is greater beneath AAE - NAI path than that for an ordinary upper mantle, for which Q is 350 - 500, for the BUL - NAI path. Since the attenuation is greater beneath AAE - NAI path, shear velocity is expected to be lower than that ^{for} a normal mantle. This finding is in agreement with the result from surface wave dispersion studies and delay time.

No attempt has been made to invert the Q against period values to Q against depth values, because of large scatter of the observed values.

CHAPTER 7DISCUSSION AND CONCLUSION(7.1) Discussion

In fitting a theoretical model to the observed velocity data, we have assumed a relation $P = 1.74S$. This relationship observed for the crust is, generally, 1.73 and for the upper mantle varies from 1.74 near the Moho to a higher value, about 1.9, at deeper mantle. We have in fact varied the P velocity of the optimized model according to this new value and found that its effect on the phase and group velocity values is usually well below the observation error, of the order of 0.001 km/sec. But it has greater effect on the P- delay time. Therefore shear velocity - depth structures remain the same.

In using newly developed optimization program, with the new criterion used to determine the order of thickness of the layers, the thickness of the layers becomes large as one goes deep into the mantle. Therefore one criticism is that we are averaging elastic velocities over greater depth and thereby losing the geological significance of the model. Theoretical studies show clearly that this is a well known problem in surface wave studies, one cannot study fine structure of the earth and can only study mean structure using dispersion data only. But - (1) If there is any special characteristic on the dispersion curves, such as a maximum and/or minimum in the Rayleigh wave phase velocity then of course we should postulate a model with thin soft layer or layers with the neighbouring layers, as usual, thick. (2) If we have geophysical information about the structure from other studies, then this information should be included when searching for a model to satisfy the observed dispersion curve.

In the case of group velocity inversion, although solutions may be

mathematically non-unique the differences between them may be trivial. For example, if we select the thickness of the layers according to the partial derivative to have distinct effect on the dispersion curve and if we impose proper upper and lower bounds on the velocity values, then there is only one model which could satisfy the observed dispersion curve.

Even though group velocity can be derived from the phase velocity, however, in practice the group velocities are very useful. Since the phase velocity will always be subject to experimental error and the observations will not be equally well determined at all periods. Small differences between theoretical and observational dispersion of the phase velocity may show up as larger and perhaps more easily noticeable differences in the group velocity.

We think array of stations over number of parts of East Africa, because of the presence of large lateral variation^{ion}, is most suitable to study in detail the crust and upper mantle structure. Because a large number of small regions will give better resolution of the dispersive character of each region than a small number of large areas where relatively small but possibly significant lateral crustal variations are averaged out. Naturally the reduction in region size must end when the wavelength of the surface wave component becomes comparable to the dimension of the sub regions.

In certain graben areas, such as Rhine graben, it has been found that a low velocity layer could exist in the crust. If such a layer exists in East Africa and since we did not take this into account the application of surface wave method would result in either a lower average shear velocity for the crust or an improbably thick layer of sediments.

We have said that the thickness of the anomalous upper mantle beneath

NAI must be about 180 km and that beneath LWI about 90 km, but we can see from the structural model obtained for the path NAI - LWI that the mean thickness of the anomalous upper mantle is only about 20 km. The Bouguer - isanomaly map of East Africa (Fig.5) shows ^{that} E - W extension of the mantle anomaly beneath the LWI station must be to a short distance, whereas beneath the NAI it can be up to the margin of Lake Victoria. Therefore, in terms of mixed path the structure beneath Lake Victoria must be similar to that for a shield area. We have already shown in chapter 5 that the path AAE - LWI can be split into three parts, two of these parts, one near LWI and the other near AAE, equivalent to AAE - NAI and the third part equivalent to AFRIC. Therefore it seems certain that the eastern and the western rift valley systems are separated by a shield type structure,

It is very clear that none of the dispersion curves derived by us can be fitted with the sort of crust and upper mantle structure suggested for the floor of the Gregory rift by Griffiths et al (Fig.4). It is on the contrary highly significant that all dispersion data is consistent with a shield type crust. Therefore it seems the structure suggested by Griffiths et al is local, may be intrusion, and cannot be taken representing the whole length of the rift system.

The difference in the petro-chemistry of the lava flow over East Africa, from that over mid-ocean ridges may be due to differences in the thickness of the crust, and in the depth and state of the anomalous upper mantle (that is, position of the magma chamber). In East Africa, variation in lava flow between the eastern and the western rift valley systems must be mainly attributed to the difference in the upper mantle structure. The lateral variation in the petro-chemistry of the lava flow along the eastern rift may be due to, the fact that each portion Afar triangle, Ethiopian rift and Gregory rift are separate units. The Afar

triangle is known to have an oceanic crust and is found to be a part of Red Sea (Harous Tazieff, 1970). The Ethiopian rift, even though it is connected to the oceanic ridges of the Red Sea and the Gulf of Aden is found to have shield type crust out ^{of} the centre of the rift valley. The Gregory rift, which is shown to be a separate unit, separated from the Ethiopian rift by Lake Rudolf (Baker and Wohlenberg, 1971) may have the same crustal structure as that beneath Ethiopian rift, but does not have any interaction effect from the mantle process taking place beneath the oceanic ridges.

The comparisons that can be made between the structure of East Africa and the structure for the continental grabens over other parts of the world is shown in Table 13 and the comparison of the structure of East Africa with that of western United States and Iceland is shown in Table 14. Beneath East - Pacific rise about 46 km of $\beta = 3.50$ km/sec soft layer at a depth of 95 km is observed, even though the presence of such a layer beneath East Africa (especially eastern rift) is not proved in our studies, we cannot completely deny the possibility of presence of such a layer. This is due to two reasons : (a) the unavailability of very long period surface wave data, (b) the problem of Uniqueness.

As a consequence of the above comparison one can say that the structural variation over East Africa is to a great extent similar to that over North America, although one is rift system and the other transform fault (Gilluly in 1969, said that large parts of the Basin and Range province greatly resemble structurally many segments of the East African rift systems in Ethiopia, Uganda and Tanzania). The eastern rift ^{is} particularly similar to other continental grabens and also to Icelandic upper mantle. If we accept the crustal structure suggested for the floor of the Gregory rift by Griffiths et al (1971), then it looks as if the eastern rift is similar in structure to the

The Comparison of East African Structure with that for Rhine Graben and Baikal Rift

| | East Africa | Rhine graben | Baikal rift |
|---|--|--|---|
| (1) The width of the rift valley system : | 40 - 50 km | 40 km | 50 km (Belossov, 1969) |
| (2) Thickness of the crustal layer : | It varies from about 20 km beneath the centre of the eastern rift valley system to about 34 - 42 km over the rest of the region. | 28 km (Iubimova and Feldman, 1970) | 40 km (Artemjev and Artgushkov, 1971) |
| (3) Sub-Moho velocity : | Very low value beneath the eastern rift, about 7.4 km/sec. | 7.2 - 7.7 km/sec (Illies, 1969) | 7.1 - 7.5 km/sec (Artemjev and Artgushkov, 1971) |
| (4) Thickness of the low velocity channel : | It is about 190 km beneath the eastern rift and about 90 km in some part of western rift (P = 7.4 km/sec) | About 140 km (S = 4.15 km/sec) (Seidl and Knopoff, 1965) | - |

Table 13

The Comparison of East African Structure with that for western United States and Iceland

| | East Africa | western United States | Iceland |
|---|--|--|--|
| (1) Thickness of the crustal layer : | It varies from about 20 km beneath the centre of the eastern rift valley system to about 34 - 42 km over the rest of the region. | It varies from 20 km beneath the centre of the rift valley to about 50 km in plateau region. (Pakiser, 1963) | 17.8 km (Bath, 1960) |
| (2) Sub-Moho Velocity : | Very low value beneath the eastern rift, about 7.4 km/sec, to about 8.2 km/sec beneath the southern East Africa. | It varies from 7.8 km/sec beneath the centre of the rift valley system to 8.2 km/sec beneath the plateau region. (Pakiser, 1963) | 7.4 km/sec (Bath, 1960) |
| (3) Thickness of the low velocity channel : | It is about 190 km beneath the eastern rift and about 90 km in some part of western rift (P=7.4 km/sec) | It is about 180 km beneath the basin and range province and 75-100 km beneath the Sierra Nevada region (P=7.2 km/sec) (Muttli and Bolt, 1969) | About 225 km (P= 7.4 km/sec) (Francis, 1969) |
| (4) P-delay : | For eastern rift about 2.3 - 2.7 sec | 3.0 sec (Muttli and Bolt, 1969) | about 2.3 sec (Long and Mitchell 1970) |
| (5) Bouguer Anomaly : | Along the eastern rift, it vary from - 220 mgal to about - 140 mgal | It vary from - 200 to -250 mgal. (Press and Biehler, 1964) | - |
| (6) Earthquake : | shallow - focus | shallow - focus (Bruce and Byerlee, 1970) | - |

Table 14

mid-ocean ridge system, but whether it is in the initial stage of ocean formation or not cannot be answered yet, because of the fact that eastern rift as a whole has not equally developed throughout its length.

(7.2) Conclusion

To study the crust and upper mantle structure over various paths in East Africa, and to understand the process going on beneath these paths by comparing its structure with other tectonic regions, we have calculated phase - and group velocity dispersion curve for Love and Rayleigh waves. The interstation phase and group velocities run in the period range 15 to 60 sec and the single station group velocities in the period range 12 to 37 sec.

The most characteristic feature of the set of interstation Rayleigh wave phase velocity curves obtained over East Africa is that there is a definite merging of phase velocity values from longer to shorter periods. The spread at 60 sec period is 0.33 km/sec whereas at 20 sec period this is reduced to 0.1 km/sec. A comparison of phase and group velocity dispersion obtained in this study with the dispersion for other areas of the world confirm that the upper mantle velocities beneath East Africa vary from that for a shield area to that for a tectonic region. The lowest velocity values ^{are} for the path AAE - NAI.

To invert the observed dispersion data into shear velocity - depth structure we have developed a number of non-linear optimization techniques. For all these new techniques one needs to derive phase and group velocity partial derivative curves for both Rayleigh and Love waves. Such a derivation shows that in the period range 15 - 62 sec Love wave is much more suitable to study the crustal structure and Rayleigh wave for upper mantle structure. Further, the effective depth of penetration for Love waves is about 0.3λ and for Rayleigh wave it is about 0.45λ (where λ is the wave length). We then investigated the problem of Non-uniqueness

and the capability of the new optimization techniques. (a) It is found that Non-uniqueness arises mainly due to interference of one parameter with the other, that is change in the phase and group velocity spectrum caused by a change in the value of one active parameter is to a great extent compensated by a change in the value of some other active parameter or parameters. For example, in the two dimensional shear velocity space (say, β_1 and β_2) the contour of the RMSD value would be inclined to the axes of co-ordinates if there is interference between the two, β_1 and β_2 . So that a set of combination of shear velocities, β_1 and β_2 , would have the same RMSD value (At the minimum). (b) It is found that Powell - conjugate direction method and the Steepest descent method are the two useful optimization techniques which can be used to derive shear velocity - depth structure from dispersion data. Further, Powell - conjugate direction method has a number of advantages over Steepest descent method. Theoretical studies show that provided we select the thicknesses of the layers in such a way that the active parameters have distinct effect on the dispersion curve (in other words Auto or cross-correlation function of phase and group velocity partial derivative with respect to active parameters is small) then we can recover the value of the active parameters to a very great accuracy depending on the accuracy of the observed data. It is also found that using phase - and group velocities, instead of phase velocities only, improve the final model (that is, inclusion of group velocities in most cases decrease the correlation function).

In this study the Powell conjugate direction method is mainly used to derive shear velocity - depth structure. The derived structures show that the total thickness of the crustal layers is roughly the same throughout East Africa, and is between 34 to 42 km; except along the centre of the eastern rift valley system where crustal thinning is indicated by refraction and gravity studies. There is some indication

of modification of the lower crustal layer, to higher shear velocity, along the flanks of the eastern rift valley system. Thinning of the crustal layer towards the coast of Indian Ocean is also revealed, in agreement with gravity data (Khan and Mansfield, 1971).

The profiles (the red lines) along which we have information about the upper mantle structure ^{are} shown in Fig. 36. The red-dashed portion of the profiles are the places beneath which we believe there is large anomaly in the upper mantle, mean Bouguer anomaly for this part of the profiles is about 160 mgal (The background anomaly is about 100 mgal) and the undashed portion of the interstation paths are the places where the upper mantle structure is likely to be similar to that for a shield type area. The red-hatched profiles are the places where anomalous uppermost upper mantle velocity is derived from single-station group velocity measurement.

The observed P- and S- delay times at AAE, NAI and LWI with respect to BUL ^{are} given in table 11.

The comparison of the derived structural models for East Africa with ^{those} for other similar areas in the world show that the structural variation over East Africa is to a great extent similar to that over North America, although one is rift system and the other transform fault. The eastern rift in particular is similar to other continental grabens, such as Baikal rift, Rhine graben, and also to Icelandic upper mantle. Even though the crust and upper mantle structure suggested for the floor of the Gregory rift by Khan and Mansfield (1971) is similar to that found beneath mid-ocean ridge in Iceland, the fact that crustal extension decreases from the centre sector of the Gregory rift to its extremities and the large variation in petro-chemistry of the lava flow along the eastern rift valley system indicate that the eastern rift valley has not yet developed to a stage as

comparable to mid-ocean ridge. Each part of the rift system is probably associated with separate thermal processes taking place beneath them (because they are not equally developed right throughout its length).

COMPUTER PROGRAM 1

STEEPEST DESCENT METHOD

SSTEP Step-length taken by each variable

Acc Accuracy of the observed data points

IMPLICIT REAL*8(A-H,O-Z), INTEGER*4(I-N)

DIMENSION A(100,4,4),C(50,5),E(4,4),Q(100,4,4),R(100,4,4),S(50,5),
 1T(50),U(50),V(100,4),ACCEL(100),FA(4,4),PV(50),GV(50),
 2B(100,2),D(250,2),THVAL(500),DVEL(250),RVEL(250),VA(100,4),DD(250,
 32),ORMSD(50)

COMMON A,C,E,K,M,Q,R,S,T,U,V,ACCEL,C1,C2,C3,CS0,DELTA1,DELTA2,
 1DT,FA,KLAST,KMAX,NLAY,NTRLS,WVND,PV,GV,B,D,THVAL,DVEL,RVEL,NUMPTS,
 2NCBPTS,LOVE,MODENO,NTRLMX,KWRITE,VA,DC,DD,CRMSD,GRMSD,MOBPTS
 DIMENSION STEP(20)

ABS(X)=DABS(X)

MYRASI=0

READ(5,603) SSTEP,ACC

WRITE(6,603) SSTEP,ACC

603 FORMAT(2F10.5)

9999 READ(5,190) NOBPTS

190 FORMAT(I3)

READ(5,201)((D(M,N),N=1,2),M=1,NOBPTS)

201 FORMAT(2F8.4)

WRITE(6,201)((D(M,N),N=1,2),M=1,NOBPTS)

READ(5,1190)MOBPTS

1190 FORMAT(I3)

READ(5,1201)((DD(M,N),N=1,2),M=1,MOBPTS)

1201 FORMAT(2F8.4)

WRITE(6,1201)((DD(M,N),N=1,2),M=1,MOBPTS)

500 READ(5,502)NLAY

502 FORMAT(I3)

800 READ(5,503)((VA(M,N),N=1,4),M=1,NLAY)

503 FORMAT(4F8.5)

28 WRITE(6,511)((VA(M,N),N=1,4),M=1,NLAY)

511 FORMAT(46H0 THICKNESS ALPHA BETA RHC//(1H,4F
 112.5))

READ(5,504)T(1),DT,C1,DC,KMAX,LOVE,MODENO,NTRLMX,KWRITE

504 FORMAT(10X,4F8.5,8X,I3,1X,I1,1X,I1,1X,I2,1X,I1)

WRITE(6,504)T(1),DT,C1,DC,KMAX,LOVE,MODENO,NTRLMX,KWRITE

LMN=3

901 CONTINUE

305 CALL PV7(RMSD,MYRASI)

PRMSD=RMSD

MLAY=NLAY-2

DO 300 IJK=4,6

VA(IJK,LMN)=VA(IJK,LMN)-SSTEP

CALL PV7(RMSD,MYRASI)

VA(IJK,LMN)=VA(IJK,LMN)+SSTEP

666 ORMSD(IJK)=RMSD

STEP(IJK)=-SSTEP

IF(PRMSD.GT.ORMSD(IJK)) GO TO 310

VA(IJK,LMN)=VA(IJK,LMN)+SSTEP

CALL PV7(RMSD,MYRASI)

ORMSD(IJK)=RMSD

VA(IJK,LMN)=VA(IJK,LMN)-SSTEP

STEP(IJK)=SSTEP

310 WRITE(6,601) VA(IJK,LMN),ORMSD(IJK)

601 FORMAT(2F10.5)

ORMSD(IJK)=(PRMSD-ORMSD(IJK))

```
300 CCNTINUE
GRMSD=0.0
DO 301 IJK=3,MLAY
IF(GRMSD.GT.ORMSD(IJK)) GO TO 301
GRMSD=ORMSD(IJK)
JKLM=IJK
301 CCNTINUE
IF(GRMSD.EQ.0) GO TO 900
IJK=JKLM
309 VA(IJK,LMN)=VA(IJK,LMN)+STEP(IJK)
CALL PV7(RMSD,MYRASI)
WRITE(6,602) RMSD
602 FORMAT(F10.5)
IF(PRMSD-RMSD)304,304,303
304 VA(IJK,LMN)=VA(IJK,LMN)-STEP(IJK)
GO TO 305
303 PRMSD=RMSD
GO TO 309
900 CCNTINUE
WRITE(6,606) ((VA(I,J),J=1,4),I=1,NLAY)
606 FORMAT(4F10.4)
DO 605 IJK=1,MLAY
ORMSD(IJK)=(SSTEP/ORMSD(IJK))*(ACC-PRMSD)
WRITE(6,604) IJK,ORMSD(IJK)
604 FORMAT(I5,F10.5)
605 CONTINUE
MYRASI=1
CALL PV7(RMSD,MYRASI)
DEBUG UNIT(6),SUBCHK
END
```

SUBROUTINE PV7(RMSD,MYRASI)
 IMPLICIT REAL*8(A-H,U-Z),INTEGER*4(I-N)

DIMENSION A(100,4,4),C(50,5),E(4,4),Q(100,4,4),R(100,4,4),S(50,5),
 1T(50),U(50),V(100,4),ACCEL(100),FA(4,4),PV(50),GV(50),
 2B(100,2),D(250,2),THVAL(500),DVEL(250),RVEL(250),VA(100,4),DD(250,
 32)

COMMON A,C,E,K,M,Q,R,S,T,U,V,ACCEL,C1,C2,C3,CSQ,DELTA1,DELTA2,
 1DT,FA,KLAST,KMAX,NLAY,NTRLS,WVNO,PV,GV,B,D,THVAL,DVEL,RVEL,NUMPTS,
 2NCBPTS,LOVE,MODENO,NTRLMX,KWRITE,VA,DC,DD,CRMSD,GRMSD,MOBPTS

ABS(X)=CABS(X)
 AMAX1(X,Y)=DMAX1(X,Y)
 SQRT(X)=DSQRT(X)

602 DO 2 K=1,4
 K1=K+1
 DO 1 L=K1,5
 S(K,L)=0.0
 C(K,L)=0.0
 1 CONTINUE
 2 CONTINUE
 DO 4 I=1,4
 DO 3 J=1,4
 E(I,J)=0.0
 3 CONTINUE
 4 CONTINUE

C1=2.2
 801 RADIUS=6371.0
 DO 901 M=1,NLAY
 V(M,1)=VA(M,1)
 V(M,3)=VA(M,3)
 V(M,2)=1.74*V(M,3)
 V(M,4)=VA(M,4)
 901 CONTINUE
 IF(LOVE.GT.0) GO TO 701
 Z=0.0
 NLAY1=NLAY-1
 DO 702 M=1,NLAY1
 Z=Z+V(M,1)/2.0
 V(M,3)=V(M,3)*RADIUS/(RADIUS-Z)
 702 Z=Z+V(M,1)/2.0
 V(NLAY,3)=V(NLAY,3)*RADIUS/(RADIUS-Z)
 701 BTAMX=ABS(V(1,3))
 DO 6 M=2,NLAY
 BTAMX=AMAX1(BTAMX,ABS(V(M,3)))
 6 CONTINUE
 ACCEL(3)=KWRITE
 ACCEL(2)=60.0
 9 DO 10 K=2,KMAX
 T(K)=T(K-1)+DT
 10 CONTINUE
 MODE=MODENO-1
 803 K=1
 ACCEL(1)=LOVE
 IF(ACCEL(1))11,12,11

```

11 DELTA1=DLTAR3(C1,T(1))
GO TO 15
12 DELTA1=CLTAL1(C1,T(1))
GO TO 15
14 C1=C2
DELTA1=DELTA2
15 C2=C1+DC
IF (ABS (C2-0.5*BTAMX)-0.5*BTAMX)17,17,16
16 WRITE(6,510)
GO TO 34
17 IF (ACCEL(1))18,19,18
18 DELTA2=DLTAR3(C2,T(1))
GO TO 20
19 DELTA2=CLTAL1(C2,T(1))
20 CONTINUE
807 IF (ABS (DELTA2-DELTA1)-ABS (DELTA2+DELTA1))14,14,23
23 CALL FOLCV4
C COMPUTATION SUBROUTINE CALLED.
C
504 IF (KLAST-5)24,27,27
24 IF (KLAST)900,900,25
25 DO 26 K=1,KLAST
U(K)=0.0
26 CONTINUE
GO TO 900
27 CALL GPVEL2
C GPVEL2 SUBROUTINE CALLED
C
IF (LOVE.LT.1) GO TO 900
502 DO 505 K=1,KLAST
U(K)=U(K)*(1.0+(0.00016*T(K))*(1.0-U(K)/C(K,1)))
C(K,1)=C(K,1)*(1.0+0.00016*T(K))
505 CONTINUE
900 CONTINUE
C
251 DO 254 K=1,KMAX
THVAL((2*K)-1)=T(K)
254 CONTINUE
DO 255 K=1,KMAX
THVAL(2*K)=C(K,1)
255 CONTINUE
C
260 M=1
PCOR1=D(1,1)
OBVEL1=D(1,2)
CALL LAGRAN (THVAL,KMAX,PCOR1,ANS)
RVEL(1)=ANS
DVEL(1)=OBVEL1-ANS
SDVEL=0.0
SDVEL=SDVEL+DVEL(1)**2
261 M=M+1
IF (M-NOBPTS)262,262,263
262 PCOR2=D(M,1)
OBVEL2=D(M,2)
CALL LAGRAN(THVAL,KMAX,PCOR2,ANS)
RVEL(M)=ANS
DVEL(M)=OBVEL2-ANS
SDVEL=SDVEL+(DVEL(M)**2)

```

GO TO 261

C

```

263 SDVEL=SDVEL/NOBPTS
   CRMSD=SQRT(SDVEL)
   DO 1254 K=1,KMAX
   THVAL((2*K)-1)=T(K)
1254 CONTINUE
   DO 1255 K=1,KMAX
   THVAL(2*K)=U(K)
1255 CONTINUE
1260 M=1
   PCOR1=DD(1,1)
   OBVEL1=DD(1,2)
   CALL LAGRAN (THVAL,KMAX,POOR1,ANS)
   RVEL(1)=ANS
   DVEL(1)=OBVEL1-ANS
   SDVEL=0.0
   SDVEL=SDVEL+DVEL(1)**2
1261 M=M+1
   IF(M-MOBPTS)1262,1262,1263
1262 PCOR2=DD(M,1)
   OBVEL2=DD(M,2)
   CALL LAGRAN(THVAL,KMAX,POOR2,ANS)
   RVEL(M)=ANS
   DVEL(M)=OBVEL2-ANS
   SDVEL=SDVEL+(DVEL(M)**2)
   GO TO 1261
1263 SDVEL=SDVEL/MOBPTS
   GRMSD=SQRT(SDVEL)
   RMSD=CRMSD+GRMSD
   IF(MYRAS1.EQ.0) GO TO 34
   WRITE(6,600) (T(K),C(K,1),U(K),K=1,KLAST)
600  FORMAT(3F10.5)
C
510  FORMAT (42HOC IS GREATER THAN BTAMX OR LESS THAN ZERO)
34  CONTINUE
   RETURN
   END

```

COMPUTER PROGRAM 2

POWELL CONJUGATE DIRECTION METHOD

LOBPTS No of Love wave data points (phase or group);

PP(M,1) Period of Love wave data;

D(M,1) Love wave phase velocity at PP(M,1);

DD(M,1) Love wave group velocity at PP(M,1);

MOBPTS No of Rayleigh wave data points;

PP(M,2) Period of Rayleigh wave data;

D(M,2) Rayleigh wave phase velocity at PP(M,2);

DD(M,2) Rayleigh wave group velocity at PP(M,2).

NLAY No of layers;

VA(J,J) A Thickness, Alpha, Beta and Rho for all the layers;

THICK Total depth up to which delay time would be attributed;

TIME 1 (1) Travel time up to a depth THICK by P wave for a shield type structure;

TIME 1 (2) Travel time up to a depth THICK by S wave for a shield type structure;

D TIME 1 (1) P - delay time after corrected for angle of emergence and height correction;

D TIME 1 (2) S - delay time after corrected for angle of emergence and height correction;

T (1) Period of first point on the curve;

DT Interval between point on the period axis;

Cl Phase velocity at which the search for the dispersion curve is begun.

DC Phase velocity interval between trial points.

KMA X Number of points required on dispersion curve.

LOVE Love = 1, causes the program to compute a Rayleigh mode. If LOVE = 0, a Love mode.

MODE NO A digit 1 to 9 cause the program to follow the dispersion curve corresponding to the first to ninth root crossed after the beginning of the initial search.

NTRIMX Maximum number of trials for each point
(= 60 if NTRIMX = 0).

KWRITE KWRITE = 1, causes the results of every trial solution to be printed with the output.
KWRITE = 0, eliminate the printing of trial solutions.

NX Number of unknowns.

MAXIT Number of iterations.

XXX(I) Starting value for each of the variables

XLO (I) Lower bound .

XUP (I) Upper bound.

FF Function to be minimized.

EE (I) Absolute accuracy to which its optimum value is required. EE (I) are approximately proportional to the magnitude of the corresponding variables XXX (I).

ESCALE ESCALE limits the maximum change in the variables at a single step. XXX(I) will not be changed by more than ESCALE, EE (I).

IPRINT IPRINT controls printing. If it is set to zero there will be no printing. If it is set to one the variables and the function will be printed after every search along a line (Approx. every other function value). If it is set to two then will be printed after each iterations, that is (N + 1) searches along a line.

ICON must be set to 1 or 2. It controls the ultimate convergence criterion. The routine will be left regardless after MAXIT iterations have been completed.

The minimum will practically never be found in less than N iterations. The function is calculated at least $2n$ times per iterations. The method is such that each iteration causes the function to decrease, except when the ultimate convergence criterion is being applied with $ICON = 2$.

The Ultimate Convergence Criterion

This will normally be satisfactory if $ICON$ is set to one. However, if low accuracy is required or if it is suspected that the required accuracy is not being achieved. $ICON$ should be set to two and a more thorough check on the ultimate convergence will be made at the expense of increasing the execution time by may be as much as 30% with $ICON = 1$ convergence will be assumed when iteration changes each variables by less than 10% of the required accuracy, with $ICON = 2$ such a point is found and it is then displaced by ten times the required accuracy in each variable. Minimisation is continued from the new point until a change of less than 10% is again made by an iteration.

The two estimates of the minimum are then compared.

Recommendations

- (i) Set $ESCALE$ as large as is reasonable remembering that it should be such that the resultant maximum step is most unlikely to be from one "Valley" to another.
- (ii) Set the required accuracy so that $ESCALE$ is at least one hundred.

- (iii) If the answers appear to be unreasonable try different initial values of the variables (XXX (I))

The function FF , to be minimized, would be made up of RMSD value between the observed dispersion data points and the one for a trial model. When using more than one set of curves, such as phase - and group - velocities of Love and Rayleigh wave; RMSD values from each curve would be weighted according to the observational error for those velocities; and then added together.

```

IMPLICIT REAL*8(A-H,O-Z), INTEGER*4(I-N)
DIMENSION A(100,4,4),C(50,5),E(4,4),Q(100,4,4),R(100,4,4),S(50,5),
1T(50),U(50),V(100,4),ACCEL(100),FA(4,4),PV(50),GV(50),
2B(100,2),D(250,2),THVAL(500),DVEL(250),RVEL(250),VA(100,4),DD(250,
32),XXX(62),EE(62)
DIMENSION PP(50,2),TIME2(2),TIME1(2),RMSD(2,2),DTIME1(2),DTIME2(2)
DIMENSION XLO(62),XUP(62)
COMMON A,C,E,K,M,Q,R,S,T,U,V,ACCEL,C1,C2,C3,CSQ,DELTA1,DELTA2,
1DT,FA,KLAST,KMAX,NLAY,NTRLS,WVND,PV,GV,B,D,THVAL,DVEL,RVEL,NUMPTS,
2MODENO,VA,DC,NTRLMX,KWRITE,NOBPTS,LOVE,DD,PP,TIME1,THICK,LOBPTS,
3MOBPTS,RMSD,DTIME1,DTIME2,XLO,XUP
READ(5,190) LOBPTS
READ(5,201) (PP(M,1),D(M,1),DD(M,1),M=1,LOBPTS)
WRITE(6,201)(PP(M,1),D(M,1),DD(M,1),M=1,LOBPTS)
READ(5,190) MOBPTS
READ(5,201) (PP(M,2),D(M,2),DD(M,2),M=1,MOBPTS)
WRITE(6,201)(PP(M,2),D(M,2),DD(M,2),M=1,MOBPTS)
190 FORMAT(I3)
201 FORMAT(3F10.5)
500 READ(5,502) NLAY
502 FORMAT(I3)
WRITE(6,502) NLAY
READ(5,300) (VA(I,1),VA(I,2),VA(I,4),I=1,NLAY)
WRITE(6,300) (VA(I,1),VA(I,2),VA(I,4),I=1,NLAY)
300 FORMAT(3F10.5)
READ(5,202) THICK,TIME1(1),TIME1(2),DTIME1(1),DTIME1(2)
WRITE(6,202)THICK,TIME1(1),TIME1(2),DTIME1(1),DTIME1(2)
202 FORMAT(5F10.5)
READ(5,504) C1,DC,LOVE,MODENO,NTRLMX,KWRITE
504 FORMAT(2F8.4,8X,I1,1X,I1,1X,I2,1X,I1)
WRITE(6,504) C1,DC,LOVE,MODENO,NTRLMX,KWRITE
READ(5,777) T(1),DT,KMAX
WRITE(6,777) T(1),DT,KMAX
777 FORMAT(2F10.5,I5)
READ(5,998) NX,ESCALE,MAXIT
998 FORMAT(I5,F15.5,I5)
WRITE(6,998) NX,ESCALE,MAXIT
READ(5,999) (XXX(I),EE(I),I=1,NX)
999 FORMAT(2F15.5)
WRITE(6,999) (XXX(I),EE(I),I=1,NX)
READ(5,999) (XLO(I),XUP(I),I=1,NX)
WRITE(6,999)(XLO(I),XUP(I),I=1,NX)
CALL VA04A(XXX,EE,NX,FF,ESCALE,2,1,MAXIT)
STOP
END

```

```

SUBROUTINE VAO4A (X,E,N,F,ESCALE,IPRINT,ICON,MAXIT)
IMPLICIT REAL*8(A-H,O-Z),INTEGER*4(I-N)
DIMENSION W(4030),X(62),E(62)
ABS(X)=DABS(X)
SQRT(X)=DSQRT(X)
AMIN1(X,Y)=DMIN1(X,Y)
AMAX1(X,Y)=DMAX1(X,Y)
DDMAG=0.1*ESCALE
SCER=0.05/ESCALE
INDRA=1
JJ=N*N+N
JJJ=JJ+N
K=N+1
NFCC=1
IND=1
INN=1
DO 1 I=1,N
DO 2 J=1,N
W(K)=0.
IF(I-J)4,3,4
3 W(K)=ABS (E(I))
W(I)=ESCALE
4 K=K+1
2 CONTINUE
1 CONTINUE
ITERC=1
ISGRAD=2
CALL CALCFX(N,X,F,INDRA)
FKEEP=ABS (F)+ABS (F)
5 ITONE=1
FP=F
SUM=0.
IXP=JJ
DO 6 I=1,N
IXP=IXP+1
W(IXP)=X(I)
6 CONTINUE
IDIRN=N+1
ILINE=1
7 DMAX=W(ILINE)
DACC=DMAX*SCER
DMAG=AMIN1 (DDMAG,0.1*DMAX)
DMAG=AMAX1(DMAG,20.*DACC)
DDMAX=10.*DMAG
GO TO (70,70,71),ITONE
70 DL=0.
D=DMAG
FPREV=F
IS=5
FA=F
DA=DL
8 DD=D-DL
DL=D
58 K=IDIRN
DO 9 I=1,N

```

```

X(I)=X(I)+DD*W(K)
K=K+1
9 CONTINUE
FSTORE=F
CALL CALCFX(N,X,F,INDRA)
NFCC=NFCC+1
GO TO (10,11,12,13,14,96),IS
14 IF(F-FA)15,16,24
16 IF (ABS (D)-DMAX) 17,17,18
17 D=D+D
GO TO 8
18 WRITE(6,19)
19 FORMAT(5X,44HVA04A MAXIMUM CHANGE DOES NOT ALTER FUNCTION)
GO TO 20
15 FB=F
DB=D
GO TO 21
24 FB=FA
DB=DA
FA=F
DA=D
21 GO TO (83,23),ISGRAD
23 D=DB+DB-DA
IS=1
GO TO 8
83 D=0.5*(DA+DB-(FA-FB)/(DA-DB))
IS=4
IF((DA-D)*(D-DB))25,8,8
25 IS=1
IF(ABS (D-DB)-DDMAX)8,8,26
26 D=DB+DSIGN(DDMAX,DB-DA)
IS=1
DDMAX=DDMAX+DDMAX
DDMAG=DDMAG+DDMAG
IF(DDMAX-DMAX)8,8,27
27 DDMAX=DMAX
GO TO 8
13 IF(F-FB)28,23,23
28 FC=FB
DC=DB
29 FB=F
DB=D
GO TO 30
12 IF(F-FB)28,28,31
31 FA=F
DA=D
GO TO 30
11 IF(F-FB)32,10,10
32 FA=FB
DA=DB
GO TO 29
71 DL=1.
DDMAX=5.
FA=FP
DA=-1.

```

```

F8=FHOLD
DB=0.
D=1.
10 FC=F
DC=D
30 A=(DB-DC)*(FA-FC)
B=(DC-DA)*(FB-FC)
IF((A+B)*(DA-DC))33,33,34
33 FA=FB
DA=DB
FB=FC
DB=DC
GO TO 26
34 D=0.5*(A*(DB+DC)+B*(DA+DC))/(A+B)
DI=DB
FI=FB
IF(FB-FC)44,44,43
43 DI=DC
FI=FC
44 GO TO (86,86,85),ITONE
85 ITONE=2
GO TO 45
86 IF (ABS (D-DI)-DACC) 41,41,93
93 IF (ABS (D-DI)-0.03*ABS (D)) 41,41,999
999 IF(ABS(F-FSTORE)-0.01*ABS(F))41,41,45
45 IF ((DA-DC)*(DC-D)) 47,46,46
46 FA=FB
DA=DB
FB=FC
DB=DC
GO TO 25
47 IS=2
IF ((DB-D)*(D-DC)) 48,8,8
48 IS=3
GO TO 8
41 F=FI
D=DI-DL
DD=SQRT ((DC-DB)*(DC-DA)*(DA-DB)/(A+B))
DO 49 I=1,N
X(I)=X(I)+D*W(IDIRN)
W(IDIRN)=DD*W(IDIRN)
IDIRN=IDIRN+1
49 CONTINUE
W(ILINE)=W(ILINE)/DD
ILINE=ILINE+1
IF(IPRINT-1)51,50,51
50 WRITE(6,52) ITERC,NFCC,F,(X(I),I=1,N)
52 FORMAT (/1X,9HITERATION,I5,I15,16H FUNCTION VALUES,
110X,3HF =,E21.14/(5E24.14))
INDRA=0
CALL CALCFX(N,X,F,INDRA)
INDRA=1
GO TO(51,53),IPRINT
51 GO TO (55,38),ITONE
55 IF (FPREV-F-SUM) 94,95,95

```

```
95 SUM=FPREV-F
   JIL=ILINE
94 IF (IDIRN-JJ) 7,7,84
84 GO TO (92,72),IND
92 FHOLD=F
   IS=6
   IXP=JJ
   DO 59 I=1,N
   IXP=IXP+1
   W(IXP)=X(I)-W(IXP)
59 CONTINUE
   DD=1.
   GO TO 58
96 GO TO (112,87),IND
112 IF (FP-F) 37,37,91
91 D=2.*(FP+F-2.*FHOLD)/(FP-F)**2
   IF (D*(FP-FHOLD-SUM)**2-SUM) 87,37,37
87 J=JIL*N+1
   IF (J-JJ) 60,60,61
60 DO 62 I=J,JJ
   K=I-N
   W(K)=W(I)
62 CONTINUE
   DO 97 I=JIL,N
   W(I-1)=W(I)
97 CONTINUE
61 IDIRN=IDIRN-N
   ITONE=3
   K=IDIRN
   IXP=JJ
   AAA=0.
   DO 65 I=1,N
   IXP=IXP+1
   W(K)=W(IXP)
   IF (AAA-ABS (W(K)/E(I))) 66,67,67
66 AAA=ABS (W(K)/E(I))
67 K=K+1
65 CONTINUE
   DDMAG=1.
   W(N)=ESCALE/AAA
   ILINE=N
   GO TO 7
37 IXP=JJ
   AAA=0.
   F=FHOLD
   DO 99 I=1,N
   IXP=IXP+1
   X(I)=X(I)-W(IXP)
   IF (AAA*ABS (E(I))-ABS (W(IXP))) 98,99,99
98 AAA=ABS (W(IXP)/E(I))
99 CONTINUE
   GO TO 72
38 AAA=AAA*(1.+DI)
   GO TO (72,106),IND
72 IF (IPRINT-2) 53,50,50
```

```
53 GO TO (109,88),IND
109 IF (AAA-0.1) 89,89,76
89 GO TO (20,116),ICON
116 IND=2
GO TO (100,101),INN
100 INN=2
K=JJJ
DO 102 I=1,N
K=K+1
W(K)=X(I)
X(I)=X(I)+10.*E(I)
102 CONTINUE
FKEEP=F
WRITE(6,702)
702 FORMAT(15H THIS CALL NO 3)
CALL CALCFX(N,X,F,INDRA)
NFCC=NFCC+1
DDMAG=0.
GO TO 108
76 IF (F-FP) 35,78,78
78 WRITE(6,80)
80 FORMAT (5X,37HVA04A ACCURACY LIMITED BY ERRORS IN F)
GO TO 20
88 IND=1
35 DDMAG=0.4*SQRT (FP-F)
ISGRAD=1
108 ITERC=ITERC+1
IF (ITERC-MAXIT) 5,5,81
81 WRITE(6,82) MAXIT
82 FORMAT(15,30H ITERATIONS COMPLETED BY VA04A)
IF (F-FKEEP) 20,20,110
110 F=FKEEP
DO 111 I=1,N
JJJ=JJJ+1
X(I)=W(JJJ)
111 CONTINUE
GO TO 20
101 JIL=1
FP=FKEEP
IF (F-FKEEP) 105,78,104
104 JIL=2
FP=F
F=FKEEP
105 IXP=JJ
DO 113 I=1,N
IXP=IXP+1
K=IXP+N
GO TO (114,115),JIL
114 W(IXP)=W(K)
GO TO 113
115 W(IXP)=X(I)
X(I)=W(K)
113 CONTINUE
JIL=2
GO TO 92
```

```
106 IF (AAA-0.1) 20,20,107  
20 RETURN  
107 INN=1  
GO TO 35  
END
```

```
SUBROUTINE CALCFX(NX,XXX,FF,INDRA)
IMPLICIT REAL*8(A-H,O-Z),INTEGER*4(I-N)
```

```
DIMENSION A(100,4,4),C(50,5),E(4,4),Q(100,4,4),R(100,4,4),S(50,5),
1T(50),U(50),V(100,4),ACCEL(100),FA(4,4),PV(50),GV(50),
2B(100,2),D(250,2),THVAL(500),DVEL(250),RVEL(250),VA(100,4),DD(250,
32),XXX(62),PP(50,2),TIME2(2),DTIME1(2),DTIME2(2),RMSD(2,2),TIME1(2
4)
```

```
DIMENSION XLO(62),XUP(62)
COMMON A,C,E,K,M,Q,R,S,T,U,V,ACCEL,C1,C2,C3,CSQ,DELTA1,DELTA2,
1DT,FA,KLAST,KMAX,NLAY,NTRLS,WVNO,PV,GV,B,D,THVAL,DVEL,RVEL,NUMPTS,
2MODENO,VA,DC,NTRLMX,KWRITE,NOBPTS,LOVE,DD,PP,TIME1,THICK,LOBPTS,
3MOBPTS,RMSD,DTIME1,DTIME2,XLO,XUP
```

```
ABS(X)=DABS(X)
AMAX1(X,Y)=DMAX1(X,Y)
SQRT(X)=DSQRT(X)
```

```
VA(1,3)=2.0
VA(2,3)=3.4
VA(3,3)=3.5
VA(4,3)=3.9
VA(7,3)=4.5
VA(NLAY,3)=4.85
```

```
FF=0.0
DO 345 KAMALA=1,2
C1=2.5
```

```
602 DO 2 K=1,4
K1=K+1
DO 1 L=K1,5
S(K,L)=0.0
C(K,L)=0.0
```

```
1 CONTINUE
2 CONTINUE
DO 4 I=1,4
DO 3 J=1,4
E(I,J)=0.0
```

```
3 CONTINUE
4 CONTINUE
LOVE=KAMALA-1
V(1,3)=VA(1,3)
V(2,3)=VA(2,3)
V(3,3)=VA(3,3)
V(4,3)=VA(4,3)
V(7,3)=VA(7,3)
```

```
V(NLAY,3)=VA(NLAY,3)
DO 303 I=1,NLAY
V(I,1)=VA(I,1)
V(I,2)=VA(I,2)
V(I,4)=VA(I,4)
```

```
303 CONTINUE
DO 302 I=5,6
N=I-4
V(I,3)=XLO(N)+(XUP(N)-XLO(N))*((DSIN(XXX(N))))**2)
```

```

V(I,2)=V(I,3)*1.74
302 CONTINUE
V(1,1)=XLO(3)+(XUP(3)-XLO(3))*((DSIN(XXX(3)))**2)
V(4,1)=XLO(4)+(XUP(4)-XLO(4))*((DSIN(XXX(4)))**2)
V(5,1)=XLO(5)+(XUP(5)-XLO(5))*((DSIN(XXX(5)))**2)
V(6,1)=180.0-V(5,1)
IF(KAMALA.GT.1) GO TO 801
DO 905 J=1,2
TIME2(J)=0.0
H=0.0
DO 901 I=1,NLAY
H=H+V(I,1)
JJ=J+1
IF(H.GT.THICK) GO TO 902
IF(I.EQ.NLAY) GO TO 904
TIME2(J)=TIME2(J)+V(I,1)/V(I,JJ)
GO TO 901
904 H=THICK-H
TIME2(J)=TIME2(J)+H/V(NLAY,JJ)
GO TO 903
902 H=H-V(I,1)
H=THICK-H
TIME2(J)=H/V(I,JJ)+TIME2(J)
GO TO 903
901 CONTINUE
903 DTIME2(J)=TIME2(J)-TIME1(J)
DTIME2(J)=ABS(DTIME1(J)-DTIME2(J))
905 CONTINUE
801 RADIUS=6371.0
IF(LOVE.GT.0) GO TO 701
Z=0.0
NLAY1=NLAY-1
DO 702 M=1,NLAY1
Z=Z+V(M,1)/2.0
V(M,3)=V(M,3)*RADIUS/(RADIUS-Z)
702 Z=Z+V(M,1)/2.0
V(NLAY,3)=V(NLAY,3)*RADIUS/(RADIUS-Z)
701 BTAMX=ABS(V(1,3))
DO 6 M=2,NLAY
BTAMX=AMAX1(BTAMX,ABS(V(M,3)))
6 CONTINUE
ACCEL(3)=KWRITE
ACCEL(2)=60.0
9 DO 10 K=2,KMAX
T(K)=T(K-1)+DT
10 CONTINUE
MODE=MODENO-1
803 K=1
ACCEL(1)=LOVE
IF(ACCEL(1))11,12,11
11 DELTA1=DLTAR3(C1,T(1))
GO TO 15
12 DELTA1=DLTAL1(C1,T(1))
GO TO 15
14 C1=C2

```

```

      DELTA1=DELTA2
15  C2=C1+DC
      IF(ABS (C2-0.5*BTAMX)-0.5*BTAMX)17,17,16
16  WRITE(6,510)
      GO TO 34
17  IF(ACCEL(1))18,19,18
18  DELTA2=DLTAR3(C2,T(1))
      GO TO 20
19  DELTA2=DLTAL1(C2,T(1))
20  CONTINUE
807 IF(ABS (DELTA2-DELTA1)-ABS (DELTA2+DELTA1))14,14,23
23  CALL FOLCV4
C    COMPUTATION SUBROUTINE CALLED.
754 IF(KLAST-5)24,27,27
C
      24 IF(KLAST)900,900,25
      25 DO 26 K=1,KLAST
          U(K)=0.0
      26 CONTINUE
          GO TO 900
      27 CALL GPVEL2
C    GPVEL2 SUBROUTINE CALLED
      IF(LOVE.LT.1) GO TO 900
753 DO 750 K=1,KLAST
      U(K)=U(K)*(1.0+(0.00016*T(K))*(1.0-U(K)/C(K,1)))
      C(K,1)=C(K,1)*(1.0+0.00016*T(K))
750 CONTINUE
C
900 CONTINUE
      IF(KAMALA.LT.2) GO TO 2510
      NOBPTS=MOBPTS
      GO TO 251
2510 NOBPTS=LOBPTS
C
251 DO 254 K=1,KMAX
      THVAL((2*K)-1)=T(K)
254 CONTINUE
      DO 255 K=1,KMAX
      THVAL(2*K)=C(K,1)
255 CONTINUE
C
260 M=1
      POOR1=PP(1,KAMALA)
      OBVEL1=D(1,KAMALA)
      CALL LAGRAN (THVAL,KMAX,POOR1,ANS)
      RVEL(1)=ANS
      DVEL(1)=OBVEL1-ANS
      SDVEL=0.0
      SDVEL=SDVEL+DVEL(1)**2
261 M=M+1
      IF(M-NOBPTS)262,262,263
262 POOR2=PP(M,KAMALA)
      OBVEL2=D(M,KAMALA)
      CALL LAGRAN(THVAL,KMAX,POOR2,ANS)
      RVEL(M)=ANS

```

```

DVEL(M)=OBVEL2-ANS
SDVEL=SDVEL+(DVEL(M)**2)
GO TO 261

```

C

```

263 SDVEL=SDVEL/NOBPTS
RMSD(1,KAMALA)=SQRT(SDVEL)
IF(INDRA) 1251,264,1251
264 WRITE(6,603) (PP(M,KAMALA),D(M,KAMALA),RVEL(M),DVEL(M),M=1,NOB
1PTS)
603 FORMAT(4F15.5)
WRITE(6,350) ((V(I,J),J=1,4),I=1,NLAY)
350 FORMAT(4F10.5)
1251 DO 1254 K=1,KMAX
THVAL((2*K)-1)=T(K)
1254 CONTINUE
DO 1255 K=1,KMAX
THVAL(2*K)=U(K)
1255 CONTINUE
1260 M=1
POOR1=PP(1,KAMALA)
OBVEL1=DD(1,KAMALA)
CALL LAGRAN (THVAL,KMAX,POOR1,ANS)
RVEL(1)=ANS
DVEL(1)=OBVEL1-ANS
SDVEL=0.0
SDVEL=SDVEL+DVEL(1)**2
1261 M=M+1
IF(M-NOBPTS)1262,1262,1263
1262 POOR2=PP(M,KAMALA)
OBVEL2=DD(M,KAMALA)
CALL LAGRAN (THVAL,KMAX,POOR2,ANS)
RVEL(M)=ANS
DVEL(M)=OBVEL2-ANS
SDVEL=SDVEL+(DVEL(M)**2)
GO TO 1261
1263 SDVEL=SDVEL/NOBPTS
RMSD(2,KAMALA)=SQRT(SDVEL)
IF(INDRA) 511,1264,511
1264 WRITE(6,604) (PP(M,KAMALA),DD(M,KAMALA),RVEL(M),DVEL(M),M=1,NOB
1PTS)
604 FORMAT(4F15.5)
WRITE(6,353) RMSD(1,KAMALA),RMSD(2,KAMALA)
353 FORMAT(2F15.5)
WRITE(6,351) DTIME2(1),DTIME2(2)
351 FORMAT(2F15.5)
511 CONTINUE
C
510 FORMAT (42HOC IS GREATER THAN BTAMX OR LESS THAN ZERO)
345 CONTINUE
FF=FF+RMSD(1,1)/2.0+RMSD(2,1)/2.0+RMSD(1,2)+RMSD(2,2)/2.0+DTIME2(1
1)/20.0
34 CONTINUE
RETURN
END

```

COMPUTER PROGRAM 3

MAPPING IN HYPERSPACE

```

IMPLICIT REAL*8(A-H,D-Z), INTEGER*4(I-N)
DIMENSION A(100,4,4),C(50,5),E(4,4),Q(100,4,4),R(100,4,4),S(50,5),
1T(50),U(50),V(100,4),ACCEL(100),FA(4,4),PV(50),GV(50),
2B(100,2),D(250,2),THVAL(500),DVEL(250),RVEL(250),DD(250,2),
3XXX(62),VVA(100,4)
COMMON A,C,E,K,M,Q,R,S,T,U,V,ACCEL,C1,C2,C3,CSQ,DELTA1,DELTA2,
1DT,FA,KLAST,KMAX,NLAY,NTRLS,WVND,PV,GV,B,D,THVAL,DVEL,RVEL,NUMPTS,
2MODENO,DC,NTRLMX,KWRITE,NOBPTS,LOVE,DD,VVA,MOBPTS
READ(5,1) NOBPTS,IN,JN,JYMN
WRITE(6,1) NOBPTS,IN,JN,JYMN
1 FORMAT(4I3)
READ(5,2) MOBPTS
2 FORMAT(I3)
NX=IN+JN
C IN NO OF PARAMETERS CHANGING IN DIRECTION I
C JN NO OF PARAMETERS CHANGING IN DIRECTION J
C NX NO OF PARAMETERS BEING MAPPED
C NX=IN+JN
C JYMN NO OF POINTS ON GRID IN EACH DIRECTION
C IV AN ARRAY OF INTEGER VALUES DENOTING THE SERIAL NUMBERS OF
C VARIABLES VARYING IN DIRECTION I
C JV AN ARRAY OF INTEGER VALUES DENOTING THE SERIAL NUMBERS OF
C VARIABLES VARYING IN DIRECTION J
C X1 COORDINATES IN THE HYPERSPACE OF FIRST POINT
C X2 COORDINATES IN THE HYPERSPACE OF SECOND POINT
C KI I-COORDINATES OF FIRST POINT
C KJ J-COORDINATES OF FIRST POINT
C INTI NO OF GRID POINTS TO SECOND POINT IN I DIRECTION FROM
C FIRST POINT
C INTJ NO OF GRID POINTS TO SECOND POINT IN J DIRECTION FROM
C FIRST POINT
CALL MAP(NX,IN,JN,JYMN)
STOP
END

```

```

SUBROUTINE MAP(NX, IN, JN, JYMN)
  IMPLICIT REAL *8(A-H, O-Z), INTEGER*4(I-N)
  DIMENSION IV(40), JV(40), X1(30), X2(30), CT(40,40), ZZ(24), VA(40,40),
  1KVA(40,40), XB(40,30), XA(30)
  DIMENSION A(100,4,4), C(50,5), E(4,4), Q(100,4,4), R(100,4,4), S(50,5),
  1T(50), U(50), V(100,4), ACCEL(100), FA(4,4), PV(50), GV(50),
  2B(100,2), D(250,2), THVAL(500), DVEL(250), RVEL(250), DD(250,2),
  3XXX(62), VVA(100,4)
  COMMON A, C, E, K, M, Q, R, S, T, U, V, ACCEL, C1, C2, C3, CSQ, DELTA1, DELTA2,
  1DT, FA, KLAST, KMAX, NLAY, NTRLS, WVNO, PV, GV, B, D, THVAL, DVEL, RVEL, NUMPTS,
  2MODENO, DC, NTRLMX, KWRITE, NOBPTS, LOVE, DD, VVA, MOBPTS
  DATA STAR/'.*'/
  DATA OH/'.O'/
  DATA ZZ/'.A', '.B', '.C', '.D', '.F', '.G', '.H', '.I', '.J', '.K', '.L',
  1'.M', '.N', '.P', '.Q', '.R', '.S', '.T', '.U', '.V', '.W', '.X', '.Y',
  2'.E'/
  READ (5,11) (X1(I), I=1, NX)
  READ (5,11) (X2(I), I=1, NX)
11 FORMAT (F15.5)
  WRITE (6,11) (X1(I), X2(I), I=1, NX)
  READ(5,12)(IV(I), I=1, IN)
  READ(5,12)(JV(J), J=1, JN)
  WRITE(6,12)(IV(I), I=1, IN)
  WRITE(6,12)(JV(J), J=1, JN)
12 FORMAT(I5)
  READ(5,13) KI, KJ, INTI, INTJ
  WRITE(6,13)KI, KJ, INTI, INTJ
13 FORMAT(4I5)
  READ(5,100)((D(I,J), J=1, 2), I=1, NOBPTS)
  WRITE(6,100)((D(I,J), J=1, 2), I=1, NOBPTS)
  READ(5,100) ((DD(I,J), J=1, 2), I=1, MOBPTS)
  WRITE(6,100) ((DD(I,J), J=1, 2), I=1, MOBPTS)
100 FORMAT(2F8.3)
  READ(5,300) NLAY
300 FORMAT(I3)
  READ(5,301) ((VVA(I,J), J=1, 4), I=1, NLAY)
  WRITE(6,301)((VVA(I,J), J=1, 4), I=1, NLAY)
301 FORMAT(4F8.3)
  READ(5,101) T(1), DT, C1, DC, KMAX, LOVE, MODENO, NTRLMX, KWRITE
101 FORMAT(4F8.5, 8X, I3, 1X, I1, 1X, I1, 1X, I2, 1X, I1)
  WRITE(6,101)T(1), DT, C1, DC, KMAX, LOVE, MODENO, NTRLMX, KWRITE
  TI=INTI
  AK=KI
  AK=AK-1.
  DO 31 I=1, IN
  L=IV(I)
  PIN=(X2(L)-X1(L))/TI
  XB(1,L)=X1(L)-AK*PIN
  DO 31 MG=1, JYMN
  AMG=MG
  AMG=AMG-1.
  XB(MG,L)=XB(1,L)+AMG*PIN
31 CONTINUE
  TJ=INTJ
  AK=KJ
  AK=AK-1.
  DO 32 J=1, JN
  L=JV(J)

```

```

PIN=(X2(L)-X1(L))/TJ
XB(1,L)=X1(L)-AK*PIN
DO 32 MG=1,JYMN
AMG=MG
AMG=AMG-1.
XB(MG,L)=XB(1,L)+AMG*PIN
32 CONTINUE
C DISTRIBUTION PARAMETERS AND CALCULATING GRID FUNCTIONS
DO 6638 II=1,JYMN
DO 6638 JJ=1,JYMN
DO 36 IM=1,IN
L=IV(IM)
XA(L)=XB(II,L)
36 CONTINUE
DO 37 JM=1,JN
L=JV(JM)
XA(L)=XB(JJ,L)
37 CCNTINUE
C THE VARIABLES ARE NOW DISTRIBUTED IN EACH OF THE XA IN APPROPRIA
C TE SERIES, EXACTLY AS IN X1,X2. HENCE
C T1 X1(1) X2(1) XA(1)
C ALPHA X1(2) X2(2) XA(2)
C AND SO ON
C ALPHA3 X1(9) X2(9) XA(9)
C DENS13 X1(11) X2(11) XA(11)
C THE CURRENT VALUES OF THE VARIABLES IS STORED IN THE APPROPRIATE
C XA.WE MAY TRANSFORM THEM INTO WHATEVER FORM SUITABLE
WRITE(6,201) II,JJ
201 FORMAT(2I5)
WRITE(6,202) (XA(KA),KA=1,NX)
202 FORMAT(10F10.5)
CALL CALCFX(NX,XA,FF)
VA(II,JJ)=FF
6638 CONTINUE
C WORKING OUT MINI.VALUE AND GENERAL EDITING
IK=KI+INTI
JK=KJ+INTJ
WRITE(6,41) VA(KI,KJ)
41 FORMAT(30HFUNCTION VALUE OF FIRST POINT=,F15.5)
WRITE(6,43) VA(IK,JK)
43 FORMAT(32HFUNCTION VALUE OF SECOND POINT= ,F15.5)
BM=VA(1,1)
AM=VA(1,2)
DO 51 I=1,JYMN
DO 51 J=1,JYMN
IF(VA(I,J)-BM)52,51,51
52 BM=VA(I,J)
51 CONTINUE
DO 53 I=1,JYMN
DO 53 J=1,JYMN
KTH=0
LTH=0
IF(VA(I,J).LT.AM) KTH=1
IF(VA(I,J).GT.BM) LTH=1
MIN=KTH*LTH
IF(MIN-1)53,54,53
54 AM=VA(I,J)
53 CONTINUE

```

```

WRITE(6,55) BM, AM
55 FORMAT(15HMINIMUM VALUE =,F15.5,5X,5HAM = ,F15.5)
WRITE(6,56) KI,KJ,IK,JK
56 FORMAT(1H0,15HFIRST POINT AT ,2I5,16HSECOND POINT AT ,2I5)
C EVALUATING AND MAPPING OUT
WRITE(6,67)
DO 20 I=1,JYMN
DO 20 J=1,JYMN
IF(AM.LT.0.01) GO TO 14
AV=(VA(I,J)/AM)*10.0
GO TO 15
14 AV=VA(I,J)/AM
15 KVA(I,J)=AV
IF(AV-99.0)28,28,27
27 KVA(I,J)=99
28 IF(AV-10.0)21,22,23
21 CT(I,J)=STAR
GO TO 20
22 CT(I,J)=OH
GO TO 20
23 AL=DLOG(AV)
LAR=AL
IF(LAR-24) 24,25,25
25 LAR=24
24 CT(I,J)=ZZ(LAR)
20 CONTINUE
DO 26 I=1,JYMN
WRITE(6,60)
60 FORMAT(1H )
WRITE(6,61)(CT(I,J),J=1,JYMN)
61 FORMAT(1X,40A3)
26 CONTINUE
WRITE(6,67)
67 FORMAT(1H1)
DO 29 I=1,JYMN
WRITE(6,62)
62 FORMAT(1H )
WRITE(6,63) (KVA(I,J),J=1,JYMN)
63 FORMAT(1X,40I3)
29 CONTINUE
RETURN
END

```

SUBROUTINE CALCFX(NX,XXX,FF)
 IMPLICIT REAL*8(A-H,O-Z),INTEGER*4(I-N)

DIMENSION A(100,4,4),C(50,5),E(4,4),Q(100,4,4),R(100,4,4),S(50,5),
 IT(50),U(50),V(100,4),ACCEL(100),FA(4,4),PV(50),GV(50),
 2B(100,2),D(250,2),THVAL(500),DVEL(250),RVEL(250),VA(100,4),DD(250,
 32),XXX(62),VVA(100,4)

COMMON A,C,E,K,M,Q,R,S,T,U,V,ACCEL,C1,C2,C3,CSQ,DELTA1,DELTA2,
 1DT,FA,KLAST,KMAX,NLAY,NTRLS,WVND,PV,GV,B,D,THVAL,DVEL,RVEL,NUMPTS,
 2MODENO,DC,NTRLMX,KWRITE,NOBPTS,LOVE,DD,VVA,MOBPTS

C
 C
 C
 ABS(X)=DABS(X)
 AMAX1(X,Y)=DMAX1(X,Y)
 SQR(X)=DSQR(X)
 602 DO 2 K=1,4
 K1=K+1
 DO 1 L=K1,5
 S(K,L)=0.0
 C(K,L)=0.0
 1 CONTINUE
 2 CONTINUE
 DO 4 I=1,4
 DO 3 J=1,4
 E(I,J)=0.0
 3 CONTINUE
 4 CONTINUE
 DO 301 I=1,NLAY
 V(I,1)=VVA(I,1)
 V(I,2)=VVA(I,2)
 V(I,3)=VVA(I,3)
 V(I,4)=VVA(I,4)
 301 CONTINUE
 DO 300 I=4,6
 N=I-3
 V(I,3)=XXX(N)
 VVA(I,3)=V(I,3)
 V(I,2)=1.74*V(I,3)
 VVA(I,2)=V(I,2)
 300 CONTINUE
 V(4,1)=XXX(4)
 V(5,1)=XXX(5)
 V(6,1)=XXX(6)
 801 RADIUS=6371.0
 IF(LOVE.GT.0) GO TO 701
 Z=0.0
 NLAY1=NLAY-1
 DO 702 M=1,NLAY1
 Z=Z+V(M,1)/2.0
 V(M,3)=V(M,3)*RADIUS/(RADIUS-Z)
 702 Z=Z+V(M,1)/2.0
 V(NLAY,3)=V(NLAY,3)*RADIUS/(RADIUS-Z)
 701 BTAMX=ABS(V(1,3))
 DO 6 M=2,NLAY
 BTAMX=AMAX1(BTAMX,ABS(V(M,3)))
 6 CONTINUE
 ACCEL(3)=KWRITE

```

ACCEL(2)=60.0
9 DO 10 K=2,KMAX
T(K)=T(K-1)+DT
10 CONTINUE
MODE=MODEND-1
803 K=1
ACCEL(1)=LOVE
IF(ACCEL(1))11,12,11
11 DELTA1=DLTAR3(C1,T(1))
GO TO 15
12 DELTA1=DLTAL1(C1,T(1))
GO TO 15
14 C1=C2
DELTA1=DELTA2
15 C2=C1+DC
IF(ABS(C2-0.5*BTAMX)-0.5*BTAMX)17,17,16
16 WRITE(6,510)
GO TO 34
17 IF(ACCEL(1))18,19,18
18 DELTA2=DLTAR3(C2,T(1))
GO TO 20
19 DELTA2=DLTAL1(C2,T(1))
20 CONTINUE
807 IF(ABS(DELTA2-DELTA1)-ABS(DELTA2+DELTA1))14,14,23
23 CALL FOLCV4
C
COMPUTATION SUBROUTINE CALLED.
C
IF(KLAST-5)24,27,27
24 IF(KLAST)900,900,25
25 DO 26 K=1,KLAST
U(K)=0.0
26 CONTINUE
GO TO 900
27 CALL GPVEL2
C
GPVEL2 SUBROUTINE CALLED
C
IF(LOVE.LT.1) GO TO 900
502 DO 505 K=1,KLAST
U(K)=U(K)*(1.0+(0.00016*T(K))*(1.0-U(K)/C(K,1)))
C(K,1)=C(K,1)*(1.0+0.00016*T(K))
505 CONTINUE
900 CONTINUE
C
251 DO 254 K=1,KMAX
THVAL((2*K)-1)=T(K)
254 CONTINUE
DO 255 K=1,KMAX
THVAL(2*K)=C(K,1)
255 CONTINUE
C
260 M=1
POOR1=D(1,1)
OBVEL1=D(1,2)
CALL LAGRAN(THVAL,KMAX,POOR1,ANS)
RVEL(1)=ANS
DVEL(1)=OBVEL1-ANS
SDVEL=0.0
SDVEL=SDVEL+DVEL(1)**2

```

```

261 M=M+1
    IF(M-NOBPTS) 262, 262, 263
262 PCOR2=D(M, 1)
    OBVEL2=D(M, 2)
    CALL LAGRAN(THVAL, KMAX, POOR2, ANS)
    RVEL(M)=ANS
    DVEL(M)=OBVEL2-ANS
    SDVEL=SDVEL+(DVEL(M)**2)
    GO TO 261
C
263 SDVEL=SDVEL/NOBPTS
    PRMSD=SQRT(SDVEL)
    DO 1254 K=1, KMAX
    THVAL((2*K)-1)=T(K)
1254 CONTINUE
    DO 1255 K=1, KMAX
    THVAL(2*K)=U(K)
1255 CONTINUE
1260 M=1
    PCOR1=DD(1, 1)
    OBVEL1=DD(1, 2)
    CALL LAGRAN(THVAL, KMAX, POOR1, ANS)
    RVEL(1)=ANS
    DVEL(1)=OBVEL1-ANS
    SDVEL=0.0
    SDVEL=SDVEL+DVEL(1)**2
1261 M=M+1
    IF(M-MOBPTS) 1262, 1262, 1263
1262 PCOR2=DD(M, 1)
    OBVEL2=DD(M, 2)
    CALL LAGRAN(THVAL, KMAX, POOR2, ANS)
    RVEL(M)=ANS
    DVEL(M)=OBVEL2-ANS
    SDVEL=SDVEL+(DVEL(M)**2)
    GO TO 1261
1263 SDVEL=SDVEL/MOBPTS
    GRMSD=SQRT(SDVEL)
    FF=PRMSD+GRMSD
C
510 FORMAT (42HQC IS GREATER THAN BTAMX OR LESS THAN ZERO)
    C1=2.2
34 CONTINUE
    END

```

R E F E R E N C E S

1. Abe, M. and Suzaki, Z. (1970) A model seismological study on the propagation of Rayleigh waves in a Medium with a Dipping Boundary between Superficial Layer and Basement, Geophysics, 20, 1 - 25. (The science reports of the Tohoku University, Ser.5.)
2. Aki, K. (1968). Seismological evidence for the existence of soft thin layers in the upper mantle under Japan, Geophys. Res., 73, 585 -
3. Alterman, Z., Jarosch, H. and Pekeris, C.L. (1961). Propagation of Rayleigh waves in the earth, Geophys. J.R. Astr. Soc., 4, 219 - 241.
4. Alexander, S.S. (1963). Surface wave propagation in the western United States, Ph.D. Thesis, Calif. Inst. of Tech.
5. Anderson, D.L. and Toksoz, M.N. (1963). Surface waves on a spherical earth, 1. Upper mantle structure from Love waves, J.Geophys. Res., 68, 3483 - 3500.
6. Anderson, D.L. and Archambeau C.B. (1964). The anelasticity of the earth, J. Geophys. Res., 69, 2071 - 2084.
7. Anderson, D.L. (1965). Recent evidence concerning the structure and composition of the earth's mantle, Physics and Chemistry of the earth, 6, 1 - 131.
8. Anderson, D.L. (1967). The anelasticity of the mantle, Geophys. J.R. Astr. Soc., 14, 135 - 164.
9. Anderson, D.L. (1967). Latest information from seismic observations, The earth's mantle, Academic Press, 355 - 420.
10. Artemjer, M.E. and Artyushkov, E.V. (1971). Structure and Isotasy of the Baikal rift and the mechanism of Rifting, J. Geophys. Res., 76, 1197 - 1211.

11. Backus, G.E. and Gilbert, J.F. (1967). Numerical application of a formalism for geophysical inverse problems, *Geophys. J.R. Astr. Soc.*, 13, 247 - 276.
12. Backus, G. and Gilbert, F. (1968). The Resolving power of Gross earth data, *Geophys. J.R. Astr. Soc.*, 16, 169 - 205.
13. Bailey, D.K. (1964). Crustal warping - A possible tectonic control of Alkaline magmatism, *J. Geophys. Res.*, 69, 1103 - 1111.
14. Baker, B.H. (1965). "An outline of the geology of the Kenya rift valley". UMG - UNESCO seminar 'The East African rift system', Nairobi. Part 2, 1 - 19.
15. Baker, B.H. and Wohlenberg, J. (1971). Structure and Evolution of the Kenya rift valley, *Nature*, 229, 538 - 542.
16. Banghar, A.R. and Sykes, L.R. (1969). "Focal mechanism of earthquakes in the Indian Ocean and adjacent regions", *J. Geophys. Res.*, 74, 632 - 649.
17. Bath, M. (1960). Crustal structure of Iceland, *J. Geophys. Res.*, 65, 1793 - 1807.
18. Bath, M. and Crampin, S., (1964). Higher modes of seismic surface waves : Relations to channel waves, *Geophys. J.R. Astr. Soc.*, 9, 309 - 321.
19. Belcsov, V.V. (1969). *Amer. Geophys. Un., Monograph*, 13, 53-.
20. Belossov, V.V., (1969). "Continental Rifts" in the Earth's crust and upper mantle, *Edit. J. Hart.*
21. Berry, M.L. and Knopoff, L. (1967). Structure of the upper mantle under western Mediterranean basin, *J. Geophys. Res.*, 72, 3613 - 3626.
22. Biswas, N.N. and Knopoff, L. (1970). Exact - earth - flattening calculation for Love waves, *Bull. Secs. Soc. Am.*, 60, 1123 - 1137.

23. Bloch, S. and Hales, A.L. (1968). New techniques for the determination of surface wave phase velocities, Bull. Seism. Soc. Am., 58, 1021 - 1034.
24. Bloch, S., Hales, A.L. and Landisman, M. (1969). Velocities in the crust and Upper Mantle of southern Africa from multi-mode surface wave dispersion, Bull. Seism. Soc. Am., 59, 1599 - 1629.
25. Bolt, B. and Dorman, J. (1961). Phase and group velocities of Rayleigh waves in spherical gravitating earth, J. Geophys. Res., 66, 2965 - 2981.
26. Bolt, B.A. (1964). Recent information on the earth's interior from studies of mantle waves and eigen vibrations, Physics and Chemistry of the earth, 5, 55 - 119.
27. Bonjer, K.P., Fuchs, K. and Wohlenberg, J. (1971). Crustal structure of the East African rift system, from spectral response ratios of long period body waves, L. Geophys. (In Press).
28. Brace, W.F. and Byerlee, J.D. (1970). California Earthquakes : Why only shallow focus, Science, 168, 1573 -
29. Brown, J.M. Geological survey of Uganda - unpublished report.
30. Brune, J., Nafe, J.N. and Oliver, J.E. (1960). A simplified method for the analysis and synthesis of dispersed wave trains, J. Geophys. Res., 65, 287 - 304.
31. Brune, J., Benioff, H., and Ewing, M. (1961). Long-period surface wave from the Chilean earthquake of May 22, 1960, recorded on linear strain seismographs, J. Geophys. Res., 66, 2895 - 2910.
32. Brune, J. and Dorman, J. (1963). Seismic waves and earth structure in the Canadian shield, Bull. Seism. Soc. Am., 53, 167 - 210.

33. Bullard, E.C., (1936). Gravity measurements in East Africa, Phil. Trans. Roy.Soc., 235, 445 - 531.
34. Capon, J. (1970). Analysis of Rayleigh wave multipath propagation at LASA, Bull. Seism. Soc. Am., 60, 1701 - 1731.
35. Crampin, S. (1964). Higher modes of seismic surface waves ; Preliminary observations, Geophys. J.R.Astro. Soc., 9, 37 - 57.
36. Crampin, S. and Bath (1965). Higher modes of seismic surface waves ; Mode separation, Geophys. J.R.Astro. Soc., 10, 81 - 92.
37. Crampin, S. (1966). Higher modes of seismic surface waves ; Phase velocities across Scandinavia, J.Geophys. Res., 69, 4801 - 4811.
38. Crampin, S. (1966). Higher modes seismic surface waves from atmospheric nuclear explosions over Novayazempeya, J. Geophys. Res., 71, 2951 - 2958.
39. Davies, K.A. (1951). The Uganda section of the western rift, Geol. Mag., 88, 377 - 385.
40. Davies, K.A. (1952). The building of Mount Elgon, Mem. Geol. Surv. Uganda, 7, 62.
41. Der, Z., Masse, R. and Landisman, M. (1970). Effects of observational errors on the resolution of surface waves at intermediate distances, J. Geophys. Res., 75, 3399 - 3409.
42. Dixey, F. (1956). "The East African rift system". Colonial Geol. and Min. resources, Bull., Suppl. No 1 , 77.
43. Dopp, S. (1964). Preliminary note on a refracted P- phase in the western rift valley of Africa, J.Geophys. Res., 69, 3027 - 3031.
44. Dorman, J., Ewing, M., and Oliver, J. (1960). Study of shear velocity distribution in the upper mantle by mantle Rayleigh waves, Bull. Seism. Soc. Am., 50, 87 - 115.

45. Dorman, J. and Ewing, M., (1962). Numerical Inversion of seismic surface wave dispersion data and crust - mantle structure in the New York - Pennsylvania area, *J. Geophys. Res.*, 67, 5227 - 5241.
46. Douglas, A. (1967). Joint Epicentre determination, *Nature*, 215, 47 - 48.
47. Dziewonski, A.M. (1970). Correlation properties of free period partial derivatives and their relation to the resolution of Gross earth data, *Bull. Seism. Soc. Am.*, 60, 741 - 768.
48. Evans, A.L., Fairhead, J.D. and Mitchell, J.G., (1971). Potassium - Argon ages from the volcanic province of northern Tanzania, *Nature*, 229, 19 - 20.
49. Ewing, M. and Press (1952). Crustal structure and surface wave dispersion. Part II Solomon Islands Earthquake of July 29, 1950, *Bull. Seism. Soc. Am.*, 42, 315 - 325.
50. Ewing, M. and Press, F. (1954). An investigation of mantle Rayleigh waves, *Bull. Seism. Soc. Am.*, 74, 127 - 147.
51. Ewing, M. and Press, F. (1954). Mantle Rayleigh waves from the Kamchatka Earthquake of Nov. 4, 1952, *Bull. Seism. Soc. Am.*, 44, 471 - 479.
52. Ewing, W.M. and Heezen, B.C. (1956). "Some problems of Antarctic Submarine Geology", *Amer. Geophys. Union, Monograph*, 1, 75 - 81.
53. Ewing, W.M., Jardetzky, W.S., and Press, F. (1957). Elastic waves in layered media, *Magraw - Hill*, pp 380.
54. Fairhead, J.D. (1968). M.Sc. Thesis, "The seismicity of the East African Rift system", University of Newcastle.
55. Freud, R. (1965). "Rift Valleys" in the World rift system". I.U.M.P. symposium, Ottawa, 330 - 344.

56. Gane, P.G., Atkins, A.R., Sellschop, J.F.F. and Seligman, P. (1956). Crustal structure in the Transvaal, Bull. Seism. Soc. Am., 46, 293 - 316.
57. Gass, I.G. (1970). A discussion of the structure and evolution of the Red Sea and the nature of the Red Sea, Gulf of Aden and Ethiopian rift junction, Phil. Trans. Roy. Soc. London, 267, 369.
58. Gilbert, F. and Backus, G.E. (1968). Approximate solutions to the inverse normal mode problem, Bull. Seism. Soc. Am., 58, 103 - 131.
59. Gilluly, J. (1969). Oceanic sediment volumes and continental drift, Science, 166, 992 - 994.
60. Girdler, R.W. (1958). "The relationship of the Red Sea to the East African rift System". Quart. J. Geol. Soc. London, 114, 79 - 105.
61. Girdler, R.W. (1963). "Geophysical studies of Rift Valleys, in Physics and Chemistry of the Earth", Editor, Ahrens, L.N., Press, F., Rankama, K., and Runcorn, S.K., Vol. 5. pp 121 - 158. London pergamon.
62. Girdler, R.W., Fairhead, J.D., Searle, R.C., and Sowerbutts, W.T.C., (1969). Evolution of rifting in Africa, Nature, 224, 1178.
63. Green, R.W.N., and Hales, A.L. (1968). The travel times of P waves to 30° in the central United States and Upper mantle structure, Bull. Seism. Soc. Am., 58, 267 - 289.
64. Griffiths, D.H., King, R.F., Khan, M.A., and Blundell, D.J. (1971). Seismic refraction line in the Gregory rift, Nature, 229, 69 - 71.
65. Gumper, F. and Pomeroy, P. (1970). Seismic wave velocities and Earth structure on the African continent, 60, 651 - 668.

66. Gutenberg, B. (1926). Untersuchungen Zur Frage, bis welcher Tiefe der Erde Kristallin ist? Zeitschr f Geophysik, 2, 24 - 29.
67. Gutenberg, B. (1954). Low velocity layers in the earth's mantle, Bull. Seism. Soc.Am., 65, 337 - 348.
68. Gutenberg, B. (1955). Wave velocities in the earth's crust, in The crust of the earth, special paper 62, A. Polder Vaart editor, Geological Society of America, 19 - 34.
69. Gutenberg, B. (1959). Physics of the Earth's interior, Academic Press, 240.
70. Hales, A.L. and Sacks, F.S. (1959). Evidence for an intermediate layer from crustal structure studies in the Eastern Transvaal, Geophy. J. R. Astro. Soc., 2, 15 - 33.
71. Harris, P.G. (1970). African Magmatism and Tectonics, Edit by Clifford, J.N. and Gass I.G., pp 433.
72. Haskell, N.H. (1953). The dispersion of surface waves on multi-layered media, Bull. Seism. Soc. Am., 43, 17 - 34.
73. Heiskanen, W.A. and Vening Meiness, F.A. (1958). The earth and its gravity field, McGraw - Hipp Book Company, New York.
74. Hoge, E. and Whitham, K. (1962). "Profile Magnetique de Mombassa (Kenya, Ocean Indian) a Torora (Uganda) au travers de La Great Rift Valley (Kenya)". Institut Royale Meteorologique de Belgique, contribution No.70, Brussels.
75. Holmes, A., (1965). Principles of Physical Geology, pp 1053.
76. Hunter, A.N. (1965). Geomagnetic studies in East Africa, in The East African rift system", UMC - UNESCO seminar, Nairobi, part 2, 50 - 52.

77. Illies, J.H. (1969). An Intercontinental belt of the World rift system, *Tectonophysics*, 8, 5 - 30.
78. Illies, J.H. (1970). "Graben problems", edit by Illies, J.H., and Mueller, st., pp 18.
79. Irvine, J.N. (1966). The World rift systems, *Geol. Surv. Canada*, 14 - 66.
80. Keffreys, H. (1925). On the surface waves of Earthquakes, *M.N. R.A.S. Geophys. Suppl.*, 1, 282 - 292.
81. Jeffreys, H. (1961). Small corrections in the theory of surface waves, *Geophys. J.R. Astro. Soc.*, 6, 115 - 117.
82. Jeffreys, H. (1962). The Earth, Cambridge University Press.
83. Johnson, L.R. (1967). Array measurements of P velocities in the upper mantle, *J. Geophys. Res.*, 72, 6309 - 6325.
84. Julian, B.R. and Anderson, D.L. (1968). Travel times, Apparent velocities and Amplitude of body waves, *Bull. Seism. Soc. Am.*, 58, 339 - 366.
85. Keilis - Borok, V.I., and Yanovskaja, T.B., (1967). Inverse problems of seismology (structural review), 13, 223 - 234.
86. Kent, P.E. (1944). The age and tectonic relationships of the East African volcanic rocks, *Geol. Mag.*, 81, 15 - 27.
87. Khan, M.A. and Mansfield, J. (1971). Gravity measurements in Gregory rift, *Nature*, 229, 72 - 75.
88. Knopoff, L. (1961). Green's function for Eigen value problems and the Inversion of Love wave dispersion data, *Geophys. J.R. Astro. Soc.*, 4, 161 - 173.

89. Knopoff, L., Muller, S. and Pilant, W.L. (1966). Structure of the crust and Upper - mantle in the Alps from the phase velocity of Rayleigh waves, Bull. Seism. Soc. Am., 56, 1009 - 1044.
90. Kovach, R.L. and Anderson, D.L. (1962). Long period Love waves in a heterogeneous spherical earth, J. Geophys. Res., 67, 5243 - 5255.
91. Kovach, R.L. and Anderson, D.L. (1964). Higher modes surface waves and their bearing on the structure of the Earth's mantle, Bull. Seis. Soc. Am., 54, 161 - 182.
92. Kovach, R.L. (1965). Seismic surface waves : Some observations and recent developments, Physics and Chemistry of Earth, 16, 251 - 314.
93. H. Lamb, (1904). On the propagation of tremors over the surface of an elastic solid, Phil. Trans. R. Soc., A. 203, 1 - 42.
94. Landisman, M. and Sato, Y. (1958). Shear wave velocities in the upper mantle, Trans. Am. Geophys. Un., 39, 522.
95. Landisman, M., Sato, Y. and Ewing, M. (1959). Surface wave dispersion in Elastic media having gradients in their physical properties, J. Geophys. Res., 64, 1113.
96. Landisman, M.A., Dziewonski, . . . and Sato (1969). Recent improvement in the analysis of surface wave observations, Geophys. J.R. Astro. Soc., 17, 369 - 403.
97. Lehmann, I. (1955). The times of P and S in North-eastern America, Am. di. Geofisica, 8, 351 - 370.
98. Lillwall and Douglass, A., (1970). Estimation of P wave travel times using the Joint Epicentre method, Geophys. J.R. Astro. Soc., 19, 165 - 181.
99. Long, R.E. and Mitchell, M.G. (1970). Teleseismic P - wave delay times in Iceland, Geophys. J.R. Astro. Soc., 20, 41 - 48.

100. Lubimova, E.A., and Feldman, I.S. (1970). Heat flow, temperature, and electrical conductivity of the crust and upper mantle in the U.S.S.R., Tectonophysics, 10, 245 - 281.
101. Magnitsky, V.A. and Kalashnikova, I.V., (1970). Problems of phase transitions in the upper mantle and its connection with the Earth's crustal structure, J. Geophys. Res., 75, 877 - 885.
102. McConnell, R.B. (1970). Evolution of Rifting in Africa, Nature, 227, 699.
103. McEvilly, T.V. (1964). Central U.S. crust - Upper mantle structure from Love and Rayleigh wave phase velocity inversion, Bull. Seism. Soc. Am., 54, 1997 - 2015.
104. McGarr, A. (1969). Amplitude variations of Rayleigh waves - Propagation across a continental margin, Bull. Seism. Soc. Am., 59, 1281 - 1305.
105. McGarr, A. (1969). Amplitude variations of Rayleigh waves - Horizontal refraction, Bull. Seism. Soc. Am., 59, 1307 - 1334.
106. McKenzie, D.P. (1970). Plate tectonics of the Red Sea and East Africa, Nature, 226.
107. McKenzie, D.P., Davies, D., and Molnar, P. (1970). Nature, 226, 243.
108. Mitchell, B.J. and Landisman, M. (1969). Electro-magnetic seismograph constants by least-square inversion, Bull. Seism. Soc. Am., 59, 1335 - 1348.
109. Mohr, P.A. (1962). "The Geology of Ethiopia", University College Press, Addis Ababa.
110. Mohr, P.A. & Gouin, P. (1968). Gravity Traverses in Ethiopia, Bull. of the Geophys. Obs. Haile Sellassie University, Addis Ababa, July, 27.

111. Mohr, P.A. (1970). Plate tectonics of the Red Sea and East Africa, *Nature*, 228, 547 - 548
112. Molnar, P. and Oliver, J. (1969). Lateral variation of attenuation in the upper mantle and discontinuities in the Lithosphere, *J. Geophys. Res.*, 74, 2648 - 2682.
113. Molnar, P. and Yash Pal Aggarwal, (1971). A micro earthquake survey in Kenya, *Bull. Seism. Soc. Am.*, 61, 195 - 201.
114. Murray, G.G. (1970). Magma Genesis and heat flow : Differences between mid-oceanic ridges and African rift valleys, *Earth and Planetary science letters*, 9, 34 - 38.
115. Niazi, M. and Anderson, D.L. (1965). Upper mantle structure of western North America from apparent velocities of P waves, *J. Geophys. Res.*, 70, 4633 - 4640.
116. Nuttli, O. (1963). Seismological evidence pertaining to the structure of the earth's upper mantle, *Res. Geophys.* 1, 351 - 400.
117. Nuttli, O.W. and Bolt (1969). P wave residuals as a function of azimuth : (2) Undulation of the mantle low velocity layer as an explanation, *J. Geophys. Res.*, 74, 6594 -
118. Ocal, N. (1965). The dispersion of surface waves and crustal structure in African continent, *Pure and Applied Geophysics*, 60, 74 - 79.
119. Oliver, J. and Ewing, M. (1957). Higher modes of continental Rayleigh waves, *Bull. Seism. Soc. Am.*, 47, 187 - 204.
120. Oliver, J. and Ewing, M. (1958). Normal modes of continental surface waves, *Bull. Seism. Soc. Am.*, 48, 33 - 49.
121. Oliver, J., Dorman, J., and Sutton, G. (1959). The second shear mode of continental Rayleigh waves, *Bull. Seism. Soc. Am.*, 49, 379 - 389.

122. Oliver, J., Sykes, L. and Isacks, B. (1969). Tectonophysics, 7, 527.
123. Pakiser, L.C. (1963). Structure of the crust and upper mantle in the western United States, J. Geophys. Res., 68,
124. Payo, G. (1970). Structure of the Crust and Upper Mantle in the Iberian shield by means of a long period triangular array, Geophy. J.R. Astro. Soc., 20, 493 - 508.
125. Pekeris, G.L. (1966). The Internal constitution of the Earth, Geophys. J.R. Astro. Soc., 11, 85 - 132.
126. Pfeffer, R.L. and Zarichny, J. (1963). Acoustic gravity wave propagation in an atmosphere with two sound channels, Geofis. Pura. e Appl., 55, 175 - 199.
127. Pilant, W.L. and Knopoff, L., (1964). Observations of multiple seismic events, Bull. Seism. Soc., Am., 54, 19 - 39.
128. Powell, J.D. (1964). "An efficient method for finding the minimum of a function of several variables without calculating derivatives", The Computer Journal, 7, 155.
129. Powell, J.D. (1965). A method for minimising a sum of squares of non-linear functions without calculating derivatives, The Computer Journal, 8, 303 - 307.
130. Press, F. and Ewing, M. (1956). A mechanism for G wave propagation, Trans. Am. Geophys. Un., 37, 355 - 356.
131. Press, F. (1959). Some implication on mantle and crustal structure from G waves and Love waves, J. Geophys. Res., 64, 565 - 568.

132. Press, F. and Biehler, S., (1964). Inferences on crustal velocities and densities from P wave delays and gravity anomalies, J. Geophys. Res., 69, 2979.
133. Press, F. (1968). The density distribution on the Earth, Science, 160, 1218.
134. Press, F. (1968). Earth models obtained by Monte Carlo Inversion, J. Geophys. Res., 73, 5223 - 5234.
135. Rayleigh, Lord (1885). On waves propagated along the plane surface of an elastic solid, Proc. Land. Math. Soc. 17, 4 - 11.
136. Roberts, D.G. (1969). Structural evolution of the rift zones in the Middle East, Nature, 223, 55.
137. Rothe, (1954). "La Zone Seismique Mediane Indo - Atlantique", Proc. Roy. Soc., A., 222, 387 - 400.
138. Saggerson, E.F. and Baker, B.H. (1965). "Post - Jurassic Erosion surfaces in eastern Kenya and their deformation in relation to rift structure", Quart. J. Geol. Soc., London, 121, 51 - 72.
139. Santo, T.A. (1965). Lateral Variation of Rayleigh wave dispersion character. Part I observational data, Pure and Applied Geophysics. (pageoph) 62, 49 - 60.
140. Santo, T.A. (1965). Lateral variation of Rayleigh wave dispersion character. Part II. Eurasia, Pure and Applied Geophysics, 62, 67 - 80.
141. Santo, T.A. (1965). Lateral variation of Rayleigh wave dispersion character. Part III. Atlantic ocean, Africa and Indian Ocean, Pure and Applied Geophysics, 63, 40 - 59.
142. Sato, Y. (1955). Analysis of dispersed surface waves, Part I, Bull. Earthquake Res. Inst. 33, 33 - 47.

143. Sato, Y. (1956). Analysis of dispersed surface waves, Part II. Bull. Earthquake Res. Inst., 34, 9 - 18.
144. Sato, Y. (1956). Analysis of dispersed surface waves, Part III, Bull. Earthquake Res. Inst. 34, 131 - 138.
145. Sato, Y. (1958). Attenuation of dispersion and the wave guide of the G wave. Bull. Seism. Soc. Am., 48, 231 - 251.
146. Searle, R.C. (1970). Lateral extensions in the East African rift valleys, Nature, 227, 267 - 268.
147. Smith, N. and Andrew, (1960). Gravity survey of Tanganyika, Overseas Geological Survey Geophysical report, No. 8C - Unpublished.
148. Sowerbutts, W.T.C. (1969). Crustal structure of the East African plateau and rift valleys from gravity measurements, Nature, 223, 143 - 146.
149. Stoneley, R. (1925). Dispersion of seismic waves, M.N.R.A.S. Geophys. Suppl., 1, 280 - 282.
150. Sutton and Grow (1969). The Earth's Crust and Upper mantle - edit by J. Hart.
151. Sykes, L.R. and Landisman, M. (1964). The seismicity of East Africa, the Gulf of Aden and the Arabian and Red Seas, Bull. Seis. Soc. Am., 54, 1927 - 1940.
152. Takeuchi, H., Press, F. and Kobayashi, B. (1959). Rayleigh wave evidence for the low velocity zone in the mantle, Bull. Seism. Soc. Am., 49, 355 - 364.
153. Thatcher, W. and Brune, J.N., (1969). Higher mode interference and observed anomalous apparent Love wave phase velocities, J. Geophys. Res., 74, 6603 - 6611.
154. Tazieff, H. (1970). The Afar triangle, Scientific America, 32,

155. Tikhonov, A.N., Lubinova, E.A. and Vlasov, V.K. (1970). Physics and Solid earth, 2, 326 - 331.
156. Tobin, D.G., Ward, P.L., and Drake, C.L. (1969). Micro earthquakes in the rift valley of Kenya, Bull. Geol. Soc. Amer., 80, 2043 - 2046.
157. Toksoz, M.N. and Anderson, D.L. (1966). Phase velocities of long period surface waves and structure of the upper mantle, 1. Great Circle Love and Rayleigh wave data, J. Geophys. Res., 71, 1649 - 1658.
158. Toksoz, M.N., Chinnery, M.A., and Anderson, D.L. (1967). Inhomogeneities in the earth mantle, Geophys. J.R. Astro. Soc., 13, 31 - 59.
159. Valle, P.E. (1949). Sulla Misura della Velocita di Gruppo delle onde Seismiche superficiali, Annali di Geofisica, 2, No 3.
160. Vine, F.J. (1966). "Spreading of the ocean floor : New Evidence", 154, 1405 - 1415.
161. Con Herzen, R.P. and Vacquier, V. (1967). Terrestrial heat flow in Lake Malawi, Africa, J. Geophys. Res., 72, 4221 - 4226.
162. Willmore, P.L., Hales, A.L. and Gane, P.G. (1952). A seismic investigation of crustal structure in the western Transvaal, Bull. Seism. Soc. Am., 42, 53 - 80.
163. Wilson, J.T. (1969). Tectonophysics, 7, 600.
164. Witham, K. and Hage, E., (1961). "Geomagnetic Investigation in British East Africa during 1959". Ottawa, Dominion Observatory.
165. Wohlenberg, J. (1968). Veroffentl Bayer, Komm. Intern. Erdmessg., 23.
166. Wohlenberg, J. (1970). On the seismicity of the East African Rift system, International Upper mantle project, Scientific report No. 27.

167. Wohlenberg, J. (1971). The first European Earth and Planetary Physics colloquium, Reading, United Kingdom.
168. Wright, J.B. (1970). Distribution of volcanic rocks about mid-ocean ridges and the Kenya rift valley, *Geol. Mag.*, 107, 125 - 131.
169. Yi - Ben Tsai and Keiiti Aki (1969). Simultaneous determination of the seismic moment and attenuation of seismic surface waves, *Bull. Seism. Soc. Am.*, 59, 275 - 287.

